Mediators of Inflammation

Acute Lung Injury, Repair, and Remodeling: Pulmonary Endothelial and Epithelial Biology

Guest Editors: Yutong Zhao, Karen Ridge, and Jing Zhao

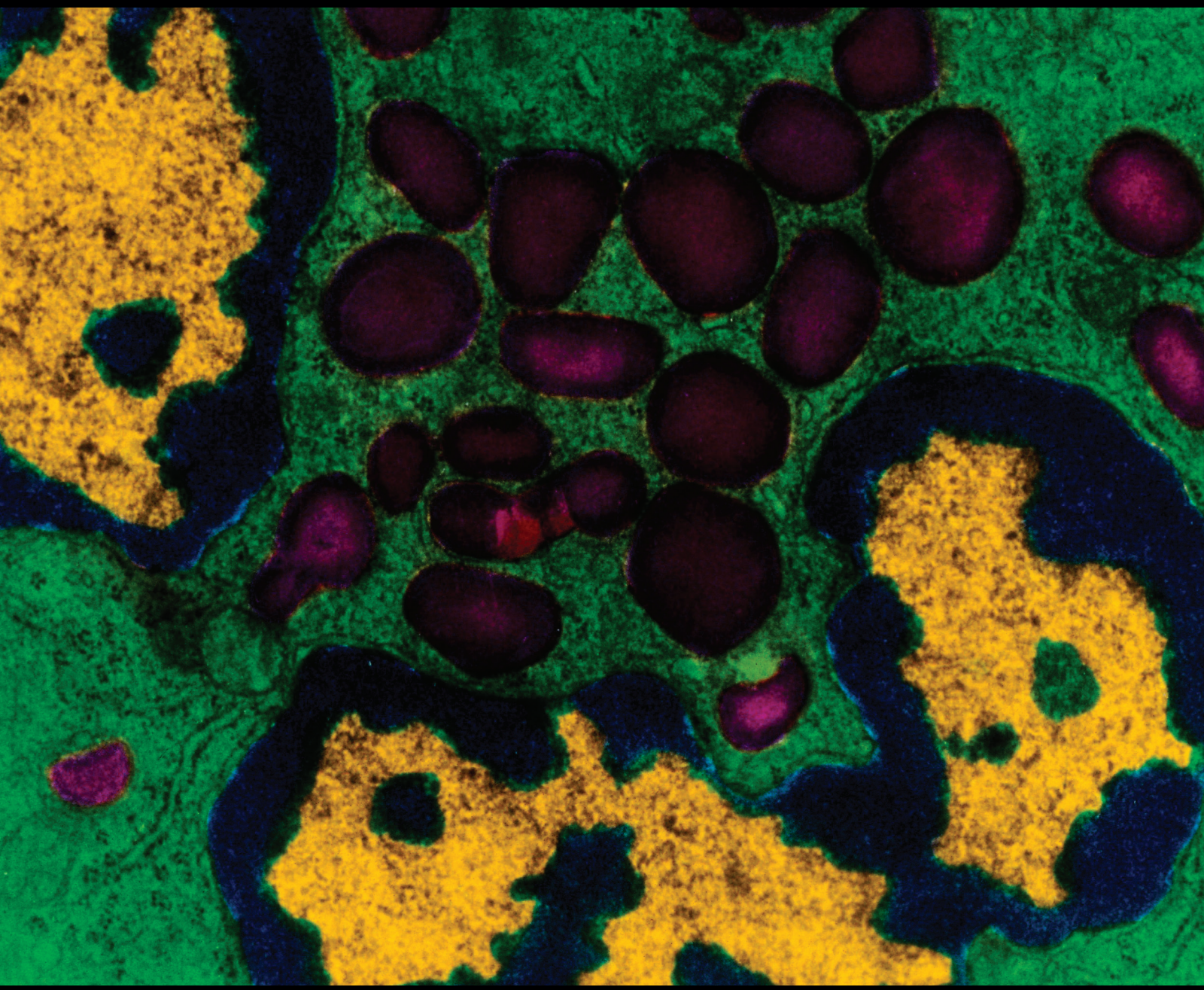

Acute Lung Injury, Repair, and Remodeling: Pulmonary Endothelial and Epithelial Biology

Mediators of Inflammation

Acute Lung Injury, Repair, and Remodeling: Pulmonary Endothelial and Epithelial Biology

Guest Editors: Yutong Zhao, Karen Ridge, and Jing Zhao

Editorial Board

Contents

Hindawi
Mediators of Inflammation
Volume 2017, Article ID 9081521, 2 pages
http://dx.doi.org/10.1155/2017/9081521

Editorial

Acute Lung Injury, Repair, and Remodeling: Pulmonary Endothelial and Epithelial Biology

Yutong Zhao,[1] Karen Ridge,[2] and Jing Zhao[1]

[1]*Department of Medicine, University of Pittsburgh, 3459 Fifth Avenue, 628 NW MUH, Pittsburgh, PA 15213, USA*
[2]*Department of Medicine, Northwestern University, McGaw Pavilion Suite M-410, 240 E Huron, Chicago, IL 60611, USA*

Correspondence should be addressed to Yutong Zhao; zhaoy3@upmc.edu

Received 21 February 2017; Accepted 21 February 2017; Published 14 March 2017

Acute lung injury (ALI) and ARDS are defined by damage to the alveolar epithelium and endothelium, which allows the exudation of protein-rich fluid into the alveolar space. ALI/ARDS are life threatening inflammatory lung diseases, most commonly caused by local or systemic inflammation, including pneumonia and sepsis. An uncontrolled cytokine storm leads to detrimental effects such as cell death, epithelial and endothelial barrier disruption, and edema. Lung repair and remodeling following ALI are crucial steps and could be a risk factor for determining morbidity and mortality. During normal repair and remodeling phases, alveolar fluid is reabsorbed and debris from dead cells and pathogens is cleared by mononuclear-linage phagocytes. Additionally, endothelial cells regenerate, epithelial cells proliferate and differentiate, and collagen fibers are formed at site of injury. Finally, excess deposits of collagen fibers are processed and removed.

Pulmonary edema is a major complication of ALI. Approaches aiming at improving and maintaining endothelial and epithelial barrier integrity and function are in high demand. The aim of this special issue is to illuminate pulmonary endothelium and epithelium biological function during ALI, repair, and remodeling. We have selected 6 original research manuscripts and 1 review article covering the range from basic research aspects to translational studies and therapeutic evaluation.

ALI/ARDS is associated with a high mortality rate between 20 and 50% and is one of the main clinical complications in severe malaria. M. L. M. Pereira et al. determine the protective role of heme oxygenase-1 (HO-1) and HO-1 inducing drug, hemin, in malaria-associated ALI. This study will potentially advance therapeutic approach in prevention of ALI/ARDS development in severe malaria. In attempt to manage the uncontrolled cytokine storm induced, a NEMO-binding domain peptide (NBD) was developed by J. Huang et al. to inhibit LPS-induced NF-κB activation; NBD limits cytokine release, neutrophil infiltration, and pulmonary vascular leakage in LPS-induced ALI mouse model. As an analysis of the enhancement of endothelium barrier integrity aspect, L. Wang et al. have investigated the protective role of pan-caspase inhibitor Q-VD in cytomix-induced pulmonary microvascular endothelial cell permeability and apoptosis. In the review article, Y. Zhuang et al. have addressed microRNA regulation in endothelial junction proteins and clinical consequence.

Lipid mediators, prostaglandin E2 (PGE_2) and Leukotriene B_4 (LTB_4), play an important role in host defense in many infections. The study by L. C. Rodrigues et al. has unveiled that Gal-1 protects against histoplasmosis by maintaining the balance of nitric oxide (NO) and PGE2. AM966 is an antagonist of lysophosphatidic acid receptor 1, which potentiates antifibrotic function in experimental study. The study by J. Cai et al. has revealed that AM966 treatment induces lung microvascular endothelial barrier disruption which is regulated by RhoA/MLC and phosphorylation of VE-cadherin. Further, P. Geraghty et al. demonstrate the ER stress in cigarette smoke-induced COPD.

In conclusion, many factors contribute to the pathogenesis of ALI/ARDS. It is important to understand the pathophysiological mechanisms of ALI/ARDS to improve the

outcome of ALI patients. These special research articles were selected to offer readers updated knowledge on new therapeutic approach development for ALI/ARDS and precaution in clinical trial medicine.

Yutong Zhao
Karen Ridge
Jing Zhao

Hindawi Publishing Corporation
Mediators of Inflammation
Volume 2017, Article ID 6893560, 12 pages
http://dx.doi.org/10.1155/2017/6893560

Research Article

AM966, an Antagonist of Lysophosphatidic Acid Receptor 1, Increases Lung Microvascular Endothelial Permeability through Activation of Rho Signaling Pathway and Phosphorylation of VE-Cadherin

Junting Cai,[1,2] Jianxin Wei,[1] Shuang Li,[1,3] Tomeka Suber,[1] and Jing Zhao[1]

[1]*Acute Lung Injury Center of Excellence, Division of Pulmonary, Asthma, and Critical Care Medicine, Department of Medicine, University of Pittsburgh, Pittsburgh, PA 15213, USA*
[2]*Third Affiliated Hospital of Xiangya Medical School, Changsha, Hunan 410013, China*
[3]*Department of General Surgery, The First Affiliated Hospital of Dalian Medical University, Dalian, Liaoning 116011, China*

Correspondence should be addressed to Jing Zhao; zhaoj@upmc.edu

Received 30 September 2016; Revised 4 January 2017; Accepted 15 January 2017; Published 27 February 2017

Academic Editor: Giuseppe Valacchi

Maintenance of pulmonary endothelial barrier integrity is important for reducing severity of lung injury. Lysophosphatidic acid (LPA) regulates cell motility, cytoskeletal rearrangement, and cell growth. Knockdown of LPA receptor 1 (LPA1) has been shown to mitigate lung injury and pulmonary fibrosis. AM966, an LPA1 antagonist exhibiting an antifibrotic property, has been considered to be a future antifibrotic medicine. Here, we report an unexpected effect of AM966, which increases lung endothelial barrier permeability. An electric cell-substrate sensing (ECIS) system was used to measure permeability in human lung microvascular endothelial cells (HLMVECs). AM966 decreased the transendothelial electrical resistance (TEER) value immediately in a dose-dependent manner. VE-cadherin and f-actin double immunostaining reveals that AM966 increases stress fibers and gap formation between endothelial cells. AM966 induced phosphorylation of myosin light chain (MLC) through activation of RhoA/Rho kinase pathway. Unlike LPA treatment, AM966 had no effect on phosphorylation of extracellular signal-regulated kinases (Erk). Further, in LPA1 silencing cells, we observed that AM966-increased lung endothelial permeability as well as phosphorylation of VE-cadherin and focal adhesion kinase (FAK) were attenuated. This study reveals that AM966 induces lung endothelial barrier dysfunction, which is regulated by LPA1-mediated activation of RhoA/MLC and phosphorylation of VE-cadherin.

1. Introduction

Lysophosphatidic acid (LPA) is a bioactive phospholipid that contributes to the pathogenesis of numerous fibrotic diseases, including pulmonary, hepatic, skin, and renal fibrosis [1–3]. Upon binding to its high-affinity G protein-coupled receptors (LPA1–6) and coupling to different downstream G proteins (Gαi/o, Gαq, and Gα12/13) [4, 5], LPA exerts multiple biological effects, including cell proliferation, migration, cytoskeletal rearrangement, and cell survival [6–8]. Studies have shown that LPA levels in bronchoalveolar lavage (BAL) fluid increase in idiopathic pulmonary fibrosis (IPF) patients [2, 9, 10]. The LPA-LPA1 pathway plays a crucial role in the development of pulmonary fibrosis via mediating fibroblast growth and recruitment [2]. AM966 is a highly selective LPA1 antagonist [11], which inhibited LPA-stimulated intracellular calcium release and LPA-induced chemotaxis in vitro and reduced lung injury and fibrosis induced by bleomycin in vivo [12]. Based on these findings, AM966 has gained considerable academic and industry attention as a treatment for IPF [12–15]. A relative compound BMS-986202 (previously AM152) has completed phase 1 clinical trials in 2011, and the phase 2

clinical trials of another structurally related molecular BMS-986020 is completed in 2016 [14, 16, 17].

Maintenance of pulmonary endothelial barrier integrity is of great importance in healthy lungs. Impaired microvascular endothelial barrier function leads to the infiltration of blood proteins and circulating cells into the tissues underlying vessels, which is related to lung injury [18, 19]. The endothelial cell-cell junctional complex that controls paracellular permeability is composed of adherens junctions, tight junctions, and desmosomes. Adherens junctions are a major part of the complex, in which VE-cadherin, an endothelium-specific component of adhesion proteins, controls both adherens junctions and endothelial barrier integrity [20, 21]. Inflammatory stimuli, such as thrombin and endotoxin, induce phosphorylation of VE-cadherin and redistribution of VE-cadherin from cell-cell junctions to the cytoplasm, thus increasing vascular permeability [20]. In addition to adherens junctions, myosin light chain- (MLC-) mediated cytoskeletal remodeling also majorly contributes to gap formation and endothelial barrier dysfunction [22, 23]. A small GTPase, RhoA, and its downstream signaling molecule, Rho kinase, regulate MLC phosphorylation and induce stress fiber, thereby causing cell retraction and endothelial leak [24, 25].

LPA has been shown to increase lung and corneal epithelial barrier integrity [26], while studies about the role of LPA in endothelial barrier function are controversial. Some earlier studies reported a protective role of LPA in endothelial cell barrier integrity [27, 28], while more recent studies demonstrated increased vascular leakage after LPA exposure [2, 29–31]. Furthermore, genetic deletion of LPA1 has been shown to induce embryonic lethality [32], indicating LPA1 signaling pathway is of great importance in healthy beings. Given the characteristic of AM966 in selectively inhibiting LPA1 receptor, we hypothesized that AM966 has a role in regulating endothelial barrier function. In the present study, we show that AM966 increases permeability in human lung microvascular endothelial cells (HLMVECs) by activation of Rho signaling pathway and phosphorylation of VE-cadherin. Our findings reveal an unexpected effect of AM966, which raises a caution for using AM966 as an antifibrotic medicine in the future.

2. Materials and Methods

2.1. Reagents and Cell Culture. Human lung microvascular endothelial cells (HLMVECs, Lonza) were cultured at 37°C in an atmosphere of 5% CO_2 with EGM-2 medium (Lonza) containing 25 mL FBS (5%), 0.5 mL hEGF, 2.0 mL hFGF-β, 0.5 mL VEGF, 0.5 mL ascorbic acid, 0.2 mL hydrocortisone, 0.5 mL R3-IGF-1, and 0.5 mL gentamycin. Phospho (T18/S19)-MLC, MLC, antibodies, and cell lysis buffer were obtained from Cell Signaling. Phospho (Y658)-VE-cadherin antibody was purchased from Invitrogen. VE-cadherin antibody was from Santa Crus Biotechnology. β-Actin antibody, scrambled siRNA, LPA1 siRNA, and LPA were from Sigma Aldrich. LPA1 antibody was obtained from Proteintech. AM966 was from Apex Bio. Horseradish peroxidase-conjugated goat anti-mouse and anti-rabbit secondary antibodies, ECL kit, and SDS-PAGE for western blotting were purchased from Bio-Rad Laboratories, Inc. For immunostaining, anti-mouse Alexa-488, anti-rabbit Alexa-568, and DAPI were from Invitrogen. Transfection reagent FuGENE HD was from Promega. All other reagents were of analytical grade.

2.2. siRNA Transfection. SiRNAs and Lipofectamine RNAi MAX reagent (Invitrogen) were diluted separately in Opti-MEM medium and then incubated together for 5 min at room temperature before adding to the cell culture. Analysis of the transfected cells was performed 72 h later.

2.3. Protein Extraction and Western Blot Analysis. Cells were lysed in lysis buffer. Samples were loaded with equal amounts of total protein (20 μg) and separated by 4–15% SDS-PAGE gels and then transferred to nitrocellulose membranes. Membranes were blocked with 5% nonfat milk and then incubated with specific primary antibodies, followed by secondary antibodies. The membranes were developed using chemiluminescence detection system.

2.4. Immunofluorescence Staining. HLMVECs were cultured in glass-bottomed dishes and were fixed with 3.7% formaldehyde in phosphate-buffered saline (PBS) for 20 min. After blocking with 1% bovine BSA in TBST for 30 min, cells were exposed to VE-cadherin for 1 h. Then, anti-rabbit Alexa-488 secondary antibody was applied for 1 h. F-Actin was immunostained with Alexa-568 Phalloidin. Nuclei were detected with DAPI. Immunofluorescent cell imaging was performed using a Zeiss LSM 510 confocal microscope.

2.5. Measurement of TEER by Electrical Cell-Substrate Impedance Sensing System (ECIS). HLMVECs grown on gold electrodes and experiments were conducted only on wells with steady-state transendothelial electrical resistance. Resistance changes were monitored in real time using ECIS (Applied Biophysics) with 4000 Hz. TEER values from each microelectrode were pooled at discrete time points and plotted versus time as the mean ± SEM.

2.6. RhoA Activity Assay. HLMVECs were treated with AM966 (1.0 μM, 15 and 30 minutes) or thrombin (1 U/mL, 30 minutes). Guanosine triphosphate- (GTP-) bound active Rho was predicated by following the manufacturer's instructions (Rho Activation Assay Kit, Millipore). The amount of activated RhoA is determined by a western blotting using a RhoA specific antibody.

2.7. Statistical Analysis. Statistical analysis was carried out by one-way ANOVA with post hoc test or Student's t-test, with a p value of < 0.05 considered indicative of significance.

3. Results

3.1. AM966 Increases Barrier Permeability and Gap Formation between Lung Microvascular Endothelial Cells. It has

been reported that LPA increases lung endothelial barrier permeability, while the effect of LPA1 antagonist on lung endothelial barrier integrity has not been reported. Our initial studies examined the effect of AM966 on HLMVECs barrier function using ECIS system, a highly sensitive system to measure endothelial cell monolayer integrity and permeability. Figures 1(a) and 1(b) show that AM966 rapidly reduces TEER in 15 min after treatment. The resistance returned to baseline within 2 h. This effect was similar to LPA treatment. The combination of LPA1 agonist (LPA) and antagonist (AM966) had no further reduction of TEER. These data suggest that both AM966 and LPA increase HLMVECs permeability and delays barrier integrity recovery time. VE-cadherin is a major junction protein, which controls endothelial barrier integrity. Next, we examined whether the effect of AM966 is dose-dependent. As shown in Figures 1(c) and 1(d), AM966 reduces TEER in a concentration-dependent manner. The TEER recovered (0.1 and 1.0 μM AM966) within 2 h, while it remained in a low level with 10 μM AM966 stimulation. Further, we examined the effect of AM966 on VE-cadherin expression on cell surface. As shown in Figure 1(e), VE-cadherin is primarily localized on cell-cell junctions. However, AM966 (1 μM, 30 min) causes paracellular gap formation and less VE-cadherin staining on cell-cell junctions. F-Actin staining shows that A966 increases stress fibers in HLMVECs (Figure 1(e)). Taken together with Figure 1, these data indicate that AM966 treatment leads to reduction of VE-cadherin expression on the cell-cell junction, increasing stress fibers, and gap formation, thus disrupting lung microvascular barrier integrity.

3.2. AM966 Activates RhoA and Increases Phosphorylation of MLC in HLMVECs. A primary mechanism of cellular contraction is the actin-myosin cross-bridge interaction. Rho/Rho kinase plays a pivotal role in direct or indirect phosphorylation of MLC [23]. Based on AM966 induction of stress fibers, we hypothesized that AM966 activates RhoA in HLMVECs. To examine whether RhoA/Rho kinase pathway contributes to AM966-increased lung endothelial permeability, we first examined the RhoA activity after AM966 treatment and found that AM966 stimulation activated RhoA (Figures 2(a) and 2(b)). Thrombin, an agent well known to activate Rho pathway, was used as a positive control (Figures 2(a) and 2(b)). Further, the effect of AM966 on MLC phosphorylation was determined. As shown in Figures 2(c) and 2(d), AM966 induced phosphorylation of MLC in a time-dependent manner, while the effect was inhibited by Rho kinase inhibitor (Figures 2(e) and 2(f)). The effect of AM966 on phosphorylation of MLC was similar to the effect by LPA (Figures 2(c) and 2(d)). To examine whether RhoA activation is involved in AM966-reduced TEER, HLMVECs were treated with Rho kinase inhibitor prior to AM966 addition. As shown in Figures 2(g) and 2(h), AM966-reduced TEER was significantly attenuated by Rho kinase inhibitor. These data suggest that RhoA activation and MLC phosphorylation play a critical role in AM966-induced lung endothelial barrier disruption.

3.3. AM966 Increases Phosphorylation of VE-Cadherin. It has been well known that tyrosine phosphorylation of VE-cadherin reduces endothelial cell-cell junctions [20]. We therefore explored the effect of AM966 on phosphorylation of VE-cadherin. Figures 3(a) and 3(b) depict a similar level of increased VE-cadherin phosphorylation after treatment with AM966 or LPA, while increase in phosphorylation of Erk1/2 was only observed in LPA treated cells. Our and others' previous studies have shown that Gαi regulates LPA-induced Erk1/2 phosphorylation [8, 33, 34]. This data suggests that AM966 induced phosphorylation of VE-cadherin is not through Gαi pathway. Furthermore, AM966 induced phosphorylation of VE-cadherin is in both a time- and concentration-dependent manner (Figures 3(c)–3(f)). These data support the hypothesis that AM966 reduces lung endothelial barrier integrity through modulation of VE-cadherin phosphorylation and reduction of VE-cadherin expression on the cell-cell junctions in HLMVECs.

3.4. AM966 Induces Phosphorylation of VE-Cadherin and Endothelial Barrier Disruption through LPA1. Though AM966 is a competitive antagonist of the LPA1 receptor, here we show that AM966 induces biological effects in HLMVECs including phosphorylation of VE-cadherin and MLC, activation of RhoA, and reduction of TEER. Thus, we hypothesized that AM966-mediated barrier disruption is through binding to LPA1 receptor. Downregulation of LPA1 expression with siRNA significantly attenuated the AM966-induced phosphorylation of VE-cadherin as shown in Figures 4(a) and 4(b). LPA1 is coupling to different downstream G proteins (Gαi/o, Gαq, and Gα12/13) to regulate multiple biological effects. To investigate the involvement of Gα12/13, we transiently transfected HLMVECs with the minigene vectors (Cue Biotech, Chicago, IL) encoding a unique peptide that specifically blocks the receptor/G protein interface. As shown in Figures 4(c) and 4(d), Gα12/13 minigene transfection resulted in attenuation of AM966-induced phosphorylation of VE-cadherin. These results indicate that Gα12/13 are essential for AM966 reduction of lung endothelial barrier integrity. The functional importance of LPA1 receptor in barrier regulation is also measured using ECIS system. LPA1 siRNA transfection markedly attenuated AM966-reduced TEER (Figures 4(e) and 4(f)). These data indicate that AM966-induced barrier disruption in HLMVECs is mediated by LPA1/Gα12/13 pathways including phosphorylation of VE-cadherin.

3.5. AM966-Induced Phosphorylation of VE-Cadherin Is Not FAK-Dependent. It has been shown that VE-cadherin phosphorylation is mediated by focal adhesion kinase (FAK) [35]. We observed that AM966 induced phosphorylation of FAK; the effect was attenuated by downregulation of LPA1 (Figures 5(a) and 5(b)), suggesting that FAK is a downstream signal molecule of AM966/LPA1. However, the FAK kinase inhibitor alone increased VE-cadherin phosphorylation, and it enhanced AM966-induced FAK phosphorylation in a dose-dependent manner (Figures 5(c) and 5(d)). The functional of FAK inhibitor in barrier regulation is also measured

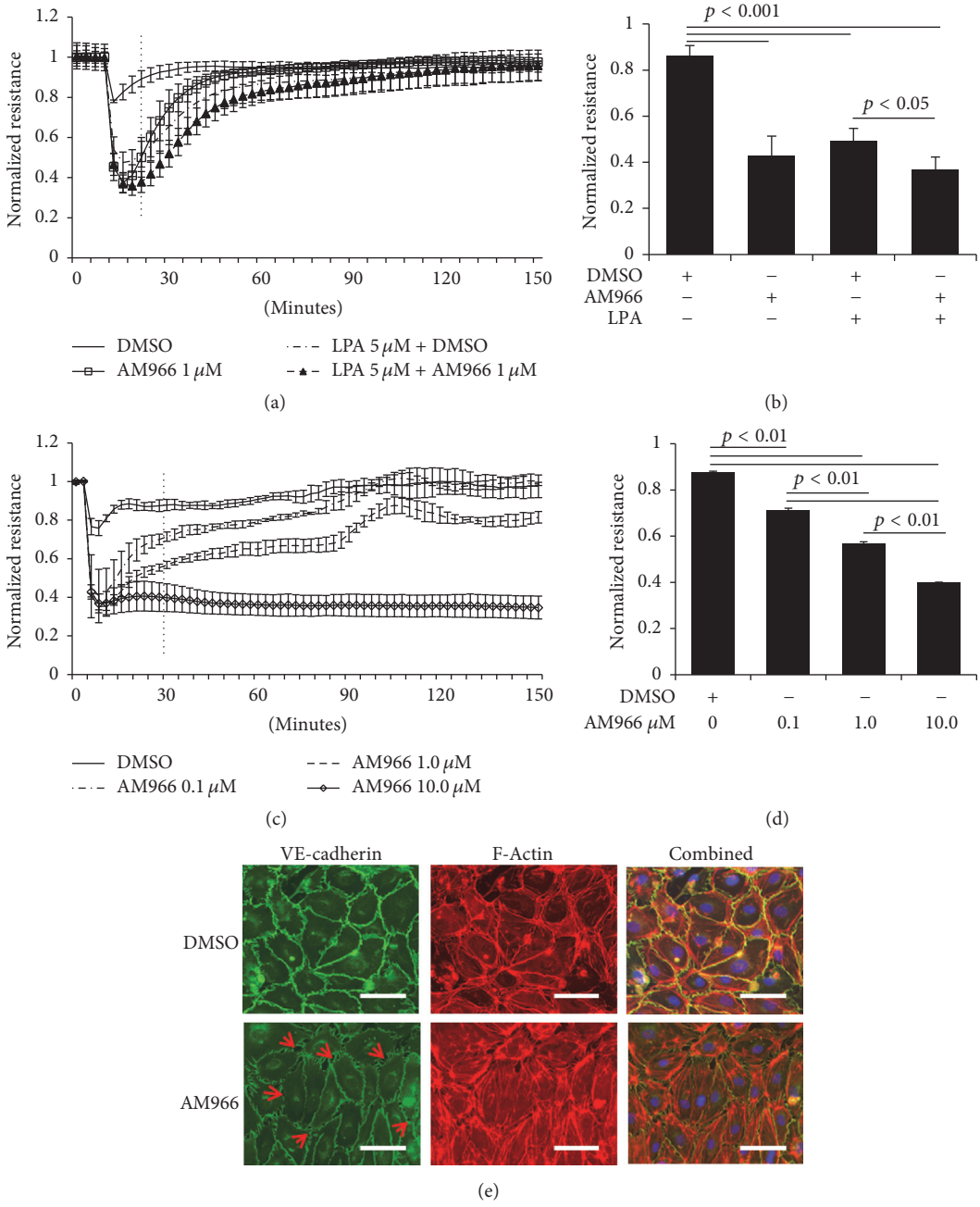

Figure 1: AM966 increases permeability in HLMVECs. (a) Confluent HLMVECs were plated on gold electrodes and TEER changes were monitored in real time using ECIS. After baseline resistance was stable, DMSO, AM966 (1.0 μM), LPA (5 μM), or AM966 + LPA was added to each well. The TEER tracing represents pooled data (±SEM) from 3 independent experiments. (b) The electrical resistance during indicated time period (a) was quantified and statistical analysis was performed. (c) Confluent HLMVECs were plated on gold electrodes and TEER changes were monitored in real time using ECIS. After baseline resistance was stable, different doses of AM966 (0.1, 1.0, or 10.0 μM) were added to each well. The TEER tracing represents pooled data (±SEM) from 3 independent experiments. (d) The resistance in response to AM966 treatments during indicated time period (c) was quantified and statistical analysis was performed. (e) HLMVECs (~100% confluence) were grown on a glass bottom coverslip and serum deprived for 3 h, and then the cells were treated with DMSO or AM966 (1 μM) for 30 min. Immunofluorescence staining of VE-cadherin (green), F-actin (red), and nuclei (blue) was examined by a Zeiss LSM 510 confocal microscope. Scale, 15 μm. Paracellular gaps are marked by arrows. Shown are representative images from three independent experiments.

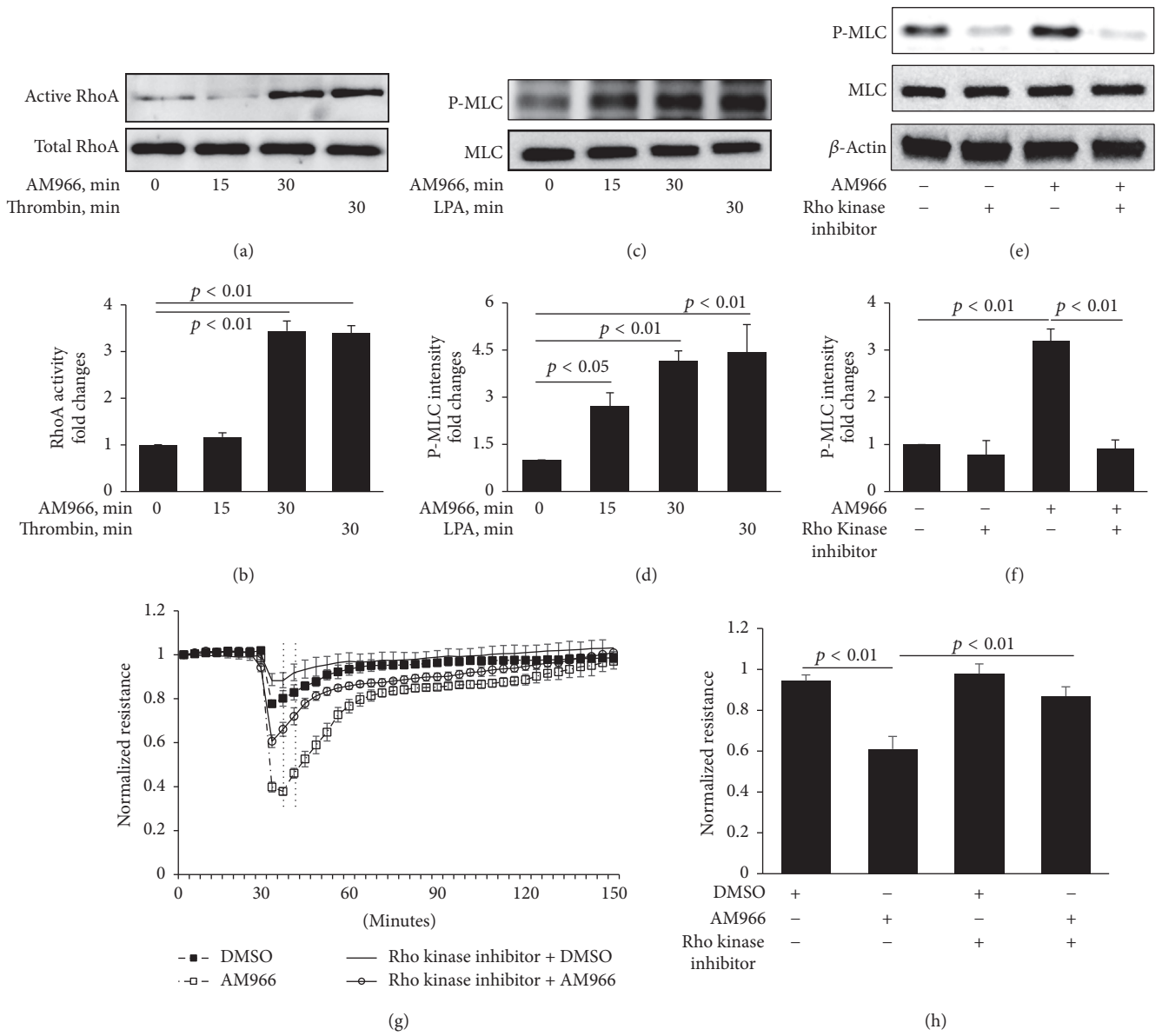

Figure 2: AM966 induces RhoA activity and phosphorylation of MLC. (a) Confluent HLMVECs were starved 3 h and treated with AM966 (1.0 μM) and thrombin (1 U/mL) for indicated time periods. Activated RhoA was immunoprecipitated from total lysates by following the manufacturer's instructions (Rho Activation Assay Kit, Millipore). The amount of activated RhoA is determined by a western blot using a RhoA specific antibody. (b) Analysis of activated RhoA by densitometry of the results in (a) were performed by Image J software ($n = 3$), and statistical analysis was shown. (c) Confluent HLMVECs were treated with AM966 (1.0 μM) or LPA (5 μM) for indicated time periods after 3 h starvation. Cell lysates were immunoblotted with phospho-MLC (P-MLC) and total MLC antibodies. (d) Analysis of P-MLC by densitometry of the results in (c) was performed by Image J software ($n = 3$), and statistical analysis was shown. (e) Serum starved confluent HLMVECs were pretreated with Rho kinase inhibitor (10 μM) for 1 h and then incubated with DMSO or AM966 (1.0 μM) for an additional 30 min. Lysates were immunoblotted with P-MLC, total MLC, and β-actin antibodies. (f) Analysis of P-MLC by densitometry of the results in (e) was performed by Image J software ($n = 3$), and statistical analysis was shown. Shown are representative blots from three independent experiments. (g) Confluent HLMVECs were plated on gold microelectrodes and pretreated with 10.0 μM Rho kinase inhibitor for 1 h and then stimulated by 1.0 μM AM966 or DMSO. The TEER tracing represents pooled data (±SEM) from 3 independent experiments. (h) The resistance in response to AM966 treatments during indicated time period (g) was quantified and statistical analysis was performed.

using ECIS system. FAK inhibitor promoted AM966-reduced TEER in a dose-dependent manner (Figures 5(e) and 5(f)). This data suggests that FAK is not the kinase that induces tyrosine phosphorylation of VE-cadherin in response to AM966 stimulation in HLMVECs.

4. Discussion

IPF is a chronic and progressive lung disorder, which may result from abnormal lung repair and remodeling [19]. LPA/LPA1-mediated fibroblast proliferation and migration

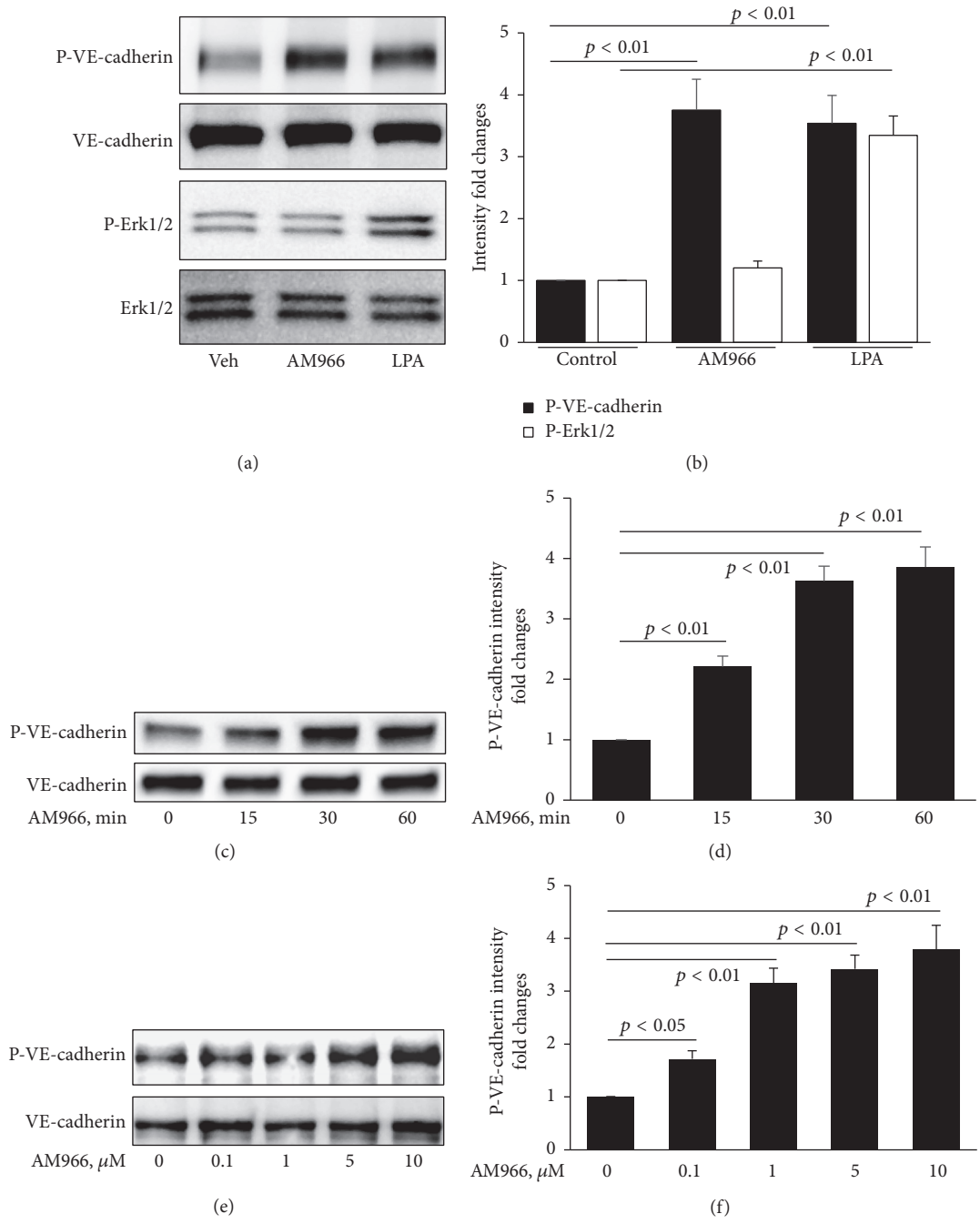

Figure 3: AM966 induces phosphorylation of VE-cadherin. (a) Confluent HLMVECs were treated with AM966 (1.0 μM) or LPA (5.0 μM) for 30 min after 3 h starvation. Cell lysates were immunoblotted with phospho-VE-cadherin (P-VE-cadherin), total VE-cadherin, phospho-Erk1/2 (P-Erk1/2), and total Erk1/2 antibodies. (b) Analysis of P-VE-cadherin and P-Erk1/2 by densitometry of the results in (a) was performed by Image J software ($n = 3$), and statistical analysis was shown. (c) Confluent HLMVECs were treated with AM966 (1.0 μM) for indicated time after 3 h starvation. Cell lysates were immunoblotted with P-VE-cadherin and total VE-cadherin antibodies. (d) Analysis of P-VE-cadherin by densitometry of the results in (c) was performed by Image J software ($n = 3$), and statistical analysis was shown. (e) Confluent HLMVECs were treated with AM966 (0 to 10.0 μM) for 30 min after 3 h starvation. Cell lysates were immunoblotted with P-VE-cadherin and total VE-cadherin antibodies. (f) Analysis of P-VE-cadherin by densitometry of the results in (e) was performed by Image J software ($n = 3$), and statistical analysis was shown. Shown are representative blots from three independent experiments.

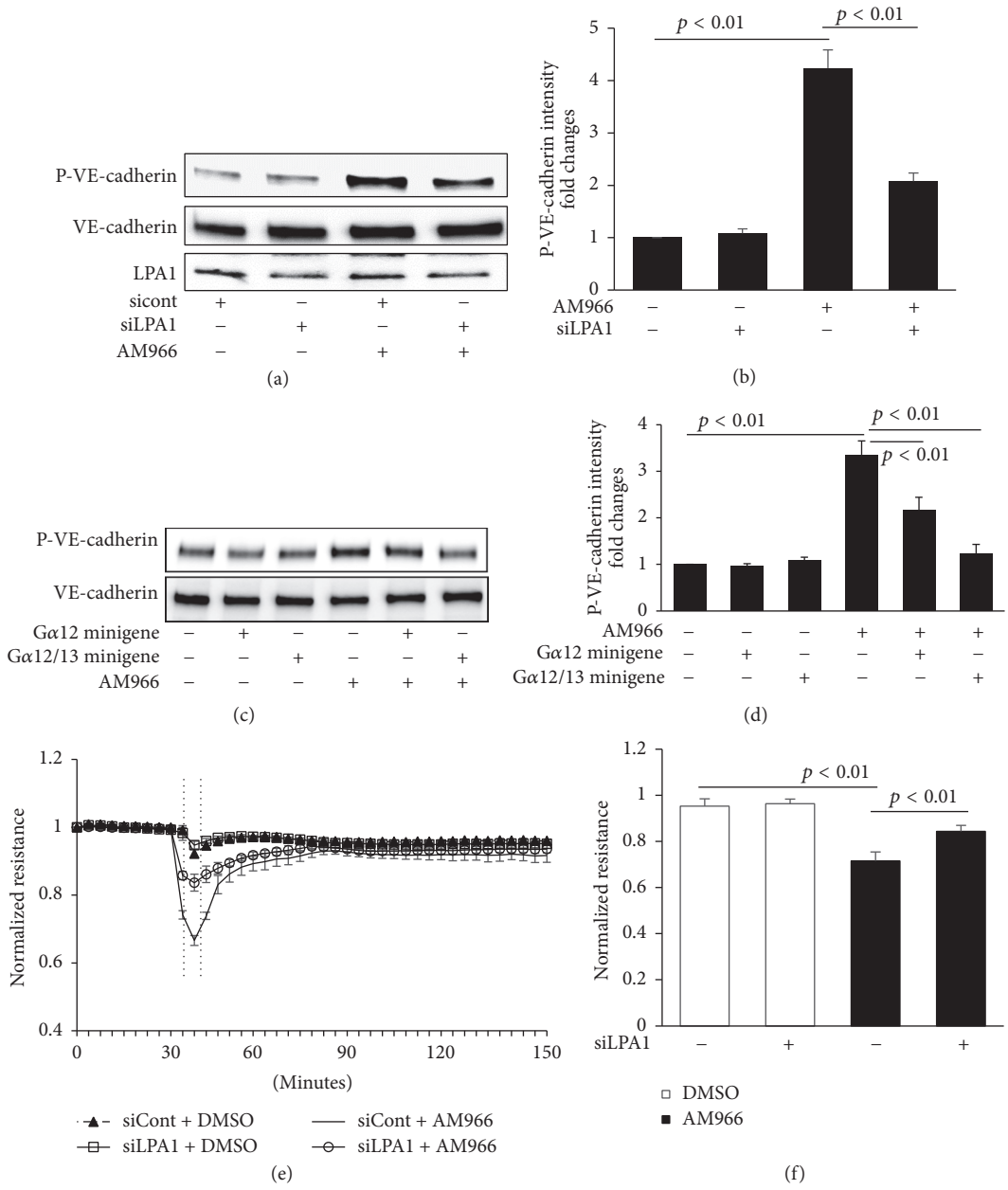

Figure 4: LPA1 is required for AM966-induced phosphorylation of VE-cadherin. (a) HLMVECs (~70% confluent) were transfected with LPA1 siRNA (siLPA1) or control (sicont) for 72 h, and then cells were treated with AM966 (1.0 μM) for 30 min. Cell lysates were immunoblotted with P-VE-cadherin, total VE-cadherin, and LPA1 antibodies. (b) Analysis of P-VE-cadherin by densitometry of the results in (a) was performed by Image J software ($n = 3$), and statistical analysis was shown. (c) HLMVECs (~70% confluent) were transfected with minigenes encoding Gα12 or Gα13 peptide for 24 h, and then cells were treated with AM966 (1.0 μM) for 30 min. Cell lysates were immunoblotted with P-VE-cadherin and total VE-cadherin antibodies. (d) Analysis of P-VE-cadherin by densitometry of the results in (c) was performed by Image J software ($n = 3$), and statistical analysis was shown. Shown are representative blots from three independent experiments. (e) HLMVECs (~70% confluent) transfected with LPA1 siRNA (siLPA1) or control (sicont) were plated on gold microelectrodes and then cells were treated with AM966 (1.0 μM) or DMSO. The TEER tracing represents pooled data (±SEM) from 3 independent experiments. (f) The resistance in response to AM966 treatments during indicated time period (e) was quantified and statistical analysis was performed.

are implicated in the pathogenesis of IPF; thus, targeting LPA1 pathway is a new potential therapeutic strategy to treat IPF. AM966 is a highly selective oral LPA1 antagonist exhibiting an antifibrotic property [12]. However, the biological effects of AM966 have not been investigated. Maintenance of pulmonary endothelial barrier integrity is of great importance for reducing severity of lung injury. The current study demonstrates that AM966 induces lung

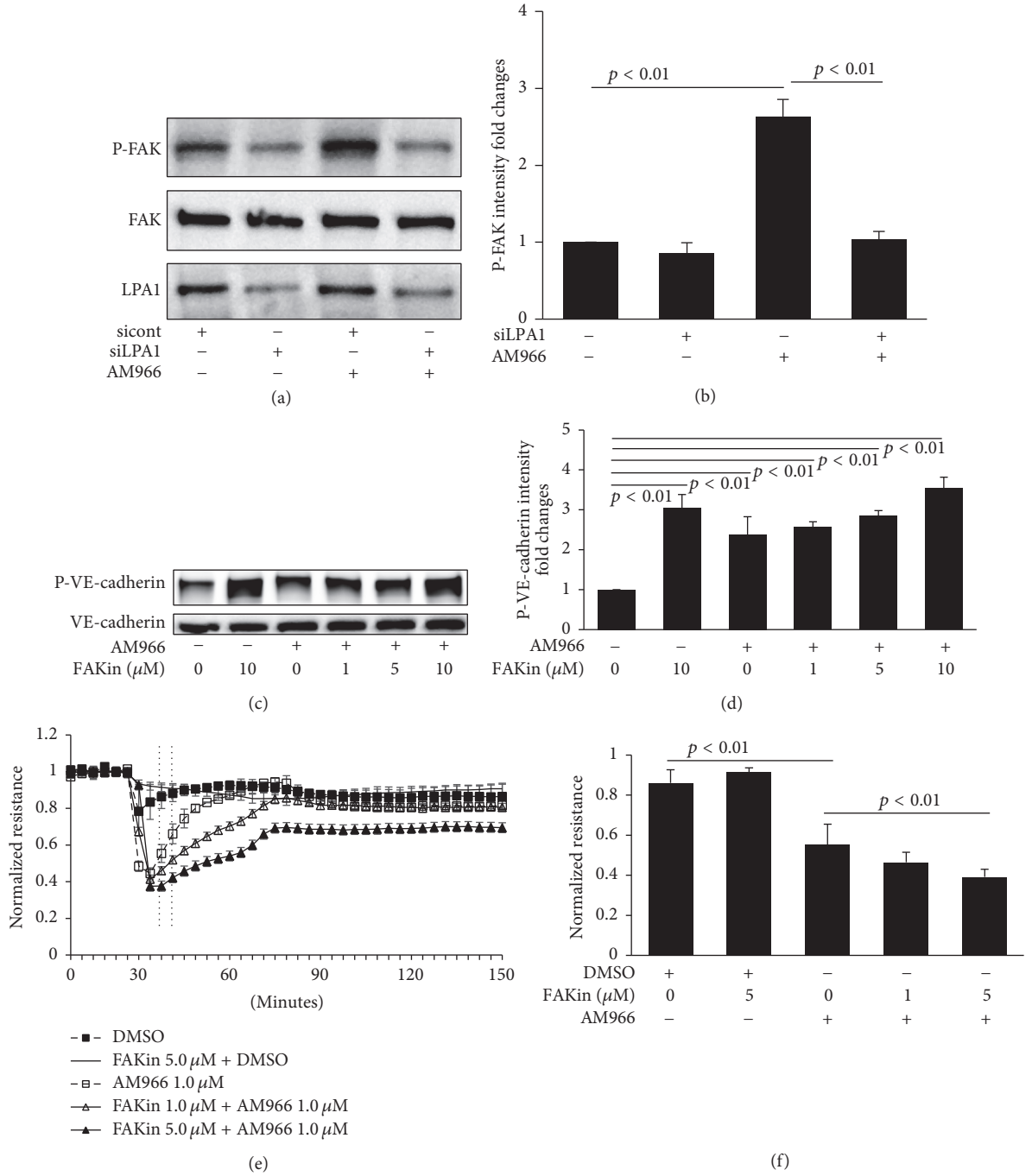

Figure 5: AM966-induced phosphorylation of VE-cadherin is not FAK-dependent. (a) HLMVECs (~70% confluent) transfected with siLPA1 or sicont were treated with AM966 (1.0 μM) or DMSO for 30 min. Cell lysates were immunoblotted with phosphospecific FAK (P-FAK), total FAK, and LPA1 antibodies. (b) Analysis of P-FAK by densitometry of the results in (a) was performed by Image J software ($n = 3$), and statistical analysis was shown. (c) Confluent HLMVECs were pretreated with FAK kinase inhibitor (0 to 10.0 μM) for 1 h, and then cells were treated with DMSO or AM966 (1.0 μM) for an additional 30 min. Cell lysates were immunoblotted with P-VE-cadherin and total VE-cadherin antibodies. (d) Analysis of P-VE-cadherin by densitometry of the results in (c) was performed by Image J software ($n = 3$), and statistical analysis was shown. Shown are representative blots from three independent experiments. (e) Confluent HLMVECs were plated on gold microelectrodes and pretreated with FAK inhibitor (1.0 or 5.0 μM) for 1 h and then stimulated by 1.0 μM AM966 or DMSO. The TEER tracing represents pooled data (±SEM) from 3 independent experiments. (f) The resistance in response to AM966 treatments during indicated time period (e) was quantified and statistical analysis was performed.

microvascular endothelial barrier disruption in vitro through modulation of VE-cadherin phosphorylation and cytoskeletal rearrangement. These effects are mediated by LPA1. This study is the first to reveal that AM966 may exhibit endothelial barrier disruption properties.

Controversial results regarding the effects of LPA on endothelial barrier integrity have been reported during the past two decades. Decreased endothelial permeability by platelet-derived LPA was first observed by Alexander et al. [28]. Further, albumin-bound LPA was found to form an active complex that increases electoral resistance across endothelial cells [36]. The effect of LPA on reduction monolayer permeability was also observed in Schlemm's canal cells [37] and in the late angiogenesis [27]. However, more recent studies demonstrated increased vascular leakage after LPA exposure [18, 38, 39], and LPA1 regulates the phenotype [39–41]. Deregulation of adherens and tight junctions [29, 42, 43], calcium release [44], and Rho-mediated cytoskeletal rearrangement [25, 30, 45, 46] contribute to LPA-induced endothelial barrier disruption. In our study, we provide evidence to show not only LPA but also LPA1 antagonist, AM966, increases permeability immediately and reversibly.

A previous study has shown that when giving 10 mg/kg of AM966 orally to nonfasted mice, plasma AM966 reached a peak concentration of 9 μM within 1 h [12], which indicates that the AM966 in our experiments were in the biological range. However, the study shows that oral administration of AM966 protects lung vascular leak after 7 days of bleomycin challenge [12]. This controversial conclusion may be due to species specificity. Pan et al. have shown that molecular regulation of gene expression of p-selection, an adhesion receptor, is different from mouse and human endothelial cells [47].

Accumulating findings have shown that, with thrombin, TNF-α, or endothelial growth factor (VEGF) treatments, stress fibers composed of actin and myosin play an important role in cell contraction and breaking down of the adherens junctions [48–50]. MLC is the light chain of myosin, and phosphorylation of MLC at either T18 or S19 is required for its interaction with actin [23]. Activation of RhoA/Rho kinase is considered to have a crucial role in the control of MLC phosphorylation and cytoskeletal rearrangements [22, 24, 46, 51–53]. LPA has been shown to activate RhoA/Rho kinase pathway in various cell types [25, 51, 54]. Our data indicate that an AM966-LPA1-RhoA/Rho kinase-MLC signaling pathway leads to cell contraction and adherens junctions disruption (Figure 6).

VE-cadherin is a fundamental component of adherens junctions in endothelium. By interacting with α-catenin, β-catenin, and p120, VE-cadherin links actin indirectly [20, 21]. Tyrosine phosphorylation of VE-cadherin increases vascular permeability [20]. There are nine tyrosine phosphorylation sites of VE-cadherin which may be phosphorylated in response to different stimuli [55]. VE-cadherin phosphorylation at Y685 is mediated by Src kinase, resulting in endothelial cell migration or hyperpermeability [56, 57], while phosphorylation at Y731 regulates the induction of leukocyte extravasation [58]. In our present study, phosphorylation of VE-cadherin at Y658 induced by AM966 leads to lung endothelial barrier dysfunction, consistent with several other

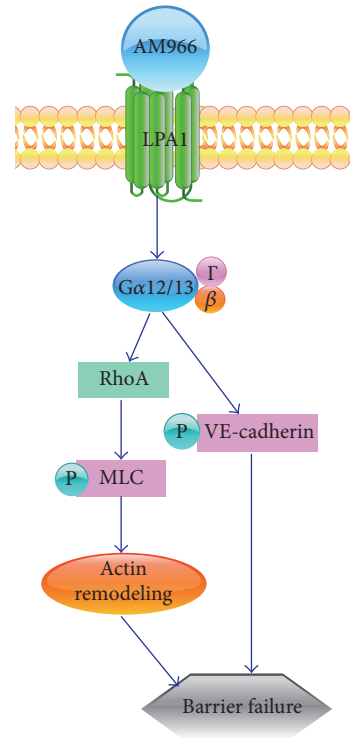

Figure 6: AM966 reduces pulmonary microvascular cell barrier integrity through LPA1/Gα12/13-mediated phosphorylation of MLC and VE-cadherin. AM966 is ligated to LPA1 and triggers RhoA/Rho kinase pathway, thereby increasing MLC phosphorylation and cytoskeletal rearrangement. AM966 induces phosphorylation of VE-cadherin. Therefore, AM966 increases lung endothelial permeability.

studies where VEGF, polychlorinated biphenyl, and silver nanoparticles are the agonists [49, 59, 60]. LPA has been reported to increase permeability by regulating Gαi/NF-kB signaling [61]. Here we show that this AM966-induced phosphorylation at Y658 is through the LPA1-Gα12/13 pathway. FAK is a tyrosine kinase that plays different roles in barrier regulation. For example, FAK contributes to VEGF-induced barrier dysfunction [62, 63], while it has been also reported that downregulation of FAK protects barrier integrity [64]. In our study, though phospho-FAK is upregulated in response to AM966 stimulation, FAK kinase inhibitor did not reduce the level of VE-cadherin phosphorylation. In addition, FAK kinase inhibitor treatment enhances AM966-induced barrier disruption. The molecular mechanism by which AM966 induces phosphorylation of VE-cadherin is our focus in future studies.

AM966 has been known to bind to LPA1; however, the signaling pathway triggered by AM966 has not been revealed. This study is the first report to reveal that AM966 binds to LPA1 and triggers RhoA/Rho kinase-MLC and VE-cadherin phosphorylation pathways. This study indicates that LPA1 agonist and antagonist share LPA1/Gα12/13 pathway regarding regulation of phosphorylation of MLC and VE-cadherin, while AM966 has no effect of activation of Gαi-coupled LPA1 pathway.

5. Conclusion

In conclusion, our study, for the first time, shows an unexpected effect of AM966 on lung microvascular barrier disruption and underlying molecular mechanisms which are regulated through RhoA/Rho kinase/MLC and VE-cadherin (Figure 6). This is overlaps with LPA activity. Future study will be performed to examine the effect of AM966 and its related compounds on endothelial barrier integrity in preclinical murine models of human diseases.

Competing Interests

All authors declare no conflict of interests.

Acknowledgments

This work was supported by the National Institutes of Health (R01GM115389 to Jing Zhao) and American Lung Association Biomedical Research Grant RG350146 (Jing Zhao).

References

[1] J.-P. Pradère, J. Klein, S. Grès et al., "LPA1 receptor activation promotes renal interstitial fibrosis," *Journal of the American Society of Nephrology*, vol. 18, no. 12, pp. 3110–3118, 2007.

[2] A. M. Tager, P. LaCamera, B. S. Shea et al., "The lysophosphatidic acid receptor LPA1 links pulmonary fibrosis to lung injury by mediating fibroblast recruitment and vascular leak," *Nature Medicine*, vol. 14, no. 1, pp. 45–54, 2008.

[3] H. Ikeda and Y. Yatomi, "Autotaxin in liver fibrosis," *Clinica Chimica Acta*, vol. 413, no. 23, pp. 1817–1821, 2012.

[4] E. J. van Corven, A. Groenink, K. Jalink, T. Eichholtz, and W. H. Moolenaar, "Lysophosphatidate-induced cell proliferation: identification and dissection of signaling pathways mediated by G proteins," *Cell*, vol. 59, no. 1, pp. 45–54, 1989.

[5] J. J. A. Contos, I. Ishii, and J. Chun, "Lysophosphatidic acid receptors," *Molecular Pharmacology*, vol. 58, no. 6, pp. 1188–1196, 2000.

[6] Y. Zhao and V. Natarajan, "Lysophosphatidic acid (LPA) and its receptors: role in airway inflammation and remodeling," *Biochimica et Biophysica Acta - Molecular and Cell Biology of Lipids*, vol. 1831, no. 1, pp. 86–92, 2013.

[7] M. Alemayehu, M. Dragan, C. Pape et al., "β-Arrestin2 regulates lysophosphatidic acid-induced human breast tumor cell migration and invasion via Rap1 and IQGAP1," *PLoS ONE*, vol. 8, no. 2, Article ID e56174, 2013.

[8] M. C. Olianas, S. Dedoni, and P. Onali, "Antidepressants activate the lysophosphatidic acid receptor LPA_1 to induce insulin-like growth factor-I receptor transactivation, stimulation of ERK1/2 signaling and cell proliferation in CHO-K1 fibroblasts," *Biochemical Pharmacology*, vol. 95, no. 4, pp. 311–323, 2015.

[9] L. Gan, J.-X. Xue, X. Li et al., "Blockade of lysophosphatidic acid receptors LPAR1/3 ameliorates lung fibrosis induced by irradiation," *Biochemical and Biophysical Research Communications*, vol. 409, no. 1, pp. 7–13, 2011.

[10] N. Oikonomou, M.-A. Mouratis, A. Tzouvelekis et al., "Pulmonary autotaxin expression contributes to the pathogenesis of pulmonary fibrosis," *American Journal of Respiratory Cell and Molecular Biology*, vol. 47, no. 5, pp. 566–574, 2012.

[11] D.-S. Im, "First-in-class antifibrotic therapy targeting type 1 lysophosphatidic acid receptor," *Archives of Pharmacal Research*, vol. 35, no. 6, pp. 945–948, 2012.

[12] J. S. Swaney, C. Chapman, L. D. Correa et al., "A novel, orally active LPA1 receptor antagonist inhibits lung fibrosis in the mouse bleomycin model," *British Journal of Pharmacology*, vol. 160, no. 7, pp. 1699–1713, 2010.

[13] A. L. Parrill, "Design of anticancer lysophosphatidic acid agonists and antagonists," *Future Medicinal Chemistry*, vol. 6, no. 8, pp. 871–883, 2014.

[14] C. B. Nanthakumar, R. J. D. Hatley, S. Lemma, J. Gauldie, R. P. Marshall, and S. J. F. Macdonald, "Dissecting fibrosis: therapeutic insights from the small-molecule toolbox," *Nature Reviews Drug Discovery*, vol. 14, no. 10, pp. 693–720, 2015.

[15] Y. Takuwa, H. Ikeda, Y. Okamoto, N. Takuwa, and K. Yoshioka, "Sphingosine-1-phosphate as a mediator involved in development of fibrotic diseases," *Biochimica et Biophysica Acta—Molecular and Cell Biology of Lipids*, vol. 1831, no. 1, pp. 185–192, 2013.

[16] C. Director and F. Squibb, "Safety and Efficacy of A Lysophosphatidic Acid Receptor Antagonist (BMS 986020) in Idiopathic Pulmonary Fibrosis," Pulmonary Fibrosis Foundation Summit, 2013.

[17] Y. Kihara, H. Mizuno, and J. Chun, "Lysophospholipid receptors in drug discovery," *Experimental Cell Research*, vol. 333, no. 2, pp. 171–177, 2015.

[18] Y. Ren, L. Guo, X. Tang et al., "Comparing the differential effects of LPA on the barrier function of human pulmonary endothelial cells," *Microvascular Research*, vol. 85, no. 1, pp. 59–67, 2013.

[19] R. M. Strieter and B. Mehrad, "New mechanisms of pulmonary fibrosis," *Chest*, vol. 136, no. 5, pp. 1364–1370, 2009.

[20] E. Dejana, F. Orsenigo, and M. G. Lampugnani, "The role of adherens junctions and VE-cadherin in the control of vascular permeability," *Journal of Cell Science*, vol. 121, no. 13, pp. 2115–2122, 2008.

[21] J. Gavard, "Endothelial permeability and VE-cadherin: a wacky comradeship," *Cell Adhesion and Migration*, vol. 8, no. 2, pp. 158–164, 2014.

[22] R. R. Rigor, Q. Shen, C. D. Pivetti, M. H. Wu, and S. Y. Yuan, "Myosin light chain kinase signaling in endothelial barrier dysfunction," *Medicinal Research Reviews*, vol. 33, no. 5, pp. 911–933, 2013.

[23] M. Hirano and K. Hirano, "Myosin di-phosphorylation and peripheral actin bundle formation as initial events during endothelial barrier disruption," *Scientific Reports*, vol. 6, Article ID 20989, 2016.

[24] T. Mizutani, K. Kawabata, Y. Koyama, M. Takahashi, and H. Haga, "Regulation of cellular contractile force in response to mechanical stretch by diphosphorylation of myosin regulatory light chain via RhoA signaling cascade," *Cell Motility and the Cytoskeleton*, vol. 66, no. 7, pp. 389–397, 2009.

[25] G. P. van Nieuw Amerongen, M. A. Vermeer, and V. W. van Hinsbergh, "Role of RhoA and Rho kinase in lysophosphatidic acid-induced endothelial barrier dysfunction," *Arteriosclerosis, Thrombosis, and Vascular Biology*, vol. 20, no. 12, pp. E127–E133, 2000.

[26] D. He, Y. Su, P. V. Usatyuk et al., "Lysophosphatidic acid enhances pulmonary epithelial barrier integrity and protects endotoxin-induced epithelial barrierdisruption and lung injury," *Journal of Biological Chemistry*, vol. 284, no. 36, pp. 24123–24132, 2009.

[27] D. English, A. T. Kovala, Z. Welch et al., "Induction of endothelial cell chemotaxis by sphingosine 1-phosphate and stabilization of endothelial monolayer barrier function by lysophosphatidic acid, potential mediators of hematopoietic angiogenesis," *Journal of Hematotherapy and Stem Cell Research*, vol. 8, no. 6, pp. 627–634, 1999.

[28] J. S. Alexander, W. F. Patton, B. W. Christman, L. L. Cuiper, and F. R. Haselton, "Platelet-derived lysophosphatidic acid decreases endothelial permeability in vitro," *American Journal of Physiology - Heart and Circulatory Physiology*, vol. 274, no. 1, pp. H115–H122, 1998.

[29] C. Schulze, C. Smales, L. L. Rubin, and J. M. Staddon, "Lysophosphatidic acid increases tight junction permeability in cultured brain endothelial cells," *Journal of Neurochemistry*, vol. 68, no. 3, pp. 991–1000, 1997.

[30] Y. Yu, J. Qin, M. Liu, Q. Ruan, Y. Li, and Z. Zhang, "Role of Rho kinase in lysophosphatidic acid-induced altering of blood-brain barrier permeability," *International Journal of Molecular Medicine*, vol. 33, no. 3, pp. 661–669, 2014.

[31] N. H. On, S. Savant, M. Toews, and D. W. Miller, "Rapid and reversible enhancement of blood-brain barrier permeability using lysophosphatidic acid," *Journal of Cerebral Blood Flow and Metabolism*, vol. 33, no. 12, pp. 1944–1954, 2013.

[32] J. J. A. Contos, N. Fukushima, J. A. Weiner, D. Kaushal, and J. Chun, "Requirement for the lp(A1) lysophosphatidic acid receptor gene in normal suckling behavior," *Proceedings of the National Academy of Sciences of the United States of America*, vol. 97, no. 24, pp. 13384–13389, 2000.

[33] L. Wang, R. Cummings, Y. Zhao et al., "Involvement of phospholipase D2 in lysophosphatidate-induced transactivation of platelet-derived growth factor receptor-β in human bronchial epithelial cells," *Journal of Biological Chemistry*, vol. 278, no. 41, pp. 39931–39940, 2003.

[34] P. Callihan, M. W. Ali, H. Salazar et al., "Convergent regulation of neuronal differentiation and Erk and Akt Kinases in Human Neural Progenitor Cells by lysophosphatidic acid, sphingosine 1-phosphate, and LIF: specific roles for the LPA1 receptor," *ASN Neuro*, vol. 6, no. 6, 2015.

[35] C. Jean, X. L. Chen, J.-O. Nam et al., "Inhibition of endothelial FAK activity prevents tumor metastasis by enhancing barrier function," *Journal of Cell Biology*, vol. 204, no. 2, pp. 247–263, 2014.

[36] F. L. Minnear, S. Patil, D. Bell, J. P. Gainor, and C. A. Morton, "Platelet lipid(s) bound to albumin increases endothelial electrical resistance: mimicked by LPA," *American Journal of Physiology—Lung Cellular and Molecular Physiology*, vol. 281, no. 6, pp. L1337–L1344, 2001.

[37] J. Kumar and D. L. Epstein, "Rho GTPase-mediated cytoskeletal organization in Schlemm's canal cells play a critical role in the regulation of aqueous humor outflow facility," *Journal of Cellular Biochemistry*, vol. 112, no. 2, pp. 600–606, 2011.

[38] N. A. Neidlinger, S. K. Larkin, A. Bhagat, G. P. Victorino, and F. A. Kuypers, "Hydrolysis of phosphatidylserine-exposing red blood cells by secretory phospholipase A2 generates lysophosphatidic acid and results in vascular dysfunction," *Journal of Biological Chemistry*, vol. 281, no. 2, pp. 775–781, 2006.

[39] M. Panchatcharam, A. K. Salous, J. Brandon et al., "Mice with targeted inactivation of Ppap2b in endothelial and hematopoietic cells display enhanced vascular inflammation and permeability," *Arteriosclerosis, Thrombosis, and Vascular Biology*, vol. 34, no. 4, pp. 837–845, 2014.

[40] S.-U. Chen, C.-H. Chou, K.-H. Chao et al., "Lysophosphatidic acid up-regulates expression of growth-regulated oncogene-α, interleukin-8, and monocyte chemoattractant protein-1 in human first-trimester trophoblasts: possible roles in angiogenesis and immune regulation," *Endocrinology*, vol. 151, no. 1, pp. 369–379, 2010.

[41] S.-U. Chen, H. Lee, D.-Y. Chang et al., "Lysophosphatidic acid mediates interleukin-8 expression in human endometrial stromal cells through its receptor and nuclear factor-κB- dependent pathway: a possible role in angiogenesis of endometrium and placenta," *Endocrinology*, vol. 149, no. 11, pp. 5888–5896, 2008.

[42] Z. Sun, M. Worden, J. A. Thliveris et al., "Biodistribution of negatively charged iron oxide nanoparticles (IONPs) in mice and enhanced brain delivery using lysophosphatidic acid (LPA)," *Nanomedicine: Nanotechnology, Biology, and Medicine*, vol. 12, no. 7, pp. 1775–1784, 2016.

[43] T. Hirase, S. Kawashima, E. Y. M. Wong et al., "Regulation of tight junction permeability and occludin phosphorylation by RhoA-p160ROCK-dependent and -independent mechanisms," *Journal of Biological Chemistry*, vol. 276, no. 13, pp. 10423–10431, 2001.

[44] M. H. Sarker, D.-E. Hu, and P. A. Fraser, "Regulation of cerebromicrovascular permeability by lysophosphatidic acid," *Microcirculation*, vol. 17, no. 1, pp. 39–46, 2010.

[45] V. Vouret-Craviari, P. Boquet, J. Pouysségur, and E. Van Obberghen-Schilling, "Regulation of the actin cytoskeleton by thrombin in human endothelial cells: role of Rho proteins in endothelial barrier function," *Molecular Biology of the Cell*, vol. 9, no. 9, pp. 2639–2653, 1998.

[46] B. Wojciak-Stothard and A. J. Ridley, "Rho GTPases and the regulation of endothelial permeability," *Vascular Pharmacology*, vol. 39, no. 4-5, pp. 187–199, 2002.

[47] J. Pan, L. Xia, and R. P. McEver, "Comparison of promoters for the murine and human P-selectin genes suggests species-specific and conserved mechanisms for transcriptional regulation in endothelial cells," *The Journal of Biological Chemistry*, vol. 273, no. 16, pp. 10058–10067, 1998.

[48] I. Petrache, A. D. Verin, M. T. Crow, A. Birukova, F. Liu, and J. G. N. Garcia, "Differential effect of MLC kinase in TNF-α-induced endothelial cell apoptosis and barrier dysfunction," *American Journal of Physiology—Lung Cellular and Molecular Physiology*, vol. 280, no. 6, pp. L1168–L1178, 2001.

[49] E. Monaghan-Benson and K. Burridge, "The regulation of vascular endothelial growth factor-induced microvascular permeability requires Rac and reactive oxygen species," *Journal of Biological Chemistry*, vol. 284, no. 38, pp. 25602–25611, 2009.

[50] H. Schnittler, M. Taha, M. O. Schnittler, A. A. Taha, N. Lindemann, and J. Seebach, "Actin filament dynamics and endothelial cell junctions: the Ying and Yang between stabilization and motion," *Cell and Tissue Research*, vol. 355, no. 3, pp. 529–543, 2014.

[51] O. Kranenburg, M. Poland, F. P. G. Van Horck, D. Drechsel, A. Hall, and W. H. Moolenaar, "Activation of RhoA by lysophosphatidic acid and Gα(12/13) subunits in neuronal cells: induction of neurite retraction," *Molecular Biology of the Cell*, vol. 10, no. 6, pp. 1851–1857, 1999.

[52] D. J. Hartshorne, M. Ito, and F. Erdödi, "Myosin light chain phosphatase: subunit composition, interactions and regulation," *Journal of Muscle Research and Cell Motility*, vol. 19, no. 4, pp. 325–341, 1998.

[53] J. Bang, M. Jang, J. H. Huh et al., "Deficiency of the 15-kDa selenoprotein led to cytoskeleton remodeling and non-apoptotic membrane blebbing through a RhoA/ROCK pathway," *Biochemical and Biophysical Research Communications*, vol. 456, no. 4, pp. 884–890, 2015.

[54] M. Mori and H. Tsushima, "Activation of Rho signaling contributes to lysophosphatidic acid-induced contraction of intact ileal smooth muscle of guinea-pig," *Canadian Journal of Physiology and Pharmacology*, vol. 78, no. 9, pp. 729–736, 2000.

[55] Y. Wallez, I. Vilgrain, and P. Huber, "Angiogenesis: the VE-cadherin switch," *Trends in Cardiovascular Medicine*, vol. 16, no. 2, pp. 55–59, 2006.

[56] A. Benn, C. Bredow, I. Casanova, S. Vukičević, and P. Knaus, "VE-cadherin facilitates BMP-induced endothelial cell permeability and signaling," *Journal of Cell Science*, vol. 129, no. 1, pp. 206–218, 2016.

[57] A. Sidibé, H. Polena, K. Pernet-Gallay et al., "VE-cadherin Y685F knock-in mouse is sensitive to vascular permeability in recurrent angiogenic organs," *American Journal of Physiology—Heart and Circulatory Physiology*, vol. 307, no. 3, pp. H455–H463, 2014.

[58] F. Wessel, M. Winderlich, M. Holm et al., "Leukocyte extravasation and vascular permeability are each controlled in vivo by different tyrosine residues of VE-cadherin," *Nature Immunology*, vol. 15, no. 3, pp. 223–230, 2014.

[59] X. Sun, J. Shi, X. Zou, C. Wang, Y. Yang, and H. Zhang, "Silver nanoparticles interact with the cell membrane and increase endothelial permeability by promoting VE-cadherin internalization," *Journal of Hazardous Materials*, vol. 317, pp. 570–578, 2016.

[60] P. Zhang, S. Feng, H. Bai et al., "Polychlorinated biphenyl quinone induces endothelial barrier dysregulation by setting the cross talk between VE-cadherin, focal adhesion, and MAPK signaling," *American Journal of Physiology—Heart and Circulatory Physiology*, vol. 308, no. 10, pp. H1205–H1214, 2015.

[61] Y.-W. Chuang, W.-M. Chang, K.-H. Chen, C.-Z. Hong, P.-J. Chang, and H.-C. Hsu, "Lysophosphatidic acid enhanced the angiogenic capability of human chondrocytes by regulating Gi/NF-kB-dependent angiogenic factor expression," *PLoS ONE*, vol. 9, no. 5, Article ID e95180, 2014.

[62] X. Chen, J.-O. Nam, C. Jean et al., "VEGF-Induced Vascular Permeability Is Mediated by FAK," *Developmental Cell*, vol. 22, no. 1, pp. 146–157, 2012.

[63] M. H. Wu, M. Guo, S. Y. Yuan, and H. J. Granger, "Focal adhesion kinase mediates porcine venular hyperpermeability elicited by vascular endothelial growth factor," *Journal of Physiology*, vol. 552, no. 3, pp. 691–699, 2003.

[64] M. Holinstat, N. Knezevic, M. Broman, A. M. Samarel, A. B. Malik, and D. Mehta, "Suppression of RhoA activity by focal adhesion kinase-induced activation of p190RhoGAP: role in regulation of endothelial permeability," *Journal of Biological Chemistry*, vol. 281, no. 4, pp. 2296–2305, 2006.

Hindawi Publishing Corporation
Mediators of Inflammation
Volume 2017, Article ID 3415380, 15 pages
http://dx.doi.org/10.1155/2017/3415380

Research Article

Inhibition of Murine Pulmonary Microvascular Endothelial Cell Apoptosis Promotes Recovery of Barrier Function under Septic Conditions

Lefeng Wang,[1,2] Sanjay Mehta,[1,2,3] Michael Brock,[1,4] and Sean E. Gill[1,2,3,4]

[1]*Centre for Critical Illness Research, Lawson Health Research Institute, London, ON, Canada*
[2]*Department of Medicine, Schulich School of Medicine and Dentistry, Western University, London, ON, Canada*
[3]*Division of Respirology, Schulich School of Medicine and Dentistry, Western University, London, ON, Canada*
[4]*Department of Physiology and Pharmacology, Schulich School of Medicine and Dentistry, Western University, London, ON, Canada*

Correspondence should be addressed to Sean E. Gill; sgill8@uwo.ca

Received 19 August 2016; Revised 25 October 2016; Accepted 20 December 2016; Published 30 January 2017

Academic Editor: Yutong Zhao

Sepsis is characterized by injury of the pulmonary microvasculature and the pulmonary microvascular endothelial cells (PMVEC), leading to barrier dysfunction and acute respiratory distress syndrome (ARDS). Our recent work identified a strong correlation between PMVEC apoptosis and microvascular leak in septic mice in vivo, but the specific role of apoptosis in septic PMVEC barrier dysfunction remains unclear. Thus, we hypothesize that *PMVEC apoptosis is likely required for PMVEC barrier dysfunction under septic conditions in vitro*. Septic stimulation (mixture of tumour necrosis factor α, interleukin 1β, and interferon γ [cytomix]) of isolated *murine* PMVEC resulted in a significant loss of barrier function as early as 4 h after stimulation, which persisted until 24 h. PMVEC apoptosis, as reflected by caspase activation, DNA fragmentation, and loss of membrane polarity, was first apparent at 8 h after cytomix. Pretreatment of PMVEC with the pan-caspase inhibitor Q-VD significantly decreased septic PMVEC apoptosis and was associated with reestablishment of PMVEC barrier function at 16 and 24 h after stimulation but had no effect on septic PMVEC barrier dysfunction over the first 8 h. Collectively, our data suggest that early septic murine PMVEC barrier dysfunction driven by proinflammatory cytokines is not mediated through apoptosis, but PMVEC apoptosis contributes to late septic PMVEC barrier dysfunction.

1. Introduction

Acute respiratory distress syndrome (ARDS), which has a 30–40% mortality rate, is characterized by severe pulmonary inflammation and high-permeability, proteinaceous edema [1, 2]. Sepsis is the most common cause of ARDS [1, 3–5]. Septic organ dysfunction, including the lung injury present in ARDS, is due in large part to systemic inflammation leading to dysfunction of the microvasculature, especially the microvascular endothelial cells (MVEC) [5–9]. Microvascular dysfunction is characterized by impaired barrier function (increased permeability leading to extravascular leak of protein-rich edema) and neutrophil (PMN) influx into organs [10–14], microvascular thrombosis [15, 16], and impaired distribution of blood flow in microvascular beds [17]. Microvascular dysfunction is clinically important, as it has been documented early in the course of sepsis in humans, and is associated with increased mortality [7, 8], especially if it persists over time [9].

Pulmonary microvascular dysfunction in sepsis and ARDS is principally due to activation, injury, and dysfunction of pulmonary MVEC (PMVEC). Multiple mechanisms promote septic PMVEC dysfunction, including activation by cytokines, mechanical interaction with activated leukocytes, and exposure to harmful leukocyte-derived molecules, such as oxidants (including nitric oxide). These factors result in PMVEC abnormalities, including disruption of inter-PMVEC junctions and cytoskeleton-driven retraction [2, 5, 10–12, 18–21]. Recently, we identified a correlation between PMVEC apoptosis in vivo and increased pulmonary microvascular permeability following cecal ligation

and perforation- (CLP-) induced sepsis in mice [22, 23]. Furthermore, we demonstrated that systemic administration of Q-VD, a synthetic inhibitor of caspases, decreased septic PMVEC apoptosis, which was associated with reduced septic pulmonary microvascular permeability [23].

Apoptosis is a highly regulated, energy-dependent, enzymatic process of cell death, important in development and tissue homeostasis, but is also activated under inflammatory/pathologic conditions, such as sepsis. Apoptotic cell death is characterized by activation of cysteine proteases known as caspases, a loss of cell membrane polarization, and fragmentation of the DNA leading to condensed nuclei [24, 25]. Initiation of apoptosis is regulated by multiple pathways, which culminate in final common effector caspase activation. One of these, the extrinsic (or receptor-mediated) pathway depends on signalling by members of the tumour necrosis factor (TNF) cytokine family (i.e., TNFα) suggesting that stimulation of PMVEC with a combination of proinflammatory cytokines (e.g., mixture of TNFα, interleukin [IL] 1β, and interferon [IFN] γ) may lead to PMVEC apoptosis [24, 26]. However, while some studies support the ability of proinflammatory cytokines (i.e., TNFα) to induce endothelial cell (EC) apoptosis, these cytokines do not consistently induce apoptosis, depending on particular EC type and method of assessment of both EC barrier function and apoptosis (Table 1) [27–42]. Further, it has not been clearly established whether PMVEC apoptosis is a driving factor in early and late septic EC barrier dysfunction or whether apoptosis has a role in recovery from septic injury and repair of the microvascular permeability barrier. Specifically, previous studies, primarily in macrovascular EC such as human umbilical vein EC (HUVEC), suggest that septic EC barrier dysfunction may correlate with EC apoptosis; however, many of these studies do not clearly demonstrate that EC apoptosis causes barrier dysfunction (Table 1). Additionally, there is also evidence that EC leak can occur in the absence of EC apoptosis (Table 1). Our previous work, however, suggests PMVEC apoptosis as a critical mechanism for the loss of PMVEC barrier function in vivo [22, 23]. Thus, we hypothesize that PMVEC apoptosis is likely required for PMVEC barrier dysfunction under septic conditions in vitro. Furthermore, it is likely that PMVEC apoptosis also prevents reestablishment of normal PMVEC barrier function.

2. Methods

2.1. PMVEC Isolation. PMVEC were isolated from the lungs of C57Bl/6 mice, as previously described [10, 43]. In brief, lungs were isolated, finely minced, and then digested with collagenase before incubation with magnetic microbeads (Dynal Biotech Inc., Lake Success, NY) coupled to anti-CD31 (platelet endothelial cell adhesion molecule, PECAM) antibodies (BD Pharmingen, Franklin Lakes, NJ). Microbead-bound PMVEC were captured, washed, suspended in growth medium (Dulbecco's modified Eagle's medium [DMEM] with 20% Fetal Bovine Serum, 5 mM glucose, 4 mM L-Glutamine, 1 mM Sodium Pyruvate, and Phenol Red; Invitrogen, Carlsbad, CA), and then seeded in gelatin-coated cell-culture flasks. Once approximately 90% confluent, cells were stained with fluorescent acetylated-low density lipoprotein (LDL) (Biomedical Technologies, Stoughton, MA) and assessed by immunofluorescence or stained with antibodies against CD31, CD34, CD146, and CD202b conjugated to pacific blue, phycoerythrin, fluorescein isothiocyanate (FITC), or allophycocyanin, respectively (VWR Scientific Inc., Radnor, PA), and assessed by flow cytometry (easyCyte Guava 12HT; Millipore, Billerica, MA, USA). Collectively, these processes resulted in PMVEC isolates with 99% homogeneity, which were then cultured and used between passages 4 and 8.

2.2. Assessment of PMVEC Barrier Integrity. PMVEC barrier function was assessed in vitro by culturing 2.5×10^4 PMVEC on gelatin-coated 24-well cell-culture inserts (3.0 μm pore, VWR) in full DMEM medium as we have done previously [10, 43]. During growth, culture medium was changed every second day and PMVEC monolayer permeability was assessed every second day by measuring transendothelial electrical resistance (TEER; EVOM2 Endothelial Voltohmmeter; World Precision Instruments, Sarasota, FL). Individual PMVEC monolayer TEER was corrected for TEER across an empty insert. A fully intact basal PMVEC permeability barrier was accepted when TEER stabilized (±5%).

PMVEC monolayer permeability under basal/resting and septic conditions (cytomix: equimolar solution of TNFα, IL1β, and IFNγ used to mimic a septic response, 0.3–100 ng/mL, PeproTech, Rocky Hill, NJ) was assessed over a time course (2–24 h) using three techniques: (i) TEER (as above), (ii) FITC-labelled dextran flux (4 kDa), and (iii) EB-labelled albumin flux (67 kDa). The levels of trans-PMVEC macromolecular flux of the smaller molecular weight FITC-labelled dextran (4 kDa) or larger molecular weight EB-labelled albumin (67 kDa) from the upper chamber into the lower chamber of the cell-culture inserts were measured over exactly 60 mins as we have done previously [10, 43]. Briefly, both EB-labelled albumin (bovine serum albumin, 33.5 μg total in 250 μL; Sigma, Oakville, Ontario) and FITC-labelled dextran (125 μg total in 250 μL; Sigma) were added directly to the upper chamber of the cell-culture insert. After 1 h, inserts were removed and the conditioned media from the lower chamber collected. EB-labelled albumin flux was determined by measuring the absorbance of the conditioned medium (620 nm) and comparing to a standard curve of EB-labelled albumin (Victor3 multilabel microplate reader, PerkinElmer, Inc. Waltham, MA, USA). Trans-PMVEC FITC-labelled dextran flux was determined by collecting the lower chamber medium, measuring the fluorescence (excitation peak wavelength: 488 nm and emission peak wavelength: 525 nm), and comparing this to completely equilibrated FITC-dextran in both chambers of control wells (labelled 100%; Victor3 multilabel microplate reader).

Basal and septic PMVEC permeability was also assessed in the presence or absence of the broad-spectrum potent caspase inhibitors carbobenzoxy-valyl-alanyl-aspartyl-[O-methyl]-fluoromethylketone (z-VAD-FMK, 100 μM, BD Biosciences, Mississauga, ON) or quinoline-valyl-aspartyl(Ome)-CH2-O-phenoxy (Q-VD, 50 μM, APExBIO, Boston, MA) [45]. For these studies, inhibitors were administered simultaneously with the septic stimulus (cytomix).

Table 1: Review of literature on relationship of endothelial cell apoptosis and barrier dysfunction in vitro.

Citation	Species	EC type	EC identification method	Septic treatment	Markers of apoptosis	Measure of trans-EC leak	Leak-apoptosis relationship	Comments
Bannerman et al. 1998 [27]	Bovine	Commercial PAEC cell line	—	LPS	DNA laddering; TUNEL	14C-albumin	+/−	Similar time course of leak and apoptosis; apoptosis inhibition (zVAD) did not affect leak
Petrache et al. 2003 [28]	Bovine	Commercial PAEC cell line	—	TNFα	Annexin V; DNA laddering; cleaved caspase 8	TEER	+/−	Apoptosis inhibition (zVAD) treatment inhibited leak; MLCK inhibition reduced apoptosis but did not affect leak
Petrache et al. 2001 [29]	Human	Commercial PAEC	—	TNFα	Nucleosome ELISA	TEER	No	No apoptosis observed
Liu et al. 2005 [30]	Human	Commercial HUVEC	—	LPS	DNA fragmentation; Annexin V	EB-albumin	+/−	Time-dependent relationship: leak at all time points, apoptosis only at later time points
Seynhaeve et al. 2006 [31]	Human	Primary HUVEC	Morphology; CD31	TNFα, IL1β, IFNγ	Annexin V; YO-PRO-1	FITC-albumin	+/−	Variable leak-apoptosis relationship depending on combinations of different cytokines
Cardoso et al. 2012 [32]	Rat	Primary brain MVEC	None	LPS	Nuclear morphology; caspase 3 activity	TEER; fluorescein	+/−	Leak-apoptosis correlation following LPS + other inflammatory stimuli, not LPS alone
Lopez-Ramirez et al. 2012 [33]	Human	Commercial brain MVEC	—	TNFα, IFNγ	Annexin V; caspase 3/7 activity; TUNEL	TEER, FITC-dextran	+/−	Apoptosis inhibition (specific caspase inhibitors) only partially rescued leak; apoptosis only assessed at single time point
Abdullah and Bayraktutan 2014 [34]	Human	Commercial brain MVEC	—	TNFα	TUNEL; caspase 3/7 activity	TEER; EB-albumin	+/−	Leak and apoptosis early; leak recovers at later time points but apoptosis increases
Bechelli et al. 2015 [35]	Human	Commercial dermal MVEC cell line	—	*Rickettsia conorii*	Annexin V	TEER	No	Leak occurs before apoptosis; markers of other types of cell death present
Yang et al. 2015 [36]	Human	Commercial pulmonary MVEC	—	LPS	Annexin V	FITC-dextran; FITC-albumin	+/−	Association at a single time point; some conditions had different effects on apoptosis and leak
Wagner et al. 2016 [37]	Human	Commercial HUVEC	—	TNFα; procalcitonin	Annexin V	FITC-dextran	+/−	Leak early at low dose; apoptosis present later at high dose
McDonnell et al. 2016 [38]	Human	Primary AoEC	None	*Staphylococcus aureus*	Annexin V	FITC-dextran	Yes	Association at only a single time point
Zhu et al. 2016 [39]	Human	Commercial HUVEC	—	TNFα and CXCL10	Cleaved caspase 3	TEER	Yes	Association at only a single time point
Wang et al. 2017 *(present study)*	Mouse	Primary pulmonary MVEC	CD31, CD34, CD176, CD202b	TNFα, IL1β, IFNγ	Annexin V; FLICA (pan-caspase activity); TUNEL	TEER, EB-albumin	Yes	Time-dependent relationship: early leak apoptosis-independent; delayed leak apoptosis-dependent

Aortic endothelial cells, AoEC; C-X-C motif chemokine 10, CXCL10; Evans blue dye, EB; endothelial cell, EC; enzyme-linked immunosorbent assay, ELISA; fluorescein isothiocyanate, FITC; human umbilical vein endothelial cell, HUVEC; interferon gamma, IFNγ; interleukin 1 beta, IL1β; lipopolysaccharide, LPS; microvascular endothelial cell, MVEC; myosin light-chain kinase, MLCK; pulmonary artery endothelial cells, PAEC; transendothelial electrical resistance, TEER; tumour necrosis factor alpha, TNFα; terminal deoxynucleotidyl transferase dUTP nick end labeling, TUNEL; carbobenzoxy-valyl-alanyl-aspartyl-O-methyl, zVAD; +/−, inconsistent/variable association.

2.3. Quantification of PMVEC Apoptosis. To identify features of apoptosis in PMVEC, three different molecular markers were assessed using fluorescence microscopy and flow cytometry under basal and septic conditions: (1) caspase activation, (2) DNA fragmentation, and (3) loss of cell membrane polarity.

To detect caspase activation, PMVEC were stained with the Sulforhodamine (SR) FLICA Poly Caspase Assay Kit as per manufacturer's instructions (Immunohistochemistry Technologies, Bloomington, MN). Briefly, SR FLICA was added to PMVEC culture medium for the final 1 h of stimulation after which PMVEC were fixed with 10% formalin. Hoechst's stain (Hoechst 33342, Life Technologies Inc., Burlington, ON) was then used to fluorescently label PMVEC nuclei. Cells were then imaged using fluorescent microscopy (FLICA excitation/emission: 550 nm/590–600 nm; Hoechst excitation/emission: 361 nm/486 nm). The number of FLICA and Hoechst positive cells per field of view was counted through the use of a macro in ImageJ (National Institutes of Health). Automated counts of positive cells were confirmed with manual counts by two blinded reviewers.

Late-stage apoptotic DNA fragmentation in PMVEC was examined by terminal deoxynucleotidyl transferase dUTP nick end labeling (TUNEL; excitation/emission: 494/521 nm; In Situ Cell Death Detection, Roche, Laval, QC). For these studies, PMVEC were fixed in 10% formalin following basal and septic (cytomix) stimulation and then permeabilized with a 1% Na^+ citrate/0.1% Triton X-100 solution. Following permeabilization, TUNEL staining was used to identify PMVEC with DNA fragmentation and Hoechst stain was used to label all PMVEC nuclei. Cells were then imaged using fluorescent microscopy and the number of TUNEL and Hoechst positive cells per field of view was determined as above.

Loss of cell membrane polarization (as indicated by presence of cell surface phosphatidylserine) was assessed by staining PMVEC with FITC-conjugated Annexin V and propidium iodide (PI; Invitrogen, Burlington, ON). For these studies, PMVEC were stimulated with PBS or cytomix, lifted by trypsinization, and stained with Annexin V and PI in binding buffer (0.1 M HEPES pH 7.4; 1.4 M NaCl; 25 mM $CaCl_2$). The presence of Annexin V and PI staining was then analyzed by flow cytometry (easyCyte Guava 12HT). Annexin V^+/PI^- cells were considered apoptotic cells, whereas Annexin V^+/PI^+ cells were considered dead cells and Annexin V^-/PI^- cells were considered live cells.

2.4. Quantification of PMVEC Detachment. The degree of PMVEC attachment was assessed under basal and septic conditions and following treatment with Q-VD. Detached cells were quantified by pooling the conditioned media collected from each well with the supernatant from a single wash (PBS) of each well. Following centrifugation at 400 RCF for 10 min at 4°C, the supernatant was removed, the cell pellet resuspended in 0.1% albumin/PBS, and the detached PMVEC cytospun onto slides. Detached PMVEC were then assessed by TUNEL/Hoechst staining as described above.

2.5. Statistical Analysis. Data are reported as mean ± SEM and were analyzed using GraphPad Prism 5. Differences between groups were assessed by t-tests (one measured variable) or by a two-way ANOVA with Bonferroni post hoc testing (two independent variables). Significance threshold was set at $\alpha = 0.05$ and experiments were replicated at least 3 times.

3. Results

3.1. Dose Response and Time Course of Cytomix-Induced PMVEC Permeability. In our previous in vivo and in vitro studies, there is significant septic PMVEC barrier dysfunction at 4 h after septic stimulation [12, 22, 23, 43]. To identify the concentration of cytomix required to induce maximal PMVEC permeability as indicated by two complementary techniques, TEER and EB-albumin flux, PMVEC were treated with a range of cytomix concentrations. Under basal conditions, PMVEC achieved a stable TEER of 23.3 ± 1.0 Ohms (Figure 1(a)). PMVEC TEER was significantly decreased (79.4 ± 0.2% versus PBS) 4 h following stimulation with 0.3 ng/mL cytomix and continued to decrease in a dose-dependent manner until 10 ng/mL cytomix (56.7 ± 4.5% versus PBS; Figure 1(a)). PMVEC permeability to protein, as measured by EB-labelled albumin flux across the PMVEC monolayer, was significantly increased versus baseline following stimulation with 1 ng/mL cytomix (264.5 ± 11.0% versus PBS; Figure 1(b)). PMVEC permeability became maximal at 30 ng/mL of cytomix (338.7 ± 21.9% versus PBS; Figure 1(b)).

The time course of septic PMVEC hyperpermeability was more rigorously defined following stimulation with 30 ng/mL cytomix. Following cytomix stimulation, TEER was significantly reduced by 2 h and was maximally reduced by 4 h (Figure 2(a)). After 4 h, TEER gradually recovered returning to baseline by 24 h after cytomix stimulation (Figure 2(a)). PMVEC permeability to small (4 kDa dextran) and large (67 kDa albumin) macromolecules was significantly increased at 4 h after cytomix and remained significantly elevated at 24 h after cytomix with no evidence of recovery (Figures 2(b) and 2(c)).

3.2. Time Course of Cytomix-Induced PMVEC Apoptosis. To begin to assess the role of PMVEC apoptosis in the increased PMVEC permeability following stimulation with cytomix, we examined three different molecular features associated with apoptosis over a time course: caspase activation (FLICA+), loss of cell membrane polarity (Annexin V+), and DNA fragmentation (TUNEL+). PMVEC apoptosis, as evidenced by greater FLICA and Annexin V staining, was significantly increased by 8 h after cytomix stimulation (237.5 ± 26.3% and 172.7 ± 21.1% versus PBS for FLICA and Annexin V, resp.), which persisted until 24 h after cytomix (569.2 ± 14.9% and 153.8 ± 15.0% versus PBS for FLICA and Annexin V, resp.; Figure 3). Similarly, TUNEL staining was significantly increased by 16 h after cytomix stimulation (866.7 ± 34.6% versus PBS) and was still evident at 24 h (900.0 ± 20.4% versus PBS; Figure 3).

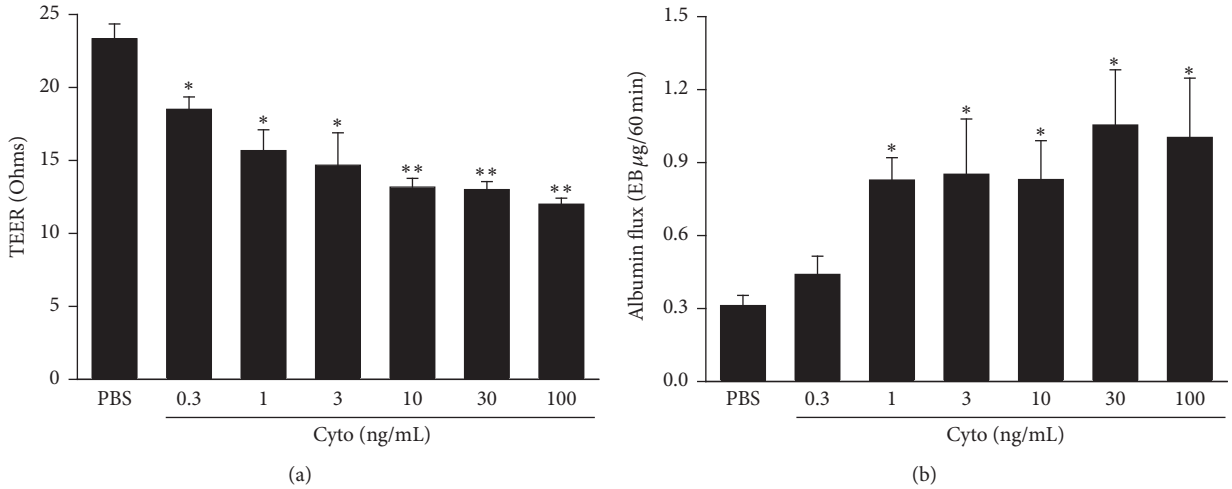

Figure 1: Cytomix induces a dose-dependent increase in mouse PMVEC permeability. PMVEC had significantly higher permeability 4 h after cytomix stimulation by 2 assays: (a) lower transendothelial electrical resistance (TEER) and (b) higher Evans blue- (EB-) labelled albumin flux. Furthermore, by both measures, permeability was maximal at 30 ng/mL cytomix. $*$ and $**$ represent $P < 0.05$ and 0.01 compared with PBS (one-way ANOVA), respectively. $n = 3$.

Caspase activation [FLICA] is considered an early marker of apoptosis whereas DNA fragmentation [TUNEL] is considered a late-stage marker of apoptosis. Examination of PMVEC double stained with FLICA and TUNEL demonstrated that at 16 h afer cytomix, 27.4 ± 7.7% of FLICA+ cells were TUNEL+, and by 24 h after cytomix, the percentage of FLICA+ cells that were also TUNEL+ increased to 70.6±7.0% (Figure 4). Most of the TUNEL+ cells were also FLICA+ at both 16 and 24 h after cytomix (Figure 4).

3.3. Effect of Caspase Inhibition on Cytomix-Induced PMVEC Leak and Apoptosis. To determine the contribution of PMVEC apoptosis to cytomix-induced loss of PMVEC barrier function, PMVEC were treated with two broad-spectrum caspase inhibitors, Z-VAD and Q-VD. Treatment with either Z-VAD or Q-VD had no effect on cytomix-induced decreases in PMVEC TEER compared to cytomix alone (Figure 5(a)). Similarly, no significant effects of Z-VAD or Q-VD were observed on cytomix-induced macromolecular flux (dextran and albumin) at 4 h and 8 h after cytomix (Figures 5(b) and 5(c)). Treatment with Z-VAD, however, significantly reduced cytomix-induced dextran flux versus cytomix alone at both 16 and 24 h and significantly reduced cytomix-induced albumin flux versus cytomix alone at 24 h (Figures 5(b) and 5(c)). Furthermore, treatment with Q-VD resulted in a significant reduction in both dextran and albumin flux at 16 and 24 h after cytomix compared to cytomix alone (Figures 5(b) and 5(c)).

Apoptosis is thought to be associated with an increase in detached cells [44]. Assessment of PMVEC detachment following cytomix stimulation revealed a significant reduction in cell attachment following 24 h of cytomix stimulation (Figure 6(a)). Furthermore, cytomix stimulation was also associated with a significant increase in the percentage of detached PMVEC at 16 h and 24 h following cytomix stimulation (360.0 ± 19.4% and 894.7 ± 8.8% versus PBS, resp.; Figure 6(b)). Importantly, treatment with Q-VD was found to significantly reduce the percentage of detached PMVEC at both 16 h (160.0 ± 23.1% versus PBS) and 24 h (210.5 ± 17.5% versus PBS) after cytomix (Figure 6(b)).

Apoptosis was then examined in Q-VD treated PMVEC to confirm that the observed decreases in cytomix-induced macromolecular flux and PMVEC detachment were due to decreases in apoptotic PMVEC death. As previously observed (Figure 3(c)), the percentage of TUNEL+ cells was significantly increased at 24 h after cytomix (890.9 ± 12.2% versus PBS); however, treatment with Q-VD resulted in a significant reduction in the percentage of TUNEL+ PMVEC following cytomix stimulation (409.1 ± 17.8% versus PBS; Figure 7(a)). Interestingly, inclusion of detached cells in the assessment of apoptosis resulted in an increase in the percentage of TUNEL+ PMVEC compared with assessment in attached cells alone (19.6 ± 2.4% versus 4.6 ± 1.0% resp.; Figure 7(a)). Similar to TUNEL+ PMVEC, the percentage of Annexin V+ PMVEC was significantly increased following cytomix stimulation (versus vehicle control), and treatment with Q-VD was associated with a significant reduction in the percentage of Annexin V+ PMVEC versus cytomix-stimulated PMVEC in the absence of Q-VD (Figure 7(b)).

4. Discussion

In the current report, we studied an in vitro model of septic ARDS by isolating, culturing, and studying murine PMVEC in vitro under septic conditions induced by exposure to multiple sepsis-relevant proinflammatory cytokines. Our current work confirms that stimulation of PMVEC with this mixture of 3 clinically relevant cytokines leads to a dose-dependent increase in PMVEC permeability over a biphasic time course, including acute 4–8 h barrier dysfunction characterized by both reduced trans-PMVEC electrical

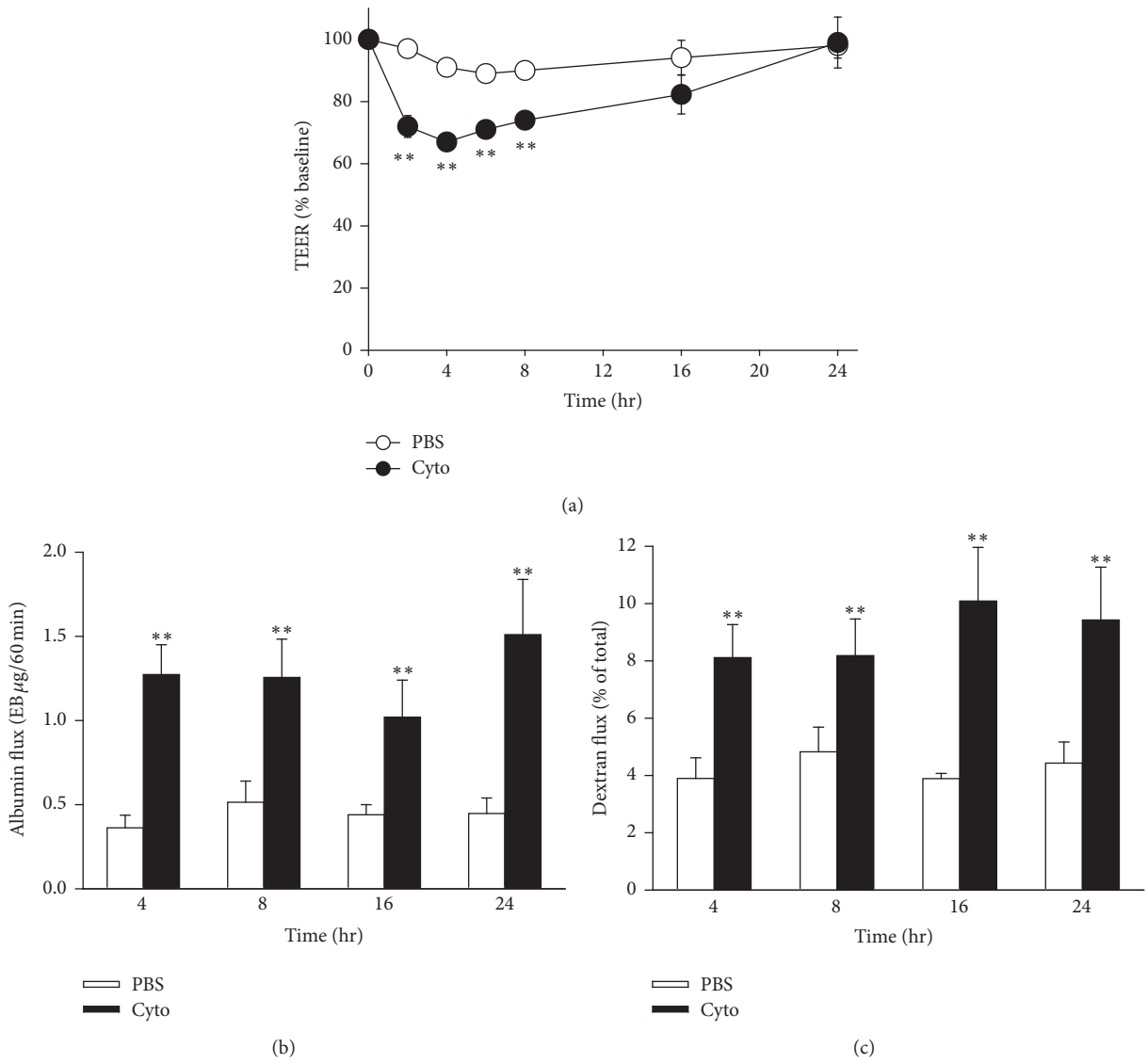

Figure 2: Time course of cytomix-induced mouse PMVEC hyperpermeability. Cytomix-stimulated PMVEC had significantly increased permeability by 4 h after stimulation versus PBS by 3 assays: lower TEER (a) and higher macromolecular flux including fluorescein isothiocyanate- (FITC-) labelled dextran (b) and EB-labelled albumin (c). Interestingly, leak as assessed by TEER appeared to recover by 16–24 h after cytomix, whereas septic enhanced macromolecular flux persisted. ∗∗ represents $P < 0.01$ compared with PBS (two-way ANOVA). $n = 8$.

resistance (TEER) and enhanced macromolecular permeability and late-phase 16–24 h persistence of this septic PMVEC macromolecule hyperpermeability despite recovery of TEER to baseline. Septic PMVEC apoptosis was documented using 3 independent and complementary markers and was found to be significant as early as 8 h and persisted at 16–24 h after cytomix stimulation. Early septic PMVEC hyperpermeability was not apoptosis-dependent; however, delayed PMVEC barrier dysfunction was abrogated following effective inhibition of apoptosis using two distinct caspase inhibitors, coincident with markedly inhibited PMVEC apoptosis and PMVEC detachment.

In sepsis, multiple organ dysfunction, including ARDS, is presumed due to systemic inflammatory injury of the microvasculature, especially the MVEC [5–9]. There is evidence for microvascular and MVEC dysfunction and injury in human sepsis. For example, microvascular dysfunction has been documented early in the course of human sepsis [7, 8, 46, 47]. In addition, increased numbers of circulating EC and soluble markers of EC damage (e.g., intercellular adhesion molecule 1, von Willebrand factor [vWF], and vascular endothelial growth factor receptor 1) correlate with more severe sepsis and higher mortality [48–54]. Furthermore, this septic microvascular dysfunction is clinically relevant as the presence of microvascular dysfunction in human sepsis is associated with more severe sepsis, organ dysfunction, and increased mortality [7, 8, 46]. Moreover, clinical outcomes including survival were especially poor if septic microvascular dysfunction persisted over time despite usual clinical management [9].

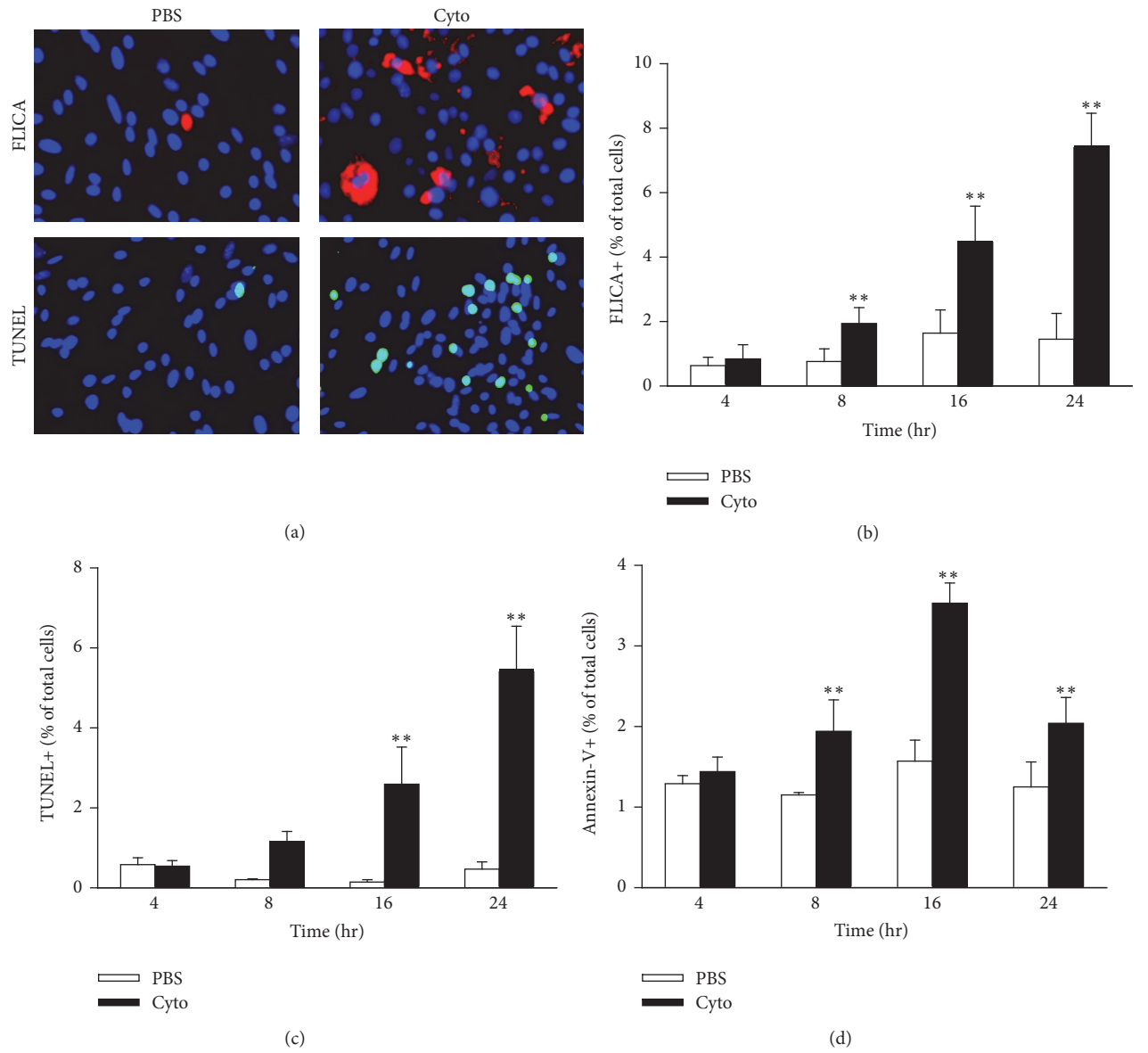

Figure 3: Cytomix induces mouse PMVEC apoptosis. (a) Cytomix stimulation for 24h leads to an increased number of cells stained positive for active caspases (fluorescent inhibitor of caspases [FLICA]; upper row; red) and fragmented DNA (terminal deoxynucleotidyl transferase dUTP nick end labeling [TUNEL]; lower row; green). Nuclei were stained with Hoechst 33342. Quantification revealed significant increases in FLICA+ (b), TUNEL+ (c), and Annexin V+/propidium iodide- (PI-) cells (d) by 8h (FLICA and Annexin V) and 16h (TUNEL) after cytomix. All 3 markers indicated persistent increases in septic PMVEC apoptosis at 24h. $^{**}P < 0.01$ compared with PBS (two-way ANOVA). $n = 5$-6.

Specifically, in ARDS, there are similar although more limited data to support pulmonary microvascular and MVEC injury and dysfunction. For example, pulmonary microvascular dysfunction, as reflected by higher measured ventilatory dead space was found to be associated with more severe ARDS and greater mortality [55]. Similarly, the presence of pulmonary vascular disease manifesting as pulmonary hypertension in patients with ARDS is an independent marker of poor prognosis [56]. In addition, elevated soluble plasma levels of several EC-derived proteins suggestive of more severe EC injury, including angiopoetin-2, thrombomodulin, and vWF in ARDS patients, are associated with higher mortality [57–60]. Specifically, for Ang-2, elevated levels are associated with a greater incidence of ARDS in patients at risk [57], and increasing levels over the first few days of infection-associated ARDS are more predictive of higher mortality than baseline levels [58]. Conceptually, pulmonary microvascular injury and dysfunction are thought to be central to indirect causes of ARDS (e.g., sepsis) and are also likely required for the development of ARDS in patients with clinical conditions characterized by direct lung insults (e.g., pneumonia and aspiration).

This septic microvascular and MVEC dysfunction is especially characterized by impaired barrier function, with

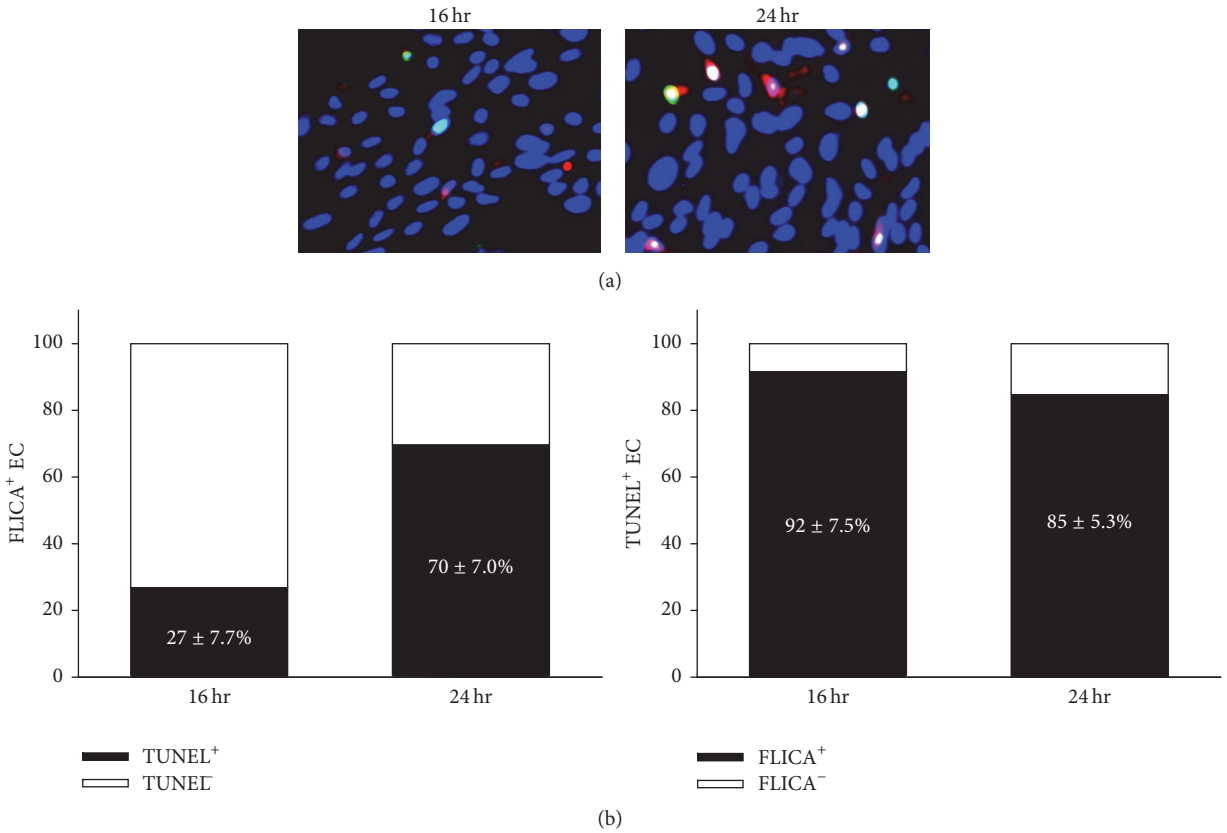

Figure 4: Caspase activation correlates with DNA fragmentation as a marker of PMVEC apoptosis. (a) Cytomix stimulation leads to an increased number of cells stained positive for both active caspases (FLICA; red) and fragmented DNA (TUNEL; green). Note that overlap between the 2 markers of apoptosis appears as yellow-white. Nuclei were stained with Hoechst 33342. (b) Quantitation of double-positive cells revealed that at 16 h, only 27 ± 7.7% of FLICA+ cells were also TUNEL+, whereas by 24 h, this number had increased to 70 ± 7.0%. Interestingly, almost all TUNEL+ cells were FLICA+ at both 16 h (92 ± 7.5%) and 24 h (85 ± 5.3%). $n = 4$.

the septic hyperpermeability resulting in protein-rich tissue edema and PMN influx into organs. Clearly, leak of protein-rich fluid from the pulmonary microvasculature into the interstitial and alveolar spaces is one of the defining pathophysiological features of ARDS [61, 62] and of animal models of sepsis-induced lung injury [11, 12, 22, 23]. Although many studies have advanced our understanding of the mechanisms regulating PMVEC barrier dysfunction in ARDS, many of these reports examined barrier function in either EC from the macrovasculature (e.g., HUVEC and pulmonary artery endothelial cells [PAEC]) or EC from systemic vascular beds (i.e., brain MVEC and corneal EC) [27–29, 33, 63–66]. While these studies provide insight into potential mechanisms, EC from the micro- and macrovasculature have different biological properties [67–71]. Moreover, the responses of EC from different vascular beds to proinflammatory cytokines vary markedly, especially with respect to apoptosis and the association of apoptosis with increased EC permeability (Table 1) [27–29, 33, 63–66]. Thus, given the importance of the pulmonary microvasculature in sepsis-associated ARDS, our current work focuses specifically on the effect of proinflammatory cytokines on PMVEC.

Multiple mechanisms of PMVEC injury in sepsis and in ARDS have been postulated. These include the actions of cytokines and other soluble circulating molecules, mechanical interaction with activated leukocytes and platelets, and paracrine exposure to injurious molecules released by these cells [2, 11, 12, 18, 19]. Ultimately, these exposures contribute to pulmonary microvascular, specifically PMVEC, injury, dysfunction, and possibly death/apoptosis [72]. EC apoptosis and resulting microvascular permeability are commonly accepted to be pathophysiologically associated, although the direct evidence in support of this relationship is limited [22, 23, 72–74]. For example, our previous work found that septic pulmonary microvascular barrier dysfunction in vivo in mice following CLP-sepsis was associated with increased PMVEC apoptosis and, moreover, that inhibition of apoptosis, via treatment of these mice with Q-VD (a synthetic caspase inhibitor), significantly reduced septic pulmonary microvascular permeability [22, 23]. Additional studies have demonstrated that inhibition of apoptosis following CLP-induced sepsis through treatment with siRNA against caspases or FAS-associated death domain (FADD) rescues septic EC dysfunction, including reducing septic hyperpermeability [72–74]. Furthermore, assessment of apoptosis in vivo revealed the presence of apoptotic EC early in the time course of sepsis (4 h) as well as much later (24 h) depending on the vascular bed studied [23, 73, 74].

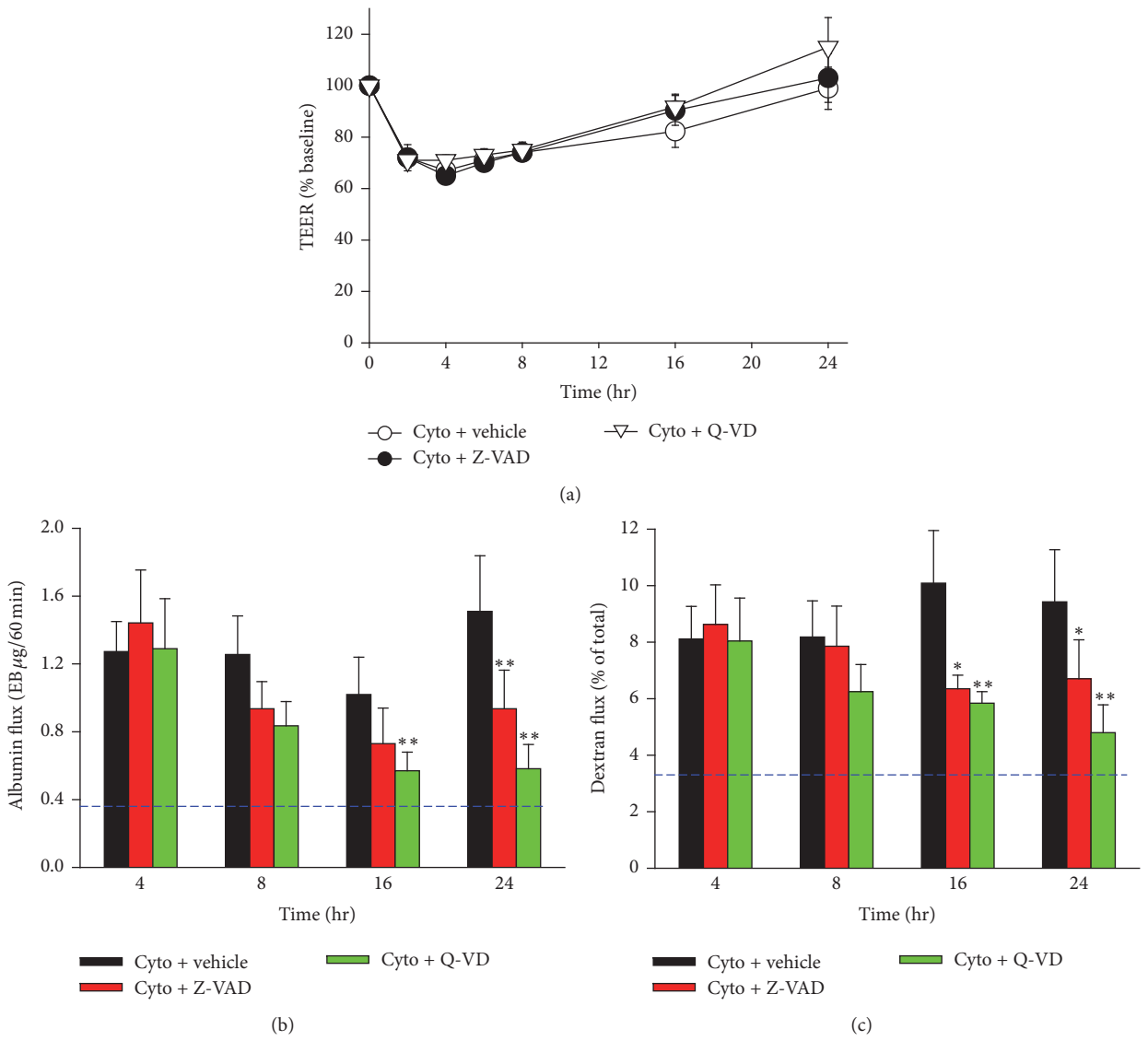

Figure 5: Caspase activity contributes to persistent septic PMVEC macromolecular hyperpermeability. (a) Inhibition of caspase activity (Z-VAD, 100 μM; Q-VD, 50 μM) following cytomix stimulation did not appear to affect mouse PMVEC TEER at any of the time points examined versus vehicle treatment (dimethyl sulfoxide [DMSO]). In contrast, septic increases in macromolecular flux across PMVEC, including EB-albumin (b) and FITC-dextran (c), were significantly attenuated at 16 h and 24 h after cytomix by inhibition of caspase activity. Dashed lines indicate average basal level (treated with vehicle alone). Of note, inhibition of caspase activity had no effect on septic PMVEC increases in macromolecular flux at earlier time points (4 h and 8 h). $*$ and $**$ represent $P < 0.05$ and 0.01 compared with PBS, respectively (two-way ANOVA). $n = 6$–8.

Despite the in vivo evidence, however, the role of apoptosis in mediating septic impaired MVEC barrier function, and hence, the pulmonary edema characteristic of ARDS, remains unclear. Multiple studies have attempted to address this question utilizing in vitro models of septic conditions in various EC types (Table 1) [27–39]. Overall, these studies demonstrated that EC stimulation with proinflammatory cytokines sometimes led to the induction of apoptosis, depending on dose, timing, and exact combination of cytokines. However, this EC apoptosis was in many cases only defined by a single marker (e.g., TUNEL), which is a serious limitation as all putative markers of apoptosis can also be observed in other nonapoptotic death mechanisms [75, 76]. Moreover, it is now widely accepted that apoptosis must be supported by a panel of multiple complementary assays, including loss of cell membrane polarization, caspase activation, and DNA fragmentation [75, 76]. Thus, the present study provides a comprehensive assessment of apoptotic cell death (3 complementary markers) over a time course clearly identifying the progressive induction of apoptosis beginning at 8 h and increasing to 24 h after cytomix.

The connection between MVEC apoptosis and barrier dysfunction has also not been firmly established and depends on the EC type, stimulation conditions, and time course

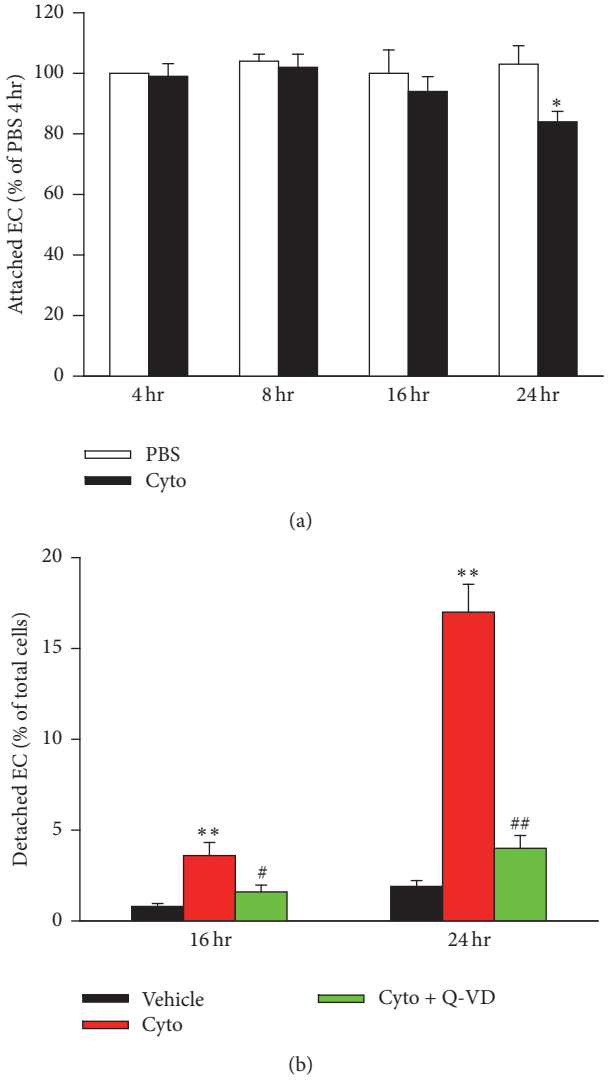

Figure 6: Inhibition of caspase activity reduces cell detachment. (a) Stimulation with cytomix significantly decreases the number of attached mouse PMVEC after 24 h. $^{*}P < 0.05$ compared with PBS (two-way ANOVA). $n = 4$–6. (b) Treatment of cytomix-stimulated PMVEC with Q-VD (50 μM) significantly increased the number of attached cells versus vehicle-treated. $^{**}P < 0.01$ compared with vehicle (DMSO); # and ## represent $P < 0.05$ and 0.01 compared with cytomix-treated group, respectively (two-way ANOVA).

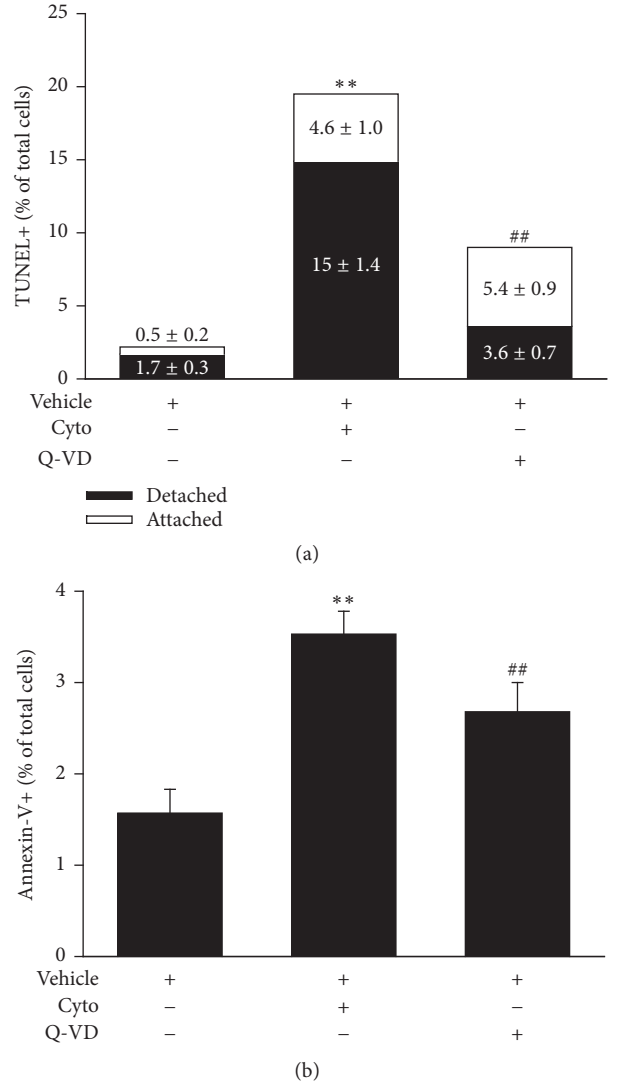

Figure 7: Inhibition of caspase activity reduces PMVEC apoptosis. (a) Stimulation of PMVEC with cytomix (24 h) led to a significant increase in TUNEL+ cells and this increase was significantly reduced by treatment with Q-VD (50 μM). $n = 6$. (b) Flow cytometric analysis revealed an increased number of early apoptotic PMVEC (Annexin V+/PI−) following cytomix stimulation (16 h) that was significantly reduced by treatment with Q-VD (50 μM). $n = 4$. ** or ## represents $P < 0.01$ compared with vehicle or cytomix group, respectively (one-way ANOVA).

with many of the studies utilizing macrovascular EC (e.g., HUVEC) and a single time point (Table 1). For example, stimulation of brain MVEC with TNFα and IFNγ for 24 h results in apoptosis that is associated with increased brain MVEC barrier dysfunction [33]. Treatment with a caspase inhibitor (Z-VAD), however, only partially restored barrier function. Additionally, stimulation of macrovascular PAEC with TNFα resulted in apoptosis as early as 4 h after stimulation that persisted at 20 h [29]. While this apoptosis was also associated with increased permeability across the PAEC monolayer, treatment with Z-VAD did not rescue the enhanced permeability at any time point [29]. It should be emphasized that the study of macrovascular EC (e.g., HUVEC and PAEC) is not biologically relevant to the study of septic microvascular/MVEC dysfunction resulting in organ dysfunction (e.g., ARDS), as MVEC are genotypically and phenotypically very distinct from macrovascular EC [67, 68]. Further, to date, there have been no studies specifically using mouse PMVEC to assess the connection between septic MVEC apoptosis and barrier dysfunction (Table 1). This is critical as septic PMVEC dysfunction is pathobiologically responsible for septic acute lung injury in mice, and mice are one of the primary models currently used for ARDS research due to the ease of genetic manipulation [1, 77]. Thus, our

examination of mouse PMVEC apoptosis over a time course clearly establishes for the first time that early septic cytomix-induced murine PMVEC barrier dysfunction is not mediated through PMVEC apoptosis.

There are multiple mechanisms through which loss of PMVEC barrier function has been found to occur; thus, it is not surprising that we found increased PMVEC permeability after 4 h of cytomix stimulation with no evidence of apoptosis. For example, TNFα has previously been found to drive loss of corneal EC barrier function through activation of p38 mitogen-activated protein (MAP) kinase and subsequent disassembly of microtubules, as well as adherens and tight junctions [66]. Additionally, examination of barrier function in mouse renal EC following stimulation with TNFα demonstrated that increased permeability to albumin was associated with altered actin cytoskeleton, as well as formation of gaps between previously confluent cells and a loss of tight junctions and the EC glycocalyx [78]. Furthermore, inhibition of Rho-associated kinase and myosin light chain kinase, but not inhibition of caspases, rescued the increased permeability as well as the loss of EC glycocalyx and tight junctions [78]. Thus, our data supports these previous studies demonstrating that early cytokine-induced leak across PMVEC is independent of apoptosis; however, it also expands on these studies by clearly demonstrating that the early apoptosis-independent leak transitions to apoptosis-dependent leak as it persists over time.

Loss of EC through loss of cell-extracellular matrix (ECM) interactions and increased EC detachment has long been thought to be involved in loss of barrier function [79]. The increased apoptosis we observed at 16 and 24 h after cytomix stimulation was found to be clearly associated with increased PMVEC detachment. This finding is supported by previous studies that found increased cell detachment following LPS and oxyhemoglobin stimulation of PAEC and brain MVEC, respectively [27, 64]. Similar to our findings, the increased cell detachment in these previous studies was also rescued by inhibition of caspases [27, 64]. Furthermore, the LPS-induced cell detachment was associated with caspase-dependent cleavage of α- and β-catenin as well as focal adhesion kinase (FAK), critical proteins involved in cell-cell and cell-ECM interactions, respectively. However, the inhibition of caspase activity, which rescued cell detachment, only prevented degradation of proteins involved in cell-ECM interactions, not cell-cell interactions, and unlike our study did not rescue the LPS-induced leak [27]. Together, these studies suggest that the increased cell detachment observed in our study may be due to loss of cell-ECM interactions. However, this remains to be determined. Furthermore, as the rescue of PMVEC detachment observed in our study was also associated with restored PMVEC barrier function, it is possible that additional mechanisms, such as altered cell-cell interactions, are involved.

Our data also demonstrates the importance of the method of assessment of EC barrier function, specifically the importance of using multiple methods to assess EC barrier function, which is not common practice (Table 1). Measurements of TEER versus macromolecular permeability reflect different aspects of EC barrier function and, not surprisingly, could respond differently to inflammatory stimulation. Specifically, the clinically relevant EB-albumin flux is a marker of paracellular and transcellular permeability to large molecules and TEER assesses permeability to charged ions [43]. The acute cytomix-induced PMVEC barrier dysfunction was consistent between TEER and both FITC-dextran and EB-albumin techniques, but persistent septic PMVEC hyperpermeability to macromolecules at later time points was divergent from the observed recovery in TEER. In addition, the acute septic cytokine-induced barrier dysfunction (both decreased TEER and increased macromolecular flux) was not rescued by caspase inhibition (Z-VAD or Q-VD), similar to previously reported studies with PAEC and corneal EC [29, 66]. However, delayed septic hyperpermeability to macromolecules at 16–24 h was rescued by treatment with Z-VAD and Q-VD. Thus, the effect of caspase (apoptosis) inhibition on persistent macromolecular flux across septic PMVEC in the absence of any effect on TEER suggests that barrier function to large molecules was enhanced by caspase inhibition, likely through increased PMVEC attachment, but that PMVEC barrier function was still impaired allowing the passage of small charged ions.

Our findings of persistent septic PMVEC barrier dysfunction at delayed time points are clinically relevant. In ARDS patients, once pulmonary microvascular injury and dysfunction are established, repair of the pulmonary alveolocapillary microvascular EC lining would be necessary and clinically important. Indeed, patients with a greater number of circulating bone-marrow derived endothelial progenitor cells (EPCs), postulated to contribute to PMVEC repopulation following loss of these cells, had better clinical outcomes, including more ventilator-free days and decreased mortality [80]. Similar resident EPC populations have also been identified in the pulmonary microvasculature [81], although their direct involvement in repair of the pulmonary alveolocapillary microvascular EC lining has not been established.

In ARDS, more prolonged clinical illness is associated with a greater need for more intensive and prolonged respiratory support, including mechanical ventilation, higher PEEP levels, and FiO2, which are associated with worse clinical outcomes, specifically greater risk of ventilator-associated pneumonia, higher rates of multisystem organ injury and dysfunction, and greater mortality [82]. As such, ongoing pulmonary microvascular alveolocapillary septic hyperpermeability and persistent high-protein interstitial and alveolar pulmonary edema would contribute to the need for more prolonged respiratory support. Future experiments to define the potential role of human PMVEC apoptosis in septic PMVEC hyperpermeability and septic ARDS, especially the presence of a similar delayed reconstitution of the pulmonary microvascular alveolocapillary permeability barrier, may suggest new therapeutic approaches to promote recovery of patients from ARDS.

Finally, we recognize that our study has limitations. Our previous work found evidence of an association between PMVEC apoptosis and septic pulmonary microvascular permeability in vivo [22, 23]. The findings of our current study, however, suggest that the initial PMVEC barrier dysfunction

following stimulation with cytokines is not dependent on apoptosis. This discrepancy is likely due to inherent differences between the natures of these studies. For example, in vivo there are many different cell types, such as pericytes and circulating inflammatory cells, which interact with PMVEC, as well as a complete interstitial ECM and the presence of the glycocalyx on the surface of the PMVEC, all of which are missing or limited in the in vitro setting [83–87]. Furthermore, our in vitro model employed PMVEC cultured alone stimulated with a mixture of three sepsis-relevant cytokines, which is still a less robust septic stimulus than EC would face in vivo (activated leukocytes and bacterial products), as well as the potentially injurious effects of shear stresses associated with blood flow present in the in vivo scenario. However, use of this simplified in vitro isolated PMVEC model as well as the comprehensive assessment of apoptosis (use of three different markers) and PMVEC permeability (use of three complementary measures) allowed for the examination of the function of specifically PMVEC over a comprehensive time course and thereby the identification of the novel potential role of apoptosis-inhibition in reestablishing the PMVEC barrier following septic injury. Future directions of our work will include assessment of apoptosis in more complex models (i.e., PMVEC-PMN coculture) as well as with cells isolated from humans to ensure clinical relevance.

In conclusion, our current data suggests for the first time using mouse cells that early septic PMVEC barrier dysfunction is independent of apoptosis but that persistent septic macromolecule leak is due to loss of adherent cells due to apoptosis, and when apoptosis (specifically caspase activity) is inhibited, PMVEC detachment is decreased, permitting restoration of the normal PMVEC permeability barrier.

Competing Interests

The authors declare that they have no competing interests.

Acknowledgments

The authors would like to thank the members of the Lung Research Group at Western University, especially Drs. Ruud Veldhuizen and Lisa Cameron, for helpful discussions. This work was supported by research funding from the Ontario Thoracic Society (S. Gill), Lawson Health Research Institute Internal Research Fund (S. Gill), the Program of Experimental Medicine (S. Gill and S. Mehta), and the Heart & Stroke Foundation of Ontario/Canada Grant no. G-13-0003039 (S. Mehta).

References

[1] A. P. Wheeler and G. R. Bernard, "Acute lung injury and the acute respiratory distress syndrome: a clinical review," *The Lancet*, vol. 369, no. 9572, pp. 1553–1564, 2007.

[2] A. B. J. Groeneveld, "Vascular pharmacology of acute lung injury and acute respiratory distress syndrome," *Vascular Pharmacology*, vol. 39, no. 4-5, pp. 247–256, 2002.

[3] L. Husak, A. Marcuzzi, J. Herring et al., "National analysis of sepsis hospitalizations and factors contributing to sepsis in-hospital mortality in Canada," *Healthcare quarterly*, vol. 13, pp. 35–41, 2010.

[4] D. C. Angus, W. T. Linde-Zwirble, J. Lidicker, G. Clermont, J. Carcillo, and M. R. Pinsky, "Epidemiology of severe sepsis in the United States: analysis of incidence, outcome, and associated costs of care," *Critical Care Medicine*, vol. 29, no. 7, pp. 1303–1310, 2001.

[5] R. S. Hotchkiss and I. E. Karl, "The pathophysiology and treatment of sepsis," *New England Journal of Medicine*, vol. 348, no. 2, pp. 138–150, 2003.

[6] M. P. Glauser, "Pathophysiologic basis of sepsis: considerations for future strategies of intervention," *Critical Care Medicine*, vol. 28, no. 9, pp. S4–S8, 2000.

[7] D. De Backer, J. Creteur, J.-C. Preiser, M.-J. Dubois, and J.-L. Vincent, "Microvascular blood flow is altered in patients with sepsis," *American Journal of Respiratory and Critical Care Medicine*, vol. 166, no. 1, pp. 98–104, 2002.

[8] S. Trzeciak, R. P. Dellinger, J. E. Parrillo et al., "Early microcirculatory perfusion derangements in patients with severe sepsis and septic shock: relationship to hemodynamics, oxygen transport, and survival," *Annals of Emergency Medicine*, vol. 49, no. 1, pp. 88.e2–98.e2, 2007.

[9] Y. Sakr, M.-J. Dubois, D. De Backer, J. Creteur, and J.-L. Vincent, "Persistent-microcirculatory alterations are associated with organ failure and death in patients with septic shock," *Critical Care Medicine*, vol. 32, no. 9, pp. 1825–1831, 2004.

[10] H. M. Razavi, L. F. Wang, S. Weicker et al., "Pulmonary neutrophil infiltration in murine sepsis: role of inducible nitric oxide synthase," *American Journal of Respiratory and Critical Care Medicine*, vol. 170, no. 3, pp. 227–233, 2004.

[11] L. Wang, R. Taneja, H. M. Razavi, C. Law, C. Gillis, and S. Mehta, "Specific role of neutrophil inducible nitric oxide synthase in murine sepsis-induced lung injury in vivo," *Shock*, vol. 37, no. 5, pp. 539–547, 2012.

[12] L. F. Wang, M. Patel, H. M. Razavi et al., "Role of inducible Nitric Oxide Synthase in pulmonary microvascular protein leak in murine sepsis," *American Journal of Respiratory and Critical Care Medicine*, vol. 165, no. 12, pp. 1634–1639, 2002.

[13] J. G. Wagner and R. A. Roth, "Neutrophil migration during endotoxemia," *Journal of Leukocyte Biology*, vol. 66, no. 1, pp. 10–24, 1999.

[14] D. N. Granger and P. Kubes, "The microcirculation and inflammation: modulation of leukocyte-endothelial cell adhesion," *Journal of Leukocyte Biology*, vol. 55, no. 5, pp. 662–675, 1994.

[15] K. Tyml, "Critical role for oxidative stress, platelets, and coagulation in capillary blood flow impairment in sepsis," *Microcirculation*, vol. 18, no. 2, pp. 152–162, 2011.

[16] N. Semeraro, C. T. Ammollo, F. Semeraro, and M. Colucci, "Sepsis, thrombosis and organ dysfunction," *Thrombosis Research*, vol. 129, no. 3, pp. 290–295, 2012.

[17] C. Lam, K. Tyml, C. Martin, and W. Sibbald, "Microvascular perfusion is impaired in a rat model of normotensive sepsis," *Journal of Clinical Investigation*, vol. 94, no. 5, pp. 2077–2083, 1994.

[18] K. S. Farley, L. F. Wang, H. M. Razavi et al., "Effects of macrophage inducible nitric oxide synthase in murine septic lung injury," *American Journal of Physiology - Lung Cellular and Molecular Physiology*, vol. 290, no. 6, pp. L1164–L1172, 2006.

[19] O. Handa, J. Stephen, and G. Cepinskas, "Role of endothelial nitric oxide synthase-derived nitric oxide in activation and dysfunction of cerebrovascular endothelial cells during early onsets of sepsis," *American Journal of Physiology—Heart and Circulatory Physiology*, vol. 295, no. 4, pp. H1712–H1719, 2008.

[20] E. Dejana, "Endothelial adherens junctions. Implications in the control of vascular permeability and angiogenesis," *Journal of Clinical Investigation*, vol. 98, no. 9, pp. 1949–1953, 1996.

[21] J. L. Shelton, L. Wang, G. Cepinskas, R. Inculet, and S. Mehta, "Human neutrophil-pulmonary microvascular endothelial cell interactions in vitro: differential effects of nitric oxide vs. peroxynitrite," *Microvascular Research*, vol. 76, no. 2, pp. 80–88, 2008.

[22] S. E. Gill, R. Taneja, M. Rohan, L. Wang, and S. Mehta, "Pulmonary microvascular albumin leak is associated with endothelial cell death in murine sepsis-induced lung injury in vivo," *PLoS ONE*, vol. 9, no. 2, Article ID e88501, 2014.

[23] S. E. Gill, M. Rohan, and S. Mehta, "Role of pulmonary microvascular endothelial cell apoptosis in murine sepsis-induced lung injury in vivo," *Respiratory Research*, vol. 16, no. 1, article no. 109, 2015.

[24] T. R. Martin, "Apoptosis and epithelial injury in the lungs," *Proceedings of the American Thoracic Society*, vol. 2, no. 3, pp. 214–220, 2005.

[25] S. J. Riedl and G. S. Salvesen, "The apoptosome: signalling platform of cell death," *Nature Reviews Molecular Cell Biology*, vol. 8, no. 5, pp. 405–413, 2007.

[26] F. Drakopanagiotakis, A. Xifteri, V. Polychronopoulos, and D. Bouros, "Apoptosis in lung injury and fibrosis," *European Respiratory Journal*, vol. 32, no. 6, pp. 1631–1638, 2008.

[27] D. D. Bannerman, M. Sathyamoorthy, and S. E. Goldblum, "Bacterial lipopolysaccharide disrupts endothelial monolayer integrity and survival signaling events through caspase cleavage of adherens junction proteins," *Journal of Biological Chemistry*, vol. 273, no. 52, pp. 35371–35380, 1998.

[28] I. Petrache, K. Birukov, A. L. Zaiman et al., "Caspase-dependent cleavage of myosin light chain kinase (MLCK) is involved in TNF-α-mediated bovine pulmonary endothelial cell apoptosis," *FASEB Journal*, vol. 17, no. 3, pp. 407–416, 2003.

[29] I. Petrache, A. D. Verin, M. T. Crow, A. Birukova, F. Liu, and J. G. N. Garcia, "Differential effect of MLC kinase in TNF-α-induced endothelial cell apoptosis and barrier dysfunction," *American Journal of Physiology—Lung Cellular and Molecular Physiology*, vol. 280, no. 6, pp. L1168–L1178, 2001.

[30] D. Liu, D. Zhang, J. Scafidi, X. Wu, C. C. Cramer, and A. E. Davis III, "C1 inhibitor prevents Gram-negative bacterial lipopolysaccharide-induced vascular permeability," *Blood*, vol. 105, no. 6, pp. 2350–2355, 2005.

[31] A. L. B. Seynhaeve, C. E. Vermeulen, A. M. M. Eggermont, and T. L. M. ten Hagen, "Cytokines and vascular permeability: an in vitro study on human endothelial cells in relation to tumor necrosis factor-α-primed peripheral blood mononuclear cells," *Cell Biochemistry and Biophysics*, vol. 44, no. 1, pp. 157–169, 2006.

[32] F. L. Cardoso, Á. Kittel, S. Veszelka et al., "Exposure to lipopolysaccharide and/or unconjugated bilirubin impair the integrity and function of brain microvascular endothelial cells," *PLoS ONE*, vol. 7, no. 5, Article ID e35919, 2012.

[33] M. A. Lopez-Ramirez, R. Fischer, C. C. Torres-Badillo et al., "Role of caspases in cytokine-induced barrier breakdown in human brain endothelial cells," *Journal of Immunology*, vol. 189, no. 6, pp. 3130–3139, 2012.

[34] Z. Abdullah and U. Bayraktutan, "NADPH oxidase mediates TNF-α-evoked in vitro brain barrier dysfunction: roles of apoptosis and time," *Molecular and Cellular Neuroscience*, vol. 61, pp. 72–84, 2014.

[35] J. Bechelli, C. Smalley, N. Milhano, D. H. Walker, and R. Fang, "Rickettsia massiliae and rickettsia conorii israeli spotted fever strain differentially regulate endothelial cell responses," *PLoS ONE*, vol. 10, no. 9, Article ID e0138830, 2015.

[36] Y. Yang, Q.-H. Chen, A.-R. Liu, X.-P. Xu, J.-B. Han, and H.-B. Qiu, "Synergism of MSC-secreted HGF and VEGF in stabilising endothelial barrier function upon lipopolysaccharide stimulation via the Rac1 pathway," *Stem Cell Research & Therapy*, vol. 6, no. 1, article no. 250, 2015.

[37] N.-M. Wagner, C. Van Aken, A. Butschkau et al., "Procalcitonin impairs endothelial cell function and viability," *Anesthesia & Analgesia*, 2016.

[38] C. J. McDonnell, C. D. Garciarena, R. L. Watkin et al., "Inhibition of major integrin $\alpha_V\beta_3$ reduces Staphylococcus aureus attachment to sheared human endothelial cells," *Journal of Thrombosis and Haemostasis*, vol. 14, no. 12, pp. 2536–2547, 2016.

[39] X. Zhu, Y. Zou, B. Wang et al., "Blockade of CXC chemokine receptor 3 on endothelial cells protects against sepsis-induced acute lung injury," *Journal of Surgical Research*, vol. 204, no. 2, pp. 288–296, 2016.

[40] J. H. Wang, H. P. Redmond, R. W. G. Watson, and D. Bouchier-Hayes, "Induction of human endothelial cell apoptosis requires both heat shock and oxidative stress responses," *American Journal of Physiology—Cell Physiology*, vol. 272, no. 5, pp. C1543–C1551, 1997.

[41] V. A. Polunovsky, C. H. Wendt, D. H. Ingbar, M. S. Peterson, and P. B. Bitterman, "Induction of endothelial cell apoptosis by TNFα: modulation by inhibitors of protein synthesis," *Experimental Cell Research*, vol. 214, no. 2, pp. 584–594, 1994.

[42] Z.-H. Liu, G. E. Striker, M. Stetler-Stevenson, P. Fukushima, A. Patel, and L. J. Striker, "TNF-alpha and IL-1 alpha induce mannose receptors and apoptosis in glomerular mesangial but not endothelial cells," *American Journal of Physiology—Cell Physiology*, vol. 270, no. 6, pp. C1595–C1601, 1996.

[43] V. Arpino, S. Mehta, L. Wang et al., "Tissue inhibitor of metalloproteinases 3-dependent microvascular endothelial cell barrier function is disrupted under septic conditions," *American Journal of Physiology—Heart and Circulatory Physiology*, vol. 310, no. 11, pp. H1455–H1467, 2016.

[44] R. S. Hotchkiss, K. W. Tinsley, P. E. Swanson, and I. E. Karl, "Endothelial cell apoptosis in sepsis," *Critical Care Medicine*, vol. 30, no. 5, pp. S225–S228, 2002.

[45] S. Subbanna, M. Shivakumar, N. S. Umapathy et al., "G9a-mediated histone methylation regulates ethanol-induced neurodegeneration in the neonatal mouse brain," *Neurobiology of Disease*, vol. 54, pp. 475–485, 2013.

[46] A. Spanos, S. Jhanji, A. Vivian-Smith, T. Harris, and R. M. Pearse, "Early microvascular changes in sepsis and severe sepsis," *Shock*, vol. 33, no. 4, pp. 387–391, 2010.

[47] D. De Backer, D. Orbegozo Cortes, K. Donadello, and J.-L. Vincent, "Pathophysiology of microcirculatory dysfunction and the pathogenesis of septic shock," *Virulence*, vol. 5, no. 1, pp. 73–79, 2014.

[48] S. Endo, K. Inada, H. Nakae et al., "Blood levels of endothelin-1 and thrombomodulin in patients with disseminated intravascular coagulation and sepsis," *Research Communications in Molecular Pathology and Pharmacology*, vol. 90, no. 2, pp. 277–288, 1995.

[49] D. B. Cines, E. S. Pollak, C. A. Buck et al., "Endothelial cells in physiology and in the pathophysiology of vascular disorders," *Blood*, vol. 91, no. 10, pp. 3527–3561, 1998.

[50] M. Mutunga, B. Fulton, R. Bullock et al., "Circulating endothelial cells in patients with septic shock," *American Journal of Respiratory and Critical Care Medicine*, vol. 163, no. 1, pp. 195–200, 2001.

[51] K. Reinhart, O. Bayer, F. Brunkhorst, and M. Meisner, "Markers of endothelial damage in organ dysfunction and sepsis," *Critical Care Medicine*, vol. 30, no. 5, pp. S302–S312, 2002.

[52] L. B. Ware, M. D. Eisner, B. T. Thompson, P. E. Parsons, and M. A. Matthay, "Significance of Von Willebrand factor in septic and nonseptic patients with acute lung injury," *American Journal of Respiratory and Critical Care Medicine*, vol. 170, no. 7, pp. 766–772, 2004.

[53] N. I. Shapiro and W. C. Aird, "Sepsis and the broken endothelium," *Critical Care*, vol. 15, no. 2, article no. 135, 2011.

[54] S. Skibsted, A. E. Jones, M. A. Puskarich et al., "Biomarkers of endothelial cell activation in early sepsis," *Shock*, vol. 39, no. 5, pp. 427–432, 2013.

[55] T. J. Nuckton, J. A. Alonso, R. H. Kallet et al., "Pulmonary dead-space fraction as a risk factor for death in the acute respiratory distress syndrome," *The New England Journal of Medicine*, vol. 346, no. 17, pp. 1281–1286, 2002.

[56] T. M. Bull, B. Clark, K. McFann, and M. Moss, "Pulmonary vascular dysfunction is associated with poor outcomes in patients with acute lung injury," *American Journal of Respiratory and Critical Care Medicine*, vol. 182, no. 9, pp. 1123–1128, 2010.

[57] A. Agrawal, M. A. Matthay, K. N. Kangelaris et al., "Plasma angiopoietin-2 predicts the onset of acute lung injury in critically ill patients," *American Journal of Respiratory and Critical Care Medicine*, vol. 187, no. 7, pp. 736–742, 2013.

[58] C. S. Calfee, D. Gallagher, J. Abbott, B. T. Thompson, and M. A. Matthay, "Plasma angiopoietin-2 in clinical acute lung injury," *Critical Care Medicine*, vol. 40, no. 6, pp. 1731–1737, 2012.

[59] A. Sapru, C. S. Calfee, K. D. Liu et al., "Plasma soluble thrombomodulin levels are associated with mortality in the acute respiratory distress syndrome," *Intensive Care Medicine*, vol. 41, no. 3, pp. 470–478, 2015.

[60] M. L. Terpstra, J. Aman, G. P. Van Nieuw Amerongen, and A. B. J. Groeneveld, "Plasma biomarkers for acute respiratory distress syndrome: a systematic review and Meta-Analysis," *Critical Care Medicine*, vol. 42, no. 3, pp. 691–700, 2014.

[61] M. A. Matthay, L. B. Ware, and G. A. Zimmerman, "The acute respiratory distress syndrome," *Journal of Clinical Investigation*, vol. 122, no. 8, pp. 2731–2740, 2012.

[62] L. B. Ware and M. A. Matthay, "The acute respiratory distress syndrome," *The New England Journal of Medicine*, vol. 342, no. 18, pp. 1334–1349, 2000.

[63] C. J. Kuckleburg, R. Tiwari, and C. J. Czuprynski, "Endothelial cell apoptosis induced by bacteria-activated platelets requires caspase-8 and -9 and generation of reactive oxygen species," *Thrombosis and Haemostasis*, vol. 99, no. 2, pp. 363–372, 2008.

[64] T. Meguro, B. Chen, A. D. Parent, and J. H. Zhang, "Caspase inhibitors attenuate oxyhemoglobin-induced apoptosis in endothelial cells," *Stroke*, vol. 32, no. 2, pp. 561–566, 2001.

[65] P. Sagoo, G. Chan, D. F. P. Larkin, and A. J. T. George, "Inflammatory cytokines induce apoptosis of corneal endothelium through nitric oxide," *Investigative Ophthalmology & Visual Science*, vol. 45, no. 11, pp. 3964–3973, 2004.

[66] M. Shivanna, G. Rajashekhar, and S. P. Srinivas, "Barrier dysfunction of the corneal endothelium in response to TNF-α: role of p38 MAP kinase," *Investigative Ophthalmology and Visual Science*, vol. 51, no. 3, pp. 1575–1582, 2010.

[67] B. R. Zetter, "The endothelial cells of large and small blood vessels," *Diabetes*, vol. 30, no. 2, pp. 24–28, 1981.

[68] J. L. Shelton, L. Wang, G. Cepinskas et al., "Albumin leak across human pulmonary microvascular vs. umbilical vein endothelial cells under septic conditions," *Microvascular Research*, vol. 71, no. 1, pp. 40–47, 2006.

[69] M. E. Gerritsen, "Functional heterogeneity of vascular endothelial cells," *Biochemical Pharmacology*, vol. 36, no. 17, pp. 2701–2711, 1987.

[70] M. K. Glassberg, K. B. Nolop, J. T. Jackowski, W. M. Abraham, A. Wanner, and U. S. Ryan, "Microvascular and macrovascular endothelial cells produce different constrictor substances," *Journal of Applied Physiology*, vol. 72, no. 5, pp. 1681–1686, 1992.

[71] Q. Wang, G. R. Pfeiffer II, T. Stevens, and C. M. Doerschuk, "Lung microvascular and arterial endothelial cells differ in their responses to intercellular adhesion molecule-1 ligation," *American Journal of Respiratory and Critical Care Medicine*, vol. 166, no. 6, pp. 872–877, 2002.

[72] N. Matsuda, S. Yamamoto, K.-I. Takano et al., "Silencing of Fas-associated death domain protects mice from septic lung inflammation and apoptosis," *American Journal of Respiratory and Critical Care Medicine*, vol. 179, no. 9, pp. 806–815, 2009.

[73] N. Matsuda, H. Teramae, S. Yamamoto, K.-I. Takano, Y. Takano, and Y. Hattori, "Increased death receptor pathway of apoptotic signaling in septic mouse aorta: effect of systemic delivery of FADD siRNA," *American Journal of Physiology—Heart and Circulatory Physiology*, vol. 298, no. 1, pp. H92–H101, 2010.

[74] N. Matsuda, Y. Takano, S.-I. Kageyama et al., "Silencing of caspase-8 and caspase-3 by RNA interference prevents vascular endothelial cell injury in mice with endotoxic shock," *Cardiovascular Research*, vol. 76, no. 1, pp. 132–140, 2007.

[75] L. Galluzzi, J. M. Bravo-San Pedro, I. Vitale et al., "Essential versus accessory aspects of cell death: recommendations of the NCCD 2015," *Cell Death & Differentiation*, vol. 22, pp. 58–73, 2015.

[76] L. Galluzzi, I. Vitale, J. M. Abrams et al., "Molecular definitions of cell death subroutines: recommendations of the Nomenclature Committee on Cell Death 2012," *Cell Death and Differentiation*, vol. 19, no. 1, pp. 107–120, 2012.

[77] G. Matute-Bello, C. W. Frevert, and T. R. Martin, "Animal models of acute lung injury," *American Journal of Physiology—Lung Cellular and Molecular Physiology*, vol. 295, no. 3, pp. L379–L399, 2008.

[78] C. Xu, X. Wu, B. K. Hack, L. Bao, and P. N. Cunningham, "TNF causes changes in glomerular endothelial permeability and morphology through a Rho and myosin light chain kinase–dependent mechanism," *Physiological Reports*, vol. 3, no. 12, Article ID e12636, 2015.

[79] M. H. Wu, "Endothelial focal adhesions and barrier function," *The Journal of Physiology*, vol. 569, no. 2, pp. 359–366, 2005.

[80] E. L. Burnham, W. R. Taylor, A. A. Quyyumi, M. Rojas, K. L. Brigham, and M. Moss, "Increased circulating endothelial progenitor cells are associated with survival in acute lung injury," *American Journal of Respiratory and Critical Care Medicine*, vol. 172, no. 7, pp. 854–860, 2005.

[81] M. C. Yoder, "Progenitor cells in the pulmonary circulation," *Proceedings of the American Thoracic Society*, vol. 8, no. 6, pp. 466–470, 2011.

[82] G. F. Curley, J. G. Laffey, H. Zhang, and A. S. Slutsky, "Biotrauma and ventilator-induced lung injury: clinical implications," *Chest*, vol. 150, no. 5, pp. 1109–1117, 2016.

[83] D. R. Potter and E. R. Damiano, "The hydrodynamically relevant endothelial cell glycocalyx observed in vivo is absent in vitro," *Circulation Research*, vol. 102, no. 7, pp. 770–776, 2008.

[84] M. I. Townsley, "Structure and composition of pulmonary arteries, capillaries, and veins," *Comprehensive Physiology*, vol. 2, no. 1, pp. 675–709, 2012.

[85] Y. Yang and E. P. Schmidt, "The endothelial glycocalyx: an important regulator of the pulmonary vascular barrier," *Tissue Barriers*, vol. 1, no. 1, Article ID e23494, 2013.

[86] C. J. Dente, C. P. Steffes, C. Speyer, and J. G. Tyburski, "Pericytes augment the capillary barrier in in vitro cocultures," *Journal of Surgical Research*, vol. 97, no. 1, pp. 85–91, 2001.

[87] D. A. Edelman, Y. Jiang, J. Tyburski, R. F. Wilson, and C. Steffes, "Pericytes and their role in microvasculature homeostasis," *Journal of Surgical Research*, vol. 135, no. 2, pp. 305–311, 2006.

Hindawi Publishing Corporation
Mediators of Inflammation
Volume 2016, Article ID 9461289, 16 pages
http://dx.doi.org/10.1155/2016/9461289

Research Article

Glutathione Peroxidase-1 Suppresses the Unfolded Protein Response upon Cigarette Smoke Exposure

Patrick Geraghty,[1,2] Nathalie Baumlin,[3] Matthias A. Salathe,[3] Robert F. Foronjy,[1,2] and Jeanine M. D'Armiento[4]

[1]*Division of Pulmonary & Critical Care Medicine, Department of Medicine, State University of New York Downstate Medical Center, Brooklyn, NY, USA*
[2]*Department of Cell Biology, State University of New York Downstate Medical Center, Brooklyn, NY, USA*
[3]*Division of Pulmonary, Allergy, Critical Care, and Sleep Medicine, University of Miami, Miami, FL, USA*
[4]*Center for Pulmonary Disease, Department of Anesthesiology, College of Physicians and Surgeons, Columbia University, New York, NY, USA*

Correspondence should be addressed to Patrick Geraghty; patrick.geraghty@downstate.edu

Received 18 August 2016; Revised 19 October 2016; Accepted 31 October 2016

Academic Editor: Karen Ridge

Oxidative stress provokes endoplasmic reticulum (ER) stress-induced unfolded protein response (UPR) in the lungs of chronic obstructive pulmonary (COPD) subjects. The antioxidant, glutathione peroxidase-1 (GPx-1), counters oxidative stress induced by cigarette smoke exposure. Here, we investigate whether GPx-1 expression deters the UPR following exposure to cigarette smoke. Expression of ER stress markers was investigated in fully differentiated normal human bronchial epithelial (NHBE) cells isolated from nonsmoking, smoking, and COPD donors and redifferentiated at the air liquid interface. NHBE cells from COPD donors expressed heightened ATF4, XBP1, GRP78, GRP94, EDEM1, and CHOP compared to cells from nonsmoking donors. These changes coincided with reduced GPx-1 expression. Reintroduction of GPx-1 into NHBE cells isolated from COPD donors reduced the UPR. To determine whether the loss of GPx-1 expression has a direct impact on these ER stress markers during smoke exposure, *Gpx-1*$^{-/-}$ mice were exposed to cigarette smoke for 1 year. Loss of *Gpx-1* expression enhanced cigarette smoke-induced ER stress and apoptosis. Equally, induction of ER stress with tunicamycin enhanced antioxidant expression in mouse precision-cut lung slices. Smoke inhalation also exacerbated the UPR response during respiratory syncytial virus infection. Therefore, ER stress may be an antioxidant-related pathophysiological event in COPD.

1. Introduction

Chronic obstructive pulmonary disease (COPD) is the third leading cause of death in the US [1], with cigarette smoking being the most important environmental risk factor. Cigarette smoke inhalation alters the expression profile of oxidants and antioxidants in the lungs and produces an enormous oxidant burden [2]. Antioxidant enzymes counter this oxidative stress [2] and deter lung inflammation responses by targeting multiple signaling pathways [3]. Detoxifying reactive oxygen species (ROS) is a therapeutic strategy to limit tissue damage in cigarette smoke-induced diseases [3]. Recently, cigarette smoke-mediated oxidative stress was shown to induce endoplasmic reticulum (ER) stress [4]. However, the ability of antioxidants to counter ER stress has not been fully characterized.

It is well established that cigarette smoke induces ER stress which activates the unfolded protein response (UPR) [5–9]. However, COPD is a complex heterogeneous disease and the significance and intensity of the UPR during the disease is unknown. The UPR is a complex stress response program that modulates multiple cellular responses and survival, via regulation of protein synthesis, folding, and degradation [10]. Three major pathways of the UPR have been characterized: (i) PKR-like ER kinase (PERK)/eIF2α/activating transcription factor (ATF) 4/CHOP, (ii) inositol-requiring

enzyme 1 (IRE1)/X-box binding protein 1 (XBP1), and the (iii) ATF6 pathway [11]. These pathways regulate ER chaperone responses and reduce protein translation following cellular stress [12]. However, persistent ER stress results in significant expression of the proapoptotic gene C/EBP homologous protein (CHOP), resulting in cell death [11]. We previously demonstrated that smoke exposure triggers a minor ER stress response in primary cells and rodent animal models [5]. However, a secondary insult may be required to provoke a significant smoke-induced UPR.

Our group demonstrated that overexpression of glutathione peroxidase- (GPx-) 1, a member of the selenoprotein family, prevents cigarette smoke-induced air space enlargement in mice [13]. GPx-1 is the most abundant GPx isoform in eukaryotic cells and deficiency of this enzyme can lead to endothelial dysfunction [14] and apoptosis [15]. GPx-1 deficiency has also been implemented as a contributor to atherosclerosis [16]. *Gpx-1* deficient mice exposed to cigarette smoke are more susceptible to cigarette smoke-induced lung inflammation and emphysema [13, 17]. Oxidative stress induces ER stress [4] and increased expression of ER stress markers is observed in the lungs of smokers [8]. GPx-1 expression, however, is reduced in COPD lungs [13]. Thus, we speculate that GPx-1 could modulate ER stress responses linked to the pathogenesis of COPD.

In view of the potential association between GPx-1 and cigarette smoke-mediated UPR, we explored whether the loss of GPx-1 expression enhanced the UPR that contributes to lung cell injury and death. Using normal human bronchial epithelial (NHBE) cells from nonsmokers, smokers, and COPD subjects, we found that ER stress markers were significantly elevated in cells isolated from COPD subjects and this increase coincided with reduced GPx-1 expression. Reintroducing GPx-1 into these cells blunted the UPR. To determine if GPx-1 depletion in the lung directly enhances ER stress, *Gpx-1*$^{-/-}$ mice were exposed to cigarette smoke for 1 year. Interestingly, the loss of GPx-1 expression activated all three branches of the UPR, PERK/eIF2α/ATF4/CHOP, IRE1/XBP1, and ATF6. This UPR coincided with elevated lung cell death in *Gpx-1*$^{-/-}$ mice following smoke exposure. Interestingly, precision-cut lung slices (PCLS) from mice had elevated GPx proteins following induction of ER stress. These findings indicate that the altered GPx-1 expression in COPD lungs contributes to heightened ER stress. In addition, early induction of ER stress induces an antioxidant response to counter oxidative stress, thereby limiting the UPR.

2. Materials and Methods

2.1. Human Primary Airway Cells. NHBE cells from nonsmokers, smokers, and COPD patients were isolated from human lungs. Lungs were obtained from organ donors whose lungs were rejected for transplant (see Table 1 for demographics). Consent for research was obtained by the Life Alliance Organ Recovery Agency of the University of Miami. All consents were IRB-approved and conformed to the Declaration of Helsinki. For lungs from donors with COPD, the diagnosis was listed in the chart before the death of the donor and we confirmed the macropathological presence of emphysema in these lungs. All COPD subjects had a significant smoking history. NHBE cells isolated from nonsmokers, smokers, and COPD subjects were dedifferentiated through expansion and redifferentiated at an air liquid interface (ALI) on 24 mm T-clear filters (Costar Corning, Corning, NY, USA) at 37°C, 5% CO_2, as previously described [18]. Cells were collected for protein and RNA analysis. CD45 and CD11C expressions were analyzed which determined a low level of inflammatory-cell contamination and confirmed NHBE cell purity. Fully differentiated NHBE cells from nonsmokers were also exposed to cigarette smoke using a Vitrocell VC-10 smoking robot (Vitrocell Systems GMBH, Waldkirch, Germany). Four cigarettes were smoked according to ISO standard 3308: six puffs per cigarette with a 35 mL volume per puff and a waiting time between each puff of 60 seconds. NHBE cells were exposed every second day, on three separate days, to 4 cigarettes. RNA was extracted from the NHBE cells for quantitative PCR (qPCR) analysis. A subset of NHBE cells from COPD subjects was protein transfected 2 μg human GPx-1 protein or human albumin (both from Signal Aldrich) using Pierce transfection reagent (ThermoFisher Scientific) as previously described [13, 19]. RNA and protein were collect 24 hours later. Human RSV strain A2 (ATCC, Manassas, VA; #VR-1540) was infected in NHBE cells as previously described [20]. RNA and protein were collect 24 hours later.

Table 1: Donor demographics for epithelial cell.

	Nonsmokers	Smokers	COPD donors
Number	9	6	9
Age (years)	36.3 ± 14.8	36.0 ± 13.2	49 ± 6.8
Gender (male/female)	2/7	3/3	5/4
Race (Caucasian/African American)	77.8%/22.2%	100%/0%	88.90%/11.1%
Pack years	0 ± 0	N/A	48.2 ± 14.5

Values are means ± SD. N/A = not available.

2.2. Animal Models. *Gpx-1*$^{-/-}$ mice were bred in C57BL/6 × CBA/J background. Eight-week-old wild type and *Gpx-1*$^{-/-}$ mice were used for all experiments. All mice were maintained in a specific pathogen-free facility at Columbia University. Both male and female mice, 8-week-old, were used at the initiation point for all experiments and each experimental parameter had at least 10 animals per group. Mice were exposed to cigarette smoke in a chamber (Teague Enterprises, Davis, CA, USA) for four hours a day, five days per week at a total particulate matter concentration of 80 mg/m^3. Smoke exposure was continued for 1 year. The University of Kentucky reference research cigarettes 3R4F (Lexington, KY, USA) were used to generate cigarette smoke. Another group of wild type animals was infected with 1×10^6 pfu of RSV following 6-month exposure to room air or cigarette smoke. The institute approved all experiments for Animal Care and Use Committee of Columbia University. This study was performed in strict accordance with the recommendations in the Guide for the

Table 2: TaqMan probe details for gene expression analysis.

Species	Gene target	NCBI reference sequence	TaqMan assay ID	Product size
Human	*DDIT3 (CHOP)*	NM_001195053.1	Hs00358796_g1	93
Human	*ATF4*	NM_001675.2	Hs00909569_g1	68
Human	*XBP1*	NM_001079539.1	Hs00231936_m1	60
Human	*HSPA5 (GRP78)*	NM_005347.4	Hs00607129_gH	146
Human	*HSP90B1 (GRP94)*	NM_003299.2	Hs00427665_g1	135
Human	*EDEM1*	NM_014674.2	Hs00976004_m1	89
Human	*GPX1 (GPx-1)*	NM_201397.1	Hs01028922_g1	70
Human	*IL-6*	NM_000600.3	Hs00985639_m1	66
Human	*ACTB*	NM_001101.3	Hs01060665_g1	63
Human	*PPFIA2 (CD45)*	NM_001220473.1	Hs00170308_m1	66
Human	*ITGAX (CD11C)*	NM_000887.3	Hs00174217_m1	119
Mouse	*Ddit3 (Chop)*	NM_001290183.1	Mm01135937_g1	92
Mouse	*Atf4*	NM_001287180.1	Mm00515325_g1	78
Mouse	*Xbp1*	NM_001271730.1	Mm00457357_m1	56
Mouse	*Hspa5 (Grp78)*	NM_001163434.1	Mm00517691_m1	75
Mouse	*Hsp90b1 (Grp94)*	NM_011631.1	Mm00441926_m1	67
Mouse	*Edem1*	NM_138677.2	Mm00551797_m1	63
Mouse	*Gpx-1*	NM_008160.6	Mm00656767_g1	134
Mouse	*Gpx-2*	NM_030677.2	Mm00850074_g1	147
Mouse	*Gpx-3*	NM_008161.3	Mm00492427_m1	99
Mouse	*Gpx-4*	NM_008162.3	Mm00515041_m1	103
Mouse	*Sod1*	NM_011434.1	Mm01344233_g1	71
Mouse	*Actb*	AK075973.1	Mm02619580_g1	143

Care and Use of Laboratory Animals of the National Institutes of Health and Institutional Animal Care and Use Committee (IACUC) guidelines.

2.3. Precision-Cut Lung Slices (PCLS). Mouse precision-cut lung slices (PCLS) were prepared as previously described [21, 22]. Briefly, mice were euthanized, the trachea was cannulated, and the animal was exsanguinated by cutting the jugular vein. The lungs were filled through the cannula with 1.5 mL low melting-point agarose solution (1.5% final concentration of agarose in PBS). Lungs were placed on ice for 15 minutes to solidify the agarose. Lobes were separated and tissue cores were prepared of the individual lobes, after which the lobes were sliced at a thickness of 300 μm using a Krumdieck tissue slicer (Alabama Research and Development, Munford, AL, USA) in Earle's balanced salt solution (Sigma Aldrich). Tissue slices were incubated in Dulbecco's modified eagle's medium/nutrient mixture F-12 HAM solution (Sigma Aldrich) at 37°C in a humid atmosphere under 5% CO_2/95% air. To remove agarose and cell debris, slices were washed every 30 minutes for 2 hours. PCLS were incubated in DMEM supplemented with penicillin (100 U/mL) and streptomycin (100 μg/mL) (Gibco® by Life Technologies). Slices were cultured at 37°C in a humidified atmosphere under 5% CO_2/95% air in 6-well tissue culture plates, using 3 slices per well. Slices were treated with 1 μM tunicamycin (Sigma Aldrich) for 24 hours. To assess the viability of the PCLS subjected to tunicamycin, lactate dehydrogenase (LDH) released from the PCLS into the incubation medium was analyzed. Maximal LDH release was determined by lysing 3 slices with 1% Triton X-100 for 30 minutes at 37°C. LDH release was determined using an assay form Sigma Aldrich.

2.4. qPCR Analysis. Total RNA was isolated from cells or mouse lung tissue using the Qiagen RNeasy Mini Kit as described by manufactures. Gene transcript levels of mouse and human specific CHOP, ATF4, XBP1, GRP78, GRP94, EDEM1, GPx-1, GPx-2, GPx-3, GPx-4, IL-6, and ACTB were quantified by real-time PCR with the use of an Bio-Rad CFX384 real-time system (Bio-Rad). TaqMan® Gene Expression Assays were purchased from Applied Biosystems (see Table 2 for details). Data is represented as relative quantification (RQ) corrected to ACTB. XBP1 splicing was also examined in NHBE cells using the following primers: 5′-TTA CGA GAG AAA ACT CAT GGC-3′ and 5′-GGG TCC AAG TTG TCC AGA ATG C-3′. XBP1 PCR products were resolved and run on a 2.5% agarose gel [23]. 289 and 286 base pair amplicons were generated from unspliced and spliced XBP1, respectively. Percent of XBP1 slicing was examined by densitometry analysis of the unspliced (XBP1u) and spliced (XBP1s) amplicons of XBP1, using Bio-Rad Laboratories Image Lab software (version 4.0, build 16).

2.5. Immunoblotting. Cell monolayers were removed by scrapping in cold phosphate-buffered saline and resuspended

in 100 μL of protein lysis buffer (50 mM HEPES, pH 7.5, 150 mM NaCl, 1% Triton X-100, 1% glycerol, 1 mM EDTA, 10 mM NaF, 2 μg/mL leupeptin, 1 μg/mL pepstatin A, 10 mM Na_3VO_4, and 1 mM phenylmethylsulfonyl fluoride), and 20 μg of protein was separated on 12% SDS-polyacrylamide gels and transferred to nitrocellulose membranes. Rabbit antibodies against CHOP (Cell Signaling; #5554), ER degradation-enhancing α-mannosidase-like (EDEM) (Santa Cruz Biotechnology; sc-27389), pho-eIF2α (Ser51) (Cell Signaling; #9721), eIF2α (Cell Signaling; #9722), pho-PERK (Thr980) (Cell Signaling; #3179), PERK (Cell Signaling; #5683), XBP-1 (Cell Signaling; #12782), IRE1α (Cell Signaling; #3294), BiP/GRP78 (Cell Signaling; #3183), GRP94 (Cell Signaling; #2104), ATF4 (Cell Signaling; #11815), ATF6 (Abcam; #ab11909), GPx-1 (Cell Signaling; #3206), GPx-2 (Abcam; #ab140130), GPx-3 (Abcam; #ab27325), GPx-4 (Cell Signaling; #2104), and β-actin (Cell Signaling; #4970) were detected with enhanced chemiluminescence reagents (Pierce). Chemiluminescence detection was performed using the Bio-Rad Laboratories Molecular Imager ChemiDoc XRS+ imaging system. Densitometry was performed on each target and represented as a ratio of pixel intensity compared to total protein or β-actin, using Bio-Rad Laboratories Image Lab software (version 4.0, build 16).

2.6. Statistical Analysis. Data are expressed as dot plots with the means ± SEM highlighted. Differences between two groups were compared by Student's t test (two-tailed). Experiments with more than 2 groups were analyzed by 2-way ANOVA with Tukey's *post hoc* test analysis. p values for significance were set at 0.05 and all significant changes were noted with $*$. All analysis was performed using GraphPad Prism Software (Version 6.0h for Mac OS X).

3. Results

3.1. NHBE Cells Isolated from COPD Donors Express More ER Stress Markers than Cells from Smokers. Our group previously demonstrated that undifferentiated NHBE cells have an increased trend in ER stress upon exposure to cigarette smoke extract (CSE) [5]. To examine whether fully differentiated NHBE cells cultured at the air liquid interface (ALI) have an UPR to smoke, NHBE cells from nonsmokers were exposed to 0 (room air, RA) or repeat exposure to four cigarettes (CS) using a Vitrocell VC-10 smoking robot (Figures 1(a)-1(b)). Repeat exposures were performed to maximize smoke stimuli without inducing apoptosis, determined by LDH release assays (Figure 1(a)). Gene expression of IL-6 was utilized as a positive control for sufficient exposure to smoke [20] (Figure 1(a)). CD45 and CD11C expressions were analyzed but detection was below significant amplification levels thereby confirming low levels of inflammatory-cell contamination (data not shown). Gene expression levels of *ATF4, XBP1, GRP78, GRP94, EDEM1,* and *CHOP* were examined. These targets are readouts for the three major pathways of the UPR. No ER stress marker was significantly altered following smoke exposure (Figure 1(b)), as we previously described in submerged cultured NHBE cells [5]. However, when comparing the same ER stress markers in NHBE cells isolated from nonsmokers, smokers, and COPD donors, expressions of *ATF4*, *XBP1*, *GRP78*, *GRP94*, *EDEM1,* and *CHOP* were all increased in cells isolated from COPD subjects (Figure 1(c)). *EDEM1* gene expression was significantly enhanced in cells isolated from smokers (Figure 1(c)). There were increased trend changes for ER stress markers in cells from smokers. Protein analysis also confirmed increased expression of ATF4, IRE1α, GRP78, GRP94, EDEM, and CHOP in cells isolated from COPD subjects (Figure 2(a)). Equally, elevated phosphorylation of eIF2 and PERK was observed only in cells isolated from COPD donors (Figure 2(a)).

XBP1 coordinates the adaptive UPR by playing a vital role in maintaining the ER function. Gene expression results showed that NHBE cells isolated from COPD subjects had enhanced XBP1 mRNA splicing compared to cells from nonsmokers and smokers (Figure 2(b)), demonstrating active XBP1 signaling; Protein analysis also confirmed increased expression of XBP1 in cells isolated from COPD donors (Figure 2(b)). Overall, the disease-state predisposes NHBE cells to enhanced ER stress. On the other hand, acute smoke exposure has only a minor impact on ER stress.

3.2. GPx-1 Regulates CHOP Expression in NHBE Cells Isolated from COPD Donors. Since oxidative stress induces ER stress [4], GPx-1 expression is reduced in the COPD lungs [13], and GPx-1 deficiency increases susceptibility to cigarette smoke-induced emphysema [13, 17], we examined whether GPx-1 expression was altered in fully differentiated NHBE cells isolated from nonsmokers, smokers, and COPD donors (Figure 3). GPx-1 expression was unchanged in NHBE cells from nonsmokers when exposed to cigarette smoke (Figure 3(a)). NHBE cells from nonsmokers and smokers expressed comparable levels of GPx-1 (Figures 3(b)-3(c)). However, cells isolated from COPD subjects had significantly reduced GPx-1 expression, confirmed by q-PCR (Figure 3(b)) and immunoblots (Figure 3(c)). Therefore, the disease-state predisposes NHBE cells to subdued GPx-1 expression.

To determine whether restoring GPx-1 levels in NHBE cells from COPD subjects would reverse heightened UPR, we protein-transfected GPx-1 protein into NHBE cells from COPD subjects. Albumin was transfected as a negative control. Transfection of GPx-1 significantly reduced CHOP gene (Figure 3(d)) and protein (Figure 3(e)) expression in NHBE cells from COPD subjects. Therefore, GPx-1 is a potent regulator of the UPR in the lungs.

3.3. Viral Exacerbations of the Lung Enhance the UPR. To determine whether a second environmental exposure could alter the UPR in our models, we infected NHBE cells and mice with respiratory syncytial virus (RSV). Viral infections have been implicated in the pathogenesis of COPD exacerbations [24, 25] and also trigger the UPR [26]. RSV infected reduced GPx-1 expression and significantly enhanced CHOP expression in NHBE cells from all subject groups (Figures 4(a)-4(b)). Similar changes to CHOP and GPx-1 expression were observed in the lungs of mice infected with RSV (Figures 4(c)-4(d)). Importantly, prior exposure to cigarette smoke

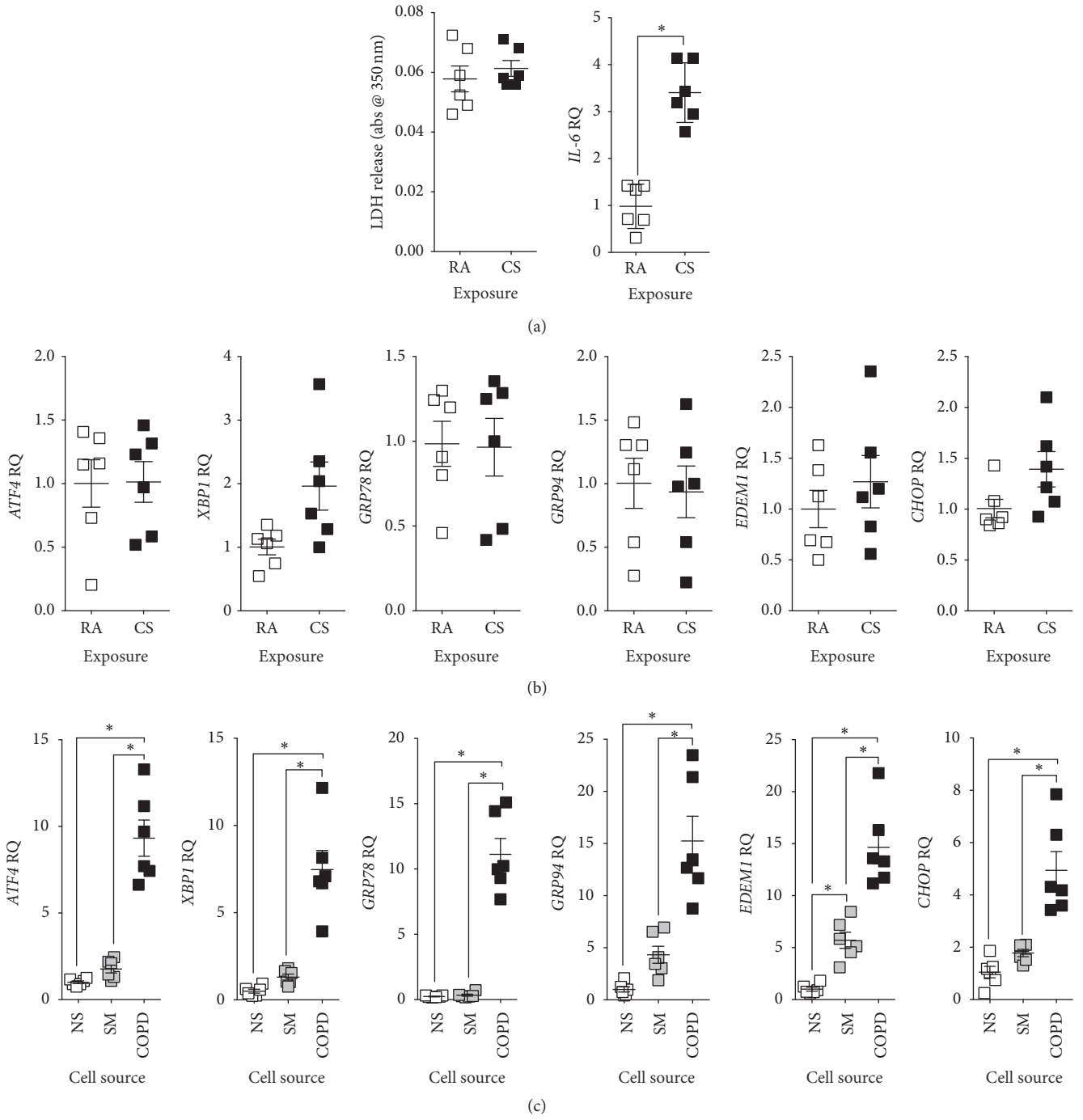

Figure 1: NHBE cells isolated from COPD donors have enhanced ER stress responses compared to nonsmokers and smokers. (a) Fully differentiated NHBE cells from nonsmoking individuals ($n = 6$) exposed to room air (RA) or cigarette smoke (CS) from 4 cigarettes every second day (3 exposures) using a Vitrocell VC-10 smoking robot. LDH release into media and *IL-6* gene expression were examined. (b) Gene expression of *ATF4*, *XBP1*, *GRP78*, *GRP94*, *EDEM1,* and *CHOP* was examined. (c) Fully differentiated NHBE cells from nonsmoker (NS), smoker (SM), and COPD (COPD) individuals ($n = 6$ donors per group) were examined for gene expression of *ATF4*, *XBP1*, *GRP78*, *GRP94*, *EDEM1,* and *CHOP*. Dot plots are represented as relative quantification (RQ) compared to ACTB expression and shown as the mean ± SEM, where each measurement was performed on 3 independent days on 6 donors/group. ∗ denotes p value < 0.05, when comparing both treatments connected by a line, determined by Student's t-test (2 groups) or 2-way ANOVA with Tukey's *post hoc* test (>2 groups).

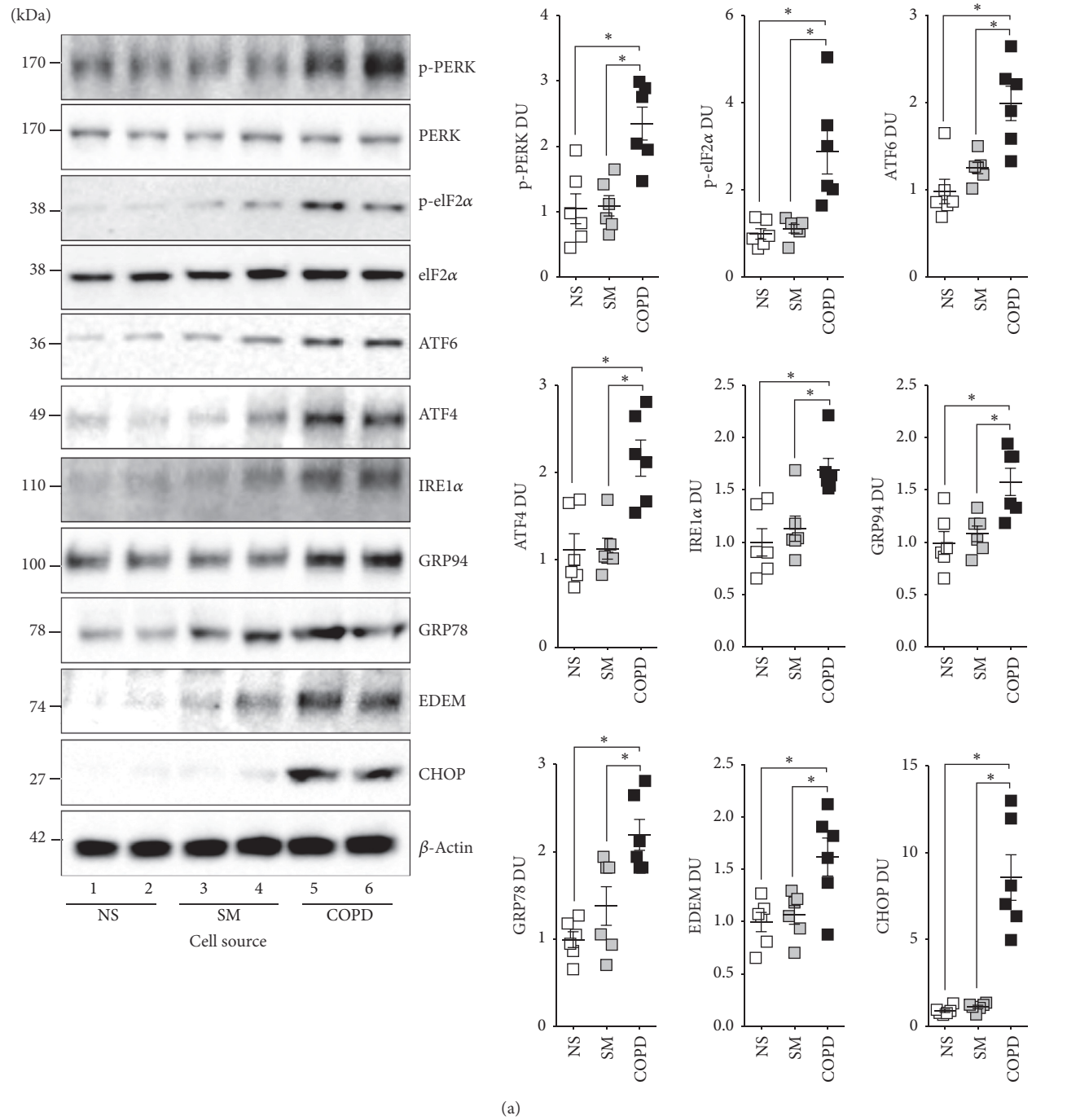

(a)

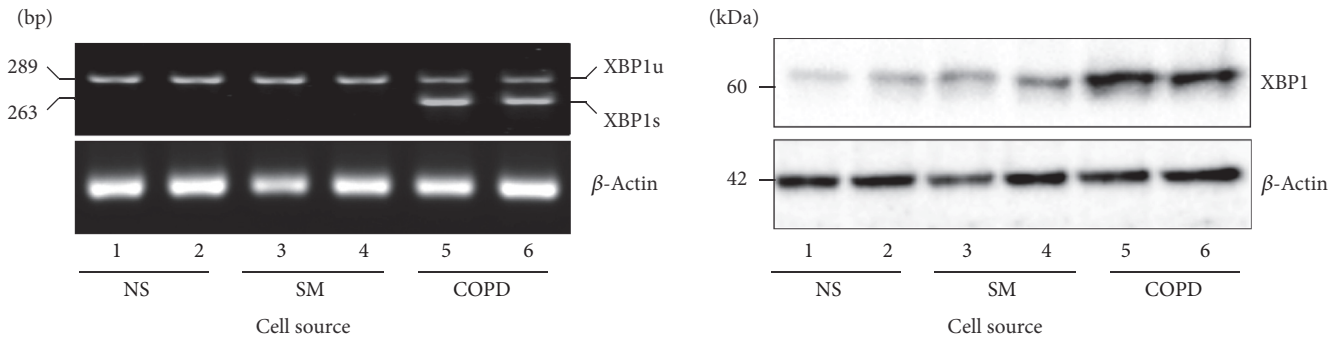

Figure 2: Continued.

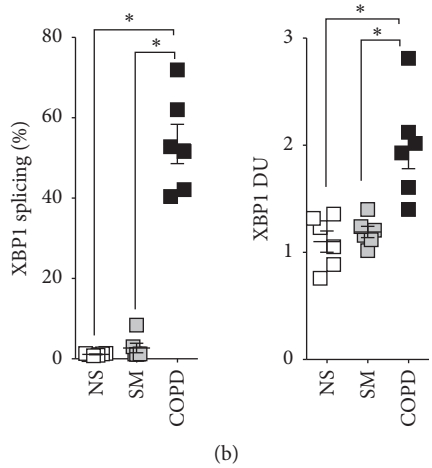

(b)

Figure 2: NHBE cells isolated from COPD donors have enhanced ER stress protein responses compared to nonsmokers and smokers. Protein was collected from fully differentiated NHBE cells from nonsmokers (NS), smokers (SM), and COPD (COPD) individuals ($n = 6$ donors per group). (a) Protein expression of ATF6, ATF4, GRP94, GRP78, EDEM, CHOP, and β-actin was examined by immunoblots. Phosphorylation of elF2 and PERK was also determined. (b) XBP1 splicing was examined on XBP1 amplified cDNA from NHBE cells from nonsmoker (NS), smokers (S), and COPD (COPD) individuals. Protein expression of XBP1 and β-actin was examined by immunoblots. (a)-(b) For each blot or gel, every lane represents an individual cell donor. Densitometry analysis was performed of XBP1s from DNA gels and other targets by analyzing immunoblots. XBP1 slicing was scored as percent of XBP1s of total XBP1. Dot plots are represented as densitometry units (DU) of pixel intensity expressed as a ratio to β-actin or total elF2 and PERK. Data are shown as mean ± SEM, where each measurement was performed on 3 independent days on 6 donors/group. $*$ denotes p value < 0.05, when comparing both treatments connected by a line, determined by 2-way ANOVA with Tukey's *post hoc* test (>2 groups).

enhanced the UPR in animals also infected with RSV compared to infected animals exposed to room air (RA) (Figure 4(d)). Therefore, the lungs of smokers and COPD subjects are likely to be more sensitive to viral infection induced ER stress, which may impact disease progression.

3.4. Gpx-1$^{-/-}$ Mice Have Heightened ER Stress and Apoptosis following Cigarette Smoke Exposure. To determine whether the loss of GPx-1 expression directly influences ER stress following inhalation of cigarette smoke *in vivo*, we examined ER stress markers in *Gpx-1*$^{-/-}$ mice and their wild type littermates exposed to cigarette smoke for 1 year. We previously demonstrated that loss of *Gpx-1* expression in mice results in enhanced air space enlargement and inflammation following long-term cigarette smoke exposure [13]. Expression levels of *Atf4*, *Xbp1*, *Grp78*, *Grp94*, *Edem1,* and *Chop* were examined in *Gpx-1*$^{-/-}$ and wild type mice. Long-term exposure to cigarette smoke did not significantly enhance ER stress marker expression in the lungs of wild type mice (Figure 5(a)). We previously observed similar findings in wild type mice [5]. However, *Gpx-1*$^{-/-}$ mice exposed to cigarette smoke had enhanced gene expression of *Atf4*, *Xbp1*, *Grp78*, *Grp94*, *Edem1,* and *Chop* (Figure 5(a)). Equally, loss of *Gpx-1* expression resulted in elevated lung tissue protein levels of ATF4, XBP1, GRP78, GRP94, EDEM, and CHOP following smoke exposure (Figure 5(b)). Densitometry analysis confirmed significant increases in lung levels of ATF4, XBP1, GRP78, GRP94, EDEM, and CHOP in *Gpx-1*$^{-/-}$ mice exposed to cigarette smoke (Figure 5(b)).

Prolonged activation of CHOP by ER stress can result in cellular apoptosis. Increased structural and immune cell apoptosis is also observed in COPD lungs [27]. Therefore, we examined whether *Gpx-1*$^{-/-}$ mice exposed to cigarette smoke had elevated apoptosis. *Gpx-1*$^{-/-}$ mice exposed to cigarette smoke had enhanced lung cell apoptosis, observed by TUNEL, caspase-3 cleavage, and lactate dehydrogenase (LDH) release assays (Figure 6). *Gpx-1*$^{-/-}$ mice exposed to cigarette smoke exhibited the highest frequency of TUNEL positive cells (Figure 6(a)). Enhanced caspase-3 cleavage was observed in *Gpx-1*$^{-/-}$ mice exposed to cigarette smoke (Figure 6(b)). Additionally, elevated levels of LDH were observed in the BALF of *Gpx-1*$^{-/-}$ mice exposed to cigarette smoke compared to the other groups (Figure 6(c)), which indicates enhanced cell membrane damage in the lung. Therefore, enhanced apoptosis in the lungs could contribute to lung remodelling and failure to clear apoptotic cells could contribute to lung inflammation.

3.5. Triggering the UPR Enhances GPx-1, GPx-2, and GPx-4 Expression in Mouse Precision-Cut Lung Slices. In *Gpx-1* and *Gpx-2* double knockout mice, apoptotic cells are increased in ileal crypts [28], suggesting that GPx proteins regulate apoptosis. However, the effect of ER stress on GPx proteins has not been directly investigated. To determine the effect of ER stress on GPx-1 expression, mouse precision-cut lung slices (PCLS) were exposed to the ER stress inducer, tunicamycin, for 24 hours. The concentration of tunicamycin tested did not induce LDH release from the PCLS (Figure 7(a)), indicating

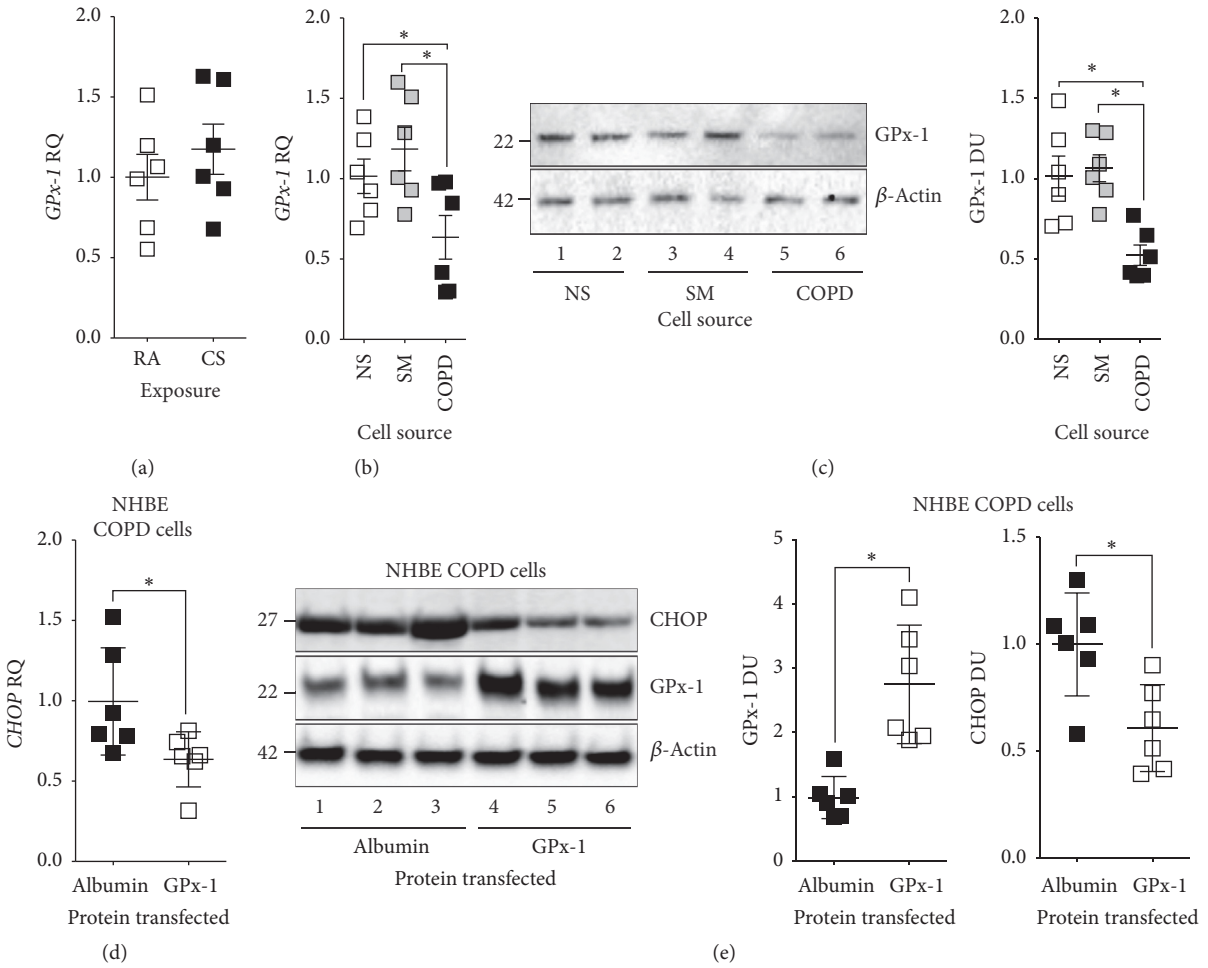

Figure 3: Reintroducing GPx-1 into NHBE cells isolated from COPD donors subdues the UPR. (a) Gene expression of *GPx-1* was determined in fully differentiated NHBE cells from nonsmoking individuals ($n = 6$) exposed to room air (RA) and cigarette smoke (CS; from 4 cigarettes every second day (3 exposures)) using a Vitrocell VC-10 smoking robot (b) RNA and (c) protein was analyzed for GPx-1 expression from fully differentiated NHBE cells from nonsmoker (NS), smokers, (SM) and COPD (COPD) individuals ($n = 6$ donors per group). (d) NHBE cells isolated from COPD subjects were transfected with albumin or GPx-1 protein and *CHOP* expression was determined by qPCR. (e) Immunoblots and corresponding densitometry analysis for CHOP, Gpx-1, and β-actin from NHBE cells from COPD subjects following albumin or GPx-1 protein transfection. In each immunoblot, every lane represents an individual cell donor. Data are shown as mean ± SEM, where each measurement was performed on 3 independent days on 6 donors/group. $*$ denotes a p value < 0.05, when comparing both treatments connected by a line, determined by Student's t-test (2 groups) or 2-way ANOVA with Tukey's *post hoc* test (>2 groups).

no induction of apoptosis. Tunicamycin induced all three branches of the UPR and CHOP expression was observed in PCLS (Figures 7(b)-7(c)). Tunicamycin enhanced gene (Figure 7(b)) and protein (Figure 7(c)) expression of ATF4, XBP1, ATF6, and CHOP in PCLS. Interestingly, tunicamycin induced GPx-1, GPx-2, and GPx-4 gene (Figure 7(d)) and protein (Figure 7(e)) expression in PCLS. Therefore, an acute ER stress induces the expression of antioxidants to counter further oxidant and ER stress.

4. Discussion

Cigarette smoking is the most relevant environmental risk factor associated with the development of COPD. However, smoke inhalation studies are problematic as long-term smoke exposure is required to trigger disease formation in animal models and a secondary event may be required to mimic the human disease-state. Here we observed that the loss of GPx-1 expression enhances cigarette smoke-induced ER stress. GPx-1 regulates the UPR following smoke exposure and we found that the expression of GPx-1 itself was triggered by an acute ER stress stimulus. NHBE cells isolated from COPD donors expressed significantly less GPx-1, which coincides with elevated UPR. Reintroducing GPx-1 protein into NHBE cells isolated from COPD donors reduced the UPR. RSV infection contributes to loss of lung GPx-1 expression, which is exaggerated in lungs exposed to smoke and coincides with elevated UPR. *Gpx-1*$^{-/-}$ mice exhibited greater UPR and subsequent enhanced apoptosis following long-term cigarette smoke exposure. Interestingly, triggering an acute ER stress in

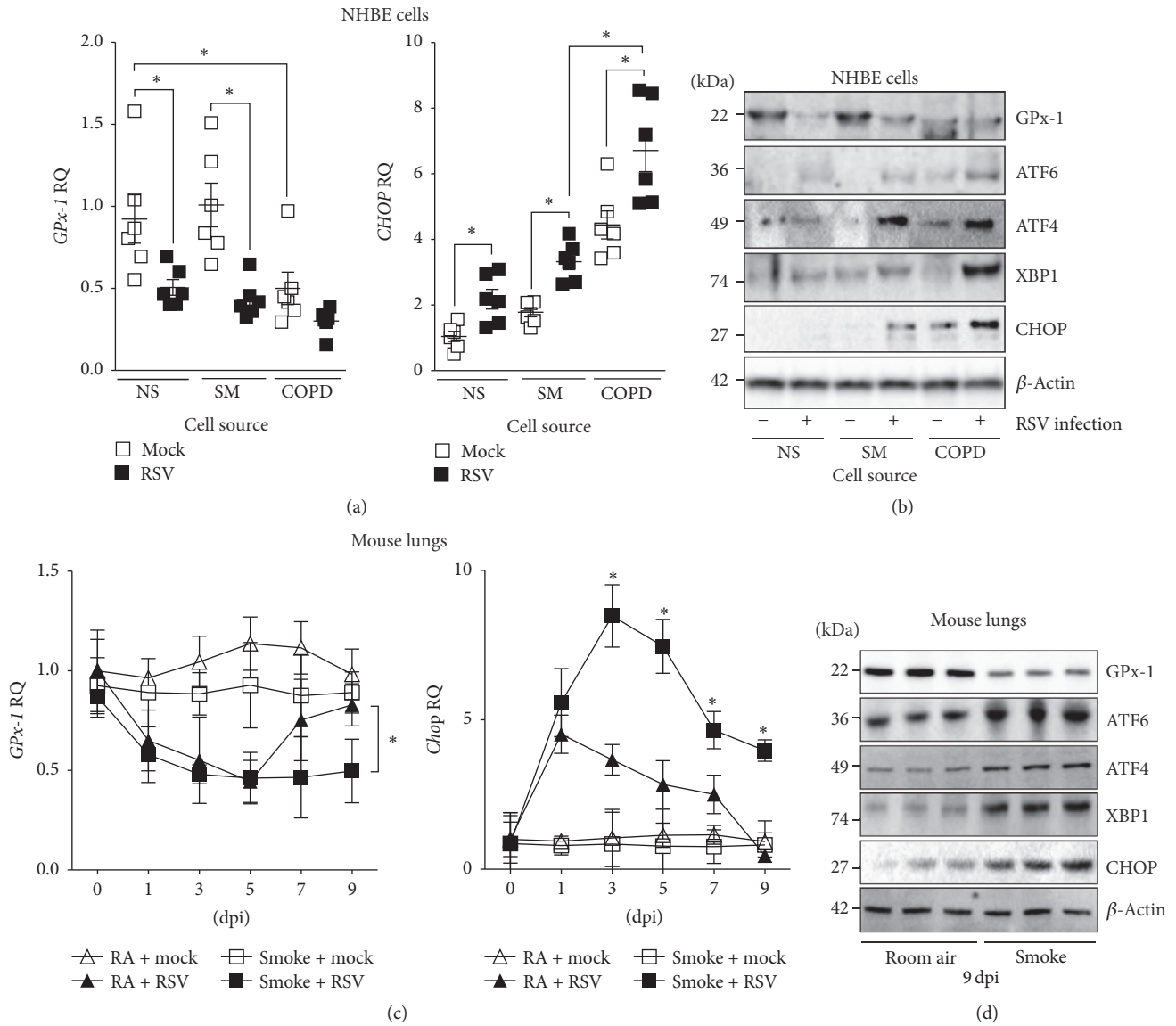

Figure 4: RSV infection enhances the UPR in the lung. (a) GPx-1 and CHOP gene expression were determined in NHBE cells isolated from nonsmoker (NS), smokers (SM), and COPD (COPD) individuals ($n = 6$ donors per group) infected with mock or RSV and analyzed by qPCR. (b) Protein expression of GPx-1, ATF6, ATF4, CHOP, and β-actin was examined by immunoblots. (c) Wild type mice were exposed to cigarette smoke or room air for six months and subsequently infected with 1×10^6 pfu of RSV. Animals were euthanized at 0, 1, 3, 5, 7, and 9 days after infection (dpi) and *Gpx-1* and *Chop* expression were determined by qPCR. (d) Protein expression of GPx-1, ATF6, ATF4, CHOP, and β-actin was examined by immunoblots. Data are shown as mean ± SEM, where each measurement was performed on 3 independent days. $*$ denotes a p value < 0.05, when comparing both treatments connected by a line or the same infection day, determined by Student's t-test (2 groups) or 2-way ANOVA with Tukey's *post hoc* test (>2 groups).

the lungs of mice induces a potent antioxidant response. This antioxidant response is diminished in the COPD lungs [29], which may explain the heightened UPR observed in NHBE cells isolated from COPD subjects. The exact role of this heightened UPR on the progression of COPD still remains to be fully determined. However, we have established that loss of GPx-1 *in vivo* leads to a marked increased in all three branches of the UPR (see Figure 8 for proposed signaling scheme) and this coincides with enhanced apoptosis and lung tissue destruction in mice [13]. Our results suggest that GPx-1 significantly regulates the UPR in COPD and enhancing GPx-1 expression may be feasible means of offsetting the UPR and lung injury responses that drive the onset and progression of this disease.

Multiple studies utilizing the *Gpx-1*$^{-/-}$ and transgenic mice demonstrated the protective role of GPx-1 in countering oxidative injury and cell death mediated by ROS [13, 30]. GPX-1 activity also affects protein kinase phosphorylation [31] and oxidant-mediated activation of NF-κB [32]. In this current study, GPx-1 was significantly reduced in NHBE cells isolated from COPD subjects compared to nonsmokers and smokers. Others have reported that the alteration of GPx-1

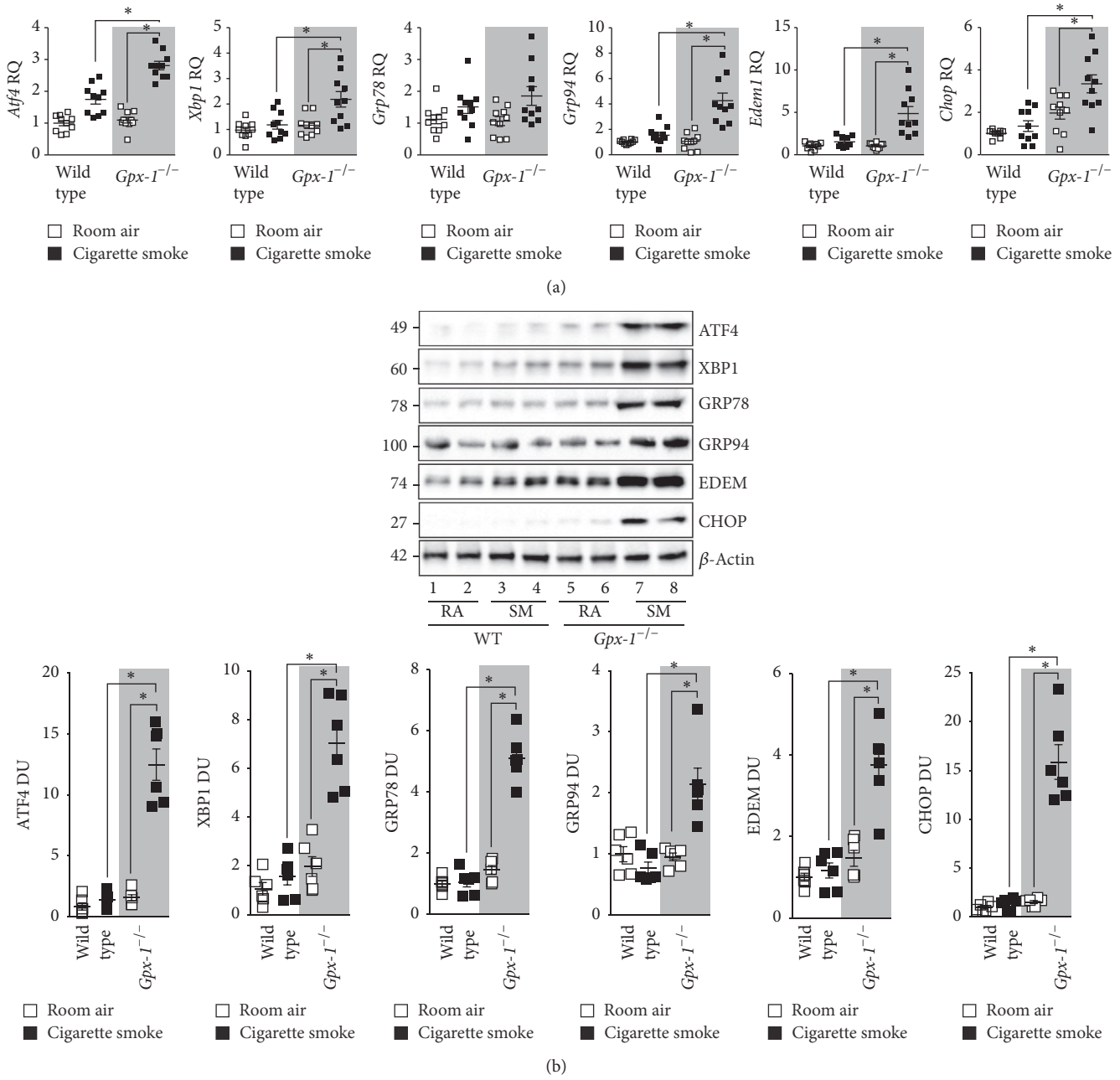

Figure 5: *Gpx-1* deficient mice have heightened ER stress in their lungs following exposure to cigarette smoke. *Gpx-1*$^{-/-}$ and wild type mice were exposed to cigarette smoke daily for 1 year. (a) Lung gene expression of *Chop*, *Atf4*, *Edem1*, *Grp78*, *Grp94*, and *Xbp1* was examined. (b) Immunoblots were performed of whole lung protein for CHOP, ATF4, EDEM, GRP78, GRP94, and XBP1. Dot plots are represented as (a) relative quantification (RQ) compared to ACTB expression or (b) densitometry units (DU) of pixel intensity expressed as a ratio to β-actin. Every lane represents an individual mouse. Data are shown as mean ± SEM, where each measurement was performed on 3 independent days on 6 donors/group. $*$ denotes a p value < 0.05, when comparing both treatments connected by a line, determined by 2-way ANOVA with Tukey's *post hoc* test (>2 groups).

expression does not affect the mRNA or activity expression of other selenoproteins [33], which suggests no compensation expression of other selenoproteins following loss of GPx-1 expression. Currently the mechanism by which cigarette smoke regulates GPx-1 expression is not fully elucidated but considering our GPx-1 reintroduction data further analysis of GPx-1 regulation is critical. GPx-1 expression and activity have been reported to be regulated by Nrf2 [34], the transcription factor TFAP2C [35], CpG methylation of the GPx-1 promoter [35], Bcr-Abl/mTOR [36], selenium [37], estrogen [38], adenosine [39], Sec-insertion sequence (SECIS) factors [40], EGFR [41], and homocysteine [42]. Specifically, within

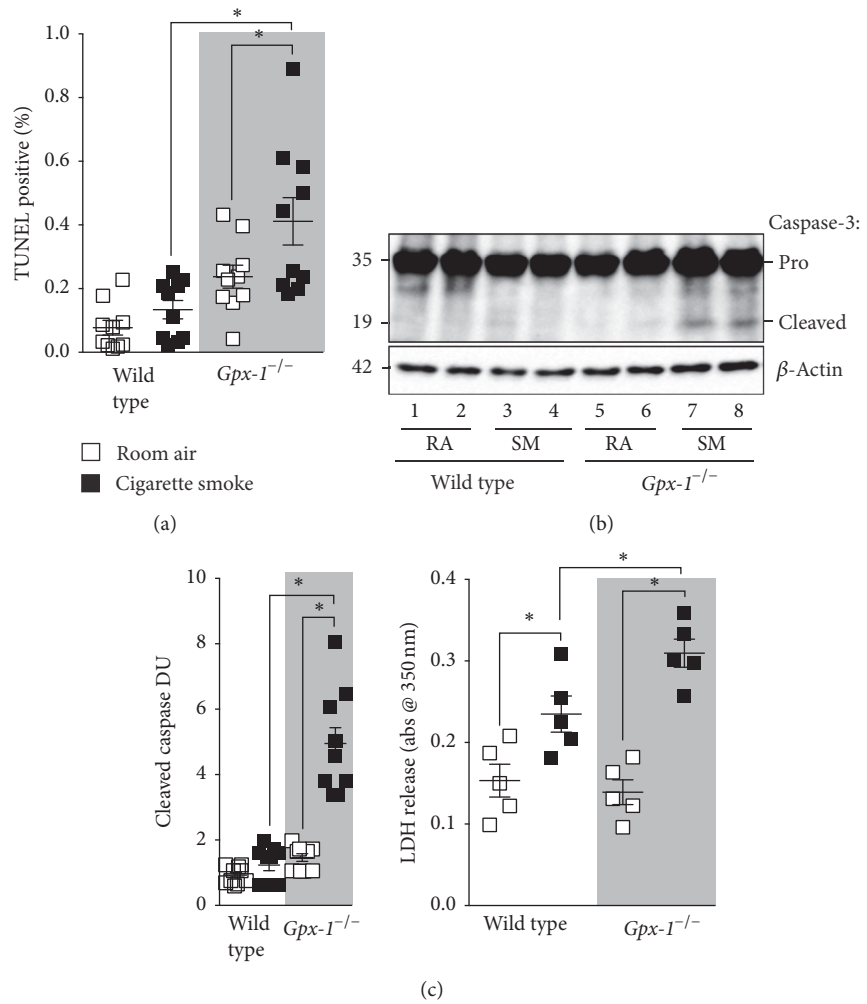

Figure 6: *Gpx-1* deficient mice have heightened ER stress in their lungs following exposure to cigarette smoke. $Gpx\text{-}1^{-/-}$ and wild type mice were exposed to cigarette smoke daily for 1 year. (a) TUNEL analysis was performed on lung tissue from each mouse group. (b) Enhanced lung tissue caspase-3 cleavage coincided with (c) elevated LDH into BALF of $Gpx\text{-}1^{-/-}$ exposed to cigarette smoke. Every lane in (b) represents an individual mouse and densitometry units (DU) of pixel intensity expressed as a ratio to total caspase-3 levels. Dot plots are represented as mean ± SEM, where each measurement was performed on 3 independent days on 6 donors/group. ∗ denotes a p value < 0.05, when comparing both treatments connected by a line, determined by 2-way ANOVA with Tukey's *post hoc* test (>2 groups).

the lung during smoke exposure, Singh et al. show elevated GPx-1 expression in the lungs following one-month cigarette smoke exposure that was regulated by Nrf2 [34]. However, Nrf2 expression is lost in COPD subjects suggesting that this secondary event could result in reduced GPx-1 expression and heightened ER stress. Loss of Nrf2 in mice results in enhanced susceptibility to cigarette smoke [43, 44] and elastase [45] induced emphysema in mice. However genomic studies in $Nrf2^{-/-}$ mouse samples suggest that Nrf2 may regulate other GPx genes but not GPx-1 [46]. Whether RSV infection alters regulation of GPx-1 expression in a similar manner to chronic smoke is unknown. Interestingly, the UPR upon RSV infection can counter viral proliferation [26]. Further studies on the regulation of GPx-1 in smoke exposure and COPD and the significance of ER stress in the lungs are required. This will be a major area for our future work.

Since GPx-1 expression regulates all three branches of the UPR, GPx-1 may affect a common mediator of the UPR or each branch individually. Dissociation of GRP78/BiP upon ER stress is required for all three branches of the UPR. GPx-1 expression directly regulated the gene expression of GRP78. However, whether GPx-1 impacts on GRP78 dissociation during ER stress is unknown. Nrf2 interacts directly with PERK [47] and may play a major role in GPx-1 expression thereby regulating the UPR. The ER stress inducer, thapsigargin, induces Nrf2 protein production in 16-HBE cells [47], which suggests that the UPR induces a Nrf2 response to reverse ER stress. We observe a similar effect on GPx-1 expression in PCLS following tunicamycin treatment. Equally, XBP1 regulates several antioxidants, including catalase, SOD1, and thioredoxin TRX1 [48]. However, XBP1 does not regulate GPx proteins [48] but XBP1 expression is regulated by GPx-1. The

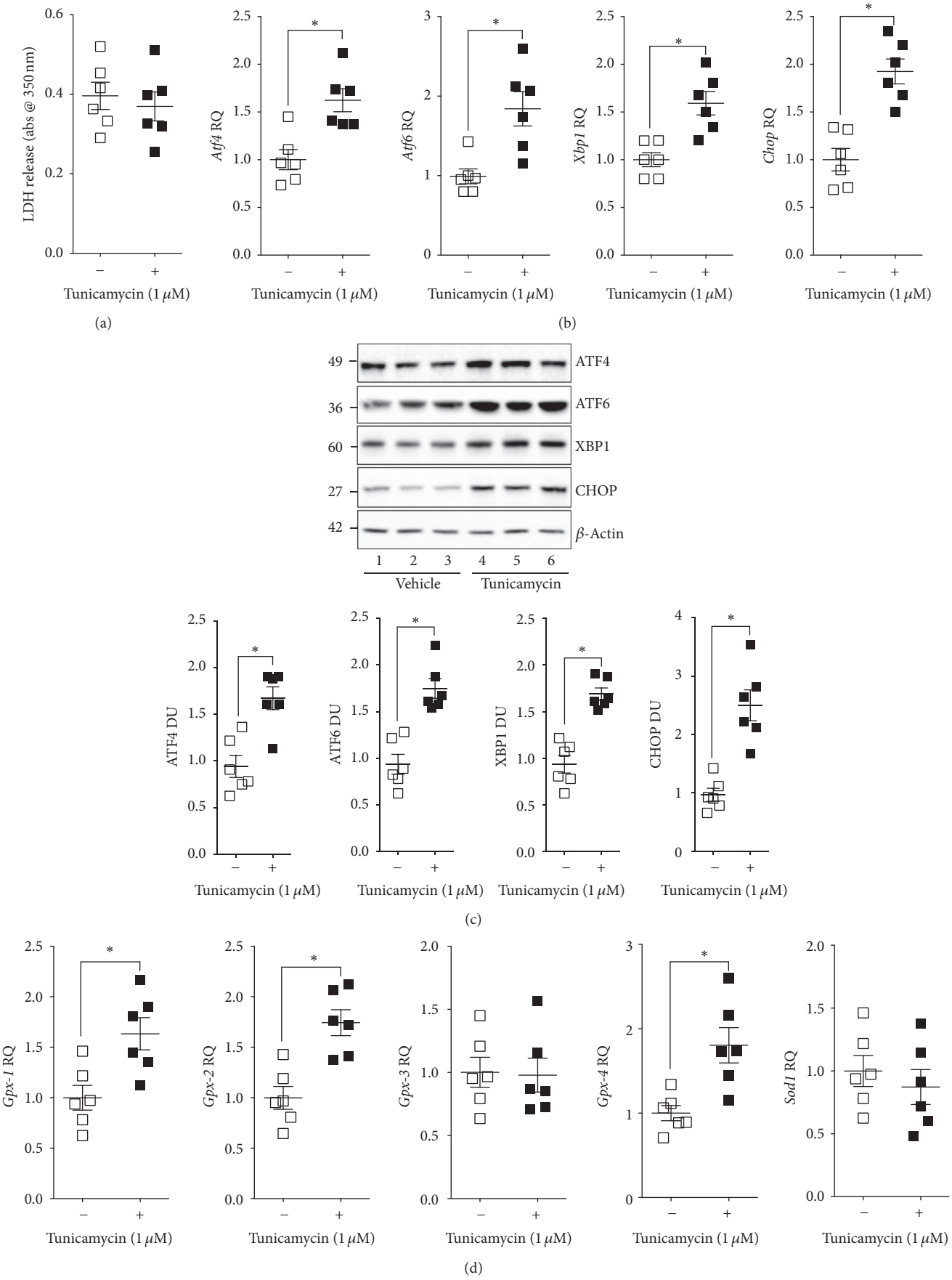

Figure 7: Continued.

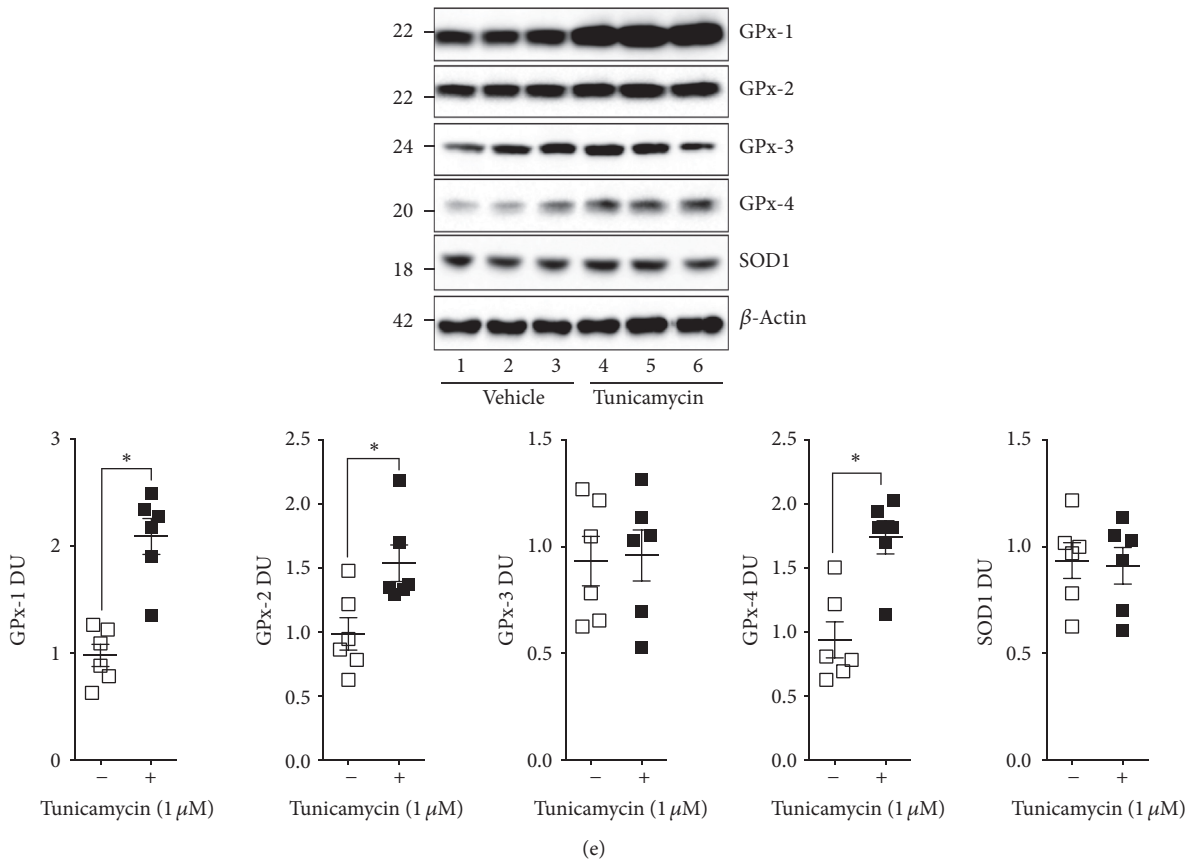

Figure 7: Effect of ER stress-induced tunicamycin on the antioxidant expression profile in mouse precision-cut lung slices (PCLS). PCLS were obtained from wild type mice and were exposed to tunicamycin (1 μM) for 24 hours. (a) LDH release into media and (b) *Chop*, *Atf4*, *Atf6*, and *Xbp1* gene expression were examined. (c) Immunoblots were conducted for *Chop*, *Atf4*, *Atf6, Xbp1, and* β-actin. (d) *GPx-1, GPx-2, GPx-3, GPx-4,* and *Sod1* were quantified by qPCR and (e) immunoblots analysis. Every lane represents an individual mouse. Dot plots are represented as relative quantification (RQ) compared to ACTB expression or densitometry units (DU) of pixel intensity expressed as a ratio to β-actin. Data are shown as the mean ± SEM, where each measurement was performed on 3 independent days on 6 donors/group. $*$ denotes a p value < 0.05, when comparing both treatments connected by a line, determined by Student's t-test (2 groups).

XBP1 regulated gene, *EDEM1*, was also enhanced in *Gpx-1*$^{-/-}$ mice exposed to smoke, which further confirms that GPx-1 regulation of XBP1 signaling. ATF6 requires translocation to the Golgi to undergo cleavage and subsequent translocation to the nucleus to act as a transcription factor [49]. Whether GPx-1 modulates this signaling has yet to be determined. This crosstalk between antioxidant signaling and the UPR is partially lost in COPD and may play a critical step in the pathogenesis of this disease.

The role of the UPR on apoptosis is dependent on the stimulus, exposure duration, and intensity of this signaling. Loss of GPx-1 expression directly impacts cell death and cell death is an important factor in COPD progression [50]. Smoke-induced apoptosis has been associated with several processes, such as ceramide signaling [51], damage-associated molecular pattern molecules (DAMPs) [52], and tumor necrosis factor-related apoptosis-inducing ligand (TRAIL) [53]. The loss of *Gpx-1* exacerbated cigarette smoke-induced cell apoptosis in mice, suggesting that *Gpx-1*$^{-/-}$ genotype exacerbated cell death at least partially through the induction of the UPR. Our group has previously demonstrated that GPx-1 also regulates the activation of protein tyrosine phosphatase 1B (PTP1B) and protein phosphatase 2A (PP2A) [13]. Both of these phosphatases could impact smoke-induced cell survival [54, 55]. Equally, Nrf2 deficient cells undergo enhanced cell death following exposure to ER stress [47], which may be dependent on GPx-1 expression. Therefore, the data presented here suggests that enhanced CHOP expression in NHBE cells and mouse lungs may contribute to apoptosis. Other studies also suggest that certain elements of the UPR have several antiapoptotic and anti-inflammatory effects in other organs. XBP1 reduces CSE-induced CHOP and thereby is protected from CSE-induced apoptosis in a retinal pigment epithelia (RPE) cell line [56], via regulation of eIF2α and p38 phosphorylation [4]. Loss of CHOP expression exacerbated cell death through the downregulation of Nrf2 in RPE cells [4]. CHOP deficiency enhances apoptosis in hippocampal cells and impaired memory-related behavioural performances in mice with tunicamycin treatment [57]. Recently, deficiency of CHOP exaggerated lipopolysaccharide- (LPS-) induced inflammation and kidney injury in mice [58]. The importance of ER stress and the role of each member of

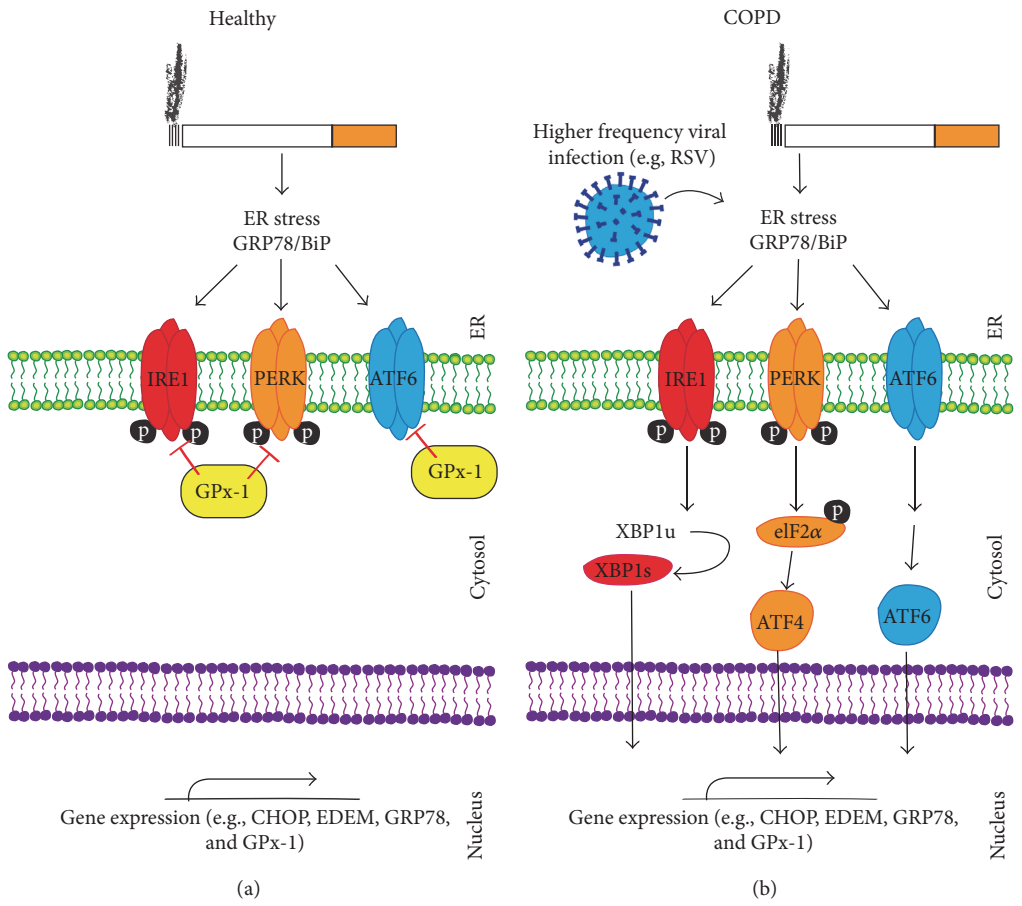

Figure 8: Possible signaling mechanism for GPx-1 regulation of the UPR. Evidence presented in this study indicates that following smoke exposure GPx-1 prevents ER stress (a). However, in the disease-state GPx-1 expression is subdued and results in enhanced UPR (b). RSV infection significantly contributes to reduced GPx-1 expression that coincides with enhanced UPR.

the UPR in the development of lung disease still remain to be fully addressed. However, we have demonstrated that enhanced UPR coincides with worsening of symptoms that are countered with the expression of GPx-1 in mice.

5. Conclusion

Here we demonstrate that GPx-1 expression is reduced in NHBE cells isolated from COPD subjects, GPx-1 is a major regulator of the UPR under smoke exposure conditions, and acute ER stress induces lung GPx-1 expression. Together, our data indicate that the loss of GPX-1 expression in COPD lungs could contribute to disease progression by enhancing the UPR. These studies suggest that enhancing GPX-1 activity may be an effective therapeutic approach to prevent the damage induced by UPR in the lung.

Competing Interests

None of the authors have a financial relationship with a commercial entity that has an interest in the subject of this manuscript.

Acknowledgments

This work was supported by grants made available to Patrick Geraghty (Flight Attendant Medical Research Institute (YCSA 113380)), Robert F. Foronjy (US National Institutes of Health 5R01HL098528-05 and Flight Attendant Medical Research Institute (CIA 130020)), Matthias A. Salathe (Flight Attendant Medical Research Institute CIA 103027 and 130033; the James and Esther King Biomedical Research Program of the State of FL 5JK02), and Jeanine M. D'Armiento (R01 HL086936-07).

References

[1] J. Xu, S. L. Murphy, K. D. Kochanek, and B. A. Basstian, "Deaths: final data for 2013," in *National Vital Statistics Reports*, pp. 1–119, National Center for Health Statistics, Hyattsville, Md, USA, 2016.

[2] R. F. Foronjy, O. Mirochnitchenko, O. Propokenko et al., "Superoxide dismutase expression attenuates cigarette smoke- or elastase-generated emphysema in mice," *American Journal of Respiratory and Critical Care Medicine*, vol. 173, no. 6, pp. 623–631, 2006.

[3] E. Bargagli, C. Olivieri, D. Bennett, A. Prasse, J. Muller-Quernheim, and P. Rottoli, "Oxidative stress in the pathogenesis of diffuse lung diseases: a review," *Respiratory Medicine*, vol. 103, no. 9, pp. 1245–1256, 2009.

[4] C. Huang, J. J. Wang, J. H. Ma, C. Jin, Q. Yu, and S. X. Zhang, "Activation of the UPR protects against cigarette smoke-induced RPE apoptosis through up-regulation of Nrf2," *Journal of Biological Chemistry*, vol. 290, no. 9, pp. 5367–5380, 2015.

[5] P. Geraghty, A. Wallace, and J. M. D'Armiento, "Induction of the unfolded protein response by cigarette smoke is primarily an activating transcription factor 4-C/EBP homologous protein mediated process," *International Journal of Chronic Obstructive Pulmonary Disease*, vol. 6, no. 1, pp. 309–319, 2011.

[6] A. Hengstermann and T. Müller, "Endoplasmic reticulum stress induced by aqueous extracts of cigarette smoke in 3T3 cells activates the unfolded-protein-response-dependent PERK pathway of cell survival," *Free Radical Biology and Medicine*, vol. 44, no. 6, pp. 1097–1107, 2008.

[7] E. Jorgensen, A. Stinson, L. Shan, J. Yang, D. Gietl, and A. P. Albino, "Cigarette smoke induces endoplasmic reticulum stress and the unfolded protein response in normal and malignant human lung cells," *BMC Cancer*, vol. 8, article 229, 2008.

[8] S. G. Kelsen, X. Duan, R. Ji, O. Perez, C. Liu, and S. Merali, "Cigarette smoke induces an unfolded protein response in the human lung: a proteomic approach," *American Journal of Respiratory Cell and Molecular Biology*, vol. 38, no. 5, pp. 541–550, 2008.

[9] Y. Tagawa, N. Hiramatsu, A. Kasai et al., "Induction of apoptosis by cigarette smoke via ROS-dependent endoplasmic reticulum stress and CCAAT/enhancer-binding protein-homologous protein (CHOP)," *Free Radical Biology and Medicine*, vol. 45, no. 1, pp. 50–59, 2008.

[10] R. J. Kaufman, "Stress signaling from the lumen of the endoplasmic reticulum: coordination of gene transcriptional and translational controls," *Genes & Development*, vol. 13, no. 10, pp. 1211–1233, 1999.

[11] P. Walter and D. Ron, "The unfolded protein response stress pathway to homeostatic regulation," *Science*, vol. 334, no. 6059, pp. 1081–1086, 2011.

[12] A.-H. Lee, N. N. Iwakoshi, and L. H. Glimcher, "XBP-1 regulates a subset of endoplasmic reticulum resident chaperone genes in the unfolded protein response," *Molecular and Cellular Biology*, vol. 23, no. 21, pp. 7448–7459, 2003.

[13] P. Geraghty, A. A. Hardigan, A. M. Wallace et al., "The glutathione peroxidase 1-protein tyrosine phosphatase 1B-protein phosphatase 2A axis. A key determinant of airway inflammation and alveolar destruction," *American Journal of Respiratory Cell and Molecular Biology*, vol. 49, no. 5, pp. 721–730, 2013.

[14] M. A. Forgione, N. Weiss, S. Heydrick et al., "Cellular glutathione peroxidase deficiency and endothelial dysfunction," *American Journal of Physiology—Heart and Circulatory Physiology*, vol. 282, no. 4, pp. H1255–H1261, 2002.

[15] J. B. De Haan, C. Bladier, M. Lotfi-Miri et al., "Fibroblasts derived from Gpx1 knockout mice display senescent-like features and are susceptible to H2O2-mediated cell death," *Free Radical Biology and Medicine*, vol. 36, no. 1, pp. 53–64, 2004.

[16] P. Lewis, N. Stefanovic, J. Pete et al., "Lack of the antioxidant enzyme glutathione peroxidase-1 accelerates atherosclerosis in diabetic apolipoprotein E-deficient mice," *Circulation*, vol. 115, no. 16, pp. 2178–2187, 2007.

[17] C. Duong, H. J. Seow, S. Bozinovski, P. J. Crack, G. P. Anderson, and R. Vlahos, "Glutathione peroxidase-1 protects against cigarette smoke-induced lung inflammation in mice," *American Journal of Physiology—Lung Cellular and Molecular Physiology*, vol. 299, no. 3, pp. L425–L433, 2010.

[18] M.-C. Nlend, R. J. Bookman, G. E. Conner, and M. Salathe, "Regulator of G-protein signaling protein 2 modulates purinergic calcium and ciliary beat frequency responses in airway epithelia," *American Journal of Respiratory Cell and Molecular Biology*, vol. 27, no. 4, pp. 436–445, 2002.

[19] A. M. Wallace, A. Hardigan, P. Geraghty et al., "Protein phosphatase 2A regulates innate immune and proteolytic responses to cigarette smoke exposure in the lung," *Toxicological Sciences*, vol. 126, no. 2, pp. 589–599, 2012.

[20] R. F. Foronjy, M. A. Salathe, A. J. Dabo et al., "TLR9 expression is required for the development of cigarette smoke-induced emphysema in mice," *American Journal of Physiology—Lung Cellular and Molecular Physiology*, vol. 311, no. 1, pp. L154–L166, 2016.

[21] A. R. Ressmeyer, A. K. Larsson, E. Vollmer, S. E. Dahlèn, S. Uhlig, and C. Martin, "Characterisation of guinea pig precision-cut lung slices: comparison with human tissues," *European Respiratory Journal*, vol. 28, no. 3, pp. 603–611, 2006.

[22] H.-D. Held, C. Martin, and S. Uhlig, "Characterization of airway and vascular responses in murine lungs," *British Journal of Pharmacology*, vol. 126, no. 5, pp. 1191–1199, 1999.

[23] C. Chen, J. J. Wang, J. Li, Q. Yu, and S. X. Zhang, "Quinotrierixin inhibits proliferation of human retinal pigment epithelial cells," *Molecular Vision*, vol. 19, pp. 39–46, 2013.

[24] J. A. Wedzicha, "Airway infection accelerates decline of lung function in chronic obstructive pulmonary disease," *American Journal of Respiratory and Critical Care Medicine*, vol. 164, no. 10, pp. 1757–1758, 2001.

[25] P. Mallia and S. L. Johnston, "Mechanisms and experimental models of chronic obstructive pulmonary disease exacerbations," *Proceedings of the American Thoracic Society*, vol. 2, no. 4, pp. 361–366, 2005.

[26] I. Hassan, K. S. Gaines, W. J. Hottel et al., "Inositol-requiring enzyme 1 inhibits respiratory syncytial virus replication," *Journal of Biological Chemistry*, vol. 289, no. 11, pp. 7537–7546, 2014.

[27] S. Hodge, G. Hodge, M. Holmes, and P. N. Reynolds, "Increased airway epithelial and T-cell apoptosis in COPD remains despite smoking cessation," *European Respiratory Journal*, vol. 25, no. 3, pp. 447–454, 2005.

[28] F.-F. Chu, R. S. Esworthy, P. G. Chu et al., "Bacteria-induced intestinal cancer in mice with disrupted *Gpx1* and *Gpx2* genes," *Cancer Research*, vol. 64, no. 3, pp. 962–968, 2004.

[29] M. Tomaki, H. Sugiura, A. Koarai et al., "Decreased expression of antioxidant enzymes and increased expression of chemokines in COPD lung," *Pulmonary Pharmacology and Therapeutics*, vol. 20, no. 5, pp. 596–605, 2007.

[30] W.-H. Cheng, Y.-S. Ho, B. A. Valentine, D. A. Ross, G. F. Combs Jr., and X. G. Lei, "Cellular glutathione peroxidase is the mediator of body selenium to protect against paraquat lethality in transgenic mice," *Journal of Nutrition*, vol. 128, no. 7, pp. 1070–1076, 1998.

[31] M. A. Nasr, M. J. Fedele, K. Esser, and A. M. Diamond, "GPx-1 modulates AKT and P70S6K phosphorylation and Gadd45 levels in MCF-7 cells," *Free Radical Biology and Medicine*, vol. 37, no. 2, pp. 187–195, 2004.

[32] Q. Li, S. Sanlioglu, S. Li, T. Ritchie, L. Oberley, and J. F. Engelhardt, "GPx-1 gene delivery modulates NFκB activation following diverse environmental injuries through a specific

subunit of the IKK complex," *Antioxidants and Redox Signaling*, vol. 3, no. 3, pp. 415–432, 2001.

[33] W.-H. Cheng, Y.-S. Ho, D. A. Ross, B. A. Valentine, G. F. Combs Jr., and X. G. Lei, "Cellular glutathione peroxidase knockout mice express normal levels of selenium-dependent plasma and phospholipid hydroperoxide glutathione peroxidases in various tissues," *Journal of Nutrition*, vol. 127, no. 8, pp. 1445–1450, 1997.

[34] A. Singh, T. Rangasamy, R. K. Thimmulappa et al., "Glutathione peroxidase 2, the major cigarette smoke-inducible isoform of GPX in lungs, is regulated by Nrf2," *American Journal of Respiratory Cell and Molecular Biology*, vol. 35, no. 6, pp. 639–650, 2006.

[35] M. V. Kulak, A. R. Cyr, G. W. Woodfield et al., "Transcriptional regulation of the GPX1 gene by TFAP2C and aberrant CpG methylation in human breast cancer," *Oncogene*, vol. 32, no. 34, pp. 4043–4051, 2013.

[36] E. N. Reinke, D. N. Ekoue, S. Bera, N. Mahmud, and A. M. Diamond, "Translational regulation of GPx-1 and GPx-4 by the mTOR pathway," *PLoS ONE*, vol. 9, no. 4, Article ID e93472, 2014.

[37] L. Flohe, W. A. Günzler, and H. H. Schock, "Glutathione peroxidase: a selfnoenzyme," *FEBS Letters*, vol. 32, no. 1, pp. 132–134, 1973.

[38] J. M. Lean, C. J. Jagger, B. Kirstein, K. Fuller, and T. J. Chambers, "Hydrogen peroxide is essential for estrogen-deficiency bone loss and osteoclast formation," *Endocrinology*, vol. 146, no. 2, pp. 728–735, 2005.

[39] Y. Zhang, D. E. Handy, and J. Loscalzo, "Adenosine-dependent induction of glutathione peroxidase 1 in human primary endothelial cells and protection against oxidative stress," *Circulation Research*, vol. 96, no. 8, pp. 831–837, 2005.

[40] C. B. Allan, G. M. Lacourciere, and T. C. Stadtman, "Responsiveness of selenoproteins to dietary selenium," *Annual Review of Nutrition*, vol. 19, pp. 1–16, 1999.

[41] C. Duval, N. Augé, M.-F. Frisach, L. Casteilla, R. Salvayre, and A. Nègre-Salvayre, "Mitochondrial oxidative stress is modulated by oleic acid via an epidermal growth factor receptor-dependent activation of glutathione peroxidase," *Biochemical Journal*, vol. 367, no. 3, pp. 889–894, 2002.

[42] D. E. Handy, Y. Zhang, and J. Loscalzo, "Homocysteine down-regulates cellular glutathione peroxidase (GPx1) by decreasing translation," *Journal of Biological Chemistry*, vol. 280, no. 16, pp. 15518–15525, 2005.

[43] T. Rangasamy, C. Y. Cho, R. K. Thimmulappa et al., "Genetic ablation of Nrf2 enhances susceptibility to cigarette smoke-induced emphysema in mice," *Journal of Clinical Investigation*, vol. 114, no. 9, pp. 1248–1259, 2004.

[44] T. Iizuka, Y. Ishii, K. Itoh et al., "Nrf2-deficient mice are highly susceptible to cigarette smoke-induced emphysema," *Genes to Cells*, vol. 10, no. 12, pp. 1113–1125, 2005.

[45] Y. Ishii, K. Itoh, Y. Morishima et al., "Transcription factor Nrf2 plays a pivotal role in protection against elastase-induced pulmonary inflammation and emphysema," *Journal of Immunology*, vol. 175, no. 10, pp. 6968–6975, 2005.

[46] J.-M. Lee, M. J. Calkins, K. Chan, Y. W. Kan, and J. A. Johnson, "Identification of the NF-E2-related factor-2-dependent genes conferring protection against oxidative stress in primary cortical astrocytes using oligonucleotide microarray analysis," *Journal of Biological Chemistry*, vol. 278, no. 14, pp. 12029–12038, 2003.

[47] S. B. Cullinan, D. Zhang, M. Hannink, E. Arvisais, R. J. Kaufman, and J. A. Diehl, "Nrf2 is a direct PERK substrate and effector of PERK-dependent cell survival," *Molecular and Cellular Biology*, vol. 23, no. 20, pp. 7198–7209, 2003.

[48] Y. Liu, M. Adachi, S. Zhao et al., "Preventing oxidative stress: a new role for XBP1," *Cell Death and Differentiation*, vol. 16, no. 6, pp. 847–857, 2009.

[49] K. Haze, H. Yoshida, H. Yanagi, T. Yura, and K. Mori, "Mammalian transcription factor ATF6 is synthesized as a transmembrane protein and activated by proteolysis in response to endoplasmic reticulum stress," *Molecular Biology of the Cell*, vol. 10, no. 11, pp. 3787–3799, 1999.

[50] L. Segura-Valdez, A. Pardo, M. Gaxiola, B. D. Uhal, C. Becerril, and M. Selman, "Upregulation of gelatinases A and B, collagenases 1 and 2, and increased parenchymal cell death in COPD," *Chest*, vol. 117, no. 3, pp. 684–694, 2000.

[51] I. Petrache, V. Natarajan, L. Zhen et al., "Ceramide upregulation causes pulmonary cell apoptosis and emphysema-like disease in mice," *Nature Medicine*, vol. 11, no. 5, pp. 491–498, 2005.

[52] R. F. Foronjy, P. O. Ochieng, M. A. Salathe et al., "Protein tyrosine phosphatase 1B negatively regulates S100A9-mediated lung damage during respiratory syncytial virus exacerbations," *Mucosal Immunology*, vol. 9, no. 5, pp. 1317–1329, 2016.

[53] T. J. Haw, M. R. Starkey, P. M. Nair et al., "A pathogenic role for tumor necrosis factor-related apoptosis-inducing ligand in chronic obstructive pulmonary disease," *Mucosal Immunology*, vol. 9, no. 4, pp. 859–872, 2016.

[54] P. Geraghty, E. Eden, M. Pillai, M. Campos, N. G. McElvaney, and R. F. Foronjy, "α1-antitrypsin activates protein phosphatase 2A to counter lung inflammatory responses," *American Journal of Respiratory and Critical Care Medicine*, vol. 190, no. 11, pp. 1229–1242, 2014.

[55] C. Van Hoof and J. Goris, "Phosphatases in apoptosis: to be or not to be, PP2A is in the heart of the question," *Biochimica et Biophysica Acta*, vol. 1640, no. 2-3, pp. 97–104, 2003.

[56] M. Cano, L. Wang, J. Wan et al., "Oxidative stress induces mitochondrial dysfunction and a protective unfolded protein response in RPE cells," *Free Radical Biology and Medicine*, vol. 69, pp. 1–14, 2014.

[57] C.-M. Chen, C.-T. Wu, C.-K. Chiang, B.-W. Liao, and S.-H. Liu, "C/EBP homologous protein (CHOP) deficiency aggravates hippocampal cell apoptosis and impairs memory performance," *PLoS ONE*, vol. 7, no. 7, Article ID e40801, 2012.

[58] V. Esposito, F. Grosjean, J. Tan et al., "CHOP deficiency results in elevated lipopolysaccharide-induced inflammation and kidney injury," *American Journal of Physiology - Renal Physiology*, vol. 304, no. 4, pp. F440–F450, 2013.

Hindawi Publishing Corporation
Mediators of Inflammation
Volume 2016, Article ID 5078627, 6 pages
http://dx.doi.org/10.1155/2016/5078627

Review Article

MicroRNA Regulation of Endothelial Junction Proteins and Clinical Consequence

Yugang Zhuang,[1,2] Hu Peng,[1] Victoria Mastej,[2] and Weiguo Chen[2]

[1]*Department of Emergency Medicine, Shanghai Tenth People's Hospital, Tongji University, Shanghai, China*
[2]*Division of Pulmonary, Critical Care, Sleep and Allergy, Department of Medicine, University of Illinois College of Medicine, Chicago, IL, USA*

Correspondence should be addressed to Weiguo Chen; weiguo@uic.edu

Received 10 September 2016; Accepted 3 November 2016

Academic Editor: Yutong Zhao

Cellular junctions play a critical role in structural connection and signal communication between cells in various tissues. Although there are structural and functional varieties, cellular junctions include tight junctions, adherens junctions, focal adhesion junctions, and tissue specific junctions such as PECAM-1 junctions in endothelial cells (EC), desmosomes in epithelial cells, and hemidesmosomes in EC. Cellular junction dysfunction and deterioration are indicative of clinical diseases. MicroRNAs (miRNA) are ~20 nucleotide, noncoding RNAs that play an important role in posttranscriptional regulation for almost all genes. Unsurprisingly, miRNAs regulate junction protein gene expression and control junction structure integrity. In contrast, abnormal miRNA regulation of junction protein gene expression results in abnormal junction structure, causing related diseases. The major components of tight junctions include zonula occluden-1 (ZO-1), claudin-1, claudin-5, and occludin. The miRNA regulation of ZO-1 has been intensively investigated. ZO-1 and other tight junction proteins such as claudin-5 and occludin were positively regulated by miR-126, miR-107, and miR21 in different models. In contrast, ZO-1, claudin-5, and occludin were negatively regulated by miR-181a, miR-98, and miR150. Abnormal tight junction miRNA regulation accompanies cerebral middle artery ischemia, brain trauma, glioma metastasis, and so forth. The major components of adherens junctions include VE-cadherin, β-catenin, plakoglobin, P120, and vinculin. VE-cadherin and β-catenin were regulated by miR-9, miR-99b, miR-181a, and so forth. These regulations directly affect VE-cadherin-β-catenin complex stability and further affect embryo and tumor angiogenesis, vascular development, and so forth. miR-155 and miR-126 have been shown to regulate PECAM-1 and affect neutrophil rolling and EC junction integrity. In focal adhesion junctions, the major components are integrin β4, paxillin, and focal adhesion kinase (FAK). Integrin β4 has been regulated by miR-184, miR-205, and miR-9. Paxillin has been regulated by miR-137, miR-145, and miR-218 in different models. FAK has been regulated by miR-7, miR-138, and miR-135. Deregulation of miRNAs is caused by viral infections, tumorigenesis, and so forth. By regulation of posttranscription, miRNAs manipulate junction protein expression in all cellular processes and further determine cellular fate and development. Elucidation of these regulatory mechanisms will become a new alternative therapy for many diseases, such as cancers and inflammatory diseases.

1. Introduction

Cellular junctions are connective structures between cells existing in various tissues, such as epithelium, endothelium, and intestine. Although the cellular junction components and types may vary in different tissues, the majority of components in junctions are similar. Cellular junctions usually have tight junctions, adherens junctions, and focal adhesion junctions. In the endothelium, two identical PECAM-1s also form a junction and stabilize the major junctions. In addition to barrier function, some junction proteins, such as connexins, form a junction between cells which functions as an ion or water exchange channel (connexon). Integrins associate with focal adhesion kinase (FAK) and paxillin to form a focal adhesion complex, anchoring cells on the basal membrane. The focal adhesion complex also functions as a mechanical sensor which transduces extracellular signal into an intracellular downstream signaling pathway. Thus, these cellular junctions regulate cell function in their own ways.

MicroRNAs (miRNAs) are noncoding RNAs typically ~20 nucleotides in length and transcribed by RNA polymerase II from individual miRNA genes or coding gene introns. Most miRNAs are associated with RNA-induced silencing complex (RISC) and destabilize or inhibit target mRNA translation via binding to the 3′ untranslated terminal (3′UTR). miRNAs provide precise posttranscriptional control of target gene mRNA. Dysfunctional miRNA causes an abnormally high transcription level of the target mRNA and related clinical consequences. The large number and variable function of miRNA identified to date indicate that miRNAs are involved in a vast array of cellular processes, including development, growth, and tumorigenesis [1, 2]. However, the importance of miRNAs for cellular junction gene transcription has not been fully characterized.

Here, we review the important role of miRNAs in the processes of endothelial junction protein transcription and clinical relationships. It will help us to better understand the mechanism behind miRNA regulation of endothelial junctions and provide alternative therapies for the diseases caused by endothelial junction abnormality.

2. Tight Junction Proteins

2.1. Zonula Occludens-1 (ZO-1)/Occludin/Claudin-5. miRNA regulation of tight junctions has been systemically reviewed [3], and more miRNAs have been found involving tight junction expression. Moreover, the clinical consequence of miRNA regulation has not been reviewed, particularly endothelial tight junction regulation.

miRNA-107 abrogated the amyloid-beta (Abeta) protein-induced disruption of blood-brain barrier (BBB) and endothelial cell dysfunction. 3-UTR assay showed that endophilin-1 mRNA is the direct target of miR-107, which further affected endothelial junction by upregulation of ZO-1, occludin, and claudin-5 [4]. The rat permanent middle cerebral artery occlusion (MCAO) model showed that MCAO significantly increased BBB permeability in MCAO area. The expression of claudin-5 was decreased in MCA ischemic areas after upregulation of miR-150. Dual-luciferase assay confirmed that miR-150 directly regulated angiopoietin receptor Tie2 and then downregulated claudin-5 [5]. Deletion of miR-150 or knockout miR-150 caused irreversible increase in vascular permeability in mouse and cell model [6]. Interestingly, miR-21 increased in the brain following traumatic brain injury, promoting junction protein expression and exerting a protective effect on BBB by activating Ang-1/Tie2 axis [7].

In vitro and in vivo models showed that miR-98 negatively regulated tight junction proteins, such as ZO-1, by targeting hypoxia-inducible factor-1 (HIF-1) [8]. Diabetes (DM) rats had significant decrease in miR-126, claudin-5, occluding, and ZO-1 expression and worsened blood retinal barrier. Niaspan treatment reversed these deleterious effects and enhanced miR-126 level. This observation indicated that miR-126 plays an important role in the Niaspan-mediated antidiabetic effect and enhances endothelial barrier by targeting tight junction protein expression [9]. In glioma ECs, upregulation of miR-181a targeted Kruppel-like factor 6 (KLF6), downregulating ZO-1, occluding, and claudin-5, and increased permeability of the blood-tumor barrier (BTB) [10].

Similarly, by targeting runt-related transcriptional factor 1 (RUNX1), miR-18a downregulated mRNA of ZO-1, occludin, and claudin-5 in glioma vascular endothelial cells (GECs) and increased the permeability of BTB [11]. In metastatic breast cancer cells, miR-105 downregulated ZO-1 and increased endothelial barrier permeability, although the underlying mechanism was unclear [12]. By targeting HIV-1 Tat protein C (HIV-1 Tat C), miR-101 downregulated VE-cadherin, further downregulated claudin-5, and changed BMVECs permeability [13] (Table 1).

3. Adherens Junction Proteins

3.1. VE-Cadherin. The major components of adherens junctions include cadherins, β-catenin, plakoglobin, p120, and vinculin. These adherens proteins play an important role not only in cellular connection, but also in cellular signal exchange, contact-induced growth inhibition, and so forth [14]. Adherens junctions exist in all types of cellular connections and are relatively stable. As a major component of adherens junctions, E-cadherin (CDH1, existing in epithelium), VE-cadherin (CDH5, existing in vascular endothelium), and N-cadherin (CDH2, existing in neurons) have been extensively studied in past decades and miRNA regulation has been reported. miR-9 downregulated E-cadherin accompanying tumor metastasis or osteoblast differentiation [15, 16].

Early studies showed that miR-99b, miR-181a, and miR-181b potentiated the mRNA and protein expression of PECAM-1 and VE-cadherin accompanying differentiation of human embryonic stem cells to vascular endothelial cells [17]. miR-21 also regulated induced pluripotent stem cell (iPSC) differentiation into ECs by directly targeting VE-cadherin [18]. miR-125b inhibited VE-cadherin translation and in vitro tube formation by tumor ECs [19]. Overexpression of miR-142a-3p resulted in loss of vascular integrity, hemorrhage, and vascular remodeling during zebrafish embryonic development, while loss of function of miR-142a-3p caused abnormal vascular remodeling. MiR-142a-3p functions in part by directly repressing VE-cadherin [20]. VE-cadherin also played a role in HIV-associated neurological disorders. HIV-1 Tat protein C increased the expression of miR-101, which led to downregulation of VE-cadherin and further caused an adverse effect on blood-brain barrier integrity and permeability [13]. By directly targeting VE-cadherin, ectopic expression of miR-27a blocked capillary tube formation and angiogenesis [21]. MiR-302c and miR-26b-5p also showed similar function during hepatocarcinoma vascular tube formation [22, 23]. By regulation of signal pathways, such as TGF-β and TGF-β2 signal pathways, several miRNAs, such as miR-20a and miR-21, indirectly modulated adherens junction protein expression and endothelial-mesenchymal transition [18, 24] (Table 1).

3.2. β-Catenin. β-Catenin is not only a central molecule of many signaling pathways, such as the Wnt signaling pathway, but also a critical part of the VE-cadherin junction complex.

Table 1: The major components of EC junction and their targeting miRNAs.

Junction protein	Targeting miRNAs	Clinical consequence
ZO-1/occludin/claudin-5	miR-105, miR-181a, miR-18a, miR-21, miR-150, miR-101, miR-126	EC barrier disruption Tumorigenesis
VE-cadherin	miR-99b, miR-181a, miR-181b, miR-21, miR-125b, miR-142a-3p, miR-101, miR-27a, miR-302c, miR-26b-5p, miR-20a	EC barrier disruption Tumorigenesis
β-Catenin	miR-1826, miR-23b	Growth, apoptosis, invasion
PECAM-1	miR-126, miR-155	EC barrier disruption Tumorigenesis
Integrin β4	miR-184, miR-205, miR-9	Tumor metastasis
Paxillin	miR-137, miR-145, miR-218, miR-125b	Tumor metastasis Infection
FAK	miR-135, miR-138, miR-543	Tumorigenesis Tumor invasion

By association with VE-cadherin, the β-catenin/VE-cadherin complex plays an important role in maintaining EC junction integrity. By far, of the majority of these studies focused on the role of miRNAs in tumorigenesis or EMT [15, 25]. For example, miR-1826 level was much lower in bladder cancer (BC) cell lines compared to normal bladder cell lines. Transfection of miR-1826 into BC cells inhibited BC cell viability, invasion, and migration by interfering with the VEGF-β-catenin-ERK signaling pathway [26]. Downregulation of miR-23b triggered glioma growth inhibition, induced apoptosis, and suppressed invasion by inhibition of β-catenin/Tcf4 and HIF-1α/VEGF signaling pathways [27]. Moreover, miRNA-184 downregulated β-catenin and deleteriously changed endothelial cell adherens junction structure and functions in HUVECs and HCE [28] (Table 1).

4. PECAM-1

PECAM-1 is specifically expressed in blood and endothelial cells. PECAM-1 on circulating platelets and leukocytes functions as an inhibitory receptor that limits cellular activation responses. However, PECAM-1 is highly expressed at endothelial cell intercellular junctions, where it functions as a mechanical sensor, regulator of leukocyte trafficking, and in the maintenance of endothelial junction integrity [29]. Inhibition of miR-155 improved neurological impairment of rats with cerebral infarction accompanying enhancement of PECAM-1 expression and EC junction integrity improvement [30]. Interestingly, polyphenolics inhibited high glucose-mediated inflammatory response and decreased PECAM-1 and ICAM-1 protein levels in human vascular endothelial cells (HUVECs). MicroRNA screens indicated that miR-126 may be modulated by polyphenolics as the underlying mechanism to inhibit expression of PECAM-1 and ICAM-1 [31]. A hyperoxia-induced bronchopulmonary dysplasia study resulted in lower levels of PECAM-1 mRNA and protein. MicroRNA screening indicated miRNAs may participate in the occurrence and development of bronchopulmonary dysplasia, including PECAM-1 expression. However, the underlying mechanism of miRNA-mediated PECAM-1 regulation and clinical consequence has not yet been determined [32] (Table 1).

5. Focal Adhesion Junction Proteins

5.1. Integrin β4. In EC focal adhesion junctions, the major components include integrin β4, paxillin, and focal adhesion kinase (FAK). Integrin β4 associates with integrin α6 to form a complex which anchors ECs on the basal membrane and functions as a mechanical sensor. Unlike other integrin β isoforms, integrin β4 has a unique long cytosolic domain which functions as a dock for tyrosine kinases, such as Src and Fny. Once integrin β4 receives stimulation from the basal membrane, its cytosolic domain recruits a tyrosine kinase and activates downstream signaling pathway. Single-nucleotide polymorphisms (SNPs) studies in breast cancer (BC) samples indicated that an A allele of the SNP rs 743554 in the integrin β4 gene has strong association with oestrogen receptor-negative tumors and it is believed to affect binding efficiency with microRNAs. Compared with wild type genotype carriers, those with the A allele have a poor survival significantly associated with aggressive tumor characteristics: high grade, lymph node metastasis, and high stage [33]. MicroRNAs miR-184 and miR-205 competitively bind to the complementary sequences within the 3′untranslated region (3′UTR) of integrin β4 mRNA. Mutated miR-184 failed to compete with miR-205 for the overlapping target sites on the 3′ UTRs of integrin β4 and resulted in familial severe keratoconus [34]. MiR-205 also regulated tumor cell basal membrane deposits of lamin-332 and its receptor integrin β4

[35]. Silico analysis showed that miR-9 also regulated integrin β4 mRNA but had no experimental results validating it [36] (Table 1).

5.2. Paxillin. Knockdown of paxillin or ectopic expression of miR-137 inhibited tumor growth and metastasis of colorectal cancer (CRC) cells in vivo. A dual-luciferase reporter gene assay validated paxillin as a direct target of miR-137 [37]. A similar inhibitory effect of miR-137 was also observed in a non-small cell lung cancer model [38]. MiR-145 also inhibited paxillin expression by binding to the paxillin mRNA 3′UTR. Higher expression of paxillin and lower expression of miR-145 were observed in colorectal cancer tissues than corresponding paracancerous tissue [39]. Among high-risk human papillomavirus (HPV) 16-infected oral cavity squamous cell carcinoma (OCSSC), HPV16/18 infection was negatively associated with miR-218 expression and positively associated with paxillin expression. This observation indicated there is an inverse relationship between miR-218 and paxillin in HPV-infected OCSCC [40]. More interestingly, microRNAs have been found to modulate paxillin expression by epigenetic mechanisms [41, 42]. Alternatively, paxillin also functions as a regulator of microRNA expression, such as miR-125b, to further regulate tumorigenesis [43] (Table 1).

5.3. Focal Adhesion Kinase (FAK). Focal adhesion kinase (FAK) is the key component of the focal adhesion complex, which links focal adhesions to the cytosolic signaling pathway. By modification of FAK, such as phosphorylation or dephosphorylation of tyrosine or serine, FAK transduces extracellular stimuli into downstream signaling, further regulating the cytoskeleton and cellular junction. miR-7 has been shown directly targeting FAK and is negatively correlated with lymph node metastasis and tumor node metastasis staging in colon cancer (CC) [44, 45]. miR-543 level decreased in endometrial cancer cells and inversely correlated with mRNA levels of FAK and Twist homolog 1 (TWIST1) [46]. By binding with the 3′UTR of mRNA, miR-138 and miR-135 inhibited FAK protein expression in different cancer cell lines, such as HeLa cell, SW480, and A375 cell. Moreover, regulation of FAK expression by miR-135 and miR-138 also affected cancer cell invasion, drug sensitivity, and tumor growth in both in vitro and in vivo models [47]. Finally, by targeting an upstream kinase of FAK, some miRNAs indirectly regulate FAK phosphorylation status and further affect cell functions, such as junction integrity, cell growth, and migration [48] (Table 1).

6. Summary

Junction proteins are groups of structural proteins involved in various critical cellular processes, including cellular connection and signal communication, cell growth, and migration. So far, endothelial junction integrity has shown to be involved in many diseases, such as edema, inflammatory cell infiltration, and tumor cell invasion. Accordingly, comprehensive understanding of cell junction protein regulation is crucial for both junction function study and clinical therapy. Among all of the regulatory mechanisms of junction protein expression, miRNAs have emerged as particularly promising targets for their structural and functional characteristics. In this review, we systemically reviewed the miRNAs and their targeting proteins of tight junctions, adherens junctions, focal adhesion junctions, and PECAM-1 junctions. Although some miRNAs –junction protein regulatory relationships were observed in models other than endothelial junctions, they still provide insights into understanding the importance of these miRNAs (Table 1). Moreover, the phenotypes of these regulatory miRNAs on targeting junction proteins are also presented and certainly help us better understand the importance of these miRNAs in clinical regards.

Competing Interests

The authors declare that they have no competing interests.

Authors' Contributions

Yugang Zhuang and Hu Peng equally contribute to this study.

Acknowledgments

This work was supported by the National Scientific Foundation of China (NSFC-81671938, Hu Peng; NSFC-81270133, Weiguo Chen).

References

[1] J. Amiel, L. de Pontual, and A. Henrion-Caude, "MiRNA, development and disease," *Advances in Genetics*, vol. 80, pp. 1–36, 2012.

[2] A. Henrion-Caude, M. Girard, and J. Amiel, "MicroRNAs in genetic disease: rethinking the dosage," *Current Gene Therapy*, vol. 12, no. 4, pp. 292–300, 2012.

[3] C. Cichon, H. Sabharwal, C. Rüter, and M. A. Schmidt, "MicroRNAs regulate tight junction proteins and modulate epithelial/endothelial barrier functions," *Tissue Barriers*, vol. 2, no. 4, Article ID e944446, 2014.

[4] W. Liu, H. Cai, M. Lin et al., "MicroRNA-107 prevents amyloid-beta induced blood-brain barrier disruption and endothelial cell dysfunction by targeting Endophilin-1," *Experimental Cell Research*, vol. 343, no. 2, pp. 248–257, 2016.

[5] Z. Fang, Q. He, Q. Li et al., "MicroRNA-150 regulates blood-brain barrier permeability via Tie-2 after permanent middle cerebral artery occlusion in rats," *The FASEB Journal*, vol. 30, no. 6, pp. 2097–2107, 2016.

[6] C. Rajput, M. Tauseef, M. Farazuddin et al., "MicroRNA-150 suppression of angiopoetin-2 generation and signaling is crucial for resolving vascular injury," *Arteriosclerosis, Thrombosis, and Vascular Biology*, vol. 36, no. 2, pp. 380–388, 2016.

[7] X. Ge, Z. Han, F. Chen et al., "MiR-21 alleviates secondary blood-brain barrier damage after traumatic brain injury in rats," *Brain Research*, vol. 1603, pp. 150–157, 2015.

[8] D. Hu, Y. Yu, C. Wang, D. Li, Y. Tai, and L. Fang, "microRNA-98 mediated microvascular hyperpermeability during burn shock phase via inhibiting FIH-1," *European Journal of Medical Research*, vol. 20, no. 1, article 51, 2015.

[9] Y. Wang and H. Yan, "MicroRNA-126 contributes to Niaspan treatment induced vascular restoration after diabetic retinopathy," *Scientific Reports*, vol. 6, Article ID 26909, 2016.

[10] J. Ma, Y. Yao, P. Wang et al., "MiR-181a regulates blood-tumor barrier permeability by targeting Krüppel-like factor 6," *Journal of Cerebral Blood Flow & Metabolism*, vol. 34, no. 11, pp. 1826–1836, 2014.

[11] Y.-S. Miao, Y.-Y. Zhao, L.-N. Zhao et al., "MiR-18a increased the permeability of BTB via RUNX1 mediated down-regulation of ZO-1, occludin and claudin-5," *Cellular Signalling*, vol. 27, no. 1, pp. 156–167, 2015.

[12] W. Zhou, M. Y. Fong, Y. Min et al., "Cancer-Secreted miR-105 destroys vascular endothelial barriers to promote metastasis," *Cancer Cell*, vol. 25, no. 4, pp. 501–515, 2014.

[13] R. Mishra and S. K. Singh, "HIV-1 Tat C modulates expression of miRNA-101 to suppress VE-cadherin in human brain microvascular endothelial cells," *Journal of Neuroscience*, vol. 33, no. 14, pp. 5992–6000, 2013.

[14] E. Dejana, "Endothelial cell-cell junctions: happy together," *Nature Reviews Molecular Cell Biology*, vol. 5, no. 4, pp. 261–270, 2004.

[15] Y. Khew-Goodall and G. J. Goodall, "Myc-modulated miR-9 makes more metastases," *Nature Cell Biology*, vol. 12, no. 3, pp. 209–211, 2010.

[16] J. Qu, D. Lu, H. Guo, W. Miao, G. Wu, and M. Zhou, "MicroRNA-9 regulates osteoblast differentiation and angiogenesis via the AMPK signaling pathway," *Molecular and Cellular Biochemistry*, vol. 411, no. 1-2, pp. 23–33, 2016.

[17] N. M. Kane, L. Howard, B. Descamps et al., "Role of microRNAs 99b, 181a, and 181b in the differentiation of human embryonic stem cells to vascular endothelial cells," *Stem Cells*, vol. 30, no. 4, pp. 643–654, 2012.

[18] E. Di Bernardini, P. Campagnolo, A. Margariti et al., "Endothelial lineage differentiation from induced pluripotent stem cells is regulated by microRNA-21 and transforming growth factor $\beta 2$ (TGF-$\beta 2$) pathways," *The Journal of Biological Chemistry*, vol. 289, no. 6, pp. 3383–3393, 2014.

[19] F. Muramatsu, H. Kidoya, H. Naito, S. Sakimoto, and N. Takakura, "microRNA-125b inhibits tube formation of blood vessels through translational suppression of VE-cadherin," *Oncogene*, vol. 32, no. 4, pp. 414–421, 2013.

[20] M. K. Lalwani, M. Sharma, A. R. Singh et al., "Reverse genetics screen in zebrafish identifies a role of miR-142a-3p in vascular development and integrity," *PLoS ONE*, vol. 7, no. 12, Article ID e52588, 2012.

[21] J. A. Young, K. K. Ting, J. Li et al., "Regulation of vascular leak and recovery from ischemic injury by general and VE-cadherin-restricted miRNA antagonists of miR-27," *Blood*, vol. 122, no. 16, pp. 2911–2919, 2013.

[22] Y. Wang, B. Sun, H. Sun et al., "Regulation of proliferation, angiogenesis and apoptosis in hepatocellular carcinoma by miR-26b-5p," *Tumor Biology*, vol. 37, no. 8, pp. 10965–10979, 2016.

[23] K. Zhu, Q. Pan, L.-Q. Jia et al., "MiR-302c inhibits tumor growth of hepatocellular carcinoma by suppressing the endothelial-mesenchymal transition of endothelial cells," *Scientific Reports*, vol. 4, article 5524, 2014.

[24] A. C. P. Correia, J.-R. A. J. Moonen, M. G. L. Brinker, and G. Krenning, "FGF2 inhibits endothelial-mesenchymal transition through microRNA-20a-mediated repression of canonical TGF-β signaling," *Journal of Cell Science*, vol. 129, no. 3, pp. 569–579, 2016.

[25] M. I. Almeida, R. M. Reis, and G. A. Calin, "MYC-microRNA-9-metastasis connection in breast cancer," *Cell Research*, vol. 20, no. 6, pp. 603–604, 2010.

[26] H. Hirata, Y. Hinoda, K. Ueno, K. Nakajima, N. Ishii, and R. Dahiya, "MicroRNA-1826 directly targets beta-catenin (CTNNB1) and MEK1 (MAP2K1) in VHL-inactivated renal cancer," *Carcinogenesis*, vol. 33, no. 3, pp. 501–508, 2012.

[27] L. Chen, L. Han, K. Zhang et al., "VHL regulates the effects of miR-23b on glioma survival and invasion via suppression of HIF-1α/VEGF and β-catenin/Tcf-4 signaling," *Neuro-Oncology*, vol. 14, no. 8, pp. 1026–1036, 2012.

[28] R. Zong, T. Zhou, Z. Lin et al., "Down-regulation of MicroRNA-184 is associated with corneal neovascularization," *Investigative Opthalmology & Visual Science*, vol. 57, no. 3, pp. 1398–1407, 2016.

[29] J. R. Privratsky and P. J. Newman, "PECAM-1: regulator of endothelial junctional integrity," *Cell and Tissue Research*, vol. 355, no. 3, pp. 607–619, 2014.

[30] Y.-C. Meng, Z.-Y. Ding, H.-Q. Wang, L.-P. Ning, and C. Wang, "Effect of microRNA-155 on angiogenesis after cerebral infarction of rats through AT1R/VEGFR2 pathway," *Asian Pacific Journal of Tropical Medicine*, vol. 8, no. 10, pp. 829–835, 2015.

[31] G. D. Noratto, G. Angel-Morales, S. T. Talcott, and S. U. Mertens-Talcott, "Polyphenolics from Açaí (Euterpe oleracea Mart.) and red muscadine grape (Vitis rotundifolia) protect human umbilical vascular endothelial cells (HUVEC) from glucose- and lipopolysaccharide (LPS)-induced inflammation and target microRNA-126," *Journal of Agricultural and Food Chemistry*, vol. 59, no. 14, pp. 7999–8012, 2011.

[32] Y. Xing, J. Fu, H. Yang et al., "MicroRNA expression profiles and target prediction in neonatal Wistar rat lungs during the development of bronchopulmonary dysplasia," *International Journal of Molecular Medicine*, vol. 36, no. 5, pp. 1253–1263, 2015.

[33] A. Brendle, H. Lei, A. Brandt et al., "Polymorphisms in predicted microRNA-binding sites in integrin genes and breast cancer: ITGB4 as prognostic marker," *Carcinogenesis*, vol. 29, no. 7, pp. 1394–1399, 2008.

[34] A. E. Hughes, D. T. Bradley, M. Campbell et al., "Mutation altering the miR-184 seed region causes familial keratoconus with cataract," *The American Journal of Human Genetics*, vol. 89, no. 5, pp. 628–633, 2011.

[35] P. Gandellini, V. Profumo, A. Casamichele et al., "*miR-205* regulates basement membrane deposition in human prostate: implications for cancer development," *Cell Death & Differentiation*, vol. 19, no. 11, pp. 1750–1760, 2012.

[36] W. Chen, M. C. Harbeck, W. Zhang, and J. R. Jacobson, "MicroRNA regulation of integrins," *Translational Research*, vol. 162, no. 3, pp. 133–143, 2013.

[37] D.-L. Chen, D.-S. Wang, W.-J. Wu et al., "Overexpression of paxillin induced by miR-137 suppression promotes tumor progression and metastasis in colorectal cancer," *Carcinogenesis*, vol. 34, no. 4, pp. 803–811, 2013.

[38] Y. Bi, Y. Han, H. Bi, F. Gao, and X. Wang, "miR-137 impairs the proliferative and migratory capacity of human non-small cell lung cancer cells by targeting paxillin," *Human Cell*, vol. 27, no. 3, pp. 95–102, 2014.

[39] J. Qin, F. Wang, H. Jiang, J. Xu, Y. Jiang, and Z. Wang, "MicroRNA-145 suppresses cell migration and invasion by targeting paxillin in human colorectal cancer cells," *International Journal of Clinical and Experimental Pathology*, vol. 8, no. 2, pp. 1328–1340, 2015.

[40] D.-W. Wu, C.-Y. Chuang, W.-L. Lin, W.-W. Sung, Y.-W. Cheng, and H. Lee, "Paxillin promotes tumor progression and predicts survival and relapse in oral cavity squamous cell carcinoma by microRNA-218 targeting," *Carcinogenesis*, vol. 35, no. 8, pp. 1823–1829, 2014.

[41] D. Li, Z. Li, J. Xiong et al., "MicroRNA-212 functions as an epigenetic-silenced tumor suppressor involving in tumor metastasis and invasion of gastric cancer through down-regulating PXN expression," *American Journal of Cancer Research*, vol. 5, pp. 2980–2997, 2015.

[42] J. Qin, J. Ke, J. Xu et al., "Downregulation of microRNA-132 by DNA hypermethylation is associated with cell invasion in colorectal cancer," *OncoTargets and Therapy*, vol. 8, pp. 3639–3648, 2015.

[43] A. Sen, H. Prizant, A. Light et al., "Androgens regulate ovarian follicular development by increasing follicle stimulating hormone receptor and microRNA-125b expression," *Proceedings of the National Academy of Sciences of the United States of America*, vol. 111, no. 8, pp. 3008–3013, 2014.

[44] X. Kong, G. Li, Y. Yuan et al., "MicroRNA-7 inhibits epithelial-to-mesenchymal transition and metastasis of breast cancer cells via targeting FAK expression," *PLoS ONE*, vol. 7, no. 8, Article ID e41523, 2012.

[45] C.-Y. Zeng, Y.-S. Zhan, J. Huang, and Y.-X. Chen, "MicroRNA-7 suppresses human colon cancer invasion and proliferation by targeting the expression of focal adhesion kinase," *Molecular Medicine Reports*, vol. 13, no. 2, pp. 1297–1303, 2016.

[46] L. Bing, C. Hong, S. Li-Xin, and G. Wei, "MicroRNA-543 suppresses endometrial cancer oncogenicity via targeting FAK and TWIST1 expression," *Archives of Gynecology and Obstetrics*, vol. 290, no. 3, pp. 533–541, 2014.

[47] V. M. Golubovskaya, B. Sumbler, B. Ho, M. Yemma, and W. G. Cance, "MiR-138 and MiR-135 directly target focal adhesion kinase, inhibit cell invasion, and increase sensitivity to chemotherapy in cancer cells," *Anti-Cancer Agents in Medicinal Chemistry*, vol. 14, no. 1, pp. 18–28, 2014.

[48] A. M. Mahmoud, W. Yang, and M. C. Bosland, "Soy isoflavones and prostate cancer: a review of molecular mechanisms," *Journal of Steroid Biochemistry and Molecular Biology*, vol. 140, pp. 116–132, 2014.

Hindawi Publishing Corporation
Mediators of Inflammation
Volume 2016, Article ID 4158698, 12 pages
http://dx.doi.org/10.1155/2016/4158698

Research Article

Association of Heme Oxygenase 1 with Lung Protection in Malaria-Associated ALI/ARDS

Marcelo L. M. Pereira,[1] Luana S. Ortolan,[1] Michelle K. Sercundes,[2] Daniela Debone,[2] Oscar Murillo,[3] Flávia A. Lima,[3] Claudio R. F. Marinho,[3] and Sabrina Epiphanio[2]

[1]*Departamento de Imunologia, Instituto de Ciências Biomédicas, Universidade de São Paulo, São Paulo, SP, Brazil*
[2]*Departamento de Análises Clínicas e Toxicológicas, Faculdade de Ciências Farmacêuticas, Universidade de São Paulo, São Paulo, SP, Brazil*
[3]*Departamento de Parasitologia, Instituto de Ciências Biomédicas, Universidade de São Paulo, São Paulo, SP, Brazil*

Correspondence should be addressed to Sabrina Epiphanio; sabrina.epiphanio@gmail.com

Received 17 August 2016; Revised 10 October 2016; Accepted 18 October 2016

Academic Editor: Jing Zhao

Malaria is a serious disease, caused by the parasite of the genus *Plasmodium*, which was responsible for 440,000 deaths in 2015. Acute lung injury/acute respiratory distress syndrome (ALI/ARDS) is one of the main clinical complications in severe malaria. The murine model DBA/2 reproduces the clinical signs of ALI/ARDS in humans, when infected with *Plasmodium berghei* ANKA. High levels of HO-1 were reported in cases of severe malaria. Our data indicated that the HO-1 mRNA and protein expression are increased in mice that develop malaria-associated ALI/ARDS (MA-ALI/ARDS). Additionally, the hemin, a HO-1 inducing drug, prevented mice from developing MA-ALI/ARDS when administered prior to the development of MA-ALI/ARDS in this model. Also, hemin treatment showed an amelioration of respiratory parameters in mice, high VEGF levels in the sera, and a decrease in vascular permeability in the lung, which are signs of ALI/ARDS. Therefore, the induction of HO-1 before the development of MA-ALI/ARDS could be protective. However, the increased expression of HO-1 on the onset of MA-ALI/ARDS development may represent an effort to revert the phenotype of this syndrome by the host. We therefore confirm that HO-1 inducing drugs could be used for prevention of MA-ALI/ARDS in humans.

1. Introduction

Malaria is a serious disease caused by the *Plasmodium* parasite and transmitted through the bite of the *Anopheles* mosquito. It is estimated that there were about 214 million cases of malaria in 2015, resulting in approximately 440,000 deaths, most of which originating from sub-Saharan Africa and in children under 5 years of age [1].

Malaria is characterized by signs and symptoms such as severe anemia, fever, vomiting, and fatigue [2]. During the symptomatic phase of malaria several clinical complications can occur and are defined as severe malaria. These complications are anemia, cerebral malaria, placental malaria, and acute lung injury/acute respiratory distress syndrome (ALI/ARDS) [3]. The ALI/ARDS has been diagnosed in patients suffering from malaria caused by all the species that cause disease in humans, including *P. knowlesi* [4]; however it is more common in *P. falciparum* and *P. vivax* malaria [5].

ALI/ARDS is characterized by high morbidity and, although more common in adults, also affects children and pregnant woman. The most common manifestations of this syndrome are noncardiogenic pulmonary edema, increased phagocytic activity, dyspnea, reduction in the capacity of gas exchange, and increased levels of inflammatory mediators [6]. ALI/ARDS is most commonly caused by bacteria, sepsis, viral pneumonia, gastric aspiration, severe trauma, adverse drug reactions, and fungal or parasitic infections of the lung [7]. The mechanisms that are critical in the initial and later stages of ALI/ARDS are not well defined [8]. However, it is known that the presence of intravascular fluid in the lungs, due to increased permeability of the alveolar capillary

membrane, is the key pathophysiological mechanism of ALI/ARDS [9].

Multiple factors are possibly involved in the increased vascular permeability, such as endothelium injury, increased levels of proinflammatory cytokines such as TNF-α (tumor necrosis factor alpha), interleukin 1 (IL-1), or IL-6 and IL-8, and endovascular occlusion associated with the accumulation of erythrocytes with reduced deformability, leukocytes, and platelets [6, 9].

Different mouse models have been developed for the study of MA-ALI/ARDS, showing similar aspects to human ALI/ARDS [10–13]. DBA/2 strain mice develop ALI/ARDS when infected with the parasite *Plasmodium berghei* ANKA (PbA) [10]. In this model, an average of 50% of the mice that die between days 7 and 12 after infection have dyspnea, hypoxemia, and reduced respiratory rate. Postmortem studies revealed that these mice had pleural effusion, containing cells such as neutrophils, lymphocytes, monocytes, and macrophages [10, 14]. Furthermore, the vascular endothelial growth factor (VEGF) has been identified as critical in increased pulmonary vascular permeability, a hallmark of ALI/ARDS [10, 15].

The protective role of HO-1 enzyme and carbon monoxide (CO) in experimental severe malaria episodes has been demonstrated in animal models [10, 15, 16]. Additionally, HO-1 was found to be increased in peripheral blood leukocytes, plasma, tissue macrophages, and monocytes of humans with severe malaria [17, 18]. HO-1 is an enzyme encoded by *hmox-1* gene and is considered "protective" due to its anti-inflammatory, antiapoptotic, and antiproliferative actions in different cell types, including endothelial cells [19]. This enzyme participates in the free heme degradation, generating equimolar amounts of CO, iron, and biliverdin and plays a protective role in modulating tissue response to injury in various organs, including the lung [20–22]. The malaria infection leads to the release of reactive oxygen species and free heme, harmful to the endothelial cells of the host. When exposed to free heme, host cells increase expression of HO-1 [23]. HO-1 catabolizes free heme into iron, biliverdin, and CO, which are less toxic to the cells. Therefore, some studies have shown that inducers of HO-1 such as hemin and cobalt protoporphyrin IX (CoPPIX) protected mice infected with malaria, or suffering from other diseases such as polymicrobial sepsis, from developing ALI/ARDS [16, 24, 25]. Additionally, it was observed in previous publications that HO-1 inducers are protective against experimental cerebral malaria [16] and that treatment of DBA/2 mice with a CO-releasing molecule is protective against MA-ALI/ARDS [15]. Meanwhile, in this study, it was observed, for the first time that HO-1 expression is increased in PbA infected DBA/2 mice lungs which develop ALI/ARDS and that the induction of HO-1 protects these mice from developing ALI/ARDS.

2. Materials and Methods

2.1. Mice, Parasites, and Infection. Six- to ten-week-old male DBA/2 mice were bred under pathogen-free conditions in isogenic mouse facilities, at the Biomedical Sciences Institute of the University of São Paulo. In all experiments, the welfare of the animals was taken into consideration. Mice had *ad libitum* access to water and food (Nuvilab CR-1, Quintia S/A, São Paulo, Brazil). Mice were intraperitoneally infected with 1×10^6 *Plasmodium berghei* ANKA (clone 1.49L) infected red blood cells (iRBCs), as previously described [10]. Parasitemia levels were monitored daily using Giemsa-stained peripheral blood smears. All experiments were performed in accordance with the ethical guidelines for experiments with mice, and the protocols were approved by the Animal Health Committee of the Biomedical Sciences Institute of the University of São Paulo (CEUA number 146, page 136, book 2). The guidelines for animal use and care were based on the standards established by The Brazilian College of Animal Experimentation (COBEA). All efforts were made to prevent undue stress or pain to the mice. Twenty days after infection, all surviving animals were euthanized. The mice were euthanized with an anesthetic overdose of ketamine (150 mg/kg) (Vetbrands, Brazil) and xylazine (15 mg/kg) (Syntec, Brazil), and consciousness was checked by testing the pedal reflex, heartbeats, and breathing movements.

2.2. Histological Evaluations. Necropsy was performed in mice dying naturally from malaria or mice euthanized on the 20th day after infection (DAI) to complete the experiment and to avoid animal suffering. The lungs were collected and fixed in buffered 10% formalin for 24 hours and 70% alcohol for 24–48 hours and then embedded in paraffin, sectioned at 5 μm onto slides, and stained with hematoxylin-eosin (HE) according to standard protocol. Histopathological analyses were performed under a Axio Imager M2 (Zeiss) microscope using the Axio Cam HRc (Zeiss) and the software Axio Vision, version 4.9.1.0. In order to determine the alveolar area percentage, 20 pictures per lung HE section were taken and the software Gimp, version 2.8.16 (https://www.gimp.org/) was used to determine the alveolar area in pixels of each picture. The percentage of alveolar area relatively to total area of the pictures were determined in ALI/ARDS versus HP and in hemin treated versus nontreated (saline) mice.

2.3. Determination of Respiratory Pattern. Respiratory patterns (respiratory frequency (RF) and enhanced pause (Penh)) were monitored on the 7th DAI by placing the mice in the plethysmography chamber (WBP, Buxco Electronics, Wilmington, North Carolina, USA) for 10 minutes (basal level) as described before [14]. The data were collected using Biosystems XA software and included the RF (breaths/minute) and variables to calculate the Penh, a theoretical variable that correlates with both pulmonary resistance and intrapleural pressure [26]. The Penh is calculated by the following equation [27]:

$$\text{Penh} = \frac{\text{peak expiratory height}}{\text{peak inspiratory height}} \times \left(\frac{\text{expiratory time}}{\text{relaxation time}} - 1 \right). \quad (1)$$

2.4. Identifying ALI/ARDS in Mice before Death. Identification of ALI/ARDS in mice before death was done as described before [14]. In short, we used two groups of PbA infected mice (10–12 mice per group): the survival group and the euthanized group in which the mice were euthanized on the 7th DAI. In the survival group, in any mouse that died between the 7th and 12th DAI showing pleural effusion or red and congested lungs at necropsy, the cause of death was attributed to ALI/ARDS. In contrast, in mice without pleural effusion that died after 13th DAI with pale lungs and high levels of parasitemia, the cause of death was attributed to hyperparasitemia (HP) and, consequently, anemia. In the euthanized group, mice were classified as having been likely to die of ALI/ARDS or HP, by comparing their respiratory patterns and parasitemia levels with the survival group, in which the *causa mortis* was known, as previously published [14].

2.5. HO-1 Immunohistochemistry. To perform the immunohistochemistry of HO-1, slides containing the tissue sections were placed in an incubator at 60°C for 20 minutes. Then they were incubated in xylene twice for 15 min at 60°C and afterwards passed in absolute ethanol, in 95% alcohol, in 70% alcohol, in distilled water, and finally in 1x PBS pH 7.2 to 7.4. For the antigen retrieval, the slides were incubated in sodium citrate buffer pH 6 for 45 minutes at 95°C. Endogenous peroxidase was blocked with 3% hydrogen peroxide for 15 minutes, twice, at room temperature and protected from light. The tissue was probed with rabbit polyclonal to HO-1 (1 : 1000) antibody (Abcam, ab13243) overnight at 4°C and then the kit REVEAL mouse/rabbit (SPRING-Code SPD-015) was used in accordance with the manufacturer's instructions. The quantification of HO-1 in lung tissue was done by calculating the marked area in the entire tissue section. The calculation was done in ImageJ (version 1.50b) software (https://imagej.nih.gov/ij/), using the plugin IHC toolbox (http://rsb.info.nih.gov/ij/plugins/ihc-toolbox/index.html) [28].

2.6. Western Blot. Fresh frozen mice lung tissues were sonicated and homogenized in ice using the Radio-Immunoprecipitation Assay (RIPA) buffer composed of 50 mM Tris-HCl pH 8.0, 150 mM NaCl, 0.5% sodium deoxycholate, 0.1% sodium dodecyl sulphate (SDS), 1 mM sodium orthovanadate, 1 mM NaF, and a protease inhibitor tablet. The samples were analyzed for protein content using a Bradford protein assay (BioRad) according to manufacturer's instructions. Each sample was quantified, and then 9 μg of protein was loaded onto a 12% Tris-glycine SDS-polyacrylamide gel, according to the manufacturer's protocol (BioRad). The gel was transferred to a PVDF membrane by electrophoresis at 30 V for 16 h. The membrane was blocked in PBS with 0.1% Tween 20 (PBS-T) and 10% nonfat milk at room temperature for 2 h. All antibodies were diluted in the same buffer (PBS-T) with 1% nonfat milk.

The membrane was then probed with rabbit polyclonal HO-1 antibody (Abcam, ab13243, 1 : 20,000) and then incubated for 1 h at room temperature. After incubation, the membrane was washed five times with PBS-T and incubated with horseradish peroxidase–conjugated goat anti-rabbit IgG (Millipore, ap307p, 1 : 20,000) for 1 h at room temperature. After washing five times with PBS-T, an ECL system (Clarity Western ECL Blotting Substrate, Biorad) was used for detection of the proteins in a ChemiDoc XRS+ System (Biorad). The HO-1 expression was calculated by densitometry, in the software ImageJ (version 1.50b) of the HO-1 bands in the immunoblot relative to the housekeeping protein β-actin (rabbit monoclonal to β-actin, Novus biologicals, NB600-501, 1 : 500,000).

2.7. HO-1 and Bilirubin Quantification by ELISA. On the 7th DAI, mice were anesthetized, and their serum was collected by cardiac puncture. ELISAs kits were used to quantify HO-1 levels in serum and macerated lung tissue (Enzo Lifesciences, ADI-960-071) and bilirubin levels (an indirect measure of HO-1 activity) (Biomatik, EKU08395) according to the manufacturer's instructions. The HO-1 level of the ALI/ARDS and HP mice was expressed as fold increase in relation to noninfected mice. The bilirubin values were presented in logarithm of the concentration in micrograms per milliliter.

2.8. Quantitative RT-PCR. Extraction of total RNA from lungs of mice was performed using RNeasy Mini Kit (Qiagen), according to the manufacturer's instructions. Noninfected mice were used as controls and as baseline levels. One microgram of total RNA was reverse-transcribed to single-strand cDNA using the First-Strand cDNA Synthesis Kit (Roche) AMV Reverse Transcriptase protocol (Roche Applied Science). HO-1 transcripts in the cDNA obtained from the reverse transcriptase reaction were quantified by real-time quantitative fluorogenic PCR performed in the 7500 Fast Instrument (Applied Biosystems). SYBR Green PCR Master Mix (Applied Biosystems) was used to quantify gene expression according to the manufacturer's instructions. The gene expression was normalized by the housekeeping gene hypoxanthine guanine phosphoribosyltransferase (HPRT) and using the relative quantification method $2^{(-\Delta\Delta CT)}$ as described before [29]. The primers used were as follows: HO-1: 5′-TCTCAGGGGGTCAGGTC-3′ (forward) and 5′-GGAGCGGTGTCTGGGATG-3′ (reverse); IFN-γ: 5′-CACACTGCATCTTGGCTTTG-3′ (forward) and 5′-TCTGGCTCTGCAGGATTTTC-3′; HPRT: 5′-TGCTCGAGATGTGATGAAGG-3′ (forward) and 5′-TCCCCTGTTGACTGGTCATT-3′ (reverse).

2.9. HO-1 Induction by Hemin. Hemin (Sigma-Aldrich) was diluted in 0.2 M NaOH to a final concentration of 5 mM and pH 7.4. Hemin was administered in two doses: the first was two days before the infection and another at 4th DAI in single doses of 17 mg/kg or with saline solution (control group), intraperitoneally. To measure parasitemias and survival rate of hemin treated and saline treated mice, they were kept alive until the 20th DAI. HO-1 induction by hemin was also used to measure lung vascular permeability and VEGF and cytokine serum levels.

2.10. Lung Vascular Permeability. To investigate lung vascular permeability on the 7th DAI, the hemin treated or saline treated infected mice and noninfected mice were injected intravenously with 0.2 mL of 1% Evans Blue (Sigma). The mice were euthanized 45 minutes later, and the lungs were weighed and placed in 2 mL of formamide (Merck) for 48 hours at 37°C. The absorbance of the formamide was then measured at λ620 nm. The amount of Evans Blue staining per gram of lung tissue was calculated from a standard curve. The lung permeability was expressed as fold increase in relation to the noninfected mice.

2.11. VEGF Quantification in Serum. On the 7th DAI, hemin treated or saline treated infected mice and noninfected mice were anesthetized, and their serum was collected by cardiac puncture. An ELISA kit (R&D Systems) was used to quantify VEGF levels in the serum according to the manufacturer's instructions. The VEGF level was expressed as fold increase in relation to that of the noninfected mice.

2.12. Cytokine Levels Measurement. The cytokine levels were measured in serum from the hemin treated and saline treated DBA/2 mice. Mice Inflammation CBA Cytokine Kit (Cytometric Bead Array, Becton-Dickinson) was used to measure interferon, IFN-γ, tumor necrosis factor, TNF-α, and IL- and IL-10 levels. This kit was used for dosing cytokines from lung tissue lysates using flow cytometer (BD FACS Calibur system, Becton-Dickinson) and using the software Cell Quest Pro, version 5.2. The individual standard curve range for a given cytokine was determined according to manufacturer instructions. The data was analyzed using FlowJo, version 10.0.7, software.

2.13. Isolation of the Primary Microvascular Lung Endothelial Cells. The primary microvascular lung endothelial cells (PMLEC) were obtained from DBA/2 mice, according to what was described before [30]. After euthanasia, the animal's body was disinfected with iodine alcohol. Then all blood was taken from the mice by cutting the carotid artery. In a laminar flow chamber, the lung tissue was cut into fragments of approximately 1 mm^2 which were distributed among 6-well polystyrene plates. After being supplemented, DMEM culture medium (20% serum fetal bovine (FBS) and antibiotics) was added to each well. The plate was then incubated at 37°C and 5% CO_2 for 72 h. After this period, the tissue fragments were removed and 50% of the medium was replaced. After 7 days of incubation, the cells were removed with trypsin 0.25% (EDTA, Gibco) for 15 min and replaced in a culture flask of 75 cm^2. The trypsinization procedure was repeated every 5 to 7 days. Finally, the cells were cultured for 15 to 20 days (3rd and 4th passage) until being used in the following trials. The isolated PMLEC were characterized by immunofluorescence with the antibodies anti-VWF, anti-VCAM, anti-ACE, anti-CD62E, anti-eNOS, anti-CD31, and anti-VE-cadherin.

2.14. Identification of Actin Microfilaments by Immunofluorescent and Morphometric Analysis of the Opening of Interendothelial Junctions. To analyze the area of opening of interendothelial junctions (OIJ), the actin filaments of PMLEC were marked. In order to achieve that, the lung endothelial cells were plated in 24 well plates (7×10^4 cells/well), adhered to gelatin on glass coverslips, and maintained at 37°C and 5% CO_2. The cells were stimulated with PbA lysate for 3 h, after incubation with hemin (5, 10, and 20 μM during 24 h), or solely with DMEM culture medium, supplemented with 20% FBS, in triplicate. Subsequently, the cells were fixed with 3.7% formaldehyde, permeabilized with acetone at −20°C, and blocked with bovine serum albumin solution (1% BSA). Actin was marked with Texas Red Phalloidin (Life Technologies) by 20 minutes. The cell nuclei were marked with Hoechst (H33342, Life Technologies).

Each slide, with fully confluent cells, was chosen randomly and ten to twenty pictures were taken and scanned in a "zig-zag" way, from top to bottom. The images were acquired in the fluorescence Axio Imager M2 (Zeiss) microscope using the Axio Cam HRc (Zeiss) and the software Axio Vision, version 4.9.1.0. The total area of OIJ was measured in each picture using the software Gimp, version 2.8.16 (https://www.gimp.org/).

2.15. Measure of Primary Microvascular Lung Endothelial Cells Permeability. The increased lung vascular permeability was analyzed in PMLEC plated on inserts of permeable membranes with pores of 0.4 μM (Transwell® Corning), pretreated with gelatin and coupled in 24-well polystyrene plates at a concentration of 2.2×10^4 cells per insert and maintained in DMEM culture at 37°C. After 96 hours, until the cells reach confluency, the extract was applied for 3 h after incubation with hemin (20 μM during 24 h) or solely with 20% FBS supplemented DMEM culture medium. Subsequently, the culture medium was replaced by Hank's balanced salt solution and in the upper compartment of each insert (in contact with the cells); 200 μL of Evans Blue was incubated at a concentration of 2 mg/mL at 37°C. After 30 min, the liquid from the lower compartment was collected and analyzed in a spectrophotometer at a wavelength of 650 nm (NanoDrop 2000, Thermo Scientific). Finally, the concentration of Evans Blue in each sample was determined from a standard curve with previously known concentrations of Evans Blue (0.2 mg/mL to 0.0031 mg/mL).

2.16. Statistical Analysis. The data were analyzed by D'Agostino-Pearson normality test. Nonparametric variables were compared using Mann–Whitney test and Kruskal–Wallis test with Dunn's multiple comparisons test. The unpaired *t*-test and one-way ANOVA with Bonferroni multiple comparison test were used for parametric variables. Statistical analyses were performed in GraphPad Prism version 5.0 (http://www.graphpad.com/scientific-software/prism/), including assessments of sensitivity and specificity. To establish cut-off from data, ROC curves were generated using the results of the control group in MedCalc version 8.2.1.0 (https://www.medcalc.org/). Survival curves were analyzed by Log-rank test. Data in graphs is presented representing means and SEM.

3. Results

3.1. P. berghei ANKA Infection of DBA/2 Mice Leads to the Development of ALI/ARDS. The development of ALI/ARDS in the DBA/2 mouse model occurred between the 7th and the 12th DAI (Figures S1A and S1B in Supplementary Material, available online at http://dx.doi.org/10.1155/2016/4158698), during which the mice have died presenting at necropsy reddish lungs, pleural effusion, and histologic changes such as congestion, alveolar edema and hemorrhage, inflammatory infiltrate, and damage to the alveolar wall (Figure S1C). Mice that survived after the 12th DAI died on the 20th DAI or were euthanized at the same day, showing grayish tone lungs, splenomegaly, and no pleural effusion, interstitial chronic pneumonia, and malarial pigment in the lung tissue (Figure S1C). These two phenotypes were described in detail previously by our group [10, 14]. Noninfected mice showed light pink lungs, and no liquid inside of the thoracic cavity was detected (Figure S1C). These changes in lung histology were consistent with the percentage of alveolar area; they were significantly lower in ALI/ARDS than in HP mice (Figure S1D).

3.2. The Expression of HO-1 Is Higher in ALI/ARDS-Developing Mice Compared to HP-Developing Mice. By using the predictive model to identify ALI/ARDS or HP in mice before death [14], the expression of HO-1 in the development of ALI/ARDS was determined in the serum and lungs of infected DBA/2 mice and compared to noninfected mice.

In order to observe the protein expression of HO-1, immunohistochemistry sections of lung tissue of DBA/2 mice were performed. The expression of HO-1 was higher in lungs of ALI/ARDS-developing mice than in HP-developing mice and noninfected mice. Quantification of immunohistochemical stain of HO-1 in the lung was performed by image analysis (Figure 1(a)).

HO-1 protein levels (Figure 1(b)) and HO-1 mRNA expression (Figure 1(c)), measured by western blot and qRT-PCR, respectively, in the mice lungs, were higher in ALI/ARDS-developing mice compared to HP-developing mice on the 7th DAI. Also, HO-1 levels in the lung tissue cell lysate and in the sera were higher in ALI/ARDS mice than in HP mice, as determined by ELISA (Figures 1(d) and 1(e)).

In addition, we checked the activity of HO-1 measuring bilirubin in PbA infected and noninfected mice by ELISA, on the 7th DAI. The levels of bilirubin were significantly higher in ALI/ARDS-developing mice than in noninfected mice (Figure 1(f)). However, the levels of bilirubin were not significantly different between ALI/ARDS and HP mice.

3.3. Induction of HO-1 Protects Plasmodium berghei-Infected DBA/2 Mice from ALI/ARDS. Mice were treated with 17 mg/kg of hemin, an inductor of HO-1, on the second day before PbA infection and on 4th DAI. The efficiency of induction of HO-1 protocol was checked and confirmed, showing that hemin treatment increased mRNA and protein levels of HO-1 in the lungs and in the serum of noninfected animals (Figures S2A and S2B, resp.), which confirms it as an inducer of HO-1.

The hemin treatment increased the survival with most of the mice alive after the 12th DAI without developing ALI/ARDS (Figure 2(a)). Additionally, the parasitemia was significantly different between the 5th and the 7th DAI (Figure 2(b)).

Mice treated with saline (control) and sacrificed on 7th DAI presented necropsy reddish lungs, pleural effusion, congestion, alveolar edema and hemorrhage, inflammatory infiltrate, and damage to the alveolar wall (Figure 2(c)), similarly to what was observed in mice that developed ALI/ARDS (Figure S1) [10, 14]. On the other hand, hemin treated mice showed a phenotype similar to noninfected mice: light pink lungs, and no liquid inside of the thoracic cavity was detected (Figure 2(c)). As it was observed in ALI/ARDS versus HP mice, saline treated mice also had significantly less percentage of alveolar area than hemin treated mice (Figure 2(d)).

3.4. Induction of HO-1 Improves Plasmodium berghei-Infected DBA/2 Respiratory Parameters and Lowers Inflammatory Cytokines Levels. Regarding the respiratory parameters, it was found that hemin treatment led to a significant amelioration, characterized by a decrease in enhanced pause (Penh) (Figure 3(a)) and an increase in the respiratory frequency at 7th DAI (Figure 3(b)). Also, treatment with hemin led to a significant reduction of IFN-γ mRNA in lung and serum protein levels, IL-10 in serum, MCP-1 protein in lung tissue lysates, and serum and TNF in serum (Figures 3(c)–3(h)).

3.5. Induction of HO-1 Protects Alveolar Capillary Barrier. The treatment of PbA infected mice with hemin led to a decrease of VEGF serum levels (Figure 4(a)), a potent inducer of ALI/ARDS in PbA infected DBA/2 [10]. Also, hemin treated mice showed protection of the alveolar capillary barrier, which can be seen by a reduction in lung vascular permeability after Evans Blue administration and quantification (Figure 4(b)). In addition, we observed the same effect in PMLEC when they were hemin treated after being stimulated with PbA lysate for 3 hours, in a transwell plate (Figure 4(c)).

To understand a possible mechanism of HO-1 action in reducing pulmonary vascular permeability, PMLEC were treated with hemin in 5, 10, and 20 μM, before PbA stimulus. The hemin action showed a significant reduction in the OIJ that are formed between the endothelial cells, when compared to nontreated cells (Figure 4(d)).

4. Discussion

The DBA/2 developed ALI/ARDS between the 7th and 12th DAI, with an incidence of 50% (average) when infected with PbA [10, 14]. Our results reinforce this finding, showing that the animals that began to die after the 7th DAI until the 12th DAI showed typical signs of ALI/ARDS, such as pleural effusion, alveolar edema and hemorrhage, alveolar wall damage, inflammatory infiltrates, and lower percentage of alveolar area. The parasitemia reaches about 20% when mice start to develop ALI/ARDS (7th DAI) and this value has a slight

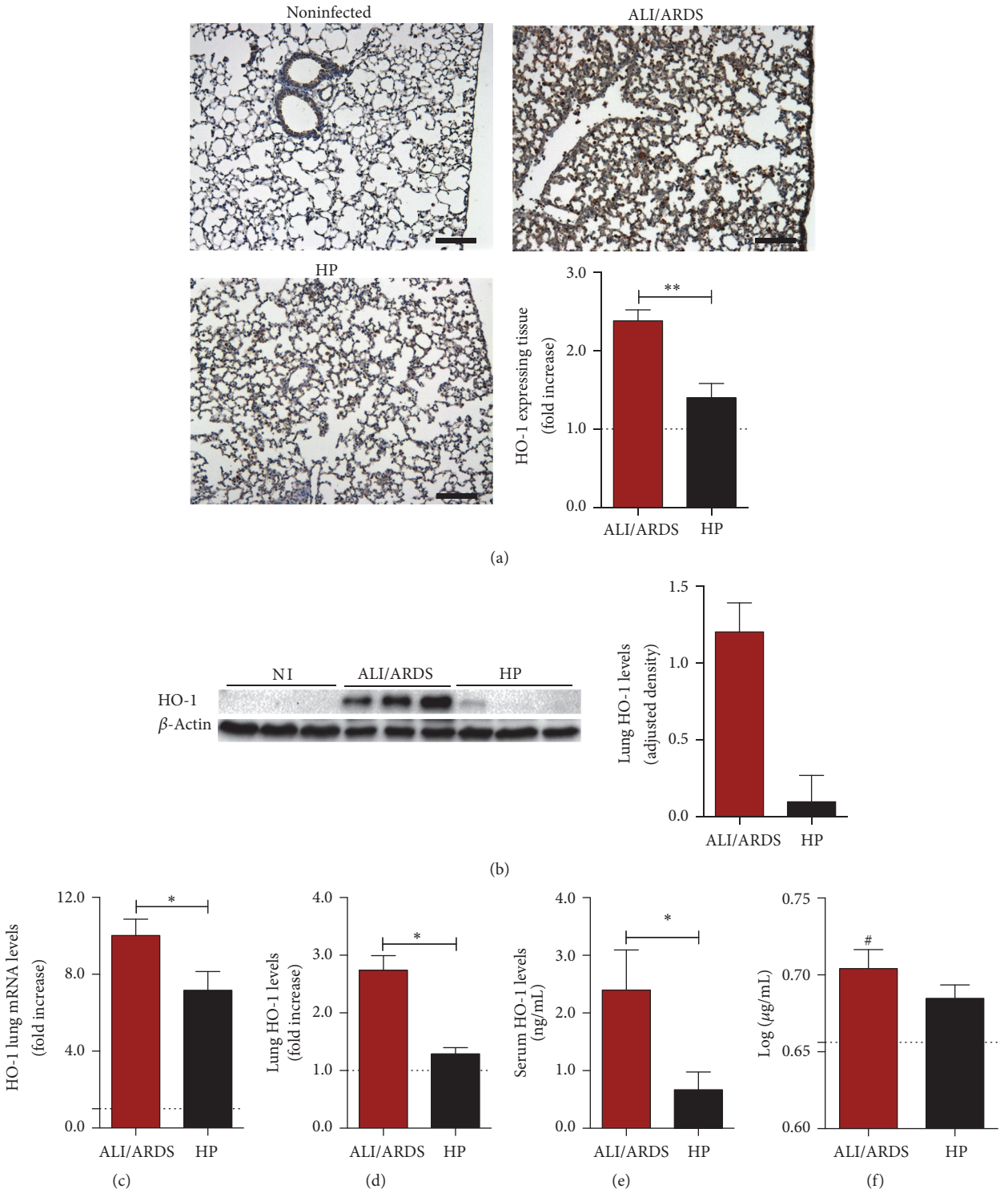

Figure 1: The expression of HO-1 is higher in ALI/ARDS-developing mice compared to HP-developing mice. (a) Representative images of lung sections subject to immunohistochemistry for detection of HO-1 protein (brown), counterstained with hematoxylin. The graph represents the quantification of protein expression of HO-1 by immunohistochemistry on the 7th day after infection (DAI). Dashed line represents the average of values from noninfected mice. (Mann–Whitney test, $n = 10$, $^{**}p \leq 0.01$). (b) Immunoblot of HO-1 and beta actin control (left). Protein levels of HO-1 measured by immunoblot densitometry (right). Values are expressed in HO-1 band densities adjusted by the beta actin control. (c) Expression of HO-1 mRNA levels in lungs of ALI/ARDS-developing mice and HP-developing mice (unpaired t-test, $n = 28$, $^{*}p \leq 0.05$). (d) Values of HO-1 in lung cell lysates of ALI/ARDS versus HP-developing mice (Mann–Whitney test, $n = 8$, $^{*}p \leq 0.05$). (e) Protein levels of HO-1 in the serum of ALI/ARDS-developing mice and HP-developing mice (Mann–Whitney test, $n = 9$, $^{*}p \leq 0.05$). (f) Bilirubin levels in the serum of ALI/ARDS and HP infected mice. Bilirubin levels are significantly higher in ALI/ARDS than in noninfected mice (one-way ANOVA with Bonferroni's multiple comparison test $n = 38$, $^{\#}p \leq 0.05$). The dashed lines represent the average values of noninfected mice (minimum $n = 3$). In graphs ((b) and (e)) the values of noninfected mice were equal or less than 0. In graphs with fold increase, the values of ALI/ARDS-developing and HP-developing mice are compared to the average values of noninfected mice.

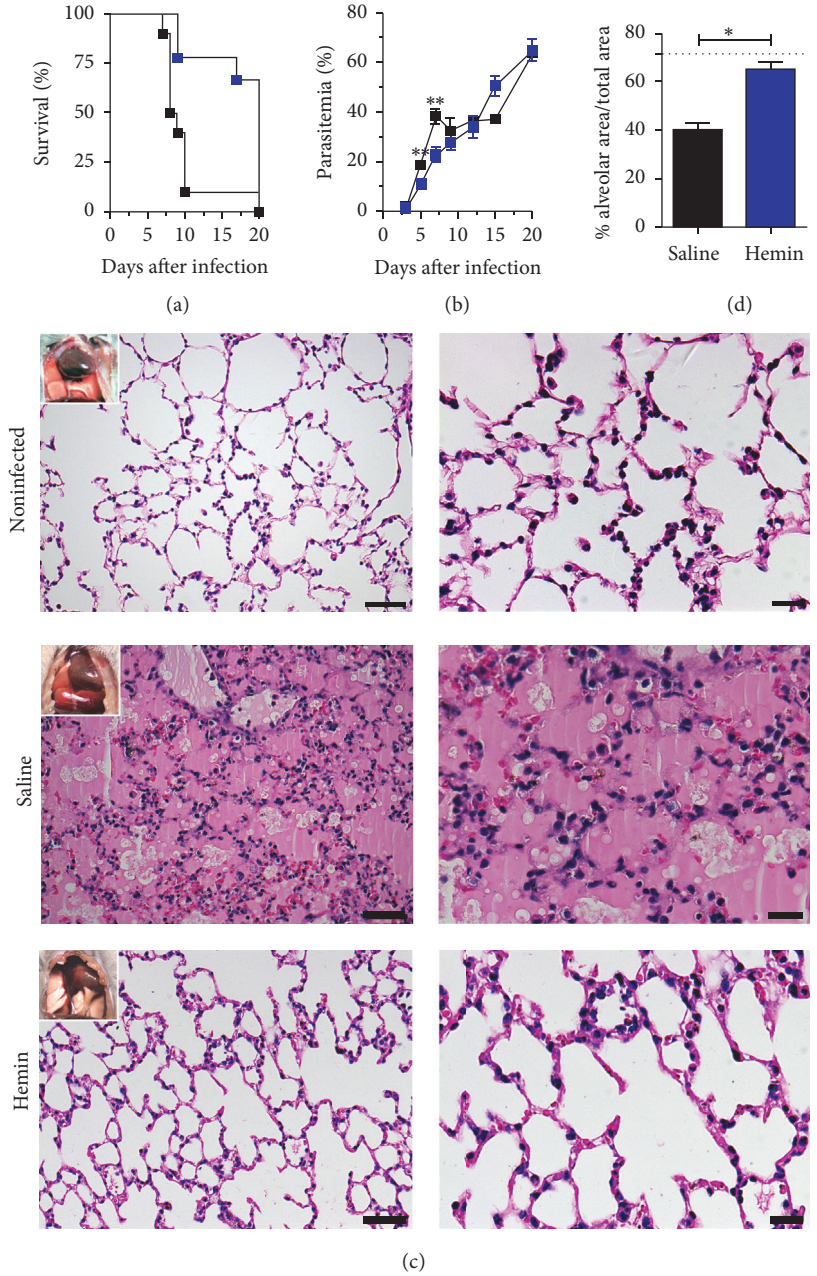

Figure 2: Hemin treatment protects *Plasmodium berghei*-infected DBA/2 mice from ALI/ARDS. Mice were treated with hemin on days 2 and 4 after infection. (a) Parasitemias of mice treated with hemin or saline (unpaired t-test, $n = 19$, $^{**}p \leq 0.01$). (b) Survival curve of mice treated with hemin or saline (log-rank test, $n = 19$, $p \leq 0.01$). (c) Representative figures of necropsies and histological lung sections of noninfected mice (top); hemin treated mice, on the 7th day after infection (middle); and saline treated mice (bottom). Scale bars: left column: 50 μm; right column: 20 μm; (d) alveolar area percentage in hemin treated versus saline treated mice (Mann–Whitney test, $n = 8$, $^{*}p \leq 0.05$).

decrease from the 12th DAI onwards. Interestingly, human malaria-associated ALI/ARDS often occurs in patients who have already begun the antimalarial treatment, which also leads to a decrease in parasitemia [5].

HO-1 showed a protective role in experimental episodes of severe malaria, including cerebral malaria [15, 16, 31]. Moreover, treatment with HO-1 inhibitors such as zinc protoporphyrin IX (ZnPPIX) or tin protoporphyrin IX (SnPPIX) led to an enhancement of ALI/ARDS signals in the case of sepsis but had no effect in the cases of hyperoxia and experimental cerebral malaria [16, 24, 32]. However, our data showed that ALI/ARDS-developing mice had increased levels of mRNA and HO-1 protein, when compared with HP-developing mice and noninfected mice. Additionally, the levels of bilirubin, which represent an indirect measure of HO-1 activity [33], were higher in ALI/ARDS mice than in noninfected mice. Although it is not known whether this increase in HO-1 levels and HO-1 activity constitutes an effort

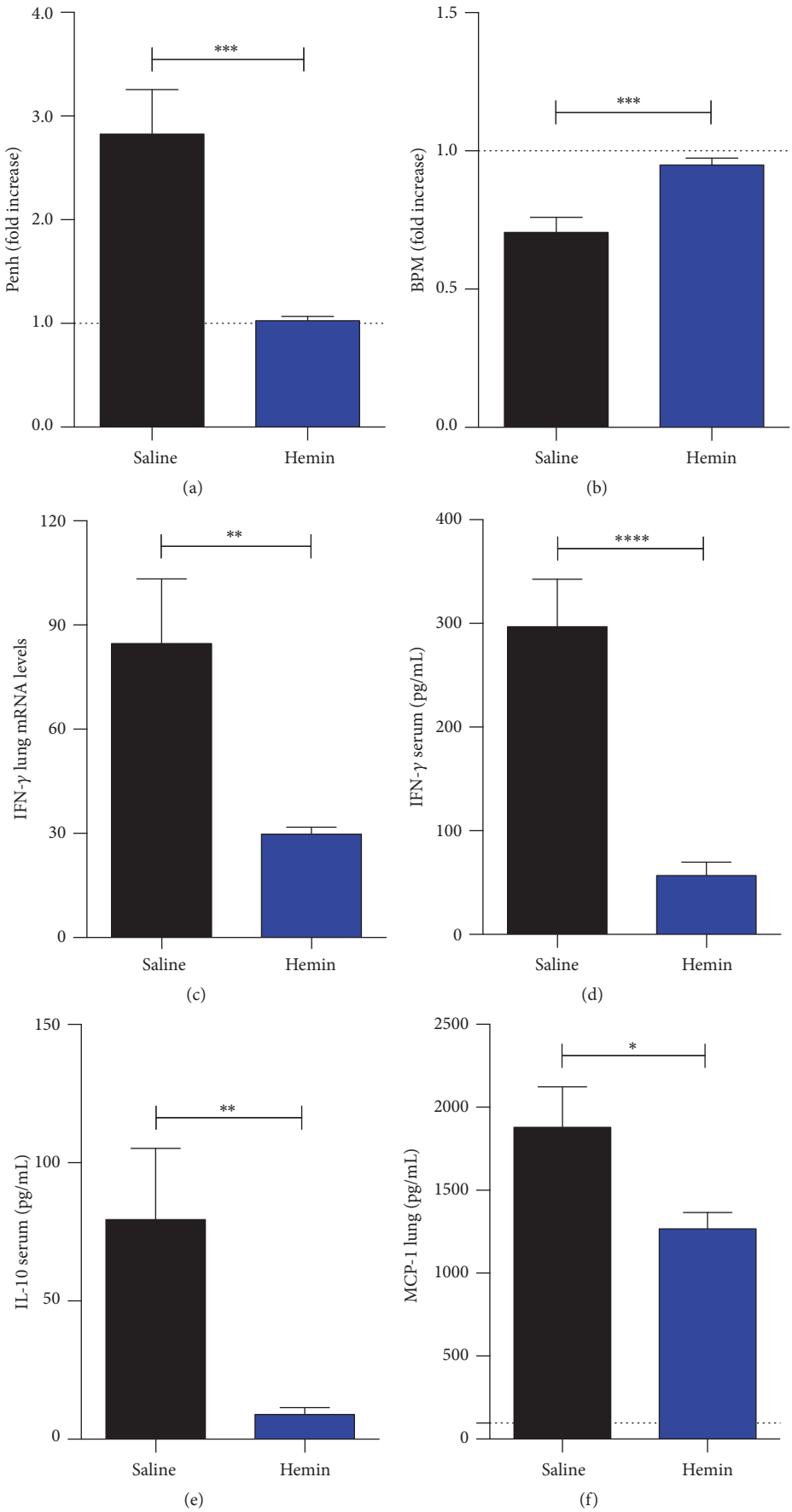

Figure 3: Continued.

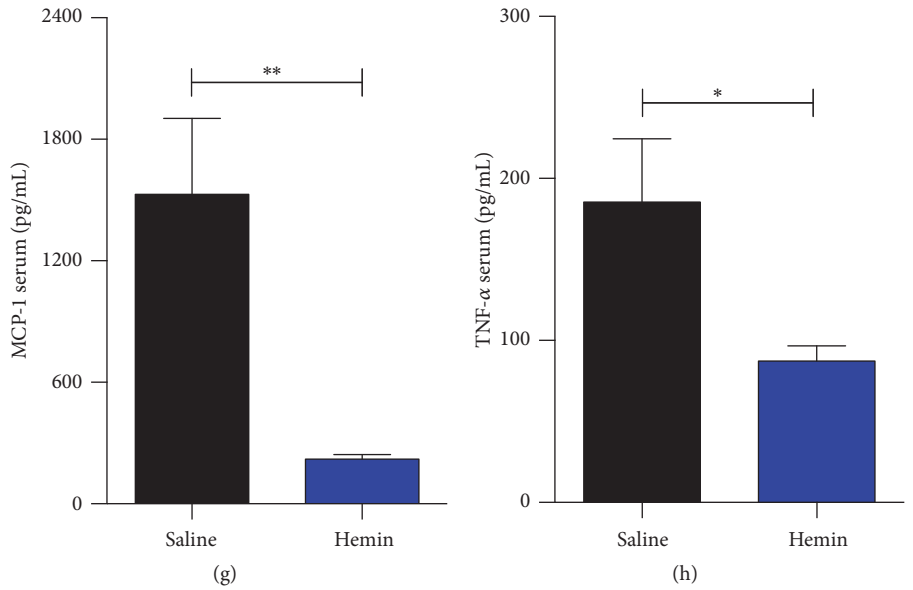

Figure 3: Induction of HO-1 improves *Plasmodium berghei*-infected DBA/2 respiratory parameters and lowers inflammatory cytokines levels. Mice were treated with hemin on days 2 and 4 after infection. ((a) and (b)) Respiratory pause and respiratory frequency of the animals treated and untreated after 7th DAI (unpaired t-test, $n = 20$, $^{***}p \leq 0.001$). (c) IFN-γ quantitative RT-PCR assay of mice lung tissue (unpaired t-test, $n = 20$, $^{**}p \leq 0.01$). ((d) to (h)) Protein levels of the cytokines IFN-γ, IL-10, MCP-1, and TNF-α in the serum and lung determined by CBA (unpaired t-test, $n = 20$, $^{*}p \leq 0.05$, $^{**}p \leq 0.01$, and $^{****}p \leq 0.0001$).

to revert the ALI/ARDS phenotype in the infected mice, it was showed in previous publications that the treatment of *P. berghei* ANKA infected DBA/2 mice with CO (a product of HO-1) [34] and with a CO-releasing molecule [15] protected them against ALI/ARDS. Therefore, in order to clarify whether HO-1 is protective in this model, its induction was performed by hemin.

The treatment with the inducer of HO-1 (hemin) had beneficial effects in PbA infected DBA/2 mice and in PMLEC in contact with PbA lysate. *In vivo*, this treatment led to an improvement in the survival rate and in lung histology, with the absence of lung edema, higher alveolar area percentage, and the absence of pleural effusion at necropsy. Hemin treatment led to a decrease in parasitemia levels. It is an interesting effect, since hemin was observed to lyse malaria parasites in culture [35]. Additionally hemin treated mice infected with *Plasmodium chabaudi adami* also have a reduction in parasitemia [36]. Possibly, the antimalarial effect of hemin is also occurring in our model. Additionally, hemin induces HO-1, which reduces the oxidative stress in the host, which may increase its capacity of parasite clearance.

Hemin also led to an improvement of respiratory parameters, with a decrease of enhanced pause (Penh) and increase of respiratory frequency reinforcing the mitigation of clinical signals of ALI/ARDS, alongside an increase in survival rate. These respiratory parameters were previously used in a predictive model of malaria-associated ALI/ARDS in DBA/2 mice [14]. Additionally, there is evidence of Penh and respiratory frequency being altered in a model of lung injury by SO_2 exposure in rats [37].

In addition to improvements in survival, lung histology, Penh, and respiratory frequency, the treatment with hemin led to a significant decrease in the levels of the proinflammatory cytokines IFN-γ, MCP-1, and TNF-α, which is in agreement with the survival increase and with improvement in lung parameters, as it was shown that TNF-α induced pulmonary vascular endothelial injury in an animal model [38]. Additionally, lung neutrophil accumulation and lung leak were abrogated in TNF-α knockout mice that were subjected to hemorrhagic shock [39]. IFN-γ was also considered to be a key contributor to ALI/ARDS in a hyperoxia mice model, where it was shown that this cytokine induced increases in lung alveolar permeability and neutrophil migration into lung air spaces [40]. Increased levels of MCP-1, chemokine involved in recruiting of monocytes, neutrophils, and lymphocytes, were found in pulmonary alveolar macrophages isolated from a rat model of immune complex-mediated acute inflammatory lung injury [41]. This shows that hemin reduced the levels of inflammatory cytokines that are important in ALI/ARDS, which corroborates with previous results showing that HO-1 induction by hemin has anti-inflammatory effects in models of sepsis and LPS induced ALI/ARDS in mice [25, 42]. As an anti-inflammatory cytokine, which was increased in hemin treated animals, which were protected against endotoxic shock [43] and whose effect in ALI/ARDS was shown to be protective [44], IL-10 was not expected to be decreased in hemin treated animals in our data. However, this cytokine was observed to be increased in mice that developed ALI/ARDS in our model before (unpublished data).

The treatment with hemin resulted in a reduction in serum levels of VEGF, a factor that promoted the development of ALI/ARDS in this model, in a previous study [10]. Furthermore, Siner and colleagues demonstrated that VEGF

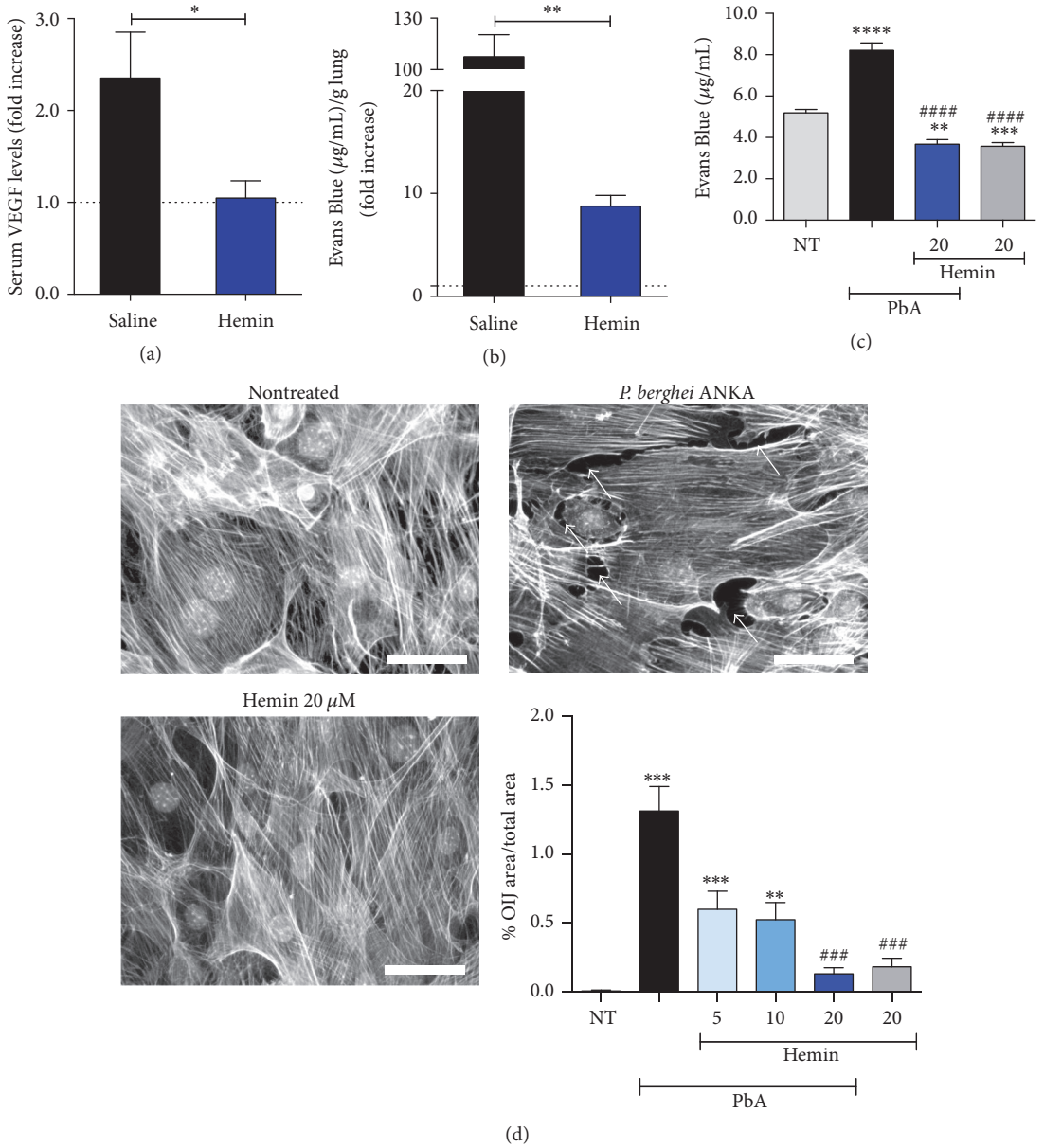

Figure 4: Induction of HO-1 defends the alveolar capillary barrier. (a) VEGF serum levels determined by ELISA (Mann–Whitney test, $n = 10$, $^{*}p \leq 0.05$). (b) Lung endothelial permeability test (Mann–Whitney test, $n = 10$, $^{**}p \leq 0.01$). (c) Permeability test of hemin treated (20 μM) and nontreated (NT) PLMC (PbA: PLMC stimulated with PbA lysate). Significant difference versus nonstimulated is represented by "$*$" and significant difference versus extract is represented by "#" (Kruskal–Wallis test with Dunn's multiple comparisons test, $n = 24$, $^{**}p \leq 0.01$, $^{***}p \leq 0.001$, $^{****}p \leq 0.0001$, and $^{\#\#\#\#}p \leq 0.0001$). (d) Pictures of PLMC by fluorescent microscopy (scale bars: 50 μm). Ten to twenty pictures were taken for each culture and the most representative are presented in (d) (white arrows are pointing to opening interendothelial junctions (OIJ)). The graph (bottom right) represents the ratio of the area of OIJ per total area of each picture (Kruskal–Wallis test with Dunn's multiple comparisons test, $n = 74$, $^{**}p \leq 0.01$, $^{***}p \leq 0.001$, and $^{\#\#\#}p \leq 0.001$). Hemin was given at 5, 10, and 20 μM.

is a potent inducer of HO-1 enzyme and that the induction of this enzyme reduced the acute lung injury in mice caused by hyperoxia [32]. The same could be happening in our model of MA-ALI/ARDS, because the VEGF levels are increased on the 7th DAI, coinciding with an increase of HO-1 levels in serum and lungs. On the other hand, it was shown that treatment of PbA infected mice with VEGF prevented them from developing experimental cerebral malaria [45]. However, the contribution of VEGF to the increase of HO-1 might not occur soon enough to revert the MA-ALI/ARDS phenotype in our model. In this model, VEGF caused a deleterious effect, increasing the lung vascular permeability [10]. Additionally, it was shown that ALF492, a CO-releasing molecule, protected PbA infected DBA/2 from ALI and reduced VEGF levels of treated mice [15]. This corroborates our results that show a reduction in VEGF levels on hemin treated mice. However

hemin treatment was also shown to have deleterious effects in a rat model of neuroinflammation, where it was responsible for increased levels of reactive oxygen species, brain tissue loss, microglial activation, and neuronal death [46].

In addition, improved pulmonary vascular permeability in hemin treated infected mice on the 7th DAI was observed. This corroborates previous studies that showed a reduction in the breakdown of alveolar capillary barriers in models of ALI/ARDS induced by LPS [42]. Additionally, in experimental cerebral malaria, the induction of HO-1 reduced the permeability of the blood brain barrier in PbA infected mice [16]. Also, *in vitro*, there was a reduction of the permeability of PMLEC stimulated with PbA and treated with hemin reinforcing the importance of HO-1 in this model.

Finally, PMLEC stimulated with PbA lysate and treated with different hemin concentrations led to a decrease in the opening of interendothelial junctions, indicating that hemin acts at the cellular level, protecting from the deleterious effect of the parasite in endothelial cells and consequently reducing the lung vascular permeability. This is in accordance with a previous publication where the presence of OIJ after acute lung injury initiation in an animal model was responsible for an increase in lung vascular permeability [47].

This data supports the hypothesis that the increase in HO-1 levels after the 7th DAI is a late effort to reverse the ALI/ARDS phenotype. Inducing HO-1 early in PbA infection has a protective effect against ALI/ARDS, making this enzyme a target for the prevention of MA-ALI/ARDS.

Competing Interests

The authors declare that they have no commercial or other associations that might pose competing interests.

Authors' Contributions

Marcelo L. M. Pereira and Luana S. Ortolan contributed equally to this work.

Acknowledgments

Financial support was provided by Grants 2009/53256-7 and 2014/20451-0 (to Sabrina Epiphanio) and 2009/53.889-0 and 2014/09964-5 (to Claudio R. F. Marinho) from the São Paulo Research Foundation (FAPESP) and from the Conselho Nacional de Desenvolvimento Científico e Tecnológico (CNPq) 306668/2012-2 and 455863/2014-8 (to Sabrina Epiphanio). Marcelo L. M. Pereira was supported by a FAPESP fellowship 2012/10081-5. The authors thank Bernardo Paulo Albe and Erika Paula Machado Peixoto for their technical support and Ana Rita Pinheiro Marques for revising this text.

References

[1] WHO, *World Malaria Report 2015*, World Health Organization, Geneva, Switzerland, 2015.

[2] "Centers for Disease Control and Prevention-Malaria," http://www.cdc.gov/malaria/about/disease.html.

[3] W. C. Aird, L. O. Mosnier, and R. M. Fairhurst, "Plasmodium falciparum picks (on) EPCR," *Blood*, vol. 123, no. 2, pp. 163–167, 2014.

[4] B. Singh and C. Daneshvar, "Human infections and detection of *Plasmodium knowlesi*," *Clinical Microbiology Reviews*, vol. 26, no. 2, pp. 165–184, 2013.

[5] A. Mohan, S. K. Sharma, and S. Bollineni, "Acute lung injury and acute respiratory distress syndrome in malaria," *Journal of Vector Borne Diseases*, vol. 45, no. 3, pp. 179–193, 2008.

[6] L. J. Monahan, "Acute respiratory distress syndrome," *Current Problems in Pediatric and Adolescent Health Care*, vol. 43, no. 10, pp. 278–284, 2013.

[7] M. A. Matthay, L. B. Ware, and G. A. Zimmerman, "The acute respiratory distress syndrome," *Journal of Clinical Investigation*, vol. 122, no. 8, pp. 2731–2740, 2012.

[8] G. Matute-Bello, C. W. Frevert, and T. R. Martin, "Animal models of acute lung injury," *American Journal of Physiology—Lung Cellular and Molecular Physiology*, vol. 295, no. 3, pp. L379–L399, 2008.

[9] M. A. Matthay and G. A. Zimmerman, "Acute lung injury and the acute respiratory distress syndrome: four decades of inquiry into pathogenesis and rational management," *American Journal of Respiratory Cell and Molecular Biology*, vol. 33, no. 4, pp. 319–327, 2005.

[10] S. Epiphanio, M. G. Campos, A. Pamplona et al., "VEGF promotes malaria-associated acute lung injury in mice," *PLoS Pathogens*, vol. 6, no. 5, Article ID e1000916, 2010.

[11] L. Hee, A. Dinudom, A. J. Mitchell et al., "Reduced activity of the epithelial sodium channel in malaria-induced pulmonary oedema in mice," *International Journal for Parasitology*, vol. 41, no. 1, pp. 81–88, 2011.

[12] F. E. Lovegrove, S. A. Gharib, L. Peña-Castillo et al., "Parasite burden and CD36-mediated sequestration are determinants of acute lung injury in an experimental malaria model," *PLoS Pathogens*, vol. 4, no. 5, Article ID e1000068, 2008.

[13] P. E. Van Den Steen, N. Geurts, K. Deroost et al., "Immunopathology and dexamethasone therapy in a new model for malaria-associated acute respiratory distress syndrome," *American Journal of Respiratory and Critical Care Medicine*, vol. 181, no. 9, pp. 957–968, 2010.

[14] L. S. Ortolan, M. K. Sercundes, R. Barboza et al., "Predictive criteria to study the pathogenesis of malaria-associated ALI/ARDS in mice," *Mediators of Inflammation*, vol. 2014, Article ID 872464, 12 pages, 2014.

[15] A. C. Pena, N. Penacho, L. Mancio-Silva et al., "A novel carbon monoxide-releasing molecule fully protects mice from severe malaria," *Antimicrobial Agents and Chemotherapy*, vol. 56, no. 3, pp. 1281–1290, 2012.

[16] A. Pamplona, A. Ferreira, J. Balla et al., "Heme oxygenase-1 and carbon monoxide suppress the pathogenesis of experimental cerebral malaria," *Nature Medicine*, vol. 13, no. 6, pp. 703–710, 2007.

[17] I. A. Clark, M. M. Awburn, C. G. Harper, N. G. Liomba, and M. E. Molyneux, "Induction of HO-1 in tissue macrophages and monocytes in fatal falciparum malaria and sepsis," *Malaria Journal*, vol. 2, article 41, 2003.

[18] M. Walther, A. de Caul, P. Aka et al., "*HMOX1* gene promoter alleles and high HO-1 levels are associated with severe malaria in Gambian children," *PLoS Pathogens*, vol. 8, no. 3, Article ID e1002579, 2012.

[19] M. P. Soares, Y. Lin, J. Anrather et al., "Expression of heme oxygenase-1 can determine cardiac xenograft survival," *Nature Medicine*, vol. 4, no. 9, pp. 1073–1077, 1998.

[20] H. Christou, T. Morita, C.-M. Hsieh et al., "Prevention of hypoxia-induced pulmonary hypertension by enhancement of endogenous heme oxygenase-1 in the rat," *Circulation Research*, vol. 86, no. 12, pp. 1224–1229, 2000.

[21] L. E. Otterbein, J. K. Kolls, L. L. Mantell, J. L. Cook, J. Alam, and A. M. K. Choi, "Exogenous administration of heme oxygenase-1 by gene transfer provides protection against hyperoxia-induced lung injury," *The Journal of Clinical Investigation*, vol. 103, no. 7, pp. 1047–1054, 1999.

[22] T. Tsuburai, Y. Ishigatsubo, M. Suzuki et al., "Adenovirus-mediated transfer and overexpression of heme oxygenase 1 cDNA in lung prevents bleomycin-induced pulmonary fibrosis via a Fas-Fas ligand-independent pathway," *Human Gene Therapy*, vol. 13, no. 16, pp. 1945–1960, 2002.

[23] A. Ferreira, J. Balla, V. Jeney, G. Balla, and M. P. Soares, "A central role for free heme in the pathogenesis of severe malaria: the missing link?" *Journal of Molecular Medicine*, vol. 86, no. 10, pp. 1097–1111, 2008.

[24] D. Fei, X. Meng, K. Kang et al., "Heme oxygenase-1 modulates thrombomodulin and activated protein c levels to attenuate lung injury in cecal ligation and puncture-induced acute lung injury mice," *Experimental Lung Research*, vol. 38, no. 4, pp. 173–182, 2012.

[25] Y.-P. Luo, L. Jiang, K. Kang et al., "Hemin inhibits NLRP3 inflammasome activation in sepsis-induced acute lung injury, involving heme oxygenase-1," *International Immunopharmacology*, vol. 20, no. 1, pp. 24–32, 2014.

[26] E. Hamelmann, J. Schwarze, K. Takeda et al., "Noninvasive measurement of airway responsiveness in allergic mice using barometric plethysmography," *American Journal of Respiratory and Critical Care Medicine*, vol. 156, no. 3, pp. 766–775, 1997.

[27] M. Lomask, "Further exploration of the Penh parameter," *Experimental and Toxicologic Pathology*, vol. 57, no. 2, pp. 13–20, 2006.

[28] Immunohistochemistry (IHC) Image Analysis Toolbox, http://rsb.info.nih.gov/ij/plugins/ihc-toolbox/index.html.

[29] K. J. Livak and T. D. Schmittgen, "Analysis of relative gene expression data using real-time quantitative PCR and the 2(-Delta Delta C(T)) method," *Methods*, vol. 25, no. 4, pp. 402–408, 2001.

[30] S.-F. Chen, X. Fei, and S.-H. Li, "A new simple method for isolation of microvascular endothelial cells avoiding both chemical and mechanical injuries," *Microvascular Research*, vol. 50, no. 1, pp. 119–128, 1995.

[31] S. Dey, S. Mazumder, A. A. Siddiqui et al., "Association of heme oxygenase 1 with the restoration of liver function after damage in murine malaria by *Plasmodium yoelii*," *Infection and Immunity*, vol. 82, no. 8, pp. 3113–3126, 2014.

[32] J. M. Siner, G. Jiang, Z. I. Cohen et al., "VEGF-induced heme oxygenase-1 confers cytoprotection from lethal hyperoxia in vivo," *The FASEB Journal*, vol. 21, no. 7, pp. 1422–1432, 2007.

[33] E. C. Araujo, B. F. Barbosa, L. B. Coutinho et al., "Heme oxygenase-1 activity is involved in the control of Toxoplasma gondii infection in the lung of BALB/c and C57BL/6 and in the small intestine of C57BL/6 mice," *Veterinary Research*, vol. 44, no. 1, article 89, 2013.

[34] S. Epiphanio, M. G. Campos, A. Pamplona et al., "VEGF promotes malaria-associated acute lung injury in mice," *PLoS Pathogens*, vol. 6, no. 5, Article ID e1000916, 2010.

[35] A. U. Orjih, H. S. Banyal, R. Chevli, and C. D. Fitch, "Hemin lyses malaria parasites," *Science*, vol. 214, no. 4521, pp. 667–669, 1981.

[36] E. Dalko, V. Gaudreault, J. Sanchez Dardon, R. Moreau, and T. Scorza, "Preconditioning with hemin decreases *Plasmodium chabaudi adami* parasitemia and inhibits erythropoiesis in BALB/c mice," *PLoS ONE*, vol. 8, no. 1, Article ID e54744, 2013.

[37] U. P. Kodavanti, M. C. Schladweiler, A. D. Ledbetter et al., "The spontaneously hypertensive rat: an experimental model of sulfur dioxide-induced airways disease," *Toxicological Sciences*, vol. 94, no. 1, pp. 193–205, 2006.

[38] S. E. Goldblum, B. Hennig, M. Jay, K. Yoneda, and C. J. McClain, "Tumor necrosis factor alpha-induced pulmonary vascular endothelial injury," *Infection and Immunity*, vol. 57, no. 4, pp. 1218–1226, 1989.

[39] Y. Song, L. Ao, C. D. Raeburn et al., "A low level of TNF-α mediates hemorrhage-induced acute lung injury via p55 TNF receptor," *American Journal of Physiology—Lung Cellular and Molecular Physiology*, vol. 281, no. 3, pp. L677–L684, 2001.

[40] M. Yamada, H. Kubo, S. Kobayashi, K. Ishizawa, and H. Sasaki, "Interferon-γ: a key contributor to hyperoxia-induced lung injury in mice," *American Journal of Physiology-Lung Cellular and Molecular Physiology*, vol. 287, no. 5, pp. L1042–L1047, 2004.

[41] J. K. Brieland, M. L. Jones, S. J. Clarke, J. B. Baker, J. S. Warren, and J. C. Fantone, "Effect of acute inflammatory lung injury on the expression of monocyte chemoattractant protein-1 (MCP-1) in rat pulmonary alveolar macrophages," *American Journal of Respiratory Cell and Molecular Biology*, vol. 7, no. 2, pp. 134–139, 1992.

[42] F. M. Konrad, U. Knausberg, R. Höne, K.-C. Ngamsri, and J. Reutershan, "Tissue heme oxygenase-1 exerts anti-inflammatory effects on LPS-induced pulmonary inflammation," *Mucosal Immunology*, vol. 9, no. 1, pp. 98–111, 2016.

[43] F. Tamion, V. Richard, S. Renet, and C. Thuillez, "Protective effects of heme-oxygenase expression against endotoxic shock: inhibition of tumor necrosis factor-α and augmentation of interleukin-10," *Journal of Trauma-Injury, Infection and Critical Care*, vol. 61, no. 5, pp. 1078–1084, 2006.

[44] H.-D. Li, Q.-X. Zhang, Z. Mao, X.-J. Xu, N.-Y. Li, and H. Zhang, "Exogenous interleukin-10 attenuates hyperoxia-induced acute lung injury in mice," *Experimental Physiology*, vol. 100, no. 3, pp. 331–340, 2015.

[45] M. Canavese, T. Dottorini, and A. Crisanti, "VEGF and LPS synergistically silence inflammatory response to *Plasmodium berghei* infection and protect against cerebral malaria," *Pathogens and Global Health*, vol. 109, no. 6, pp. 255–265, 2015.

[46] C. Tronel, G. Y. Rochefort, N. Arlicot, S. Bodard, S. Chalon, and D. Antier, "Oxidative stress is related to the deleterious effects of heme oxygenase-1 in an in vivo neuroinflammatory rat model," *Oxidative Medicine and Cellular Longevity*, vol. 2013, Article ID 264935, 10 pages, 2013.

[47] A. Kása, C. Csortos, and A. D. Verin, "Cytoskeletal mechanisms regulating vascular endothelial barrier function in response to acute lung injury," *Tissue Barriers*, vol. 3, no. 1-2, Article ID e974448, 2015.

Hindawi Publishing Corporation
Mediators of Inflammation
Volume 2016, Article ID 7349603, 11 pages
http://dx.doi.org/10.1155/2016/7349603

Research Article

NEMO-Binding Domain Peptide Attenuates Lipopolysaccharide-Induced Acute Lung Injury by Inhibiting the NF-κB Signaling Pathway

Jianhua Huang,[1,2] Li Li,[1] Weifeng Yuan,[1] Linxin Zheng,[1] Zhenhui Guo,[3,4] and Wenjie Huang[1,4]

[1]*Department of Respiratory Medicine, General Hospital of Guangzhou Military Command of PLA, Guangzhou, Guangdong, China*
[2]*Department of Pulmonary Medicine, Chenzhou No. 1 People's Hospital, Chenzhou, Hunan, China*
[3]*Department of Medical Intensive Care Unit, General Hospital of Guangzhou Military Command of PLA, Guangzhou, Guangdong, China*
[4]*Guangdong Provincial Key Laboratory of Geriatric Infection and Organ Function Support, Guangzhou, Guangdong, China*

Correspondence should be addressed to Zhenhui Guo; micugzh@126.com and Wenjie Huang; huangyelu1029@vip.163.com

Received 11 July 2016; Revised 5 September 2016; Accepted 15 September 2016

Academic Editor: Yutong Zhao

The aim of the present study is to investigate the protective effects and relevant mechanisms exerted by NEMO-binding domain peptide (NBD) against lipopolysaccharide- (LPS-) induced acute lung injury (ALI) in mice. The ALI model was induced by intratracheally administered atomized LPS (5 mg/kg) to BABL/c mice. Half an hour before LPS administration, we treated the mice with increasing concentrations of intratracheally administered NBD or saline aerosol. Two hours after LPS administration, each group of mice was sacrificed. We observed that NBD pretreatment significantly attenuated LPS-induced lung histopathological injury in a dose-dependent manner. Western blotting established that NBD pretreatment obviously attenuated LPS-induced IκB-α and NF-κBp65 activation and NOX1, NOX2, and NOX4 overexpression. Furthermore, NBD pretreatment increased SOD and T-AOC activity and decreased MDA levels in lung tissue. In addition, NBD also inhibited TNF-α and IL-1β secretion in BALF after LPS challenge. In conclusion, NBD protects against LPS-induced ALI in mice.

1. Introduction

Acute lung injury (ALI) is caused by microbial infection, sepsis, trauma, and ischemia and reperfusion, leading to epithelial integrity disruption, neutrophil accumulation, noncardiogenic pulmonary edema, severe hypoxemia, and intense pulmonary inflammatory responses. The acute respiratory distress syndrome (ARDS) is a more severe form of ALI. Both ALI and ARDS are major causes of acute respiratory failure and leading causes of morbidity and mortality in critically ill patients [1, 2]. In recent years, rapid advances in supportive care, such as mechanical ventilation, have been achieved. However, several data analyses have shown that the mortality rate associated with ALI- or ARDS-induced acute respiratory failure is still high at approximately 40% [3–5]. The pathogenesis of ALI/ARDS is characterized by polymorphonuclear cells (PMNs) infiltration into the lungs, which may cause interstitial edema. In addition, the alveoli develop fibrin leakage, resulting in increases in the levels of macrophage-derived cytokines, chemokines, and other proinflammatory mediators in the lungs [6]. The results of previous studies indicate that many specific therapies have not proven beneficial with respect to managing ALI/ARDS [7]. Therefore, investigating the mechanisms underlying ALI/ARDS is necessary, as such investigations may contribute to the development of novel effective treatments for ALI/ARDS.

ALI research relies mainly on animal models. The intratracheal lipopolysaccharide (LPS) administration model is the most commonly used clinically relevant severe lung injury model for studying the pathophysiologic mechanisms underlying ALI, as it simulates the human disease [8]. LPS

are components of gram-negative bacterial walls and play an important role in ALI by inducing PMNs infiltration into injured lung tissue, mimicking clinical ALI progression. TNF-α and keratinocyte-derived chemokines are secreted during this process and recruit intravascular PMNs into the alveolar spaces [9]. These activated PMNs generate superoxide anions (O_2^-) and release proteases via respiratory bursts and degranulation [10]. This excessive inflammatory response induces significant lipid peroxidation and antioxidant enzyme activity alterations, thereby disrupting lung endothelial integrity [11].

It is accepted that NF-κB, a critical transcriptional factor, plays an important role in the pathogenesis of ALI/ARDS [12]. A variety of experimental techniques have demonstrated that NF-κB exists in both the cytoplasm and the nucleus. NF-κB activation induces its translocation from the cytoplasm to the nucleus. NF-κB is activated by LPS and some cytokines, such as TNF-α and IL-1β. These cytokines initiate a cascade of events leading to IκB phosphorylation by IκB kinase (IKK), which triggers IκB degradation by the ubiquitin–proteasome pathway. IκB, an inhibitory protein, binds to P65 and P50, two NF-κB subunits, under normal conditions. IκB degradation removes a nuclear localization signal from NF-κB, resulting in its uncoiling and translocation into the nucleus. This uncoiling is thought to activate the transcription of cytokines and other proinflammatory mediators [13, 14]. IKK comprises three subunits, IKKα, IKKβ, and IKKγ, which are also collectively known as NEMO (NF-κB essential modulator). IKKγ has no catalytic domain and plays a critical role in biology only when being a part of the IKK complex [15]. The NH2-terminus of NEMO associates with a hexapeptide sequence (Leu-Asp-Trp-Ser-Trp-Leu) within the COOH terminus of IKKα and IKKβ termed the NEMO-binding domain (NBD). Previous studies have shown that LPS induces the NF-κB activation required for NBD activity. NBD disrupts the association between NEMO and IKKβ and blocks LPS-induced NF-κB activation in cells, which ameliorates the inflammatory response and oxidative stress in distinct animal models to some extent [16, 17]. The results of previous studies indicate that understanding the mechanisms underlying the protective effects of NBD may facilitate the development of therapies that are effective against ALI.

Therefore, the aim of the current study was to elucidate the mechanisms underlying the protective effects exerted by NBD against LPS-induced ALI.

2. Materials and Methods

2.1. Chemicals and Reagents. LPS (from *Escherichia coli* 055: B5) was purchased from Sigma-Aldrich, St. Louis, MO, USA. NBD and N-NBD (negative control) were obtained from MERCK (NBD amino acid sequence: H-Asp-Arg-Gln-Ile-Lys-IIe-Trp-Phe-Gln-Asn-Arg-Arg-Met-Lys-Trp-Lys-Lys-Thr-Ala-Leu-Asp-Trp-Ser-Trp-Leu-Gln-Thr-Glu-OH; N-NBD amino acid sequence: H2N-Asp-Arg-Gln-Ile-Lys-IIe-Trp-Phe-Gln-Asn-Arg-Arg-Met-Lys-Trp-Lys-Lys-Thr-Ala-Leu-Asp-Ala-Ser-Ala-Leu-Gln-Thr-Glu-OH). Rabbit polyclonal antibodies against p-IKKα/β, IKKα, IKKβ, p-I-κB, I-κB, p-NF-κB p65, NF-κB p65, NOX1, NOX2, and NOX4 were purchased from Cell Signaling Technology (Santa Cruz Biotechnology, Inc., Texas, USA). All secondary antibodies and β-actin were obtained from Boster (Wuhan Boster Bio-Engineering Limited Company, Wuhan, China). The TNF-α, IL-1β, IL-6, and IL-8 ELISA kits were obtained from Boster (Wuhan Boster Bio-Engineering Limited Company, Wuhan, China). The superoxide dismutase (SOD), total antioxidant capacity (T-AOC), and malondialdehyde (MDA) assay kits and the BCA Protein Assay Kit were obtained from Beyotime Biotech (Beyotime Biotech, Jiangsu, China).

2.2. Animals. Male BLAB/c mice weighing 18–22 g were obtained from the Laboratory Animal Center of Guangdong province (Guangdong, China). All mice were fed a normal standard diet and tap water ad libitum and were housed in an animal facility under controlled environmental and temperature ($24 \pm 1^{\circ}$C) conditions, 12 h light/dark cycles, and controlled humidity. All mice were allowed 7 days to adapt to their environments before the experiments. This study was approved by the Institutional Animal Ethics Committee of the General Hospital of Guangzhou Military Command of PLA and was carried out in compliance with the criteria outlined in the Provisions and General Recommendation of the Chinese Experimental Animals Administration Legislation.

2.3. LPS-Induced ALI Experimental Protocol. The animals were randomly assigned to one of six groups ($n = 6$ per group). Two control groups were intratracheally given atomized LPS (model group) or saline (control group). Three groups were experimental groups (NBD-2, NBD-6, and NBD-10 groups) that received intratracheal NBD at concentrations of 2, 6, and 10 μg/50 μL/mouse (small, middle, and large NBD groups, resp.) 30 min before intratracheal LPS (100 μg/50 μL/mouse) administration. The remaining group (N-NBD group), which served as a negative control, received a nonfunctional NBD analogue at a concentration of 6 μg/50 μL/mouse 30 min before intratracheal LPS (100 μg/50 μL/mouse) administration.

Two hours after the mice were given LPS or saline, they were sacrificed using sodium pentobarbital. Their right lung tissues were collected for histopathological and immunohistochemical analyses. Their left lungs were snap-frozen in liquid nitrogen and stored at -80°C for enzyme-linked immunosorbent assay (ELISA) and Western blotting analysis. Bronchoalveolar lavage fluid (BALF) samples were collected for protein and cell counting detecting.

2.4. Lung Histopathological Studies. After the mice were euthanized and subjected to thoracotomy, their right lungs were removed and tied off at the end of trachea to keep the lungs inflated. Then, the lungs were fixed in 4% paraformaldehyde for 18 h before being embedded in paraffin and sliced into 3 μm thick sections using a microtome and stained with hematoxylin and eosin (H&E). Lung histologic changes were evaluated by pathologists who were blinded to the study. Lung parenchyma histological alterations were quantitatively graded using the following scale ranging from 0 to 5 [18]:

(0) no reaction in the alveolar walls; (1) diffuse reaction in the alveolar walls—primarily neutrophilic—without alveolar wall thickening; (2) diffuse inflammatory cell (neutrophil and mononuclear cell) infiltration in the alveolar walls, with slight thickening; (3) distinct (2-3 times) alveolar wall thickening due to the presence of inflammatory cells; (4) alveolar wall thickening up to 25% above baseline; and (5) alveolar wall thickening up to 50% above baseline. The final score was calculated as the mean of scores from 50 microscopic fields.

2.5. Cytokine, Protein, and Cell Count Analyses. Blood samples were centrifuged at 4°C at 2,500 rpm for 15 min and used to estimate serum TNF-α, IL-1β, IL-6, and IL-8 levels. After thoracotomy, the trachea was identified and intubated with a tracheal cannula. The trachea and pulmonary alveoli were washed 3 times with 1 mL of sterile saline, and all lavage fluid was collected according to the study groups. The BALF was centrifuged at 500 ×g for 5 min at 4°C to obtain the supernatants, which were stored at −20°C for protein and cell counts assays. BALF protein concentrations were measured using a BCA Protein Assay Kit. Total cell counts were determined using a hemocytometer. The numbers of neutrophils were determined on BALF smear slides stained with Diff-Quick.

2.6. Measurement of SOD, T-AOC, and MDA Activity. SOD and T-AOC activity were measured using commercially available assay kits, according to the manufacturer's instructions. MDA levels were measured using a thiobarbituric acid reactive substances assay kit, according to the manufacturer's instructions.

2.7. Lung Tissue Western Blot Analysis. Frozen lung tissue samples were thawed and homogenized in radio-immunoprecipitation lysis buffer (RIPA) supplemented with protease inhibitors and phenylmethylsulfonyl fluoride (PMSF). After centrifugation, we measured protein concentrations via standard BCA assay. We subsequently added equal amounts of protein to 6x sodium dodecyl sulfate (SDS) loading buffer, after which the protein samples were heated (100°C; 5 min). The proteins were then separated by 10% SDS-PAGE and transferred to nitrocellulose membranes for the appropriate time. The membranes were blocked with Tris-buffered saline containing Tween-20 (TBST) and 5% nonfat milk (1 h; 24°C) and washed with TBS containing 0.1% Tween-20 before being incubated overnight at 4°C with the following antibodies: p-IKKα/β, IKKα, IKKβ, p-I-κB, I-κB, p-NF-κB p65, NF-κB p65, NOX1, NOX2, and NOX4. The following day, the membranes were washed in TBST three times, incubated with a 1 : 2000 (v/v) dilution of horseradish peroxidase-labeled IgG for 1 h at 37°C, and then washed three additional times in TBST. The bands were visualized using ECL Plus Reagent, and the Western blot results were quantitated using Quantity One software (Gel-doc, Bio-Rad, Germany) and normalized to the β-actin signal. The blots were representative of multiple experiments.

2.8. Immunohistochemistry (IHC). The lung tissue sections were incubated with 1 : 200 diluted mouse polyclonal antibodies against phospho-NF-κBp65 and NOX1 overnight at 4°C in a humidified chamber. Then, these immune complexes were incubated with the appropriate secondary antibody for 20 min at room temperature before being rinsed 3 times with PBS. Immunoreactivity was represented by brown staining using DAB (Beijing Biosynthesis Biotechnology Co., Ltd.). The sections were subsequently washed with distilled water, counterstained with H&E, and photographed via microscopy (Olympus Optical Co., Tokyo, Japan). The IHC staining results were evaluated by independent pathologists who were blinded to the study. Immunohistochemical staining intensity was scored using a scale ranging from 0 to 3 (negative = 0, weak = 1, moderate strong = 2, or strong = 3). Staining extent was assessed based on the percentages of positive cells as follows: 0 (negative), 1 (1–25%), 2 (26–50%), 3 (51–75%), and 4 (76–100%). The final staining score was calculated as the mean of the sums of the scores in five fields in every section, and all the sections were separated into low expression groups (final score = 1–5) and high expression groups (final score = 6–12).

2.9. Statistical Analysis. All data are expressed as the mean ± standard deviation (SD). Differences between the experimental and control groups were assessed by either the analysis of variance (ANOVA) or t-test, as applicable, using SPSS 18.0 (SPSS, 165 Inc.). Statistical significance was accepted at $P < 0.05$ for all analyses.

3. Results

3.1. Effect of NBD on Pulmonary Histopathological Changes in Mice with LPS-Induced ALI. To evaluate the lung histopathological changes caused by LPS-induced lung injury, hematoxylin-eosin staining and histopathological analyses were performed. As expected, in the control group, normal pulmonary structures were observed via light microscopy, and no histopathological changes were noted. In the model group, staining revealed the presence of excessive edema and severe hemorrhage resulting in widespread increases in alveolar wall thickness, as well as alveolar collapse and obvious inflammatory cell infiltration. However, when the mice were treated with increasing doses of intratracheally administered NBD, the abovementioned LPS-induced pathological changes were attenuated (Figure 1(a)). Semiquantitative analysis of the NBD-treated lung tissue samples yielded similar results, as NBD treatment normalized the lung wet/dry weight ratio and attenuated the abovementioned increases in alveolar wall thickness and inflammation (Figures 1(b), 1(c), and 1(d)). These findings indicate that NBD pretreatment attenuates histopathological changes in lungs subjected to LPS-induced ALI.

3.2. Effects of NBD on BALF Protein Levels and Inflammatory Cell Infiltration. Uncontrolled inflammation causes vascular leakage in the lung in CLP-induced acute lung injury. BALF protein levels were assessed at 2 h after LPS injection to

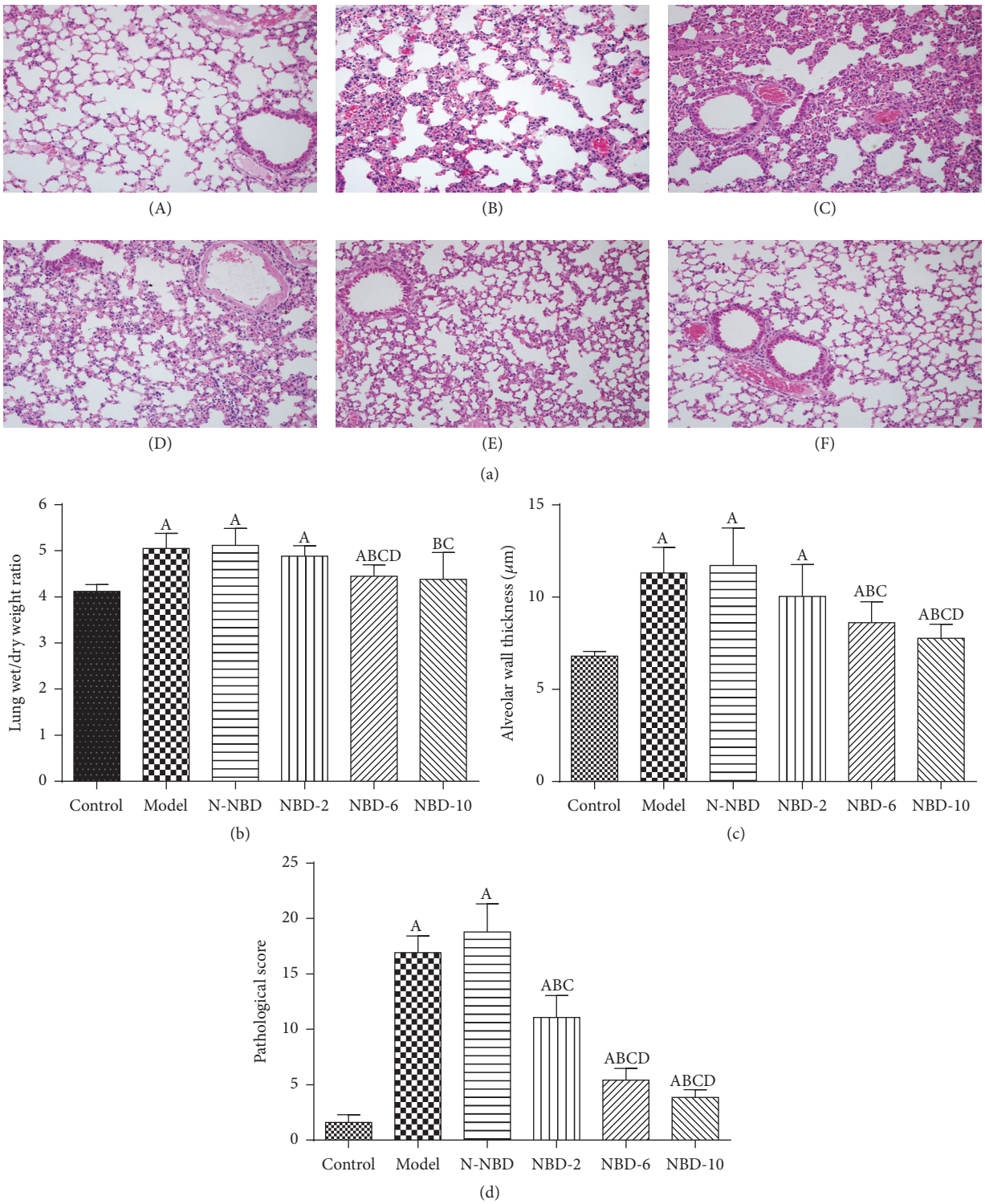

FIGURE 1: Effects of NBD on LPS-induced pulmonary histopathological changes in mice with ALI. (a) Lung sections stained with hematoxylin-eosin at 2 hours after LPS administration exhibited pulmonary histopathological changes (original magnification ×200). (A) Control group: normal structure. (B) Model group: alveolar wall thickening, hemorrhaging, alveolar collapse, and obvious inflammatory cell infiltration. (C) N-NBD group: same as the model group. (D) NBD-2 group. (E) NBD-6 group. (F) NBD-10 group. (b) Lung wet/dry weight ratios, (c) alveolar wall thickness, and (d) histopathological changes were evaluated to assess lung injury severity. LPS-induced lung injury severity was attenuated by NBD in a dose-dependent manner. Data are expressed as the mean ± SD ($n = 6$). A represents versus control group, $^{A}P < 0.05$; B represents versus model group, $^{B}P < 0.05$; C represents versus N-NBD group, $^{C}P < 0.05$; D represents versus NBD-2 group, $^{D}P < 0.05$.

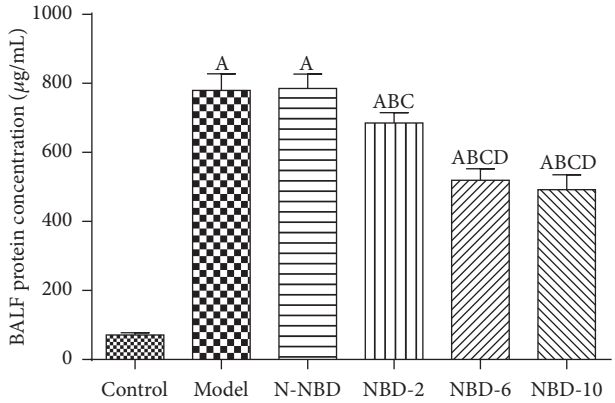

Figure 2: Effects of NBD on pulmonary vascular leakage in mice with ALI. BALF protein concentrations were assessed to evaluate pulmonary vascular leakage. The data indicated that NBD can noticeably reduce BALF protein levels. Data are expressed as the mean ± SD ($n = 6$). A represents versus control group, $^{A}P < 0.05$; B represents versus model group, $^{B}P < 0.05$; C represents versus N-NBD group, $^{C}P < 0.05$; D represents versus NBD-2 group, $^{D}P < 0.05$.

evaluate the effects of NBD on alveolar-capillary membrane barrier integrity and pulmonary vascular leakage. The results indicated that the total protein concentration in the BALF was increased after LPS administration. However, the total protein concentration was markedly decreased in a dose-dependent manner in the NBD group compared with the ALI group ($P < 0.05$) (Figure 2). The total numbers of cells and neutrophils in the BALF were also quantified at 2 h after LPS administration. The results indicated that the total numbers of cells and neutrophils in the BALF were significantly increased in the ALI group compared to the control group ($P < 0.05$). Similar to the above results, NBD treatment significantly decreased the total numbers of cells and neutrophils in the BALF ($P < 0.05$) (Figure 3).

3.3. Effects of NBD on Cytokine Levels in Mice with ALI. TNF-α and IL-1β both are the major proinflammatory cytokines that facilitate active PMNs recruitment into the lungs in all kinds of pulmonary injury [10, 19, 20].

At 2 hours after LPS administration, we observed that TNF-α and IL-1β expression levels had increased significantly in mice in the ALI group. However, mice in the NBD group exhibited concentration-dependent decreases in TNF-α and IL-1β levels (Figures 4(a) and 4(b)). IL-6 and IL-8 expression levels were also assessed to evaluate inflammation severity in ALI mice. The results showed that mice pretreated with NBD exhibited lower serum/BALF IL-6 levels after LPS challenge. Interestingly, NBD exerted dose-dependent effects on the levels of these cytokines (Figures 4(c) and 4(d)). These data suggest that NBD pretreatment attenuates LPS-induced ALI by suppressing proinflammatory cytokine production.

3.4. Effect of NBD on SOD and T-AOC Activity and MDA Concentrations in the Lung Tissues of Mice with ALI. In general, the process of LPS-induced ALI is characterized by excessive oxidative stress, which damages endothelial barrier integrity [21]. SOD and T-AOC are antioxidant enzymes that are inactivated by reactions involving ROS and membrane phospholipids that form MDA. To assess the effects of NBD on MDA production in LPS-induced ALI, we detected SOD and T-AOC activity in the lung. LPS administration significantly decreased SOD levels (Figure 5(a)) and T-AOC (Figure 5(b)) activity and increased MDA (Figure 5(c)) levels. However, the middle and large NBD concentrations exerted effects contrasting with those of sham treatment. Therefore, we concluded that NBD attenuates ALI-induced oxidative stress in LPS-treated mice.

3.5. Effects of NBD on IKK, IκB, and NF-κB p56 Activation in the Lung Tissues of Mice with ALI. It is accepted that LPS induces NF-κB activation by acting on IKK and IκB phosphorylation in lung tissue and that this effect is related to the inflammatory response [21]. At 2 hours after LPS administration, IKK, IκB-α, and NF-κBp65 phosphorylation levels increased dramatically. However, these increases were significantly attenuated in a concentration-dependent manner in mice treated with NBD before LPS administration (Figures 6(a) and 6(b)). IHC staining and semiquantitative analysis yielded similar results (Figure 7).

3.6. Effects of NBD on NOX1, NOX2, and NOX4 Expression in the Lung Tissues of Mice with ALI. Inflammation-induced oxidative stress plays an important role in ALI. Our previous results indicated that the NF-κB signaling pathway regulates NOX family expression, thereby inducing increased reactive oxygen species production leading to cellular oxidative damage. Notably, LPS stimulation significantly increased NOX1, NOX2, and NOX4 expression, while pretreatment with the middle and large NBD concentrations suppressed LPS-induced NOX family member expression (Figures 8(a) and 8(b)). These results demonstrated that NBD attenuates LPS-induced oxidative stress in ALI by inhibiting NOX production. Similar results were observed via IHC staining and semiquantitative analysis (Figure 9).

4. Discussion

This study demonstrated the effects exerted by NBD on LPS-induced inflammation and oxidative stress in mouse lung tissue. We found that NBD effectively prevented LPS-induced lung histopathological changes. We also observed that NBD pretreatment attenuated LPS-induced proinflammatory cytokine expression and oxidative stress and inhibited the NF-κB pathway.

In experimental models of ALI, intratracheal LPS administration is the classic method of mimicking the process of human ARDS and causes similar histopathological changes, such as hemorrhage, interstitial edema, and neutrophil infiltration [22]. LPS also induces significant increases in pulmonary microvascular permeability, leading to increases in extravascular lung water, as well as protein-rich fluid leakage from the intravascular space into the interstitium and air spaces [23–25]. We observed similar histopathological

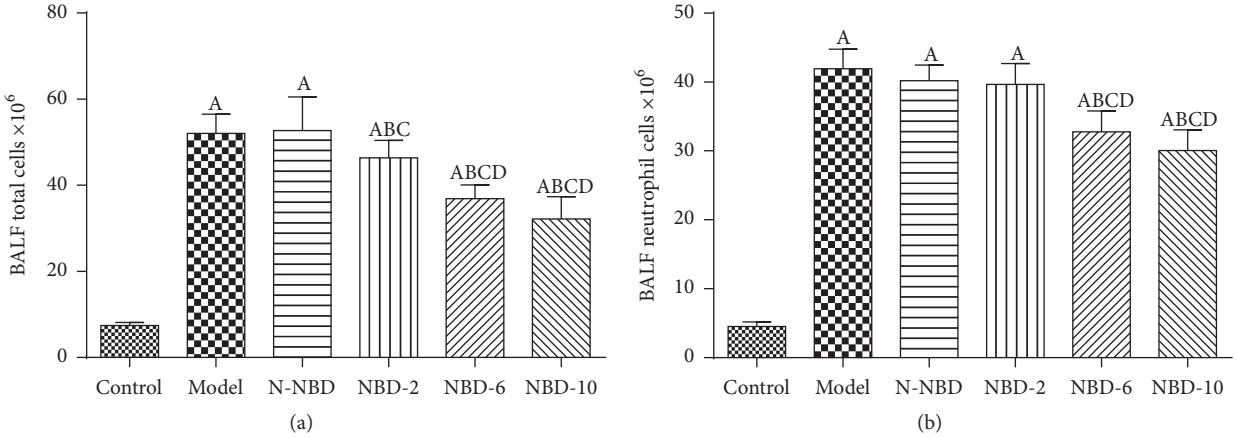

Figure 3: Effect of NBD on inflammatory cell infiltration in the BALF of mice with ALI. BALF (a) total cell and (b) neutrophil levels were assessed to evaluate inflammatory infiltration. Data are expressed as the mean ± SD ($n = 6$). A represents versus control group, $^{A}P < 0.05$; B represents versus model group, $^{B}P < 0.05$; C represents versus N-NBD group, $^{C}P < 0.05$; D represents versus NBD-2 group, $^{D}P < 0.05$.

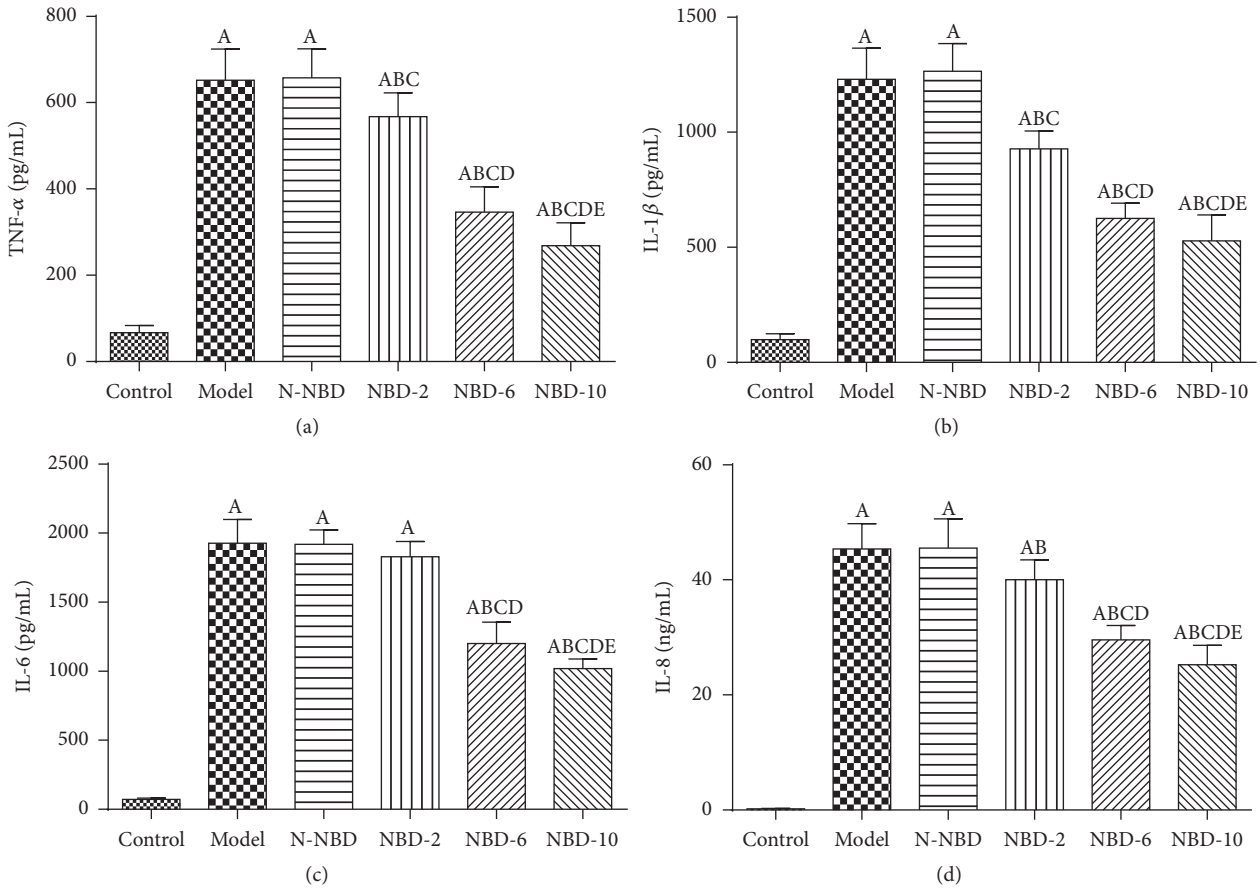

Figure 4: Effect of NBD on serum cytokine concentrations in mice with ALI. Values are expressed as the mean ± SD ($n = 6$). Increased serum TNF-α, IL-1β, IL-6, and IL-10 levels were detected in mice in response to LPS or N-NBD + LPS treatment. NBD decreased serum cytokine levels in ALI mice in a dose-dependent manner. A represents versus control group, $^{A}P < 0.05$; B represents versus model group, $^{B}P < 0.05$; C represents versus N-NBD group, $^{C}P < 0.05$; D represents versus NBD-2 group, $^{D}P < 0.05$; E represents versus NBD-6 group, $^{E}P < 0.05$.

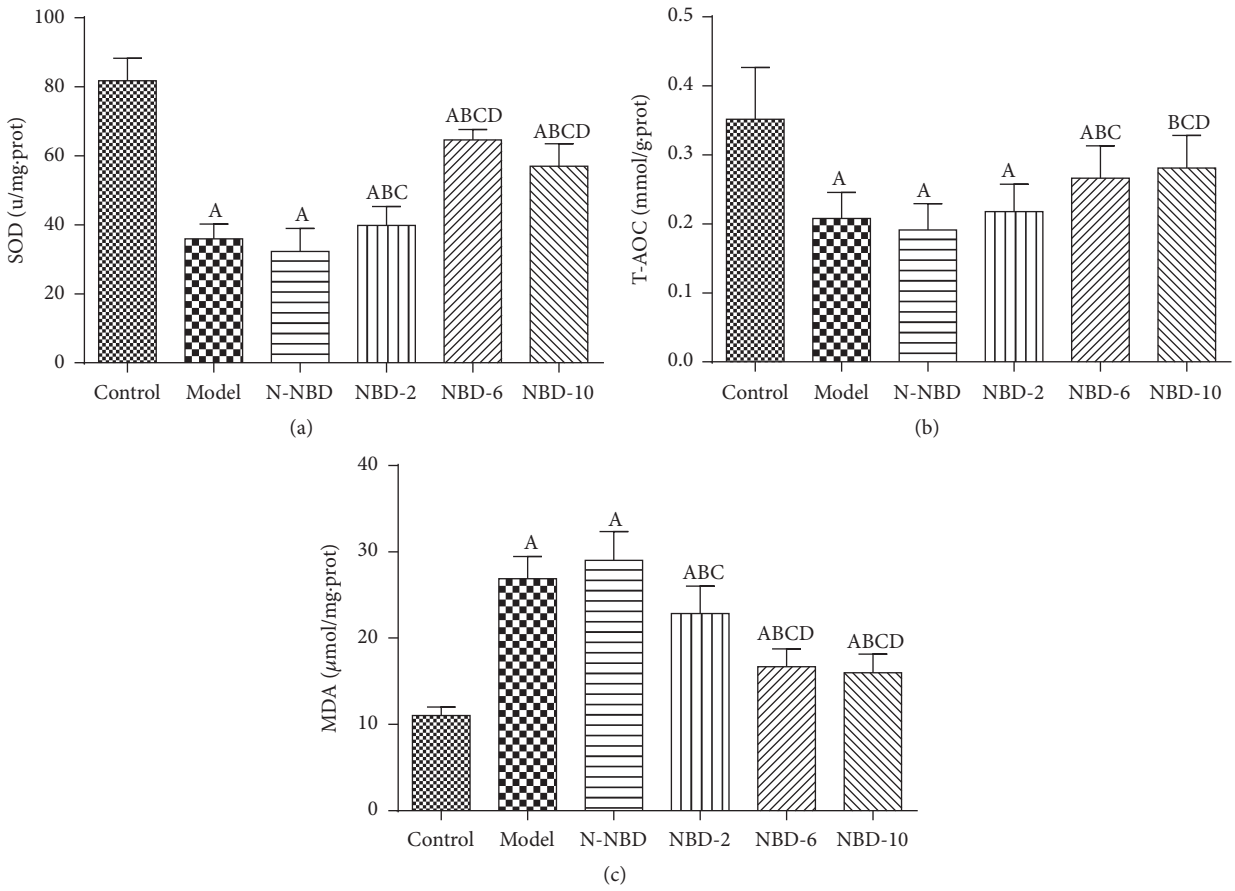

Figure 5: Effect of NBD on SOD and T-AOC activity and MDA concentrations in the lung tissues of mice with ALI. LPS challenge significantly increased MDA levels and decreased SOD and T-AOC activity compared with sham controls; however, treatment with the middle and large NBD concentrations exerted effects contrasting with those described above. Data are expressed as the mean ± SD ($n = 6$). A represents versus control group, $^{A}P < 0.05$; B represents versus model group, $^{B}P < 0.05$; C represents versus N-NBD group, $^{C}P < 0.05$; D represents versus NBD-2 group, $^{D}P < 0.05$.

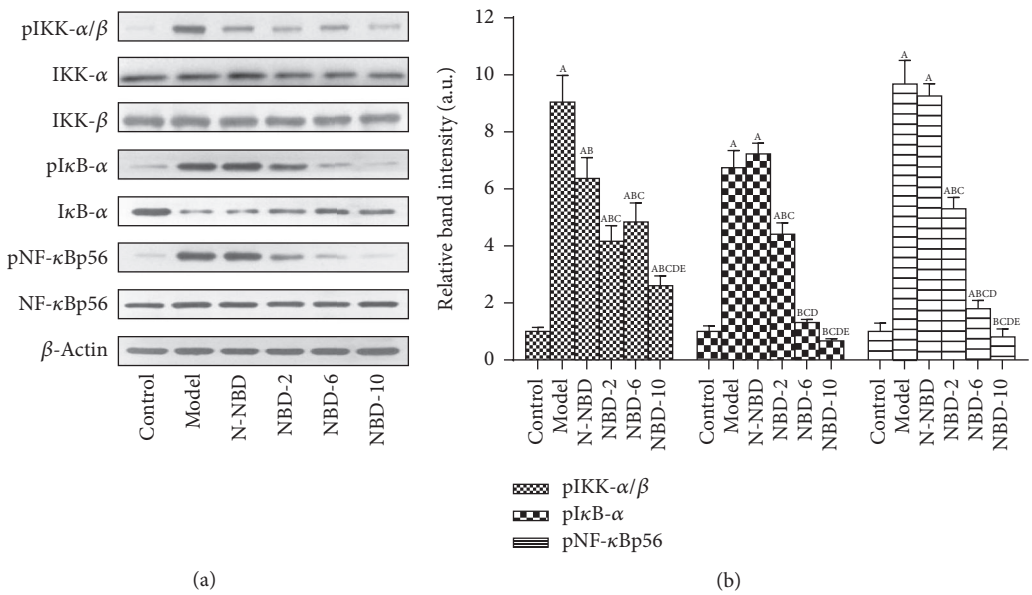

Figure 6: Effect of NBD on IKK, IκB-α, and NF-κBp65 activation in the lung tissues of mice with ALI. (a) Relative gray scale quantitation of total IκB-α, NF-κB, and β-actin phosphorylation. (b) Statistical results. IKK, IκB-α, and NF-κBp65 phosphorylation levels were increased by LPS administration, and these changes were inhibited by NBD pretreatment in a concentration-dependent manner. Data are expressed as the mean ± SD ($n = 6$). A represents versus control group, $^{A}P < 0.05$; B represents versus model group, $^{B}P < 0.05$; C represents versus N-NBD group, $^{C}P < 0.05$; D represents versus NBD-2 group, $^{D}P < 0.05$; E represents versus NBD-6 group, $^{E}P < 0.05$.

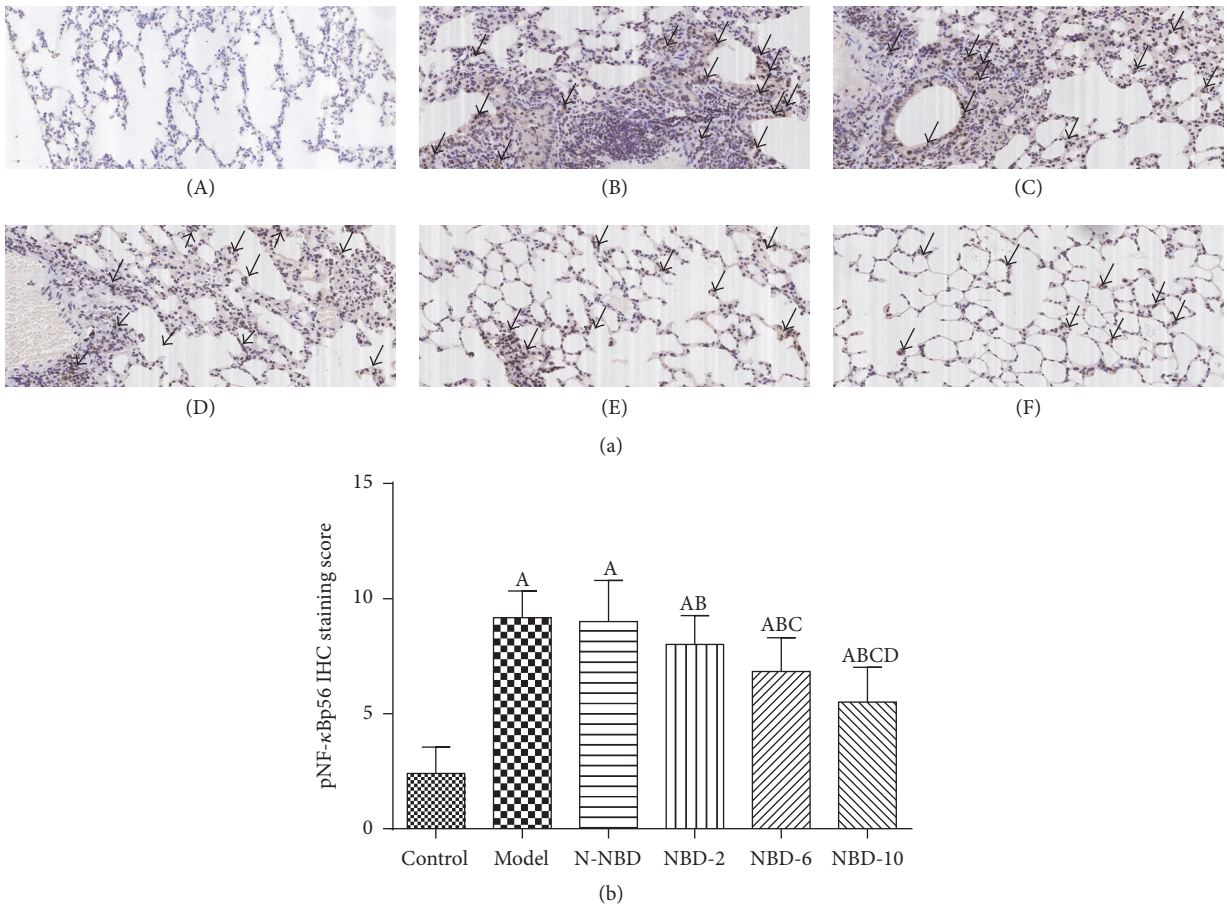

Figure 7: Effect of NBD on pNF-κBp65 expression, as determined via immunohistochemistry, in the lung tissues of mice with ALI. (a) Representative photographs of pNF-κB P65 expression in the lung (original magnification ×200). (A) Control group; (B) model group; (C) N-NBD group; (D) NBD-2 group; (E) NBD-6 group; (F) NBD-10 group. Black arrows indicate the immunohistochemically positive pNF-κBp65. (b) IHC staining scores pertaining to pNF-κB P65 expression. pNF-κBp65 expression levels were increased by LPS administration, and these changes were inhibited by NBD pretreatment in a concentration-dependent manner. Data are expressed as the mean ± SD ($n = 6$). A represents versus control group, $^{A}P < 0.05$; B represents versus model group, $^{B}P < 0.05$; C represents versus N-NBD group, $^{C}P < 0.05$; D represents versus NBD-2 group, $^{D}P < 0.05$.

changes in this study. Moreover, in this study, NBD pretreatment reversed the lung histopathological damage caused by LPS administration and attenuated protein leakage and activated PMN recruitment to the lung parenchyma. Thus, we speculated that the protective effects exerted by NBD are associated with NADPH oxidases, which contribute to the oxidative stress response in all types of inflammatory disorders. As we expected, NBD pretreatment reduced TNF-α and IL-1β release via NADPH oxidase suppression.

LPS activates alveolar macrophages and endothelial cells, increasing the levels of proinflammatory mediators, such as TNF-α, IL-6, and IL-8, which play major roles in inducing ALI by recruiting PMNs to the lungs and enhancing PMN activity [26]. IL-1β is another important proinflammatory cytokine that is generated mainly by macrophages and is involved in inflammatory and immunomodulatory processes [27]. IL-1β is a major extracellular proinflammatory cytokine that usually exerts synergistic effects with TNF-α [28]. Most studies have reported that TNF-α and IL-1β levels are increased in LPS-treated mice [29, 30]. These increases were suppressed by NBD in a concentration-dependent manner, demonstrating that NBD has significant anti-inflammatory properties, which may explain how NBD can inhibit cytokine production by inhibiting the NF-κB signaling pathway. Previous studies showed that NF-κB signaling pathway overactivation is closely related to ALI development [31, 32]. NF-κB signaling is upregulated to induce the transcription of some inflammatory factors in LPS-induced ALI [12, 33]. Under resting conditions, NF-κB is bound by IκB and maintained in a deactivated state in the cytoplasm. LPS administration induces toll-like receptors to stimulate a series of NF-κB cascades, resulting in IκB depolymerization and degradation by proteasomes. The liberated NF-κB translocates into the nucleus and binds to specific gene sequences, including gene promoter sequences or enhancer regions, suggesting that NBD-mediated NF-κB inhibition may be caused by IκB-α

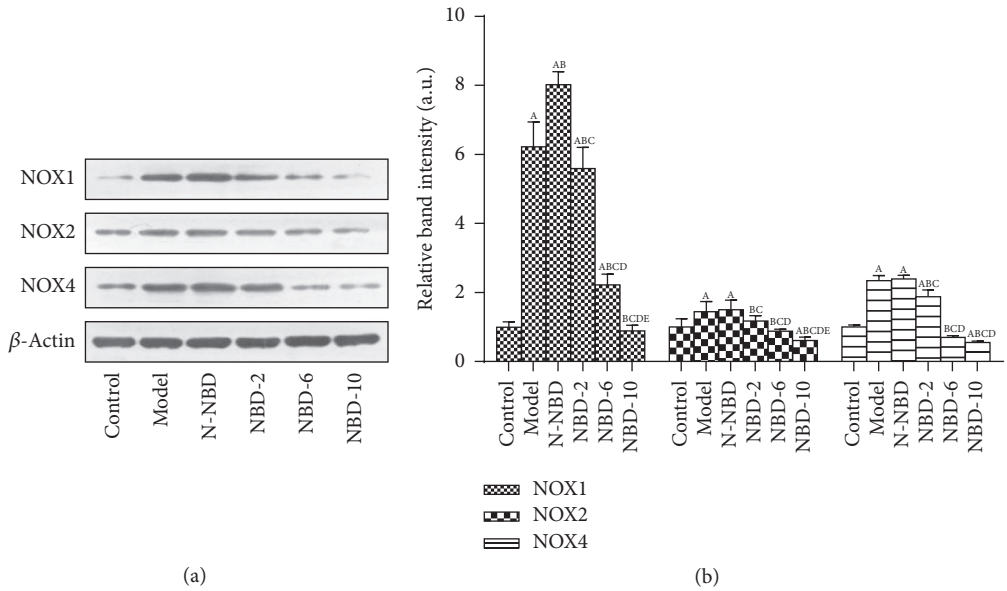

Figure 8: Effect of NBD on NOX1, NOX2, and NOX4 expression in the lung tissues of mice with ALI. (a) Relative NOX1, NOX2, NOX4, and β-actin immunointensity levels were calculated. (b) Statistical results. NOX1, NOX2, and NOX4 expression levels were increased by LPS administration, and these changes were inhibited by the middle and large NBD concentrations. Data are expressed as the mean ± SD ($n = 6$). A represents versus control group, $^{A}P < 0.05$; B represents versus model group, $^{B}P < 0.05$; C represents versus N-NBD group, $^{C}P < 0.05$; D represents versus NBD-2 group, $^{D}P < 0.05$; E represents versus NBD-6 group, $^{E}P < 0.05$.

inhibition. This mechanism entails the binding of NBD to IKKγ to block IKK assembly, which reduces IKK activity and inhibits NF-κB activation [34].

Inflammation-induced oxidative stress plays an important role in acute lung injury. The respiratory burst is an early symptom of LPS-induced acute lung injury that depends on PMNs producing reactive oxygen species (ROS), including O_2^- and hydrogen peroxide. The respiratory burst can protect organs from pathogens. However, excessive ROS can damage tissues and cause inflammation [35]. ROS attack polyunsaturated fatty acids, producing lipid peroxidation products, such as MDA, causing tissue damage [36]. In our study, pretreatment with the middle and large NBD concentrations prevented MDA generation in the lung tissues of mice with LPS-induced ALI. ROS elimination requires antioxidant enzymes, such as SOD and T-AOC, which convert O_2^- into H_2O_2, and catalase, which metabolizes H_2O_2 into hydrogen oxide and oxygen [37]. The present study revealed that LPS significantly reduced SOD and T-AOC activity in the lung. This finding is consistent with those pertaining to the effects exerted by inflammatory responses in ALI patients [37]. However, our study demonstrated that NBD treatment before LPS administration can reverse the decreases in SOD and T-AOC activity caused by LPS. Therefore, we hypothesized that NBD can reduce the inflammatory response by attenuating oxyradical formation in mice with LPS-induced ALI.

In conclusion, NBD treatment attenuates ALI by inhibiting LPS-induced NF-κB signaling pathway overactivation, thereby suppressing LPS-induced inflammation and oxidative stress. Our findings suggest that NBD has potential as a therapeutic target in the treatment of acute inflammatory diseases, including ALI, ARDS, and infectious diseases.

Disclosure

Jianhua Huang and Li Li are co-first authors.

Competing Interests

The authors declare no competing interests.

Authors' Contributions

Jianhua Huang and Li Li participated in performing the experiments and writing of the paper; they contributed equally to the work. Weifeng Yuan and Linxin Zheng participated in the data analysis. Zhenhui Guo and Wenjie Huang provided substantial advice in designing the study, assisting in the division of labor, and revising the paper; they contributed equally to the work.

Acknowledgments

The authors are indebted to all individuals who participated in or helped with this research project. This study was supported by funding from "the National Nature Science Foundation of China" (Grant no. 81370173) and "Guangzhou Science and Technology Program key projects" (Grant no. 2011B031800170).

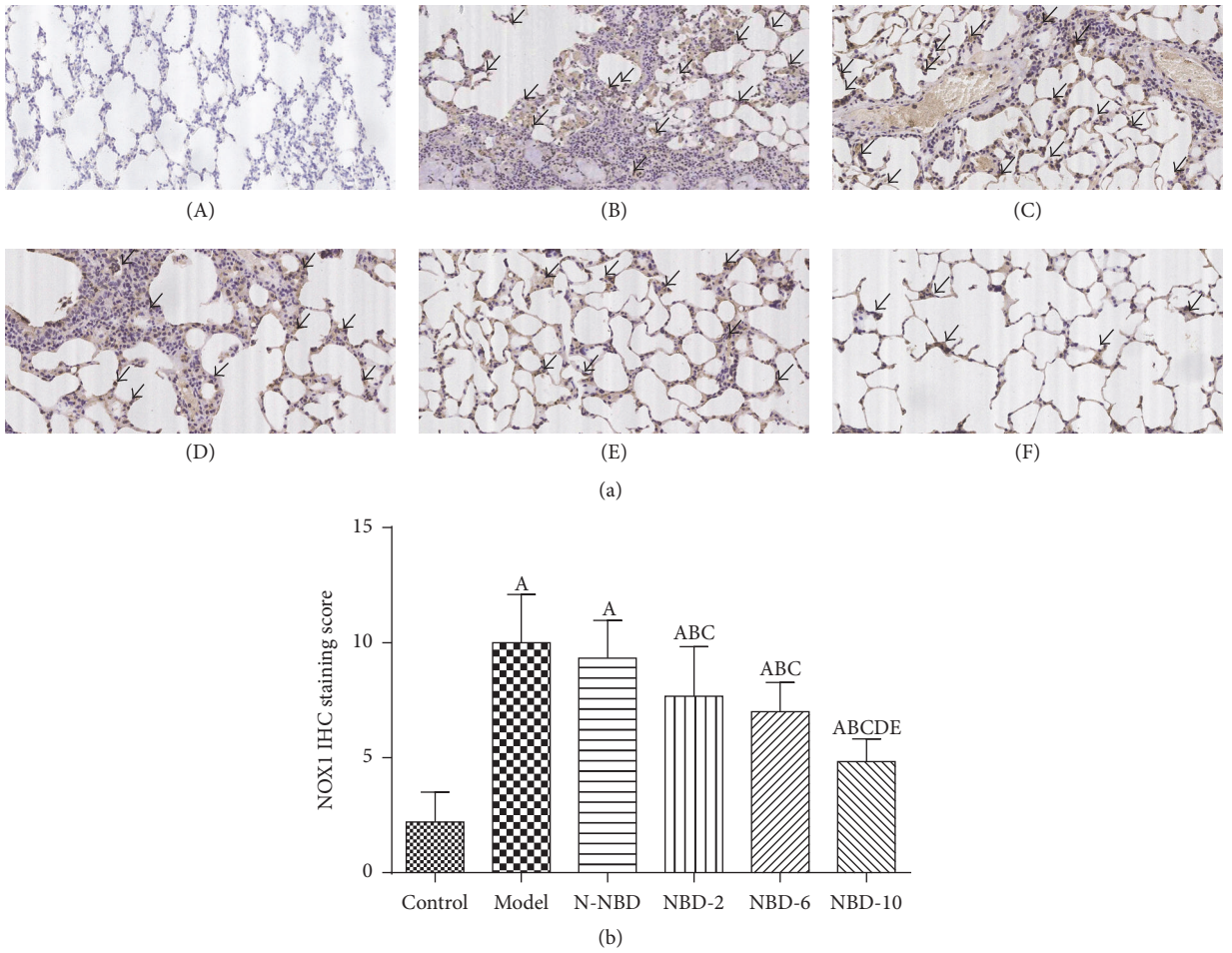

Figure 9: Effect of NBD on NOX1 expression, as determined via immunohistochemistry, in the lung tissues of mice with ALI. (a) Representative photographs of NOX1 expression in the lung (original magnification ×200). (A) Control group; (B) model group; (C) N-NBD group; (D) NBD-2 group; (E) NBD-6 group; (F) NBD-10 group. Black arrows indicate the immunohistochemically positive NOX1. (b) IHC staining scores pertaining to NOX1 expression. NOX1 expression levels were increased by LPS administration, and these changes were inhibited by NBD pretreatment in a concentration-dependent manner. Data are expressed as the mean ± SD ($n = 6$). A represents versus control group, $^{A}P < 0.05$; B represents versus model group, $^{B}P < 0.05$; C represents versus N-NBD group, $^{C}P < 0.05$; D represents versus NBD-2 group, $^{D}P < 0.05$; E represents versus NBD-6 group, $^{E}P < 0.05$.

References

[1] G. D. Rubenfeld, E. Caldwell, E. Peabody et al., "Incidence and outcomes of acute lung injury," *The New England Journal of Medicine*, vol. 353, no. 16, pp. 1685–1693, 2005.

[2] G. D. Rubenfeld and M. S. Herridge, "Epidemiology and outcomes of acute lung injury," *Chest*, vol. 131, no. 2, pp. 554–562, 2007.

[3] M. A. Matthay, L. B. Ware, and G. A. Zimmerman, "The acute respiratory distress syndrome," *The Journal of Clinical Investigation*, vol. 122, no. 8, pp. 2731–2740, 2012.

[4] C. Putensen, "Acute respiratory distress syndrome (ARDS)," in *Sepsis und MODS*, pp. 153–166, Springer, Berlin, Germany, 2015.

[5] A. M. Modrykamien and P. Gupta, "The acute respiratory distress syndrome," *Proceedings (Baylor University. Medical Center)*, vol. 28, no. 2, pp. 163–171, 2015.

[6] E. Abraham, "Neutrophils and acute lung injury," *Critical Care Medicine*, vol. 31, no. 4, pp. S195–S199, 2003.

[7] V. M. Ranieri, G. D. Rubenfeld, B. T. Thompson et al., "Acute respiratory distress syndrome: the Berlin Definition. The ARDS Definition Task Force," *The Journal of the American Medical Association*, vol. 307, no. 23, pp. 2526–2533, 2012.

[8] G. Matute-Bello, C. W. Frevert, and T. R. Martin, "Animal models of acute lung injury," *American Journal of Physiology—Lung Cellular and Molecular Physiology*, vol. 295, no. 3, pp. L379–L399, 2008.

[9] J. Grommes and O. Soehnlein, "Contribution of neutrophils to acute lung injury," *Molecular Medicine*, vol. 17, no. 3-4, pp. 293–307, 2011.

[10] P. Puneet, S. Moochhala, and M. Bhatia, "Chemokines in acute respiratory distress syndrome," *American Journal of Physiology—Lung Cellular and Molecular Physiology*, vol. 288, no. 1, pp. L3–L15, 2005.

[11] G. He, C. Dong, Z. Luan et al., "Oxygen free radical involvement in acute lung injury induced by H5N1 virus in mice," *Influenza and Other Respiratory Viruses*, vol. 7, no. 6, pp. 945–953, 2013.

[12] S. Liu, G. Feng, G.-L. Wang, and G.-J. Liu, "p38MAPK inhibition attenuates LPS-induced acute lung injury involvement of NF-κB pathway," *European Journal of Pharmacology*, vol. 584, no. 1, pp. 159–165, 2008.

[13] M. S. Hayden and S. Ghosh, "Regulation of NF-κB by TNF family cytokines," *Seminars in Immunology*, vol. 26, no. 3, pp. 253–266, 2014.

[14] S. Gerondakis, T. S. Fulford, N. L. Messina, and R. J. Grumont, "NF-κB control of T cell development," *Nature Immunology*, vol. 15, no. 1, pp. 15–25, 2014.

[15] A. Nenci, C. Becker, A. Wullaert et al., "Epithelial NEMO links innate immunity to chronic intestinal inflammation," *Nature*, vol. 446, no. 7135, pp. 557–561, 2007.

[16] M. J. May, F. D'Acquisto, L. A. Madge, J. Glockner, J. S. Pober, and S. Ghosh, "Selective inhibition of NF-κB activation by a peptide that blocks the interaction of NEMO with the IκB kinase complex," *Science*, vol. 289, no. 5484, pp. 1550–1554, 2000.

[17] J. A. DiDonato, F. Mercurio, and M. Karin, "NF-κB and the link between inflammation and cancer," *Immunological Reviews*, vol. 246, no. 1, pp. 379–400, 2012.

[18] R. J. Szarka, N. Wang, L. Gordon, P. N. Nation, and R. H. Smith, "A murine model of pulmonary damage induced by lipopolysaccharide via intranasal instillation," *Journal of Immunological Methods*, vol. 202, no. 1, pp. 49–57, 1997.

[19] M. Bhatia, R. L. Zemans, and S. Jeyaseelan, "Role of chemokines in the pathogenesis of acute lung injury," *American Journal of Respiratory Cell and Molecular Biology*, vol. 46, no. 5, pp. 566–572, 2012.

[20] T. Dolinay, Y. S. Kim, J. Howrylak et al., "Inflammasome-regulated cytokines are critical mediators of acute lung injury," *American Journal of Respiratory and Critical Care Medicine*, vol. 185, no. 11, pp. 1225–1234, 2012.

[21] T. Zhu, D.-X. Wang, W. Zhang et al., "Andrographolide protects against LPS-induced acute lung injury by inactivation of NF-κB," *PLoS ONE*, vol. 8, no. 2, Article ID e56407, 2013.

[22] D. P. Schuster, "ARDS: clinical lessons from the oleic acid model of acute lung injury," *American Journal of Respiratory and Critical Care Medicine*, vol. 149, no. 1, pp. 245–260, 1994.

[23] J. Bhattacharya and M. A. Matthay, "Regulation and repair of the alveolar-capillary barrier in acute lung injury," *Annual Review of Physiology*, vol. 75, pp. 593–615, 2013.

[24] S. Herold, N. M. Gabrielli, and I. Vadász, "Novel concepts of acute lung injury and alveolar-capillary barrier dysfunction," *American Journal of Physiology—Lung Cellular and Molecular Physiology*, vol. 305, no. 10, pp. L665–L681, 2013.

[25] J.-P. Lee, Y.-C. Li, H.-Y. Chen et al., "Protective effects of luteolin against lipopolysaccharide-induced acute lung injury involves inhibition of MEK/ERK and PI3K/Akt pathways in neutrophils," *Acta Pharmacologica Sinica*, vol. 31, no. 7, pp. 831–838, 2010.

[26] L. B. Ware, "Pathophysiology of acute lung injury and the acute respiratory distress syndrome," in *Proceedings of the Seminars in Respiratory and Critical Care Medicine*, pp. 337–349, Thieme Medical, New York, NY, USA, 2006.

[27] C. Basak, S. K. Pathak, A. Bhattacharyya, D. Mandal, S. Pathak, and M. Kundu, "NF-κB- and C/EBPβ-driven interleukin-1β gene expression and PAK1-mediated caspase-1 activation play essential roles in interleukin-1β release from *Helicobacter pylori* lipopolysaccharide-stimulated macrophages," *The Journal of Biological Chemistry*, vol. 280, no. 6, pp. 4279–4288, 2005.

[28] J. Wang, Y.-T. Liu, L. Xiao, L. Zhu, Q. Wang, and T. Yan, "Anti-inflammatory effects of apigenin in lipopolysaccharide-induced inflammatory in acute lung injury by suppressing COX-2 and NF-κB pathway," *Inflammation*, vol. 37, no. 6, pp. 2085–2090, 2014.

[29] D. Wei and Z. Huang, "Anti-inflammatory effects of triptolide in LPS-induced acute lung injury in mice," *Inflammation*, vol. 37, no. 4, pp. 1307–1316, 2014.

[30] H. Wu, G. Zhao, K. Jiang et al., "Plantamajoside ameliorates lipopolysaccharide-induced acute lung injury via suppressing NF-κB and MAPK activation," *International Immunopharmacology*, vol. 35, pp. 315–322, 2016.

[31] C. Liu, J. Huang, H. Li et al., "Ghrelin accelerates wound healing through GHS-R1a-mediated MAPK-NF-κB/GR signaling pathways in combined radiation and burn injury in rats," *Scientific Reports*, vol. 6, Article ID 27499, 2016.

[32] H. Lv, Z. Yu, Y. Zheng et al., "Isovitexin exerts anti-inflammatory and anti-oxidant activities on lipopolysaccharide-induced acute lung injury by inhibiting MAPK and NF-κB and activating HO-1/Nrf2 pathways," *International Journal of Biological Sciences*, vol. 12, no. 1, pp. 72–86, 2016.

[33] K. Schuh and A. Pahl, "Inhibition of the MAP kinase ERK protects from lipopolysaccharide-induced lung injury," *Biochemical Pharmacology*, vol. 77, no. 12, pp. 1827–1834, 2009.

[34] W. Shen, J. Gan, S. Xu, G. Jiang, and H. Wu, "Penehyclidine hydrochloride attenuates LPS-induced acute lung injury involvement of NF-κB pathway," *Pharmacological Research*, vol. 60, no. 4, pp. 296–302, 2009.

[35] N. Borregaard, O. E. Sørensen, and K. Theilgaard-Mönch, "Neutrophil granules: a library of innate immunity proteins," *Trends in Immunology*, vol. 28, no. 8, pp. 340–345, 2007.

[36] D. Del Rio, A. J. Stewart, and N. Pellegrini, "A review of recent studies on malondialdehyde as toxic molecule and biological marker of oxidative stress," *Nutrition, Metabolism and Cardiovascular Diseases*, vol. 15, no. 4, pp. 316–328, 2005.

[37] J. Ueda, M. E. Starr, H. Takahashi et al., "Decreased pulmonary extracellular superoxide dismutase during systemic inflammation," *Free Radical Biology and Medicine*, vol. 45, no. 6, pp. 897–904, 2008.

Hindawi Publishing Corporation
Mediators of Inflammation
Volume 2016, Article ID 5813794, 13 pages
http://dx.doi.org/10.1155/2016/5813794

Research Article

Protective Effect of Galectin-1 during *Histoplasma capsulatum* Infection Is Associated with Prostaglandin E_2 and Nitric Oxide Modulation

Lílian Cataldi Rodrigues,[1] Adriana Secatto,[1] Carlos A. Sorgi,[1] Naiara N. Dejani,[2] Alexandra I. Medeiros,[2] Morgana Kelly Borges Prado,[1] Simone Gusmão Ramos,[3] Richard D. Cummings,[4] Sean R. Stowell,[5] Lúcia Helena Faccioli,[1] and Marcelo Dias-Baruffi[1]

[1]*Departamento de Análises Clínicas, Toxicológicas e Bromatológicas, Faculdade de Ciências Farmacêuticas de Ribeirão Preto, Universidade de São Paulo (USP), 14040-903 Ribeirão Preto, SP, Brazil*
[2]*Departamento de Ciências Biológicas, Faculdade de Ciências Farmacêuticas, Universidade Estadual Paulista (UNESP), 14801-902 Araraquara, SP, Brazil*
[3]*Departamento de Patologia, Faculdade de Medicina de Ribeirão Preto, Universidade de São Paulo (USP), 14049-900 Ribeirão Preto, SP, Brazil*
[4]*Department of Surgery, Beth Israel Deaconess Medical Center and Harvard Medical School, Boston, MA 02115, USA*
[5]*Department of Pathology, Emory University School of Medicine, Atlanta, GA 30322, USA*

Correspondence should be addressed to Marcelo Dias-Baruffi; mdbaruff@fcfrp.usp.br

Received 16 April 2016; Revised 27 July 2016; Accepted 1 August 2016

Academic Editor: Marc Pouliot

Histoplasma capsulatum is a dimorphic fungus that develops a yeast-like morphology in host's tissue, responsible for the pulmonary disease histoplasmosis. The recent increase in the incidence of histoplasmosis in immunocompromised patients highlights the need of understanding immunological controls of fungal infections. Here, we describe our discovery of the role of endogenous galectin-1 (Gal-1) in the immune pathophysiology of experimental histoplasmosis. All infected wild-type (WT) mice survived while only 1/3 of Lgals1$^{-/-}$ mice genetically deficient in Gal-1 survived 30 days after infection. Although infected Lgals1$^{-/-}$ mice had increased proinflammatory cytokines, nitric oxide (NO), and elevations in neutrophil pulmonary infiltration, they presented higher fungal load in lungs and spleen. Infected lung and infected macrophages from Lgals1$^{-/-}$ mice exhibited elevated levels of prostaglandin E_2 (PGE_2, a prostanoid regulator of macrophage activation) and prostaglandin E synthase 2 (*Ptgs2*) mRNA. Gal-1 did not bind to cell surface of yeast phase of *H. capsulatum*, *in vitro*, suggesting that Gal-1 contributed to phagocytes response to infection rather than directly killing the yeast. The data provides the first demonstration of endogenous Gal-1 in the protective immune response against *H. capsulatum* associated with NO and PGE_2 as an important lipid mediator in the pathogenesis of histoplasmosis.

1. Introduction

Histoplasmosis is a worldwide known disease caused by the fungus *Histoplasma capsulatum*. The real geographic distribution of this mycosis could be more widespread than what was previously thought [1, 2]. The incidence of this fungal disease is higher in the Mid- and Southeast USA, Latin America, China, and other world areas [2]. Additionally, asymptomatic cases are escalating and are reported to predominately affect immunocompromised individuals as an acute pulmonary infection similar to mild flu-like symptoms [1, 3, 4]. Likewise, the most severe symptomatic form of the disease, referred to as disseminated histoplasmosis, develops most commonly in immunosuppressed patients. However, unlike the mild form, disseminated histoplasmosis can lead to death [4]. Although antifungal therapies have been used against the fungus, there are no current alternative therapies to treat or protect against *H. capsulatum* infection.

H. capsulatum is a dimorphic, facultative, intracellular pathogen found as a yeast phase when in host tissue [5].

In the early stages of infection, the fungus is phagocytosed by resident alveolar macrophages, dendritic cells, and neutrophils [6]. Once phagocytosed, the fungus survives in the phagosome and consequently transforms into a yeast. In immunocompromised individuals or when left untreated, the reservoir phagocytes can travel to lymphatic tissue and spread infection. However, induction of a strong cellular immune response can contain or clear the infected phagocytes, therefore preventing the spread of the infection. An effective host defense to *H. capsulatum* infection is dependent on adequate activation of T cells and phagocytes [6, 7]. Appropriately, the balance between the Th1 and Th2 response is fundamental for solving *H. capsulatum* infection [6, 7], with Th1 proinflammatory cytokines IFN-γ (interferon-γ), interleukin-12 (IL-12), TNF-α (tumor necrosis factor-α), and GM-CSF (granulocyte macrophage colony-stimulating) being essential to elicit macrophage activation and clearance of *H. capsulatum*. In addition, a balanced production of lipid mediators, such as prostaglandin E_2 (PGE_2) and leukotriene B_4 (LTB_4), is critical for the host defense in histoplasmosis, since high levels of PGE_2 and low levels of LTB_4 impair the yeast clearance and increase the severity of this fungal disease [8, 9]. Nitric oxide also participates in the host defense against *H. capsulatum* [10, 11]; however, overproduction of this mediator increases the susceptibility of the host to yeast infection [8, 12].

In addition to cytokines and lipid mediators, a member of the galectin family, known as galectin-3 (Gal-3), has been suggested to be involved in the immune response against *H. capsulatum* infection [13]. Galectins belong to an endogenous lectin family that recognizes glycans present in microorganisms and participates in the pathophysiology of inflammatory responses, infectious diseases, autoimmunity, and cancer [14–18].

Interestingly, galectin-1 (Gal-1) has been shown to participate in an innate and adaptive immune response to different models of experimental infections such as in *Trypanosoma cruzi* (*T. cruzi*) [19], situation in which a dual role for this lectin was described. These authors showed that, in a low concentration, Gal-1 was able to decrease proinflammatory interleukin-12 (IL-12) and nitric oxide (NO), while in a high concentration, it has induced infected macrophage apoptosis. Gal-1 was also found to promote *Human Immunodeficiency Virus-1* (HIV-1) infectivity [20]; in dengue virus infection, it could cause an inhibitory effect on virus replication [21]. Thus, several Gal-1 exogenous properties have been related to CRD binding to cell surface receptors, modulating immune cell functions, migration, differentiation, activation, and cell survival [22–27]. Nevertheless, the interactions of this lectin with the intracellular ligands can also occur independently to carbohydrates [28, 29].

Although Gal-1 can participate in various pathophysiological processes, there is little information about the role of Gal-1 in fungal infections. Therefore, the present study evaluated the biological impact of the absence of Gal-1 on a murine model of histoplasmosis. While mice genetically deficient in Gal-3 ($Lgals3^{-/-}$) were able to clear *H. capsulatum* infection more efficiently than wild-type (WT) mice [13], it was reported for the first time that Gal-1 ($Lgals1^{-/-}$) mice are more susceptible to *H. capsulatum* infection compared to WT group. This unique immune phenotype suppresses the host response against the fungus and is followed by high levels of neutrophil infiltration and proinflammatory cytokines in the lungs which causes a strong anti-inflammatory response with high levels of PGE_2 and NO. These findings indicate a novel contribution of endogenous Gal-1 to the development of a protective immune response to *H. capsulatum*.

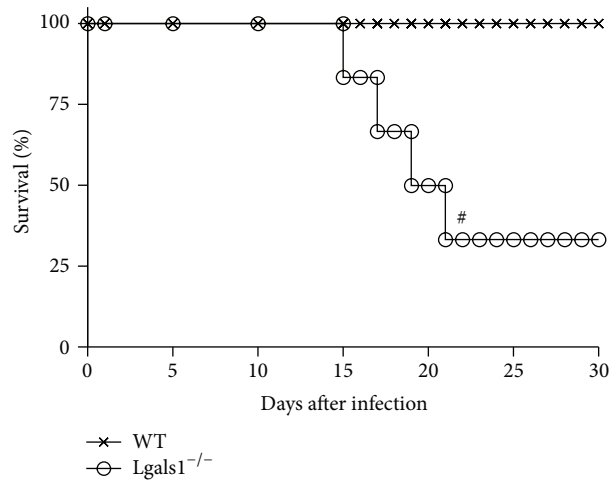

Figure 1: Gal-1 knockout mice are sensitive to *H. capsulatum* infection. WT and $Lgals1^{-/-}$ mice were infected i.t. with 5×10^5 viable *H. capsulatum* yeast (sublethal inoculum) and survival was monitored for 30 days. Control mice (uninfected) received i.t. 100 μL PBS (data not shown). Data are representative of one of the two experiments performed independently ($n = 10$ per group) and Mantel-Cox log-rank (χ^2 "chi-squared") was used. $^{\#}p < 0.05$ WT versus $Lgals1^{-/-}$, both infected.

2. Results

2.1. $Lgals1^{-/-}$-Infected Mice Fail to Control H. capsulatum Infection. WT and $Lgals1^{-/-}$ mice were injected with 5×10^5 *H. capsulatum* yeasts cells directly into the lungs and survival was monitored up to 30 days. 14 days after infection, $Lgals1^{-/-}$-infected mice began to die. 33% of $Lgals1^{-/-}$-infected mice survived 30 days after infection, whereas 100% of the infected WT mice survived over that period (Figure 1).

2.2. $Lgals1^{-/-}$-Infected Mice Have a Higher Yeast Load and Infiltration of Neutrophils in the Lung. To determine if the high mortality rate in $Lgals1^{-/-}$ mice is correlated with impaired fungal clearance, the *H. capsulatum* load was quantified in the lung and spleen. Considering that $Lgals1^{-/-}$ mice began to die day 14 after infection and that day 15 after infection is a critical point on the evolution of experimental histoplasmosis using mutant mice and a sublethal fungus dose [9], on day 15 after infection, lung parenchymal histopathological analysis and quantification of fungal

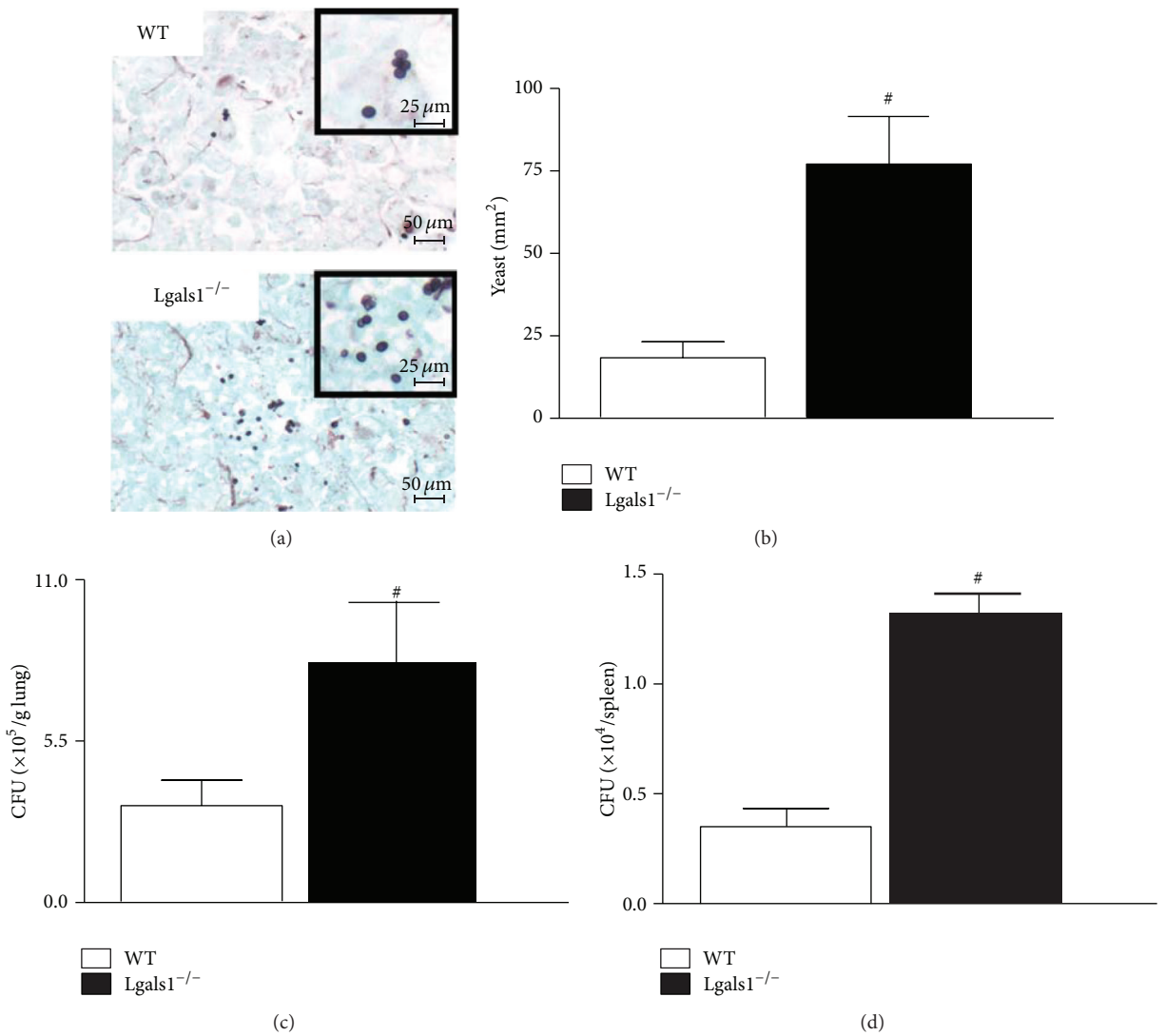

FIGURE 2: Lgals1$^{-/-}$ mice have a higher yeast burden in the lung and spleen day 15 after infection. On day 15 after infection with *H. capsulatum* (5×10^5 viable yeasts), animals were sacrificed and tissue samples were harvested. (a) Lung sections (5 μm) from WT and Lgals1$^{-/-}$ mice were stained with silver (Grocott's methanamine silver (GMS); bar: 50 μm; insert bar: 25 μm) and (b) yeast cells were quantified (yeast/mm^2 lung) using magnifications ×400. Fungal burden was quantified from tissue homogenates and expressed as the number of colony-forming units (CFU) per gram of tissue CFU/g in lung (c) and CFU per spleen (d). Data are representative of one of the two experiments performed independently ($n = 10$ per group). Values are mean ± SEM. $^{\#}p < 0.05$ WT versus Lgals1$^{-/-}$, both infected.

burden in the lung and spleen were performed. Lgals1$^{-/-}$-infected mice presented a higher number of yeast cells in pulmonary parenchyma (Figures 2(a) and 2(b)) and higher fungal load in lung (Figure 2(c)) and spleen (Figure 2(d)). Even though infected Lgals1$^{-/-}$ mice presented a higher fungal burden in the lung, an increased neutrophil influx was detected in their pulmonary tissue (Figures 3(a) and 3(b)). It is known that an efficient immune response against *H. capsulatum* is associated with fungicidal/fungistatic effects of pulmonary infiltrated phagocytes [6, 30]. Thus, these findings suggest that endogenous Gal-1 is required to develop a protective immune response against *H. capsulatum* and that Gal-1 could be associated with the control of fungal replication as an efficient anti-*H. capsulatum* activity along with effectors functions and regulation of tissue accumulation of neutrophils.

2.3. Lgals1$^{-/-}$-Infected Mice Show Increased Proinflammatory Cytokines in the Lung. It is well known that increased expression of inflammatory cytokines, including IL-12, IFN-γ, and TNF-α, is critical for the immune-protective response in *H. capsulatum*-infected mice [31–34]. Thus, to analyze the pattern of inflammatory cytokines in WT and Lgals1$^{-/-}$ mice day 15 after *H. capsulatum* infection, the levels of IL-12p40, TNF-α, IL-1α, IL-10, IL-4, and IL-6 in the pulmonary homogenates were measured. There were higher levels of IL-12p40 (Figure 4(a)) and IL-1α (Figure 4(c)) and similar

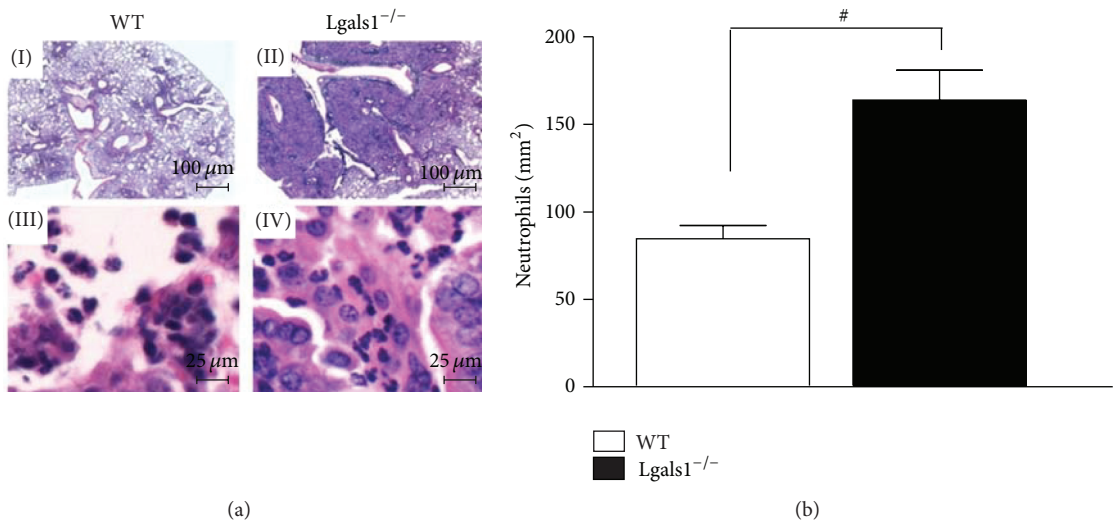

FIGURE 3: Lgals1$^{-/-}$ mice have increased neutrophil infiltration in the lung parenchyma. *H. capsulatum*-infected mice were euthanized on day 15 after infection and lung sections (5 μm) were embedded in paraffin blocks. Lung sections from WT + *H. capsulatum* (I, bar: 100 μm; III, bar: 25 μm) and Lgals1$^{-/-}$ + *H. capsulatum* (II, bar: 100 μm; IV, bar: 25 μm) were stained with hematoxylin (a) and neutrophils were quantified (neutrophils/mm^2) using magnifications ×400 (b). Data are representative of one of the two experiments performed independently ($n = 10$ per group). Values are mean ± SEM. $^{\#}p < 0.05$ WT versus Lgals1$^{-/-}$, both infected.

concentrations of TNF-α (Figure 4(b)) in homogenized lungs of Lgals1$^{-/-}$-infected mice, when compared to WT infected mice. Furthermore, no statistically significant differences in TNF-α (Figure 4(b)) were observed, and IL-10, IL-4, and IL-6 (data not shown) were not produced in detectable levels.

2.4. Lgals1$^{-/-}$-Infected Mice Demonstrate Prostaglandin E_2 and Nitric Oxide Overproduction. Based on the aforementioned results, it was also analyzed whether inflammatory mediators, such as NO and PGE_2, are associated with increased levels of proinflammatory cytokines and consequently immunosuppression in the absence of endogenous Gal-1 in experimental histoplasmosis. It has been reported that the inhibition of COX-2 improves the host defense against *H. capsulatum* [8]. Therefore, PGE_2 was quantified from homogenized lungs derived from infected WT and Lgals1$^{-/-}$ mice on day 15 after *H. capsulatum* infection. The lungs of infected Lgals1$^{-/-}$ mice exhibited higher levels of PGE_2 (Figure 5(a)) when compared to infected WT mice. Thus, consistent with other published results [8, 35], these findings suggest that higher levels of PGE_2 may contribute to susceptibility of infected Lgals1$^{-/-}$ mice. Interestingly, not only PGE_2 but also NO levels in the lung of this group were increased when compared to WT (Figure 4(d)).

2.5. Uninfected Lgals1$^{-/-}$ Macrophages Express High Levels of Prostaglandin E Synthase 2 after Fungal Infection. The immune response against *H. capsulatum* is mediated by Th1 cells, which requires macrophages activation [6, 7]. The pathogenic yeast fungus replicates inside these cells and results in metabolites of arachidonic acids production, such as prostaglandins and leukotrienes [35]. To assess the role of endogenous Gal-1 in PGE_2 production, prostaglandin E synthase 2 (Ptges2) mRNA expression in peritoneal macrophages from Lgals1$^{-/-}$ and WT mice infected or not with *H. capsulatum in vitro* was evaluated. Interestingly, 24 hours after *H. capsulatum* infection, Lgals1$^{-/-}$ macrophages had increased Ptges2 mRNA expression when compared to infected WT macrophages. In addition, higher levels of PGE_2 were detected in the supernatants 24 hours after the infection of Lgals1$^{-/-}$ macrophages when compared to WT macrophages (Figure 5(c)). Thus, the *in vitro* results correlate with overproduction of prostaglandins *in vivo* (Figure 5(a)).

2.6. Galectin-1 Does Not Bind to and Kill the Yeast Form of H. capsulatum. Recently, it was reported that galectins can bind glycans not only on the host cell surface, but also on molecules on pathogens, which has been found to result in pathogen killing and modulation of immune responses against bacterial infections [36, 37]. To assess the binding capacity of Gal-1 on *H. capsulatum* surface, biotinylated-human recombinant Gal-1 (hrGal-1 : 1 μM and 4 μM) was incubated with the yeast form of *H. capsulatum*. Gal-1 did not bind to the yeast form of this fungus (Figure 6(a)) although the hrGal-1 was active, since it did bind to glycans on HL-60 cells (Figure 6(b)). As expected, different concentrations of hrGal-1 (0.5, 1.0, 2.5, 4.0, and 10.0 μM) did not alter the viability of *H. capsulatum* after 24 and 48 h of *in vitro* incubation (Figure 6(c)). This result suggests that the binding effect can be related to killing activity as Stowell et al. [36] described for *E. coli* strains in the presence of Gal-4 and Gal-8. Thus, the yeast form of *H. capsulatum* seems not to express ligands for Gal-1 and indicates that the protective mechanistic effects of Gal-1 to *H. capsulatum* infection do not involve Gal-1 binding to the yeast.

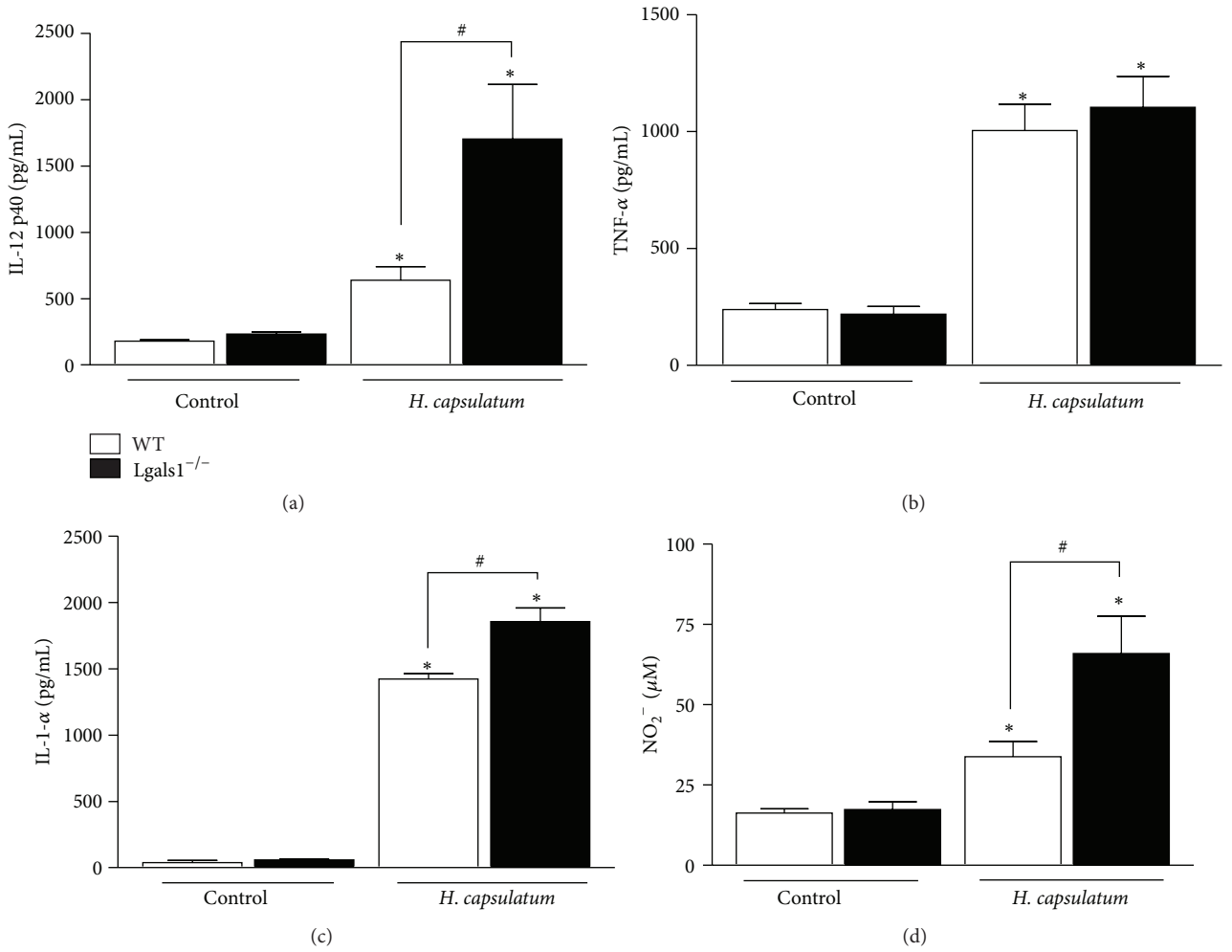

FIGURE 4: Lgals1$^{-/-}$ mice exhibit increased inflammatory response day 15 after infection with *H. capsulatum*. Cytokines IL-12p40 (a), TNF-α (b), IL-1-α (c), and NO_2^- (d) were quantified from homogenized lungs on day 15 after infection with *H. capsulatum*. Cytokines levels (pg/mL) were determined in the supernatants by ELISA and NO_2^- (μM) by using a Griess reaction. Data are representative of one of the two experiments performed independently ($n = 10$ per group). Values are mean ± SEM. $^*p < 0.05$ infected mice versus control (uninfected), $^\#p < 0.05$ WT versus Lgals1$^{-/-}$, both infected.

3. Discussion

Galectins have been described as regulators of immune response in models of inflammatory and infectious diseases and host pathogen recognition [14, 25, 27, 36, 38–41]. Gal-1 and Gal-3 are the best studied members of the galectin family and the expression of these proteins is increased or decreased in distinct cell types following infections caused by different pathogens [42, 43]. Previous reports demonstrate that Gal-3 participates in yeast infections [13, 39, 44]; however, the role of Gal-1 in fungal diseases has not yet been explored. Although the expression of Gal-3 in dendritic cells is not upregulated in WT mice infected with *H. capsulatum*, mice genetically deficient in Gal-3 clear this fungal infection more efficiently than WT mice [13], showing that high Gal-3 expression in WT mice is not required for the participation in the immune response against *H. capsulatum* and may actually contribute to pathogenesis [13].

Unexpectedly, Gal-3 knockout mice are more susceptible to *Candida albicans* infection than WT mice and the susceptibility is associated with high fungal burden in the brain. Additionally, Gal-3, but not Gal-1, can induce yeast cell death upon binding to β-1,2-linked oligomannosides on the surface of pathogenic fungus *Candida albicans* [44]. Thus, Gal-3 and Gal-1 appear to be differentially involved in host defense mechanisms against fungal infections, and this feature may arise from the specific pathogen. In disseminated candidiasis model, the absence of Gal-3 is responsible for increased susceptibility [39]. In the present study, in contrast to Gal-3-deficient mice [13], the novel observation that the absence of endogenous Gal-1 increased susceptibility to *H. capsulatum* accompanied by higher fungal loads in the lung and spleen was made. Recently, it was reported that Lgals1$^{-/-}$ mice infected intradermally with *T. cruzi* are resistant to this parasitic infection compared to their WT counterparts and this resistant phenotype could be associated

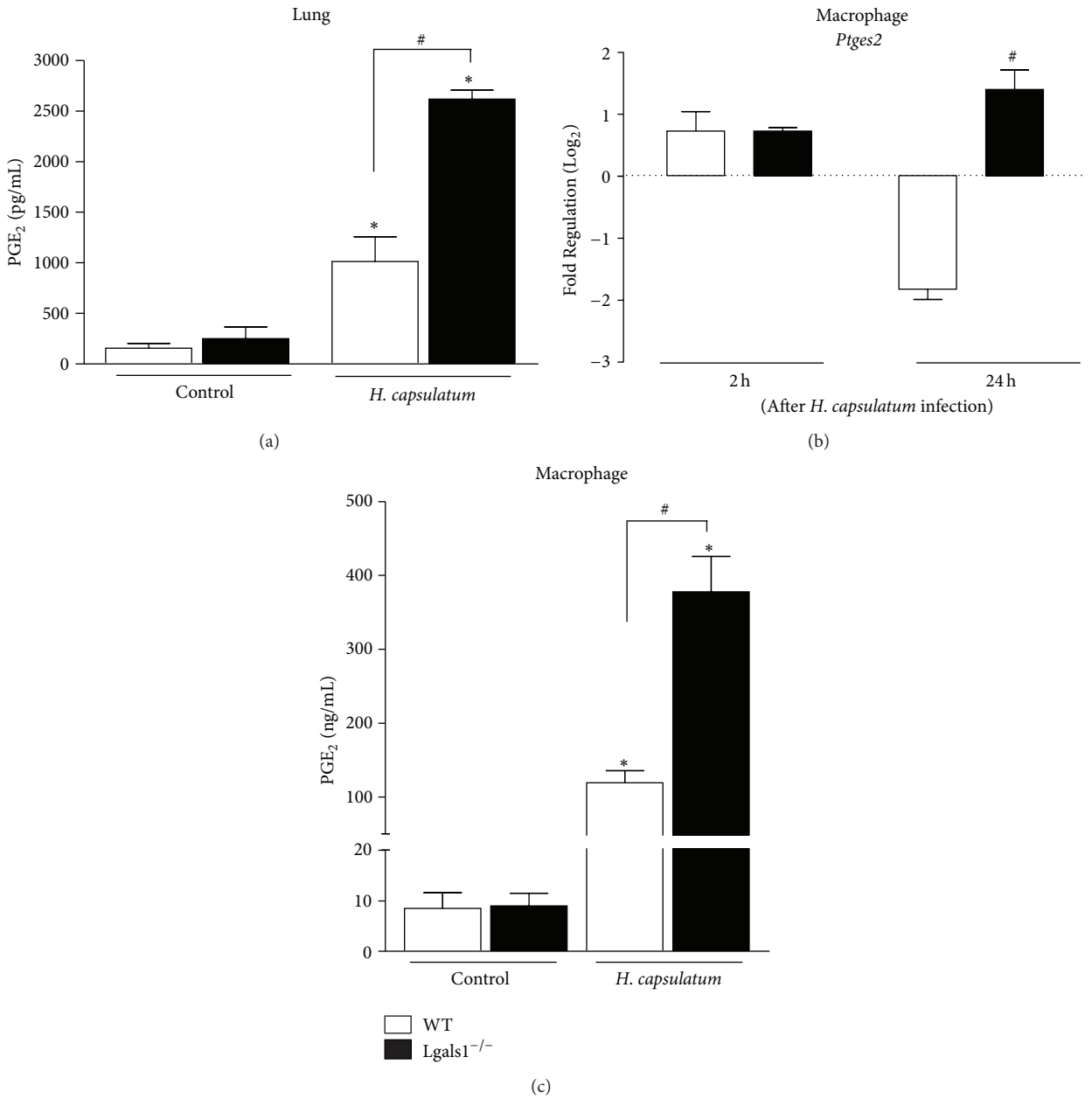

FIGURE 5: Absence of endogenous Gal-1 increases prostaglandin PGE_2 production and Ptges2 expression in peritoneal macrophages. (a) *In vivo* prostaglandin E_2 was quantified in supernatants from homogenized lungs on day 15 after infection with *H. capsulatum* (5×10^5 yeasts/mice) by ELISA. (b) 5×10^5 peritoneal macrophages were incubated *in vitro* with *H. capsulatum* (MOI 1 : 1) during 2 and 24 hours and mRNA levels for Ptges2 were quantified and plotted as Fold Regulation by Log_2. In addition, PGE_2 was assessed *in vitro* in the supernatants by ELISA 24 hours after infection (c). *In vivo* data are representative of one of the two experiments performed independently ($n = 10$ per group). Values are mean ± SEM. $^*p < 0.05$ infected mice versus control (uninfected), $^\#p < 0.05$ WT versus Lgals1$^{-/-}$, both infected.

with a dysfunction in the regulatory properties of Gal-1 followed by high production of Th1 proinflammatory cytokines and improvement of Th1 and $CD8^+$ T cells responses [25]. However, another report from the same group described that Lgals1$^{-/-}$ mice infected intraperitoneally with *T. cruzi* showed elevated parasitemia, less tissue inflammation, and higher mortality rates as compared to infected WT mice [45]. These authors suggest that this discrepancy could be associated with the presence of different phagocytes at sites of infection and distinct local immune response induced by *T. cruzi*. Based on these reports and the present data, it is suggested that the infection of Lgals1$^{-/-}$ mice, intratracheally, with *H. capsulatum* promotes a unique immunophenotype that suppresses the host response against the fungus. This special immunological scenario is characterized by an imbalanced inflammation associated with high levels of neutrophil

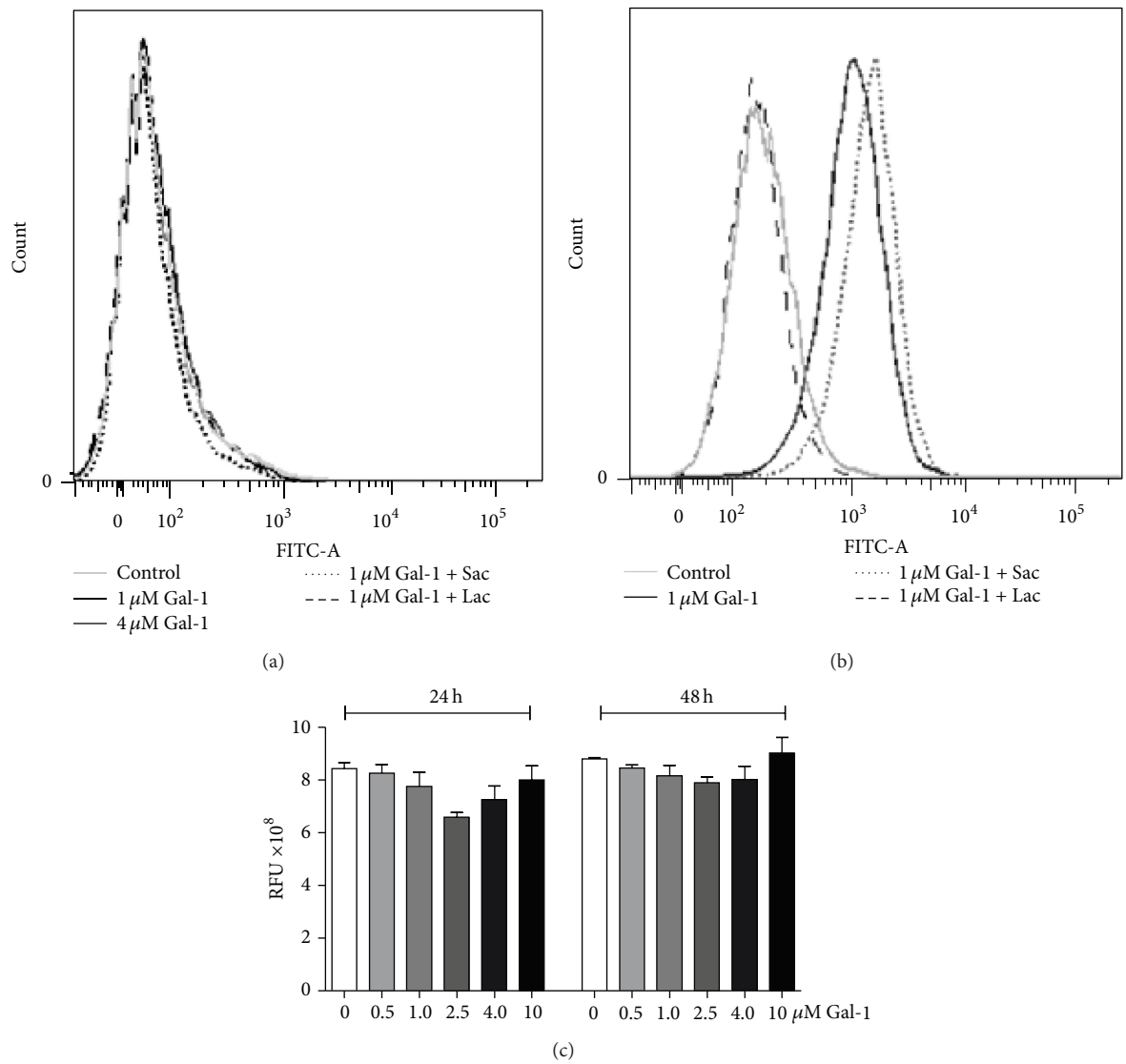

Figure 6: Gal-1 does not bind and kill the yeast form of *H. capsulatum*. (a) Yeasts were incubated for 1 hour at 4°C with 1.0 μM and 4.0 μM biotinylated-hrGal-1, in the presence or absence of 20 mM lactose (Gal-1 inhibitor) or sucrose (control, noninhibitor). After that, yeasts were incubated with streptavidin-FITC and labeled cells were acquired on a FACS Canto (Becton Dickinson, Mountain View, CA, USA) and analyzed in the DIVA software (Becton Dickinson). (b) As a control, HL-60 cells (1×10^6) were incubated with 1 μM biotinylated-hrGal-1 for 1 hour at 4°C, in presence or absence of 20 mM lactose or sucrose. (c) Several hrGal-1 concentrations (0.5, 1.0, 2.5, 4.0, and 10 μM) were incubated with 1×10^6 *H. capsulatum* cells during 24 and 48 h. After each time, relative fluorescent units (RFU) (560–590 nm) were measured and represent yeast cells metabolically active through the dye resazurin reagent. Data are representative of two independent experiments and expressed as the mean ± SEM.

infiltration and proinflammatory cytokines in the lungs that causes a strong anti-inflammatory response induced by high levels of PGE_2 and nitric oxide that could modulate phagocyte and T cell functions.

Based on evidence that Gal-4 and Gal-8 can bind and kill bacteria that express a human blood group B-like antigen and a common mammalian antigen α-Gal [36, 46], it is hypothesized that Gal-1 might have the same effect on the yeast form of *H. capsulatum*. However, in contrast to Gal-4 and Gal-8 killing activities toward bacteria, Gal-1 neither bound to nor killed the yeast form (Figure 6). This data suggests that the ability of Gal-1 to contribute to proper control of the fungal infection arises from an indirect contribution, since Gal-1 is clearly involved in the modulation of immune response against *H. capsulatum*.

Next, it was evaluated whether the absence of Gal-1 could interfere with the recruitment of neutrophils to the lungs during the infection, since this lectin could modulate the inflammatory response [24, 47]. It is known that neutrophil migration to sites of infection helps the clearance of pathogens [48]. Human neutrophils are able to impair the growth of *H. capsulatum* yeast form, and this microbiostatic effect is

mediated mostly by compounds present in the azurophil granules [49]. Moreover, in experimental histoplasmosis, depletion of GR-1$^+$ cells, primarily neutrophils, promotes the increase in fungal load in the lungs and spleens and decreases the survival of animals even in the presence of high levels of TNF-α and NO [50]. Previous reports demonstrate that mice genetically deficient in Gal-1 have enhanced neutrophil emigration in response to IL-1β compared to their wild-type counterparts [51]. Furthermore, in an animal model of zymosan-induced peritonitis, exogenous Gal-1 was shown to cause decreased production of proinflammatory cytokines and expression of adhesion molecules on the surface of neutrophils, thus diminishing their rates of migration [47]. The present results are consistent with those of others, indicating that *H. capsulatum* promotes intense neutrophil recruitment in the lung of Lgals1$^{-/-}$ mice (Figure 3); however, these phagocytes were not able to clear the fungus in the lung pulmonary parenchyma. Other authors have demonstrated that upregulation of proinflammatory cytokines/chemokines resulted in higher numbers of lung neutrophils and also reduced the capacity of the host defense to eliminate the fungus [9]. Since Gal-1 can modulate the adhesion molecules expression as well as releasing mediators of immune response [22–24, 47], it was evaluated whether the increase of neutrophil infiltration into the lung was associated with exacerbation of cytokines during the inflammatory response against *H. capsulatum* infection. The intense neutrophil accumulation in the lung of Lgals1$^{-/-}$ mice could be explained by high levels of IL-1α (Figure 4(c)), since this cytokine is a chemoattractant for neutrophils [52, 53]. Moreover, the presence of high number of neutrophils may be a major source of IL-12 detected in the lung from infected-Lgals1$^{-/-}$ mice, as neutrophils have been reported to produce IL-12 [54]. Curiously, inhibition of dectin-1 expression, a host receptor for fungal beta-glucan, reduces the severity of fungus infection and its effect was associated with decrease of proinflammatory cytokines, including IL-12, and neutrophil infiltration [55]. Furthermore, it is known that proinflammatory cytokines, including IL-12 [32, 34, 56, 57], are essential for host defense against *H. capsulatum*. Conversely, on the present model, the increase of IL-12 did not promote fungal clearance in the lungs of Lgals1$^{-/-}$ mice. Based on these results, it may be hypothesized that the excessive production of IL-12p40 and IL-1α in Lgals1$^{-/-}$-infected mice is deleterious to the animals. Interestingly, Lgals1$^{-/-}$ mice are more resistant to *Trypanosoma cruzi* infection than wild-type mice and this phenotype is associated with upregulation of IFN-γ and no significant production of IL17A [25]. However, the HSV-1 infection in Lgals1$^{-/-}$ mice promotes a severe disease, compare to wild-type, that is correlated with the elevated number of neutrophil infiltrations and IFN-γ-producing CD4 T cells and no significant change of IL-17-producing T cell in the ocular [58]. Then, considering that (i) immunoregulatory properties of Gal-1 are associated with regulation of T_H 1 and T_H 17 responses [59], (ii) IL-12 and IL-23 share p40 subunit [60], and (iii) IL-17/IL-23-axis cytokines participate in immune response against *H. capsulatum* infection [33], further investigation should be done in order to elucidate the impact of IL17/IL23 in experimental histoplasmosis in the absence of endogenous Gal-1. In addition to cytokine production, it was analyzed whether microbicidal factors, such as NO, could be modulated by the deficiency of Gal-1, which could underlie the suppression of host defense against *H. capsulatum*. It was found that the deficiency of Gal-1 promotes the increase of NO concentration in the lung of infected mice when compared with infected WT mice. These results are in concordance with other studies that show that Gal-1 negatively modulates the NO production by activating macrophage or microglia-like cells [23, 61] and activated microglia from Lgals1$^{-/-}$ mice produce high concentration of NO [62]. Moreover, the high levels of NO produced (Figure 4(d)) in the lung have no microbicidal effect on *H. capsulatum,* since lungs from Gal-1 *Lgals1*$^{-/-}$ mice had higher CFU (Figure 2). Thus, NO appears to be important for the host defense against primary infection by *H. capsulatum* [11]; nonetheless, the overproduction of NO has also been shown to suppress phagocytic activities of macrophage in *H. capsulatum* infection and inhibit the CD4 T cells proliferation response to *T. cruzi* infection [12, 34, 50].

Alveolar macrophages are the first line of host defense in the lung against respiratory pathogens, and this phagocyte is an important source of lipid mediators, such as PGE_2 in infected lung [63]. PGE2 has an important role in suppression of host defense involved modulation of alveolar macrophages functions in different pulmonary infection models, such as *Streptococcus pneumoniae* [64], *Klebsiella pneumoniae* [65], *Pseudomonas aeruginosa* [66], and recently *H. capsulatum* [8]. Lung and macrophages from Lgals1$^{-/-}$-infected mice produced higher levels of PGE_2 when compared to WT mice. Then, it is hypothesized that high levels of NO and PGE_2 in the lungs of Lgals1$^{-/-}$-infected mice inhibit the effector functions of macrophages and neutrophils against *H. capsulatum*. Whether the absence of endogenous Gal-1 can inhibit the effector functions of neutrophils against *H. capsulatum* remains unknown, though.

PGE_2 is able to inhibit IL-12 production by macrophage and dendritic cells [67], although lung parenchyma from infected Lgals1$^{-/-}$ mice contained higher levels of IL-12 than those from infected WT mice even in the presence of high levels of PGE_2. This finding is in agreement with other studies reporting that the inhibition of prostaglandin has no effects on the production of IL-12 in *H. capsulatum*-infected mice [8]. In addition, the present data is similar to others, demonstrating that the immunoregulatory effects of Gal-1 (endogenous or exogenous) are associated with suppression of Th1 cytokines, including the negative modulation of IL-12 production by activated macrophage or tolerogenic dendritic cells [19, 68–71].

Because of the low yield of murine alveolar macrophages, peritoneal macrophages from Lgals1$^{-/-}$ mice were used to examine the ability of endogenous Gal-1 to modulate the expression of mRNA *Ptges2* and PGE_2 after *H. capsulatum* infection (Figure 5(b)). The high fungus burden in lungs and spleen in infected Lgals1$^{-/-}$ mice could be associated with the downregulation effects of PGE_2 in antimicrobial functions of phagocytes [8, 72].

Exaggerated inflammatory response could be responsible for higher production of PGE_2 in lungs of *H. capsulatum*-infected Lgals1$^{-/-}$ mice that inhibited fungal clearance, since the PGE_2 biosynthesis is increased under inflammatory conditions, and this prostanoid has been described to impair phagocytosis and kill by alveolar macrophages [73]. In addition, the effector functions of phagocytes from Lgals1$^{-/-}$ could be altered, since Gal-1 is a multifunctional molecule with intra- and extracellular effects [28, 29]. This immune suppressive effect is in line with current results, demonstrating the positive impact on mRNA *Ptgs2* expression and PGE_2 secretion of the Gal-1 deficiency in macrophages from Lgals1$^{-/-}$ mice after fungal infection. This data is in agreement with the results described by Rabinovich and colleagues, since this lectin can reduce arachidonic acid release and PGE_2 secretion from activated macrophage [27]. Besides that, celecoxib treatment, a selective cyclooxygenase 2 inhibitor, improved the immune response against *H. capsulatum* infection through the inhibition of prostaglandin production [8]. Curiously, celecoxib induces expression of Gal-1 in activated macrophage and Gal-1 could be involved in the anti-inflammatory mechanisms of this drug [74]. Furthermore, Gal-1 inhibited the expression of activating transcription factor 3, a negative regulator of mRNA *Ptgs2* in macrophage [75]. Despite that, further investigations are needed to elucidate the mechanism by which Gal-1 inhibits *Ptgs2* expression. It has now been shown that PGE_2 is a DAMP (damage-associated molecular patterns) and is induced and released by dying cells, which leads to suppressed expression of genes associated with inflammation and thereby limits immunostimulatory activities [76]. Also, PGE_2 is downregulated in human systemic inflammatory diseases and mice with reduced PGE_2 exhibit systemic inflammation [77]. In summary, the present results demonstrate that the endogenous Gal-1 plays an important role in host defense against *Histoplasma capsulatum* modulating of PGE_2, IL-12, and NO production, as well as pulmonary neutrophil accumulation. Future studies are needed to better understand the cellular and molecular mechanisms in which endogenous galectin-1 could participate in host defense against fungus infection.

4. Materials and Methods

4.1. Animals. Six-to-eight-week-old wild-type (WT) male mice and mice genetically deficient in Gal-1 (Lgals1$^{-/-}$), both in a C57BL/6J background, were housed and bred at the animal facility of the School of Pharmaceutical Sciences of Ribeirão Preto (University of São Paulo, Brazil). Wild-type mice were originally purchased from The Jackson Laboratory (Bar Harbor, ME, USA) and Lgals1$^{-/-}$ mice were provided by Dr. Richard D. Cummings (Department of Surgery, Beth Israel Deaconess Medical Center and Harvard Medical School, Boston, MA, USA). The experimental protocol was approved and conducted in accordance with guidelines of the Institutional Animal Care Committee. To check the depletion of Lgals1, Gal-1 expression (mRNA and protein) analysis on WT and Lgals1$^{-/-}$ cells were performed as previously described [21] using conventional RT-PCR and western blot, respectively (data not shown). We used C57BL/6J mice as wild-type counterparts in our experiments.

4.2. H. capsulatum Strain and Infection of Mice. *H. capsulatum* strain was isolated from a patient at the Clinical Hospital, School of Medicine of Ribeirão Preto, University of São Paulo, and the characterization and preparation of *H. capsulatum* yeast cells were performed as previously described [9, 78, 79]. The yeast cultures were used at ≥90% viability according to fluorescein diacetate (Sigma-Aldrich, St. Louis, MO) and ethidium bromide (Sigma-Aldrich) staining [80]. Mice were given intratracheally (i.t.) dispersion containing 100 μL phosphate buffered saline (PBS, vehicle control) or a sublethal dose in PBS (5×10^5 yeasts/animal). The appropriate inoculum size was chosen based on procedure described by Sá-Nunes and colleagues [78]. On day 15 after infection, both uninfected and infected mice were euthanized in a CO_2 chamber, and lungs and spleens were collected for analyses.

4.3. Fungal Load and Histopathology. *H. capsulatum*-infected mice were euthanized on day 15 after infection and tissue samples were harvested. Lung sections (5 μM) were embedded in paraffin blocks and stained with Grocott's methanamine silver (GMS) and quantification of yeasts was expressed as yeast/mm^2 (original magnification: 400x). Also, fungal burden was determined from homogenized lung and spleen (Mixer Homogenizer; Labortechnik, Staufen, Germany) as previously described [7, 9]. Serial dilutions of these tissue homogenates were plated onto BHI blood agar and incubated at 37°C for 21 days. The results were expressed as mean colony-forming units (CFU) per gram of lung ± SEM (CFU/g) or CFU per whole spleen ± SEM (CFU/spleen). Lungs were collected, fixed in 10% formaldehyde, and embedded in paraffin blocks. For neutrophils analyses, lung sections (5 μm) were stained with hematoxylin and eosin (H&E) and the cells were quantified in the ocular lens containing 10 × 10 graticules (0.0624 mm^2 each in magnifications: 400x). The results are expressed as neutrophils/mm^2.

4.4. Measurement of Cytokines, PGE_2, and Nitric Oxide. Lungs were collected 15 days after infection, weighed and homogenized (Mixer Homogenizer; Labortechnik, Staufen, Germany) in 2 mL of RPMI1640 (Sigma) and the supernatants were stored at −70°C until being assayed. Commercially available ELISA antibodies were used to measure TNF-α, IL-1α, IL-12p40, IL-10, IL-4, and IL-6 (BD OptEIA ELISA sets; BD Pharmingen) according to the instructions of the manufacturer. PGE_2 from lung homogenate and from *in vitro* assay (*in vitro* assay is described below) were purified by Sep-Pak C18 cartridges according to the manufacturer's instructions (Waters Corp., Milford, MA). Quantification of PGE_2 was assessed also by ELISA (Cayman Chemical, Ann Arbor, MI) and the results for cytokines and PGE_2 are expressed in ng/mL. The sensitivity of the assay was <10 pg/mL. Nitrite (NO_2^-) concentrations (μM) in lung homogenates was measured by Griess reaction using a standard curve with serial dilutions of $NaNO_2$ (Sigma-Aldrich). Griess reagent was used

in order to measure NO levels indirectly from nitrite as described previously [10].

4.5. Gene Expression by Real-Time Polymerase Chain Reaction (qRT-PCR)

4.5.1. In Vitro Assay. WT or Lgals1$^{-/-}$ peritoneal macrophages (5×10^5 cells/well) were incubated with *H. capsulatum* (MOI 1:1) during 2 and 24 hours. PGE_2 was assessed in the supernatants 24 hours after infection and expression of mRNA was performed in plated macrophages 2 and 24 hours after *H. capsulatum* exposure.

4.5.2. Gene Expression. Total mRNA was isolated using the RNeasy Mini kit (Qiagen Inc., Valencia, CA), according to the manufacturer's instructions. cDNA (complementary DNA) was synthesized from 600 ng of total RNA using random primers (High Capacity cDNA Reverse Transcription Kit, Applied Biosystems, Temecula, CA). Aliquots of 2 μL of the total cDNA were amplified by qRT-PCR (StepOne Plus, Applied Biosystems, Singapore) using the primers (IDT®, Integrated DNA Technologies, California, USA) for *Ptges2* (the gene encoding prostaglandin E synthase 2, Mm.PT. 58.7480753) and probe (TaqMan® Gene Expression Assay, Applied Biosystems, Foster City, USA). *Actb* (Mm00607939) was used as reference gene. Amplification was performed in duplicate under the following conditions: denaturation at 95°C for 10 min, followed by 40 cycles of 95°C for 15 s and 60°C for 1 minute. Relative quantification was performed using the ΔΔCt method and plotted as Fold Increase or Fold Regulation by Log_2.

4.6. Human Recombinant Galectin-1 (hrGal-1) Purification. hrGal-1 was prepared as previously described [26, 81]. Briefly, purified hrGal-1 was treated with 100 mM iodoacetamide (Sigma-Aldrich) in 100 mM lactose/PBS overnight at 4°C [82]. To ensure that hrGal-1 samples were endotoxin-free, Detoxi-Gel Endotoxin removing gel (Pierce Biotechnology, Rockford, IL) was used and hrGal-1 activity was assessed by haemagglutination (data not shown).

4.7. Binding by Flow Cytometry and Resazurin Cell Viability Assays. To measure the capacity of Gal-1 to bind on yeast form of *H. capsulatum*, 1 μM and 4 μM biotinylated-hrGal-1 were incubated for 1 hour at 4°C, in presence or absence of 20 mM lactose or sucrose (Sigma-Aldrich). After washing, yeasts were incubated with streptavidin-FITC (Jackson IR) for 30 minutes at 4°C, washed, and formalin-fixed (1% in PBS). Labeled cells were acquired on a FACS Canto (Becton Dickinson, Mountain View, CA, USA) and analyzed in the DIVA software (Becton Dickinson). As a control, we used HL-60 cells obtained from the American Type Culture Collection (ATCC, Manassas, VA) and maintained in RPMI medium supplemented with 10% fetal bovine serum. To test *H. capsulatum* viability in a presence of Gal-1, we incubated, *in vitro*, several hrGal-1 concentrations (10, 4, 2.4, 1, and 0.5 μM) with 1×10^6 yeast cells during 24 and 48 h. The relative fluorescent units (RFU) using a plate reader were detected (560–590 nm) in order to analyze the number of yeast cells metabolically active using the dye resazurin reagent (Sigma-Aldrich).

4.8. Statistical Analysis. The data are presented as the mean ± SEM. Comparisons were performed using an ANOVA followed by a Bonferroni posttest by the Prism 4.0 statistical program (GraphPad Software, San Diego, CA). Survival analyses were performed using the Mantel-Cox log-rank (χ^2 "chi-squared") test. Differences in survival were analyzed by the log-rank test. Values of $p < 0.05$ were considered statistically significant.

Abbreviations

Gal-1:	Galectin-1
Lgals1$^{-/-}$:	Galectin-1 deficient mice
WT:	Wild-type mice
Th1 and Th2:	Helper T cell responses
IFN:	Interferon
IL:	Interleukin
TNF-α:	Tumor necrosis factor-α
GM-CSF:	Granulocyte macrophage colony-stimulating
PGE_2:	Prostaglandin E2
Ptgs2:	Prostaglandin E synthase 2
NO_2^-:	Nitrite
NO:	Nitric oxide
HIV:	Human Immunodeficiency Virus-1
HTLV-1:	Human T Lymphotropic Virus-1
BALF:	Bronchoalveolar Lavage Fluid.

Competing Interests

The authors declare no competing interests.

Acknowledgments

The authors thank Dr. Seema R. Patel for the critical review of the manuscript, Dr. Connie M. Arthur for helpful discussions, and Rubens Eduardo da Silva for the excellent assistance with animal handling and technical support. This work was supported by Fundação de Amparo à Pesquisa do Estado de São Paulo (FAPESP, Grant nos. 2007/02487-3, 2007/00840-8, and 2011/17611-7), Conselho Nacional de Desenvolvimento Científico e Tecnológico (CNPq, Grant nos. 557403/2008-1, 467646/2014-7), Coordenação de Aperfeiçoamento de Pessoal de Nível Superior (CAPES, Grant no. BEX 9320/13-0), and National Institutes of Health (NIH, AL101982, to Richard D. Cummings). Also, the research leading to these results has received support and funding from the Núcleo de Apoio à Pesquisa em Doenças Inflamatórias (NAPDIN, Grant no. 11.1.21625.01.0).

References

[1] R. Allendoerfer and G. S. Deepe Jr., "Infection with *Histoplasma capsulatum*: host-fungus interface," *Revista Iberoamericana de Micologia*, vol. 15, no. 4, pp. 256–260, 1998.

[2] S. Antinori, "*Histoplasma capsulatum*: more widespread than previously thought," *The American Journal of Tropical Medicine and Hygiene*, vol. 90, no. 6, pp. 982–983, 2014.

[3] G. D. Brown, D. W. Denning, N. A. R. Gow, S. M. Levitz, M. G. Netea, and T. C. White, "Hidden killers: human fungal infections," *Science Translational Medicine*, vol. 4, no. 165, Article ID 165rv13, 2012.

[4] A. A. Adenis, C. Aznar, and P. Couppié, "Histoplasmosis in HIV-infected patients: a review of new developments and remaining gaps," *Current Tropical Medicine Reports*, vol. 1, pp. 119–128, 2014.

[5] G. S. Deepe Jr., R. S. Gibbons, and A. G. Smulian, "Histoplasma capsulatum manifests preferential invasion of phagocytic subpopulations in murine lungs," *Journal of Leukocyte Biology*, vol. 84, no. 3, pp. 669–678, 2008.

[6] D. N. Kroetz and G. S. Deepe, "The role of cytokines and chemokines in *Histoplasma capsulatum* infection," *Cytokine*, vol. 58, no. 1, pp. 112–117, 2012.

[7] R. Allendoerfer, G. P. Boivin, and G. S. Deepe Jr., "Modulation of immune responses in murine pulmonary histoplasmosis," *Journal of Infectious Diseases*, vol. 175, no. 4, pp. 905–914, 1997.

[8] P. A. T. Pereira, B. C. Trindade, A. Secatto et al., "Celecoxib improves host defense through prostaglandin inhibition during histoplasma capsulatum infection," *Mediators of Inflammation*, vol. 2013, Article ID 950981, 11 pages, 2013.

[9] A. I. Medeiros, A. Sá-Nunes, E. G. Soares, C. M. Peres, C. L. Silva, and L. H. Faccioli, "Blockade of endogenous leukotrienes exacerbates pulmonary histoplasmosis," *Infection and Immunity*, vol. 72, no. 3, pp. 1637–1644, 2004.

[10] T. E. Lane, B. A. Wu-Hsieh, and D. H. Howard, "Antihistoplasma effect of activated mouse splenic macrophages involves production of reactive nitrogen intermediates," *Infection and Immunity*, vol. 62, no. 5, pp. 1940–1945, 1994.

[11] T. E. Lane, G. C. Otero, B. A. Wu-Hsieh, and D. H. Howard, "Expression of inducible nitric oxide synthase by stimulated macrophages correlates with their antihistoplasma activity," *Infection and Immunity*, vol. 62, no. 4, pp. 1478–1479, 1994.

[12] B. A. Wu-Hsieh, W. Chen, and H.-J. Lee, "Nitric oxide synthase expression in macrophages of *Histoplasma capsulatum*-infected mice is associated with splenocyte apoptosis and unresponsiveness," *Infection and Immunity*, vol. 66, no. 11, pp. 5520–5526, 1998.

[13] S.-Y. Wu, J.-S. Yu, F.-T. Liu, S.-C. Miaw, and B. A. Wu-Hsieh, "Galectin-3 negatively regulates dendritic cell production of IL-23/IL-17-axis cytokines in infection by *Histoplasma capsulatum*," *The Journal of Immunology*, vol. 190, no. 7, pp. 3427–3437, 2013.

[14] G. A. Rabinovich and A. Gruppi, "Galectins as immunoregulators during infectious processes: from microbial invasion to the resolution of the disease," *Parasite Immunology*, vol. 27, no. 4, pp. 103–114, 2005.

[15] D. J. Laderach, D. Compagno, M. A. Toscano et al., "Dissecting the signal transduction pathways triggered by galectin-glycan interactions in physiological and pathological settings," *IUBMB Life*, vol. 62, no. 1, pp. 1–13, 2010.

[16] F.-T. Liu, R.-Y. Yang, and D. K. Hsu, "Galectins in acute and chronic inflammation," *Annals of the New York Academy of Sciences*, vol. 1253, no. 1, pp. 80–91, 2012.

[17] S. Thiemann and L. G. Baum, "Galectins and immune responses—just how do they do those things they do?" *Annual Review of Immunology*, vol. 34, no. 1, pp. 243–264, 2016.

[18] K. Wdowiak, W. Spychalowicz, M. Fajkis, and J. Wojnar, "Galectins in hematological malignancies-role, functions and potential therapeutic targets," *Postępy Higieny i Medycyny Doświadczalnej*, vol. 70, pp. 95–103, 2016.

[19] E. Zúñiga, A. Gruppi, J. Hirabayashi, K. I. Kasai, and G. A. Rabinovich, "Regulated expression and effect of galectin-1 on *Trypanosoma cruzi*-infected macrophages: modulation of microbicidal activity and survival," *Infection and Immunity*, vol. 69, no. 11, pp. 6804–6812, 2001.

[20] M. Ouellet, S. Mercier, I. Pelletier et al., "Galectin-1 acts as a soluble host factor that promotes HIV-1 infectivity through stabilization of virus attachment to host cells," *The Journal of Immunology*, vol. 174, no. 7, pp. 4120–4126, 2005.

[21] K. A. Toledo, M. L. Fermino, C. Del Cistia Andrade et al., "Galectin-1 exerts inhibitory effects during DENV-1 infection," *PLoS ONE*, vol. 9, no. 11, article e112474, 2014.

[22] S. R. Stowell, Y. Qian, S. Karmakar et al., "Differential roles of galectin-1 and galectin-3 in regulating leukocyte viability and cytokine secretion," *Journal of Immunology*, vol. 180, no. 5, pp. 3091–3102, 2008.

[23] S. G. Correa, C. E. Sotomayor, M. P. Aoki, C. A. Maldonado, and G. A. Rabinovich, "Opposite effects of galectin-1 on alternative metabolic pathways of L-arginine in resident, inflammatory, and activated macrophages," *Glycobiology*, vol. 13, no. 2, pp. 119–128, 2003.

[24] L. V. Norling, A. L. F. Sampaio, D. Cooper, and M. Perretti, "Inhibitory control of endothelial galectin-1 on in vitro and in vivo lymphocyte trafficking," *The FASEB Journal*, vol. 22, no. 3, pp. 682–690, 2008.

[25] C. V. Poncini, J. M. Ilarregui, E. I. Batalla et al., "Trypanosoma cruzi infection imparts a regulatory program in dendritic cells and T cells via galectin-1-dependent mechanisms," *Journal of Immunology*, vol. 195, no. 7, pp. 3311–3324, 2015.

[26] M. Dias-Baruffi, H. Zhu, M. Cho, S. Karmakar, R. P. McEver, and R. D. Cummings, "Dimeric galectin-1 induces surface exposure of phosphatidylserine and phagocytic recognition of leukocytes without inducing apoptosis," *Journal of Biological Chemistry*, vol. 278, no. 42, pp. 41282–41293, 2003.

[27] G. A. Rabinovich, C. E. Sotomayor, C. M. Riera, I. Bianco, and S. G. Correa, "Evidence of a role for galectin-1 in acute inflammation," *European Journal of Immunology*, vol. 30, no. 5, pp. 1331–1339, 2000.

[28] F.-T. Liu, R. J. Patterson, and J. L. Wang, "Intracellular functions of galectins," *Biochimica et Biophysica Acta (BBA)—General Subjects*, vol. 1572, no. 2-3, pp. 263–273, 2002.

[29] M. C. Vladoiu, M. Labrie, and Y. St-Pierre, "Intracellular galectins in cancer cells: potential new targets for therapy (review)," *International Journal of Oncology*, vol. 44, no. 4, pp. 1001–1014, 2014.

[30] N. Kurita, E. Brummer, S. Yoshida, K. Nishimura, and M. Miyaji, "Antifungal activity of murine polymorphonuclear neutrophils against histoplasma capsulatum," *Medical Mycology*, vol. 29, no. 3, pp. 133–143, 1991.

[31] R. Allendoerfer and G. S. Deepe Jr., "Intrapulmonary response to *Histoplasma capsulatum* in gamma interferon knockout mice," *Infection and Immunity*, vol. 65, no. 7, pp. 2564–2569, 1997.

[32] G. S. Deepe Jr., R. Gibbons, and E. Woodward, "Neutralization of endogenous granulocyte-macrophage colony-stimulating factor subverts the protective immune response to *Histoplasma capsulatum*," *The Journal of Immunology*, vol. 163, no. 9, pp. 4985–4993, 1999.

[33] G. S. Deepe Jr. and R. S. Gibbons, "Interleukins 17 and 23 influence the host response to Histoplasma capsulatum," *Journal of Infectious Diseases*, vol. 200, no. 1, pp. 142–151, 2009.

[34] P. Zhou, M. C. Sieve, J. Bennett et al., "IL-12 prevents mortality in mice infected with Histoplasma capsulatum through induction of IFN-γ," *Journal of Immunology*, vol. 155, no. 2, pp. 785–795, 1995.

[35] J. E. Wolf, S. E. Massof, and S. P. Peters, "Alterations in murine macrophage arachidonic acid metabolism following ingestion of nonviable *Histoplasma capsulatum*," *Infection and Immunity*, vol. 60, no. 7, pp. 2559–2564, 1992.

[36] S. R. Stowell, C. M. Arthur, M. Dias-Baruffi et al., "Innate immune lectins kill bacteria expressing blood group antigen," *Nature Medicine*, vol. 16, no. 3, pp. 295–301, 2010.

[37] J. P. Cerliani, S. R. Stowell, I. D. Mascanfroni, C. M. Arthur, R. D. Cummings, and G. A. Rabinovich, "Expanding the universe of cytokines and pattern recognition receptors: galectins and glycans in innate immunity," *Journal of Clinical Immunology*, vol. 31, no. 1, pp. 10–21, 2011.

[38] S. Sato, C. St-Pierre, P. Bhaumik, and J. Nieminen, "Galectins in innate immunity: dual functions of host soluble β-galactoside-binding lectins as damage-associated molecular patterns (DAMPs) and as receptors for pathogen-associated molecular patterns (PAMPs)," *Immunological Reviews*, vol. 230, no. 1, pp. 172–187, 2009.

[39] J. R. Linden, M. E. De Paepe, S. S. Laforce-Nesbitt, and J. M. Bliss, "Galectin-3 plays an important role in protection against disseminated candidiasis," *Medical Mycology*, vol. 51, no. 6, pp. 641–651, 2013.

[40] R. N. Fichorova, H. S. Yamamoto, T. Fashemi et al., "Trichomonas vaginalis lipophosphoglycan exploits binding to galectin-1 and -3 to modulate epithelial immunity," *Journal of Biological Chemistry*, vol. 291, no. 2, pp. 998–1013, 2016.

[41] C. I. Muglia, R. P. Gobbi, P. Smaldini et al., "Inflammation controls sensitivity of human and mouse intestinal epithelial cells to galectin-1," *Journal of Cellular Physiology*, vol. 231, no. 7, pp. 1575–1585, 2016.

[42] I. Camby, M. Le Mercier, F. Lefranc, and R. Kiss, "Galectin-1: a small protein with major functions," *Glycobiology*, vol. 16, no. 11, pp. 137R–157R, 2006.

[43] G. R. Vasta, "Roles of galectins in infection," *Nature Reviews Microbiology*, vol. 7, no. 6, pp. 424–438, 2009.

[44] L. Kohatsu, D. K. Hsu, A. G. Jegalian, F.-T. Liu, and L. G. Baum, "Galectin-3 induces death of *Candida* species expressing specific β-1,2-linked mannans," *Journal of Immunology*, vol. 177, no. 7, pp. 4718–4726, 2006.

[45] A. F. Benatar, G. A. García, J. Bua et al., "Galectin-1 prevents infection and damage induced by *Trypanosoma cruzi* on cardiac cells," *PLOS Neglected Tropical Diseases*, vol. 9, no. 10, Article ID e0004148, 2015.

[46] S. R. Stowell, C. M. Arthur, R. McBride et al., "Microbial glycan microarrays define key features of host-microbial interactions," *Nature Chemical Biology*, vol. 10, no. 6, pp. 470–476, 2014.

[47] C. D. Gil, C. E. Gullo, and S. M. Oliani, "Effect of exogenous galectin-1 on leukocyte migration: modulation of cytokine levels and adhesion molecules," *International Journal of Clinical and Experimental Pathology*, vol. 4, no. 1, pp. 74–84, 2010.

[48] E. Kolaczkowska and P. Kubes, "Neutrophil recruitment and function in health and inflammation," *Nature Reviews Immunology*, vol. 13, no. 3, pp. 159–175, 2013.

[49] S. L. Newman, L. Gootee, and J. E. Gabay, "Human neutrophil-mediated fungistasis against Histoplasma capsulatum: localization of fungistatic activity to the azurophil granules," *The Journal of Clinical Investigation*, vol. 92, no. 2, pp. 624–631, 1993.

[50] A. Sá-Nunes, A. I. Medeiros, C. A. Sorgi et al., "Gr-1+ cells play an essential role in an experimental model of disseminated histoplasmosis," *Microbes and Infection*, vol. 9, no. 12-13, pp. 1393–1401, 2007.

[51] D. Cooper, L. V. Norling, and M. Perretti, "Novel insights into the inhibitory effects of Galectin-1 on neutrophil recruitment under flow," *Journal of Leukocyte Biology*, vol. 83, no. 6, pp. 1459–1466, 2008.

[52] N. Schmitz, M. Kurrer, M. F. Bachmann, and M. Kopf, "Interleukin-1 is responsible for acute lung immunopathology but increases survival of respiratory influenza virus infection," *Journal of Virology*, vol. 79, no. 10, pp. 6441–6448, 2005.

[53] L. H. Faccioli, G. E. P. Souza, F. Q. Cunha, S. Poole, and S. H. Ferreira, "Recombinant interleukin-1 and tumor necrosis factor induce neutrophil migration 'in vivo' by indirect mechanisms," *Agents and Actions*, vol. 30, no. 3-4, pp. 344–349, 1990.

[54] L. Romani, A. Mencacci, E. Cenci et al., "Neutrophil production of IL-12 and IL-10 in candidiasis and efficacy of IL-12 therapy in neutropenic mice," *The Journal of Immunology*, vol. 158, no. 11, pp. 5349–5356, 1997.

[55] J. Zhong, W. Huang, Q. Deng et al., "Inhibition of *TREM-1* and *Dectin-1* alleviates the severity of fungal keratitis by modulating innate immune responses," *PLoS ONE*, vol. 11, no. 3, Article ID e0150114, 2016.

[56] R. Allendoerfer and G. S. Deepe Jr., "Regulation of infection with *Histoplasma capsulatum* by TNFR1 and -2," *The Journal of Immunology*, vol. 165, no. 5, pp. 2657–2664, 2000.

[57] G. S. Deepe Jr., "Immune response to early and late *Histoplasma capsulatum* infections," *Current Opinion in Microbiology*, vol. 3, no. 4, pp. 359–362, 2000.

[58] N. K. Rajasagi, A. Suryawanshi, S. Sehrawat et al., "Galectin-1 reduces the severity of herpes simplex virus-induced ocular immunopathological lesions," *Journal of Immunology*, vol. 188, no. 9, pp. 4631–4643, 2012.

[59] M. A. Toscano, G. A. Bianco, J. M. Ilarregui et al., "Differential glycosylation of TH1, TH2 and TH-17 effector cells selectively regulates susceptibility to cell death," *Nature Immunology*, vol. 8, no. 8, pp. 825–834, 2007.

[60] D. M. Floss, J. Schröder, M. Franke, and J. Scheller, "Insights into IL-23 biology: from structure to function," *Cytokine & Growth Factor Reviews*, vol. 26, no. 5, pp. 569–578, 2015.

[61] J. Wang, J. Xia, F. Zhang et al., "Galectin-1-secreting neural stem cells elicit long-term neuroprotection against ischemic brain injury," *Scientific Reports*, vol. 5, article 9621, 2015.

[62] D. Pineda, C. Ampurdanés, M. G. Medina et al., "Tissue plasminogen activator induces microglial inflammation via a noncatalytic molecular mechanism involving activation of mitogen-activated protein kinases and Akt signaling pathways and AnnexinA2 and Galectin-1 receptors," *Glia*, vol. 60, no. 4, pp. 526–540, 2012.

[63] S. L. Hempel, M. M. Monick, and G. W. Hunninghake, "Lipopolysaccharide induces prostaglandin H synthase-2 protein and mRNA in human alveolar macrophages and blood monocytes," *The Journal of Clinical Investigation*, vol. 93, no. 1, pp. 391–396, 1994.

[64] D. M. Aronoff, C. Lewis, C. H. Serezani et al., "E-prostanoid 3 receptor deletion improves pulmonary host defense and

protects mice from death in severe Streptococcus pneumoniae infection," *Journal of Immunology*, vol. 183, no. 4, pp. 2642–2649, 2009.

[65] C. H. Serezani, J. Chung, M. N. Ballinger, B. B. Moore, D. M. Aronoff, and M. Peters-Golden, "Prostaglandin E2 suppresses bacterial killing in alveolar macrophages by inhibiting NADPH oxidase," *American Journal of Respiratory Cell and Molecular Biology*, vol. 37, no. 5, pp. 562–570, 2007.

[66] R. Domingo-Gonzalez, S. Katz, C. H. Serezani, T. A. Moore, A. M. LeVine, and B. B. Moore, "Prostaglandin E2-induced changes in alveolar macrophage scavenger receptor profiles differentially alter phagocytosis of *Pseudomonas aeruginosa* and *Staphylococcus aureus* post-bone marrow transplant," *Journal of Immunology*, vol. 190, no. 11, pp. 5809–5817, 2013.

[67] M. Rodríguez, E. Domingo, C. Municio et al., "Polarization of the innate immune response by prostaglandin E2: a puzzle of receptors and signals," *Molecular Pharmacology*, vol. 85, no. 1, pp. 187–197, 2014.

[68] L. Santucci, S. Fiorucci, N. Rubinstein et al., "Galectin-1 suppresses experimental colitis in mice," *Gastroenterology*, vol. 124, no. 5, pp. 1381–1394, 2003.

[69] J. M. Ilarregui, D. O. Croci, G. A. Bianco et al., "Tolerogenic signals delivered by dendritic cells to T cells through a galectin-1-driven immunoregulatory circuit involving interleukin 27 and interleukin 10," *Nature Immunology*, vol. 10, no. 9, pp. 981–991, 2009.

[70] P.-L. Kuo, J.-Y. Hung, S.-K. Huang et al., "Lung cancer-derived galectin-1 mediates dendritic cell anergy through inhibitor of DNA binding 3/IL-10 signaling pathway," *Journal of Immunology*, vol. 186, no. 3, pp. 1521–1530, 2011.

[71] J. A. Fulcher, S. T. Hashimi, E. L. Levroney et al., "Galectin-1-matured human monocyte-derived dendritic cells have enhanced migration through extracellular matrix," *The Journal of Immunology*, vol. 177, no. 1, pp. 216–226, 2006.

[72] A. Medeiros, C. Peres-Buzalaf, F. Fortino Verdan, and C. H. Serezani, "Prostaglandin E_2 and the suppression of phagocyte innate immune responses in different organs," *Mediators of Inflammation*, vol. 2012, Article ID 327568, 13 pages, 2012.

[73] C. H. Serezani, J. H. Perrela, M. Russo, M. Peters-Golden, and S. Jancar, "Leukotrienes are essential for the control of Leishmania amazonensis infection and contribute to strain variation in susceptibility," *Journal of Immunology*, vol. 177, no. 5, pp. 3201–3208, 2006.

[74] F. Rezaie, M. Salimi, M. H. Ghahremani, and B. Vaziri, "Potential molecular targets in chemopreventative action of celecoxib: a proteomics analysis of J774.A1 macrophage-like cell line," *Molecular BioSystems*, vol. 7, no. 4, pp. 1306–1311, 2011.

[75] J. Hellmann, Y. Tang, M. J. Zhang et al., "Atf3 negatively regulates Ptgs2/Cox2 expression during acute inflammation," *Prostaglandins & Other Lipid Mediators*, vol. 116-117, pp. 49–56, 2015.

[76] S. Hangai, T. Ao, Y. Kimura et al., "PGE2 induced in and released by dying cells functions as an inhibitory DAMP," *Proceedings of the National Academy of Sciences of the United States of America*, vol. 113, no. 14, pp. 3844–3849, 2016.

[77] R. Duffin, R. A. O'Connor, S. Crittenden et al., "Prostaglandin E_2 constrains systemic inflammation through an innate lymphoid cell-IL-22 axis," *Science*, vol. 351, no. 6279, pp. 1333–1338, 2016.

[78] A. Sá-Nunes, A. I. Medeiros, R. Nicolete et al., "Efficacy of cell-free antigens in evaluating cell immunity and inducing protection in a murine model of histoplasmosis," *Microbes and Infection*, vol. 7, no. 4, pp. 584–592, 2005.

[79] A. I. Medeiros, C. L. Silva, A. Malheiro, C. M. L. Maffei, and L. H. Faccioli, "Leukotrienes are involved in leukocyte recruitment induced by live Histoplasma capsulatum or by the β-glucan present in their cell wall," *British Journal of Pharmacology*, vol. 128, no. 7, pp. 1529–1537, 1999.

[80] B. Corrêa, A. Purchio, C. R. Paula, W. Gambale, and M. A. Shikanai-Yasuda, "Fluorescent method (fluorescein diacetate and ethidium bromide) to study the viability of Cryptococcus neoformans in liquor," *Revista do Instituto de Medicina Tropical de Sao Paulo*, vol. 32, no. 1, pp. 46–50, 1990.

[81] M. Cho and R. D. Cummings, "Galectin-1, a β-galactoside-binding lectin in Chinese hamster ovary cells. II. Localization and biosynthesis," *The Journal of Biological Chemistry*, vol. 270, no. 10, pp. 5207–5212, 1995.

[82] P. L. Whitney, J. T. Powell, and G. L. Sanford, "Oxidation and chemical modification of lung β-galactoside-specific lectin," *Biochemical Journal*, vol. 238, no. 3, pp. 683–689, 1986.